MODEL-BASED LIFE EXTENDING CONTROL FOR ROTORCRAFT

A Dissertation
Presented to
The Academic Faculty

By

Chams Eddine Mballo

In Partial Fulfillment
of the Requirements for the Degree
Doctor of Philosophy in the
School of Aerospace Engineering

Georgia Institute of Technology

August 2022

MODEL-BASED LIFE EXTENDING CONTROL FOR ROTORCRAFT

Thesis committee:

Dr. J. V. R. Prasad, Advisor
Department of Aerospace Engineering
Georgia Institute of Technology

Dr. Joseph F. Horn
Department of Aerospace Engineering
Pennsylvania State University

Dr. Daniel P. Schrage
Department of Aerospace Engineering
Georgia Institute of Technology

Dr. Julian J. Rimoli
Department of Aerospace Engineering
Georgia Institute of Technology

Dr. Mark F. Costello
Department of Aerospace Engineering
Georgia Institute of Technology

Date approved: July 25, 2022

In the name of Allah, the Most Gracious, the Most Merciful.

“Read! In the Name of your Lord Who created,

Created man from clots.

Read! And your Lord is The Most Generous,

Who taught by the pen.

He taught man what he did not know.”

[Translation from the Arabic text]

The Quran, Surah Al-‘Alaq (Chapter 96), verses 1-5

ACKNOWLEDGMENTS

I would like to sincerely thank my PhD advisor, Professor J.V.R. Prasad, for believing in me and giving me the opportunity to work with him. Prof. Prasad introduced me to the field of rotorcraft flight mechanics and control back in 2017. Even though I faced a steep learning curve, Prof. Prasad was very patient with me and always ready to answer the millions of questions I had. Prof. Prasad is an amazing teacher, mentor, and research advisor. I will forever cherish our discussions over the past few years. I would also like to express my deep gratitude to the other four members of my dissertation committee: Professors Costello, Schrage, Horn, and Rimoli. Thank you for taking an interest in my research and providing the invaluable comments and suggestions that helped improve the quality of this thesis. My gratitude also goes to Prof. Walker for the financial assistance in the form of a fellowship he provided during my time at Georgia Tech.

I would like to thank Dr. Tom Berger and Dr. Mark Lopez for providing great feedback on my work and suggesting new research avenues I have not yet explored. Furthermore, I greatly appreciate the help received from Dr. Chengjian He and the entire Advanced Rotorcraft Technology (ART) team in resolving technical issues associated with FLIGHTLAB.

Growing up, I have had the privilege to be partly raised and educated by my beloved late grandparents: Abass Dieng and Safietou Aidara. They instilled in me a strong set of values that made me the man I am today. I especially thank them for teaching me to never take anything for granted and also be humble. This thesis is dedicated in their loving memory.

I certainly cannot express in words the appreciation, love, and respect I have for my father, Ousmane, and my mother, Khadija. My mother is my source of inspiration and motivation. She taught me, through her actions, the importance of hard-work, discipline, persistence, patience, humbleness and so much more. Thank you for all the sacrifices you made to ensure that my siblings and myself had all we needed to be successful scholars. Thank you also for showing us that with dedication and perseverance nothing is impossible.

A special thank you is due to my father for always motivating me to make learning a lifelong journey.

I want to take this opportunity to thank my beautiful wife, Fadumo Awil Farah, for your unconditional love and for always being there for me. Thank you for being so patient, kind, and supportive. I certainly would not have made it this far without you. I am looking forward to the great things we will do together.

I owe a special debt of gratitude to my siblings: Ibrahima, Cheikh Saad-Bou, Ely Cheikh, Fatima, and Makhfouz. Thank you for always being the best siblings I could ever ask for. Your support, love, and friendship played a crucial role in the completion of this thesis.

I want to express my profound gratitude to the friends and colleagues I made at Georgia Tech over the past years: Dr. Toafiq Amoloye, Dr. Yasin Ridwane, Dr. Feyyaz Guner, Dr. Abhishek Mishra, Dr. Avani Gupta, Dr. Aarohi Shah, Dr. Yong-Boon, Dr. Jeremy Epps, Dr. Nicholson Koukpaizan, Dr. Robert Walters, Mr. Mahmoud Adnan, Mr. Zhenhao Jing, Mr. Marcus Pereira, Mr. Gabriel Nakajima, Mr. Emre Yilmaz, Mr. Imran Aziz, Mr. Alha Kane, Mr. Mamadou Ba, Mr. Hamza Mir, Ms. Vinodhini Comandur, and Mr. Aqib Syed.

TABLE OF CONTENTS

LIST OF TABLES

LIST OF FIGURES

SUMMARY

Rotorcraft are subjected to fatigue loads that not only limit the fatigue life of components but also add to their cost. Most of the fatigue-critical rotorcraft components are located in the rotor system, creating challenges for real-time load and structural health monitoring of such components. Furthermore, in forward flight, as the helicopter's main rotor rotates and simultaneously advances, a very complex aerodynamic environment dominated by large dynamic loads is created. Because of the asymmetric air flow past the main rotor, the lift forces each blade generates vary depending on its location. This creates cyclic loading that occurs at the main rotor frequency of rotation (1/rev) and at higher harmonic frequencies (n/rev, n = 2, 3 ,4, etc.) which become important for vibration, fatigue, and forward flight performance. Hence, many components in the rotor system are highly loaded with cyclic loads at multiples of the rotor frequency. In addition, during aggressive maneuvers, the low-duration high magnitude cyclic loads may lead to small amounts of localized damage, for example, localized plasticity, at stress concentration regions. Therefore, it is crucial to develop control strategies that can guard against premature fatigue failure of critical helicopter components to enable component life extension. This research aims at developing real-time algorithms that estimate component level dynamic loads in order to enable real-time load monitoring of critical rotor components and control strategies which alleviate or limit fatigue damage.

A nonlinear helicopter model with 33-inflow states and elastic blade representation is modeled in FLIGHTLAB®. The developed nonlinear model gives a suitable representation of the dynamic loads that the rotor system experiences. From the nonlinear model, a first order Linear Time Periodic (LTP) model of coupled body-rotor-inflow dynamics is extracted by performing a linearization about a periodic equilibrium. The LTP model is transformed into a Linear Time Invariant (LTI) model using harmonic decomposition methodology. The obtained LTI model which has 1513 states is used to develop novel

schemes for online estimation of rotor component loads.

The fidelity of the 1513-state LTI model is assessed in the frequency domain via comparison with flight test data. A model order reduction approach based on singular perturbation theory is used to reduce the 1513-state LTI model to a 10^{th} order LTI model. The 10^{th} order LTI model retains the physical meaning of relevant states and the fidelity of the dynamic load prediction of the 1513-state LTI model.

Using the reduced order LTI model, two component load limiting strategies to limit fatigue damage are pursued. The first one is based on a receding horizon model predictive control (i.e., Load Limiting Control (LLC) scheme) while the second one is based on active rotor control (i.e., Load Alleviation Control (LAC) via IBC scheme). In both approaches, component life extension is achieved by directly limiting fatigue life usage associated with harmonic loads. In the receding horizon model predictive control formulation, an optimal control problem is formulated where given a desired user-defined maximum harmonic load limit, an estimate of the control margin associated with the component load limit is found and used in the form of pilot cueing/automatic limiting to prevent the component harmonic load from exceeding the maximum limit. In this approach, the use of the reduced order LTI model is twofold. The component harmonic load estimate generated by the reduced order LTI model is used in the detection of limit violation. Furthermore, the reduced order LTI model is used to generate a mapping between the limit and control margins. To assess the effectiveness of this scheme, its integration with a visual cueing system is performed. Subsequently, the resulting architecture is implemented within the Georgia Tech Re-configurable Rotorcraft Flight Simulator to perform real-time piloted flight simulation experiments.

The component load limiting scheme based on active rotor control uses the 10^{th} order LTI model in the synthesis of a higher harmonic individual blade controller (i.e, IBC controller). The IBC controller uses load predictions from the 10^{th} order LTI model to compute optimal higher harmonic individual blade pitch inputs to reduce specific harmonic loads. It

is found that the proposed component load limiting scheme via IBC is effective in reducing desired harmonic components of pitch link load at trim but also during maneuvering flight with no impact on the maneuver performance and vibratory hub loads. Furthermore, using the handling quality requirement for small amplitude pitch changes in forward flight, it is shown that the proposed scheme does not cause handling qualities degradation.

CHAPTER 1
INTRODUCTION

1.1 Motivation

Since inception, rotorcraft (i.e., helicopters and tilt-rotor aircraft) have been essential components of daily human life. The increasing popularity of this complex machine mainly stems from its capability to take-off and land vertically, sustain hover flight, and land on unprepared surfaces. Rotorcraft are used in a plethora of ways: disaster relief, reconnaissance, and combat missions to name a few. The expanded use over the last decade revealed new challenges which limit rotorcraft's operational capabilities and ease of flight.

Rotorcraft are known to exhibit unstable bare-airframe flight dynamics and high inter-axis coupling. The pilot is, therefore, forced to manually suppress the inter-axis coupling and stabilize the aircraft through the use of the four primary controls (collective, lateral and longitudinal cyclic, and pedal). The pilot essentially acts as a feedback controller which drastically increase her or his workload and make it extremely challenging to fly the aircraft. Furthermore, the rotorcraft flight envelope is constrained by a very complex set of limits. The flight envelope limits of a rotorcraft are related to structural/aerodynamics loads on the rotor or fuselage, engine speed and temperature, transmission loads, and loss of control (for instance, loss of tail rotor authority) [1]. Each of these limits can be described as either a "hard limit" or a "soft limit". In any case, these limits define the performance capability of the aircraft and its degree of maneuverability. Hard limits should never, under any circumstances, be exceeded as this can lead to catastrophic failures. On the other hand, soft limits can be exceeded at the expense of an increase in operational cost (i.e., increase in fatigue life usage which leads to frequent repairs and component replacement). The engine/gearbox torque and maximum fatigue load limits are examples of soft limits, whereas

stall and maximum resultant hub moment limits are examples of hard limits. Hard and soft limits are established to ensure the controllability and structural integrity of the aircraft, but also to prevent premature fatigue failure of critical airframe and rotor components. Hence, to reduced operational cost and avoid fatal accidents it is imperative for the pilot to closely monitor these limits. The simultaneous monitoring of several critical limits can have a negative effect on the pilot's workload.

The use of a flight control system helps in circumventing these issues. A flight control system is able to eliminate the inter-axis coupling and provide a stable dynamic response. This greatly reduces the pilot workload, and hence improves the handling quality of the vehicle. Most legacy helicopters (e,g,, UH-60A/L) use a partial authority flight control system. In a partial authority flight control system, the pilot can command 100% of the available actuator travel through mechanical linkages that directly connect the pilot stick input to the swashplate actuation system (or control surfaces) whereas the flight control system can only command a smaller fraction of that usually in the order of $\pm 10\%$. Limited authority is given to the flight control system. This is mainly because legacy helicopters usually have limited redundancy; therefore, it is imperative to allow the pilot to have sufficient control of the vehicle when the control system fails. With the advance of digital technology and the need for less mechanically complex aircraft, partial authority flight control systems were slowly replaced by full-authority automatic flight control system (AFCS). In a full authority fly-by-wire control system, no mechanical linkage is used. The pilot inputs are converted into electrical signals that are sent to the control surface actuators by a computer. Therefore, the pilot is no longer directly connected to the control surfaces and the control system can command 100% of the available actuator travel. The successful transition to a full authority fly-by-wire control system necessitated a control system design with a high degree of redundancy to compensate for various potential system failures during flight (i.e., sensors, actuator, flight computer failures). The switch to a full authority fly-by-wire control system allowed not only reducing weight but, more importantly, transferring the

challenging task of monitoring aircraft limits (i.e., hard and soft limits) from the pilot to the aicraft's flight control computer. This greatly reduces the pilot workload and helps mitigate issues associated with pilot attention.

Full authority fly-by-wire flight control systems allow for a much more flexible control design framework. This enables the incorporation of carefree maneuver enabling technologies and load alleviation control (LAC) schemes into the automatic flight control system. Carefree maneuvering refers to the ability of the pilot to fly the aircraft without concern for exceeding the flight envelope limits. A carefree maneuver system helps the pilot achieve such a capability. Hence, a carefree maneuver system helps in preventing envelope limit violation when the aircraft is aggressively flown near the edge of the flight envelope. Although a carefree maneuver system has tremendous benefits, its design is a challenging task for two reasons. The first reason is the difficulty in computing in real-time the proximity of the aircraft to the envelope limit. In the literature, this is known as the limit detection step which allows for the detection of impending limit violation. The second reason is the difficulty in designing advanced algorithms that can efficiently prevent limit violation without degrading the handling qualities of the vehicle. This is known as the limit avoidance step. The limit avoidance step takes preventive actions to keep the vehicle within the flight envelope. This is achieved either through pilot cueing or automatic limiting of excessively aggressive maneuvers. Load alleviation control is a scheme that aims to extend the life of helicopter components. LAC aims to reduce component level peak-to-peak dynamic loads; this reduces the peak-to-peak stresses, which can reduce fatigue life usage. LAC is achieved through modifications of the flight control system. Such modifications can take the form of the addition of feedback signals, the optimization of flight control system gains or a combination of both. The integration of carefree maneuver and load alleviation control systems within the flight control system comes with many benefits as it reduces the pilot workload, maximizes the use of the flight envelope, and helps in maintaining the structural integrity of the aircraft.

The loads a helicopter experiences during flight are very complex and different from their fixed-wing counterparts. This is mainly due to the complex coupling between the various dynamic components of a helicopter as shown in Fig. 1.1. In Figure 1.1, Professors Peters and Schrage highlight the high coupling between the rotor dynamics which comprises three groups of components: the blade aerodynamics, blade structural dynamics and external flow field, the airframe dynamics, airframe aerodynamics, powerplant/drive system dynamics, and the AFCS [2–4]

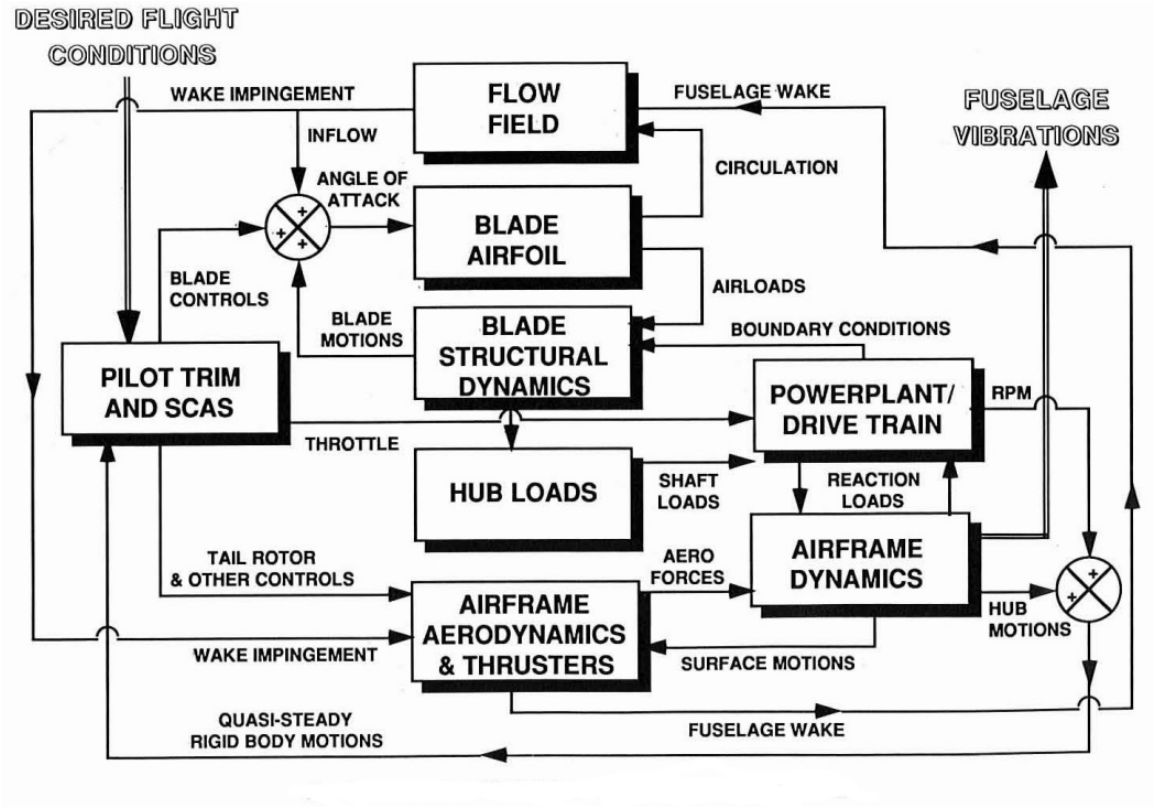

Figure 1.1: Rotorcraft multi-discipline interactions-for main lifting rotor (Ref. [2]).

Because of the complex coupling between these dynamic components, it is challenging to understand and predict or calculate the loads acting on the helicopter during flight. In fact, the calculation of rotor system loads is considered one of the most difficult problems of rotorcraft technology [2, 3]. The rotor loads are mostly dominated by 0^{th} and the first two harmonic loads [2]. The accurate prediction of rotor loads is crucial as it has a direct impact on the fatigue life of dynamic components and rotor system weight [2]. For instance,

if the loads on the rotor system are over-predicted this would lead to an early retirement of helicopter components. Furthermore, in the early design stage, an over-prediction of the rotor loads would lead to a design that is too heavy to operate efficiently [2].

In forward flight, as the helicopter's main rotor rotates and simultaneously advances, a very complex aerodynamic environment dominated by large dynamic loads is created [5]. Because of the asymmetric air flow past the main rotor, the lift forces each blade generate vary depending on the blade's location. This variation in lift forces creates cyclic loading that occurs at the main rotor frequency of rotation (1/rev) and at higher harmonic frequencies (n/rev, n = 2, 3 ,4, etc.), which becomes important for vibration, fatigue and forward flight performance. Hence, many components in the rotor system experience cyclic loads, whose frequency of application is equal to the rotor frequency or can be a multiple of the rotor frequency. In addition, during aggressive maneuvers, the low-duration high magnitude cyclic loads may lead to small amounts of localized damage, such as localized plasticity, at stress concentration regions. Therefore, it is crucial to develop control strategies in the form of LAC that can guard against premature fatigue failure of critical helicopter components to enable component life extension. This would reduce maintenance and operating cost. A full-authority fly-by-wire system facilitates this goal.

A 2012 survey of the past 30 years, carried out in Augusta Westland Limited (AWL) Materials Technology Laboratory, concluded that fatigue failures account for approximately 55% of all premature failures in helicopter components[6]. The causes of low cycle fatigue are largely due to aircraft maneuvers, gust loading, and through take-off and landing. Critical helicopter components, classified as Grade-A Vital components by regulatory authorities, are subject to significant fatigue loading in which the failure would result in a catastrophic event. A list of fatigue critical components[7] on the AH-64A Apache shows that many of the Grade-A Vital components are located in the rotor system, creating challenges for real-time load monitoring of those components but also for the development of load alleviation and load limiting control schemes.

Current methods for Structural Health and Usage Monitoring (HUMS) and Load Alleviation Control rely on distributed sensing and operational monitoring to infer usage and estimate fatigue in critical components. Such methodologies involve significant uncertainty due to the difficulty in placing sensors on rotating components and other hot-spot locations often characterized by maximum stresses. For example, past work[8] aimed at limiting pitch link loads has used proxy models of the vibratory loading. A classic example is the Equivalent Retreating Indicated Tip Speed (ERITS) parameter. ERITS has been correlated as a function of airspeed and normal load factor with vibratory pitch link loads from retreating blade stall onset and can be limited to indirectly constrain the pitch link loads. Additionally, curve fits of pitch link vibratory loads as a function of airspeed have been used to limit the peak-to-peak pitch link load. Furthermore, various non-physics based models, developed using statistical methods or neural networks[9], have been used for the synthesis of structural Health Usage and Monitoring Systems (HUMS) that could be potentially used in the development of future control strategies for component life extension[10–12].

The use of non-physics based and proxy-models for real-time load monitoring has been a major drawback in the development of control strategies for component life extension. These models suffer from at least one of the following issues:

- They are data-driven and hence require significant amounts of training data.
- They suffer from inaccuracy and often are aircraft-specific.
- They do not provide the higher-harmonic dynamics of the vibratory loads, a factor which is essential for fatigue analysis.

Therefore, there is a need for high-fidelity physics-based models that are not aircraft specific and can accurately capture, in real-time, the higher harmonic dynamics of the vibratory loads at critical helicopter components during flight. Such models can drastically improve the design of control schemes for helicopter component life extension. Recent

studies[13–15] have explored methods for approximating coupled body/rotor/inflow dynamics into a linear time invariant form that is suitable for integrated flight/rotor controller development. The developed methods use harmonic decomposition to represent higher frequency harmonics as states in a LTI state space model, and they offer the potential for real-time estimation of the effect of control inputs on component dynamic loads; these methods can be used in combination with reduced order structural models to estimate primary damage variables associated with fatigue of critical components. Such real-time estimation of component level dynamic loads, stresses and strains, etc., provides the opportunity for real-time monitoring of component damage variables, and more importantly, the development of control schemes designed to alleviate or limit component fatigue damage by automatically limiting (or provide cues to the pilot regarding) excessively aggressive maneuvers.

These higher order LTI models have been previously used in the development of an integrated flight and vibration controller to study the interaction between Higher Harmonic Control (HHC) and the augmented flight control system (AFCS) in maneuvering flight[13]. Through the use of dynamic cross-feeds, this controller has been successful in reducing vibration while not having significant impact on the handling qualities and maneuver performance. Furthermore, a harmonic analyser scheme for combining the LTI model of coupled body/rotor/inflow dynamics with a Linear Quadratic Estimator (Kalman Filter) was developed in which individual harmonic components of hub loads could be extracted in real-time from total hub load measurements[16]. Although results showed that the use of these higher order LTI models improved vibration control and real-time extraction of harmonic components of fixed-frame rotor hub loads, very few studies were focused on using these higher order LTI models in the development of life-extending control schemes for critical helicopter components.

This thesis has two main objectives. The first objective is to develop models for online estimation of rotor component harmonic loads using a novel approach, namely a purely physics-based approach. The second objective is to use the developed physics-based mod-

els to propose novel control schemes for critical rotor component life extension. The LTI model of helicopter coupled body/rotor/inflow dynamics and the linear quadratic estimator are the main tools used in this research effort.

1.2 Background

This section summarizes published work in the literature related to load alleviation control, envelope protection systems, load monitoring system for rotor components, linear time invariant approximations of linear time periodic systems, singular perturbation methods for model order reduction, and individual blade control. These six topics are used as the foundation for this current research effort.

1.2.1 Load Alleviation Control

Tilt-rotor aircraft like the V-22 Osprey can operate in both fixed-wing and rotary-wing modes. The ability to operate in both modes comes with many benefits but also many challenges. One such challenge is the excessive build-up of loads in the rotor system during trim and maneuvering flight (especially during mode transition). This excessive build-up of loads has been identified as a problem that could limit the maneuverability and agility of the vehicle[1], attributed to the high fatigue life usage resultant from the high loads maneuvers. To solve this problem, a load alleviation control strategy was proposed[17, 18]. In Refs. [17, 18], Dave Miller et al. proposed a load alleviation control scheme based on a weighted least squares assignment technique and a balanced singular value Linear Quadratic Gaussian with loop transfer recovery (LQG/LTR) technique. The load alleviation control scheme pursued in Refs. [17, 18] was used to alleviate rotor yoke chord loads. The main idea behind the proposed LAC scheme is to arrive at a feedback control law which eliminates the tendency of the rotor to lead the mast during precession. Real-time piloted simulations were used to evaluate the effectiveness of the proposed load alleviation control scheme. Results obtained from the piloted simulations suggest that the proposed scheme is

effective in alleviating rotor yoke loads while maintaining level 1 handling qualities.

Around the same period, Popelka et al. proposed another load alleviation control scheme for the V-22[19]. This time, both the airframe and rotor loads were reduced using the LAC scheme to avoid component fatigue damage exceeding a prescribed threshold during airplane and rotary-wing modes. The synthesis of such a load alleviation control scheme was achieved via modifications to the flight control system and an optimization of its gains. In the literature, many other load alleviation control laws for the V-22 Osprey were proposed[20–22]. These studies differ in the way they modify the flight control system to achieve component load alleviation while not affecting the handling qualities of the vehicle.

More recently, various studies have tried to develop load alleviation control schemes for the UH-60 helicopter[23, 24] to extend the life of rotating blade root pitch links. The proposed LAC strategies for component life extension aim at reducing component dynamic (e.g., peak-to-peak) loads, leading to reduced peak-to-peak stresses, and hence potentially leading to reduced fatigue life usage. Figure 1.2, extracted from Ref. [23], shows an example of a flight controller with pitch link load alleviation capability. The flight controller uses an Explicit Model Following (EMF) architecture to achieve stability and Rate Command and Attitude Hold (RCAH) response in the roll, pitch, and yaw axes.

The LAC schemes pursued in Refs.[23] and [24] considered a Linear Quadratic Control (LQR) solution for arriving at feedback control laws that trade between maneuver command following and load alleviation. As such, load alleviation is implicitly used in arriving at a compromise set of flight controller gains as a trade-off between maneuver performance and load. The proposed LAC schemes are seen to be effective in reducing the peak-to-peak total pitch link load during maneuvering flight. Furthermore, it is shown in Refs.[23] and [24] that with a compound helicopter (i.e., UH-60 with a wing), load alleviation can be achieved with LAC by distributing control to fix-wing surfaces and the rotor. This potentially obtains load alleviation with no impact on the handling performance of the helicopter.

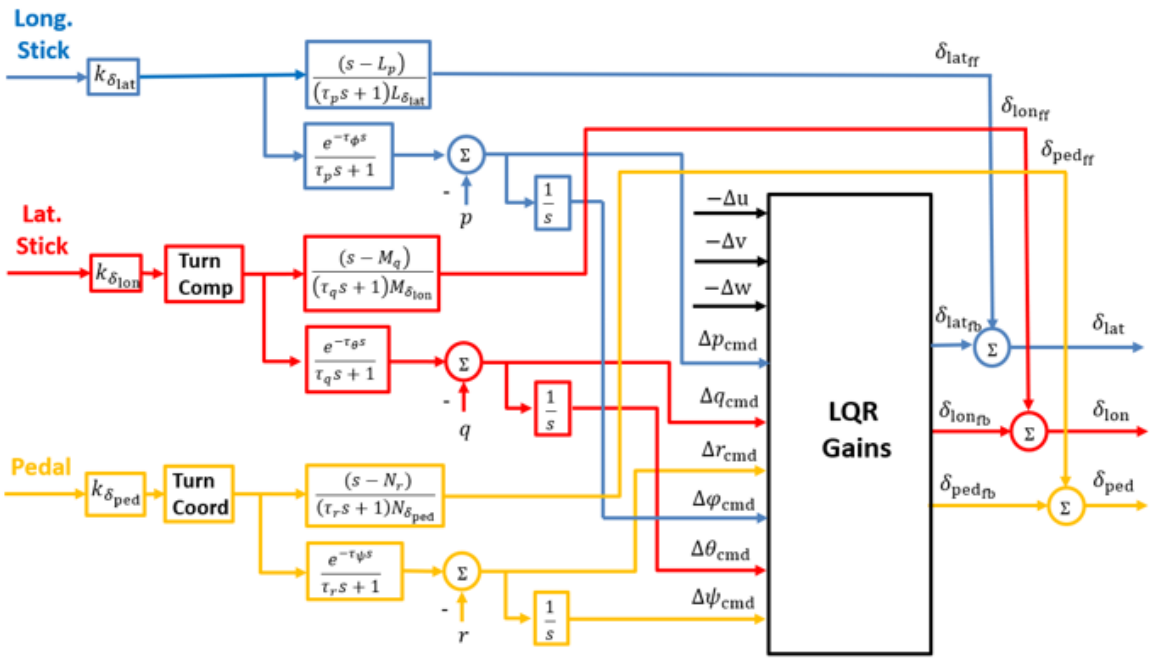

Figure 1.2: A load alleviation control scheme (Ref. [23]).

While LAC offers a computationally simpler scheme, it leads to a conservative design for two reasons. First, it is incapable of discerning aggressive from non-aggressive maneuvers. Second, it totally neglects the effect of harmonic loads on localized damage. This thesis proposes novel control schemes for critical helicopter component life extension that are more effective and less conservative than the traditional LAC scheme. For instance, a more effective control strategy for component life extension, albeit at a significant computational complexity, is to treat desired levels of component harmonic loads as limit boundaries, and hence, limit directly the fatigue life usage associated with harmonic loads.

1.2.2 Envelope Protection Systems

The recently growing performance and handling quality issues associated with the complex operating limits that constrain helicopter operations have motivated many investigations into carefree maneuver systems[25]. Carefree maneuver systems, also known as envelope protection systems, are designed to maintain vehicle operation within the operating limits. Their main purpose is to maintain the structural integrity of the vehicle. Over the past few

years, researchers have adopted many different approaches for the accurate prediction of limit violation onset as well as advanced cueing mechanisms for appropriate limit violation prevention [26]. At NASA Ames, the performance of various aural, visual and tactile cueing methodologies were assessed[25, 27–29]. The studies concluded that even though tactile cues via control inceptor are intrusive, they are better at warning the pilot of an impending flight envelope limit exceedance. Tactile cues via control inceptor showed great promise mainly because they are immediate and pilot over-ridable, but also for a more important reason: they naturally relate the proximity to a flight envelope limit with the pilot control action required to reach that flight envelope limit[25]. An envelope protection system with tactile cues on the control inceptors allows the pilot to perceive flight envelope limits as equivalent control limits on the control stick. Essentially, with these tactile cues on the control inceptors, a mapping is obtained that relates how far the vehicle is from the flight envelope limits (i.e., limit margins) to the necessary control deflections to reach the flight envelope limits (i.e., control margins) . This aspect is shown in Fig. 1.3.

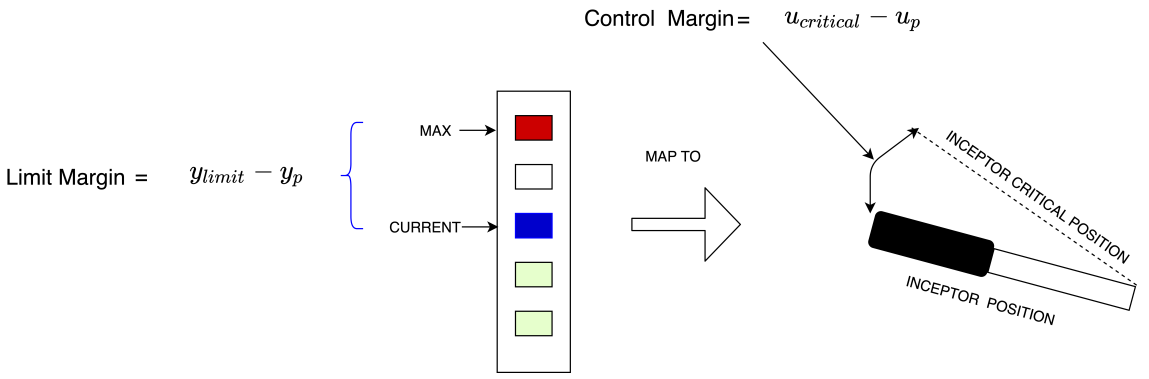

Figure 1.3: Envelope protection with tactile constraint cueing.

In Fig. 1.3, the control margin is defined as the difference between the control limit ($u_{critical}$) and the current control stick position (u_p). The control margin is the amount of control input deflection from the current stick position that will take the limit parameter (y_p) to the limit boundary (y_{limit}). The limit parameter is a standard terminology in the literature that refers to the state or parameter which limits the boundary of a flight envelope. The con-

trol limit is determined using a function that relates the limit parameter (y_p) to the control stick input (u_p). This function is usually complex and highly nonlinear. Furthermore, its true mathematical form is usually unknown. Envelope protection systems differ in the way they generate an approximation of that function. Once an approximation of the function that relates the limit parameter (y_p) to the control stick input(u_p) is obtained, one can use it to compute future values of the limit parameter over a selected time horizon, which in turn can be used to generate control limit and available control margin estimates. The selected time horizon over which a future value of the limited parameter is calculated is known as the prediction window. The prediction window should be large enough (i.e., not too small) to take into account the dynamic nature of limit parameter response. The selected prediction window provides a lead time prediction which gives enough time for the detection and avoidance of limit violations. The development of envelope protection systems which provide adequate lead time prediction has been the focus of many research efforts. In the literature, various envelope protection systems based on artificial/polynomial neural networks, dynamic trim, Linear Parameter Varying (LPV) aircraft dynamics, and nonlinear time response functions have been proposed[30–42]. For each of the proposed methods, studies show how different tools such as neural networks, dynamic trim, etc., can be used to not only generate a function that relates the limit parameter to the control stick input, but also to compute control margin estimates. The proposed methods have been successfully implemented for normal load factor, angle of attack, transient rotor RPM, rotor yoke bending loads, vertical downstop loads, main rotor hub moment, and torque limit protection within various aircraft simulation models such as the V-22 tiltrotor aircraft.

This thesis adopts a carefree maneuvering approach in the development of novel life-extending control schemes for critical helicopter components. Carefree maneuver systems have been notably used in past research to maintain the structural integrity of the vehicle. One major contribution of this research is to extend the use of carefree maneuver systems to enable component life extension. More specifically, a Load Limiting Control (LLC)

scheme for component life extension inspired by carefree maneuver systems is proposed.

1.2.3 Rotor System Load Estimation

Critical helicopter components with limited fatigue life are replaced once their prescribed Component Replacement Times (CRTs) are reached[43]. For a particular component, the prescribed replacement time is determined by the number of flying hours for which the component can be used. Once that number of flying hours is reached, the component should be automatically replaced to reduce possibilities of component failure during flight. This binary strategy for deciding whether or not a component should be replaced or not has been a standard method used by the army and defense forces for a long time. It is a conservative approach since there are possible scenarios where some components are replaced whose fatigue life has not been reached yet (i.e., premature retirement of components); or on the other extreme, where the components should have been replaced much earlier (i.e., late retirement of components). Hence, such a method can be very costly and raise many safety issues. The life of helicopter components, especially the ones in the rotor system, heavily depends on the dynamic loading they experience over a specific number of flying hours and not just on the number of flight hours. Therefore, accurate real-time load monitoring of critical helicopter components can increase safety and lead to significant cost savings at the fleet-level. Unfortunately, for most components in the rotating system, obtaining real-time load measurements is a challenge. Much work has been dedicated to finding ways to have accurate real-time estimation of component level dynamic loads to facilitate the inference of fatigue life usage but more importantly, the development of life extending control schemes in the form of load alleviation/limiting control. However, the development of load alleviation/limiting control schemes for critical rotor component life extension has suffered from the lack of methods that can provide accurate real-time estimation of component level dynamic loads. One strategy to overcome this difficulty is to rely on proxy or curve-fit models of the loads. For instance, in Refs. [8] and [28] the pitch

link load variation was constrained via a limiting of the Equivalent Retreating Indicated Tip Speed (ERITS) parameter. The ERITS parameter correlates the vehicle airspeed and the normal load factor with the vibratory pitch link loads from retreating blade stall onset. Hence, the ERITS parameter can be limited to indirectly constraint the pitch link loads.

In the literature, various models have been constructed based on statistical methods, neural networks, or a combination of both to have robust and accurate rotor component load/fatigue life estimation. More specifically, these models were developed to use fixed-system measurements for the determination of rotating system loads. The fixed system measurements are either in the form of load or flight parameter measurements. For instance, in Ref. [44], a technique based on holometrics is developed. Using fixed system data from strain gauge readings, the technique developed in Ref. [44] establishes a linear relationship in the form of a transfer coefficient matrix between fixed system and rotating system loads. Hence, this method arrives at a static mapping that relates loads in the fixed system to loads in the rotating system. Initially, this technique solely used fixed-system load measurements in the estimation of rotating frame loads but was later extended to also include flight parameter measurements. The method was applied on both a SH-2F[45] and AH-64A[46] helicopter. For the SH-2F helicopter, the pilot control stick inputs, aircraft angular rates, velocity, and normal load factor are fixed system measurements that are used in the prediction of main rotor normal bending and pushrod loads. On the other hand, for the AH-64A helicopter, various fixed system measurements are used in the prediction of damper force and twisting moment at station 104.5 of rotor blade lead-lag, lateral control actuator force, and vertical bending moment at fuselage stringer station 416. From the simulation results of Refs.[45] and [46], it is shown that holometrics can be used for load and damage monitoring of critical rotor system components, and hence, in the development of life extending control schemes. During the same year, Tang and O'Brien[47] proposed a pattern recognition approach for on-board fatigue life monitoring of dynamic components in the rotor system. The proposed approach is a semi-empirical method which correlates

already monitored quasi-static flight parameters (i.e., airspeed, normal acceleration, engine torque, etc.) with available load data from flight tests. First, a database of load time histories of critical components are used to formulate a set of load cycle spectrum types. Then, the quasi-static flight parameters associated with the load time histories are used to train a pattern recognition algorithm so as to obtain a mapping between the quasi-static flight parameters and the load cycle spectrum types. The pattern recognition algorithm is then used during flight using real-time measurement of the quasi-static flight parameters for on-line estimation of load cycle spectrum type for the rotating components to be monitored in the helicopter. The load cycle spectrum type estimates are then used to obtain real-time estimation of fatigue damage accumulation on the component. The method was successfully used for online estimation of the pitch link fatigue life usage. A similar approach was proposed by Barndt and Moon[48] where a flight condition recognition monitoring system was developed for the AH-1W helicopter to monitor aircraft usage (i.e., to monitor fatigue damage for aircraft components).

Regression is a particular statistical-based method that has received particular interest. This is mainly because regression-based models are usually computationally less expensive than neural-network based models. As an example, regression-based methods (i.e., least squares regression) have been used to determine rotating component loads (i.e., main rotor blade bending and pushrod load) from fixed system measurements on a SH-60B helicopter[49, 50]. The fixed system measurements included pedal, collective, lateral and longitudinal stick positions, roll, yaw, pitch and climb rates, load factor at CG, and velocity. Similar approaches were also used for rotor system load and fatigue life monitoring[51, 52].

Instead of using a statistical-based method, many researchers have adopted a neural network approach. Neural networks are attractive due to their capability to approximate continuous functions with a high level of accuracy (i.e., Weierstrass approximation theorem) and generalization ability[53]. Cook et al.[54] in 1994 investigated the use of an

Artificial Neural Network (ANN) for the estimation of dynamic loads in critical components using flight variable information that can be easily measured. The ANN is used to learn the relationship between flight variables and component loads through an adaptive training process that uses a database of flight parameter records and corresponding load histories as training data. The proposed scheme was tested in a simulation for the estimation of time-varying mean and oscillatory components of the tail boom bending load and the pitch link load. For this simulation, the inputs to the network are fixed system flight parameters which are the pitch rate, roll rate, yaw rate, vertical acceleration, lateral acceleration, longitudinal acceleration, longitudinal control position, and lateral control position. It is shown in Ref.[54] that the ANN was able to predict the mean and oscillatory component load with accuracy above 90%. Following this research effort, Azzam[55] proposed a novel technique based on a mathematical network instead of an artificial neural network. A mathematical network is very similar to a neural network; however, a special structure is imposed on the network by the inclusion of fundamental laws of physics. The proposed method provides more accurate fatigue life estimations when compared to techniques available in the literature. Azzam's proposed method uses flight parameters measurements to have real-time estimates of fatigue damage on critical helicopter components. The network training used sets of examples in which each training example comprises instantaneous fatigue damage induced during a small time step and flight parameters measured during the time step. This proposed technique was found to accurately predict fatigue damage of two rotating components (i.e, blade lug section and rotating pitch link) with 5% of measurement error. While Hoffman[56] studied the effect of training data selection on the load estimation of a neural network, many other researchers took a blended approach to load and fatigue life estimation of critical helicopter components by combining neural networks and regression models[10, 11].

The methods currently present in the literature for real-time load monitoring of rotor components are based on models that are constructed using either a neural network or

some form of statistical-based method, and make use of fixed system measurements (i.e., either load and flight parameter measurements). The development of these models requires obtaining a lot of data, a difficult and expensive task. Even with the data, the models developed are only associated with the specific helicopter from which the data is extracted. In other words, such models are helicopter- specific. There is, therefore, a need for a purely physics-based approach to load monitoring, more specifically, a physics-based model capable of providing real-time estimates of rotating frame loads that are not easily amenable for measurement solely using fixed system measurements. A physics-based approach would avoid reliance on a large amount of data and would develop models that are not vehicle specific.

1.2.4 Linear Time-Invariant Approximations of Linear Time-Periodic Systems

Due to the periodic nature of the helicopter rotor in forward flight, linearized nonlinear helicopter models take the form of Linear Time Periodic (LTP) systems. These LTP models have matrix coefficients which are periodic with a period of one rotor revolution. The analysis of LTP systems has been the interest of many scientists and researchers in the field of physics, mathematics, and engineering such as Matthieu Emilie[57]. More specifically, the reformulation of linear time periodic system in order to arrive at a Linear Time Invariant (LTI) formulation has been a very popular research topic. Even though the Floquet method has been extensively used for the analysis of LTP systems as well as their conversion into LTI form, the methodology is still inadequate because the generated LTI model remains inconvenient for control design and for handing qualities analysis. Similar to the Floquet method, Hill's method[58], which is a Fourier-based frequency domain reformulation, provides a time invariant state matrix approximation of the original LTP system. Hill's method is a generalization of Mathieu's equation[59]. It uses the method of infinite determinants to expand the LTP system states into various harmonic state coefficients, hence devising a corresponding linear time invariant model. In the rotary-wing field, Olcer and Prasad used

Hill's method to develop a methodology for approximating coupled body/rotor/inflow dynamics into linear time invariant form that is suitable for integrated flight/rotor controller development[14, 15]. The extraction of an LTI model from a nonlinear system model is done using a two step approach. The first step consists of linearizing the nonlinear model about a selected periodic equilibrium in order to obtain an LTP model. The linearization is performed incrementally using azimuthal steps over one complete rotor revolution. The second step consists of a harmonic expansion of the LTP states to represent higher frequency harmonics as states in a LTI state-space model. The minimum number of harmonic states to retain in the LTI formulation is determined from both time and frequency domain response characteristics between the extracted LTI model and the nonlinear model but also from a stability characteristics' comparison between the LTI and nonlinear models. The extracted LTI model has provided a successful framework to conduct integrated flight and rotor control studies.

Active rotor control is one of many research areas that has greatly benefited from the work of Olcer and Prasad[14, 15]. For instance, their method has found successful application for OBC implementations of HHC[14, 60] and the study of the interaction between HHC and the Augmented Flight Control System (AFCS)[61].

Although the method proposed by Olcer and Prasad showed great promise and received a wide range of applications, the fidelity of the obtained LTI model was not rigorously assessed. Furthermore, the developed LTI model relied on a second order formulation of the original LTP system. This second order formulation can present problems for degrees of freedom which cannot be represented explicitly in second order form. More specifically, a problem arises when performing harmonic decomposition of body and inflow states. Furthermore, for the LTI model obtained using the LTP model in second order form, harmonic states associated with velocities are not obtained via a harmonic expansion of the LTP velocity states, but rather via a kinematic relationship involving terms that depend on the rotor speed[13]. Hence, interpretation of LTI model velocities becomes a problem.

Lopez and Prasad[13, 62] proposed a more general approach which generates a linear time invariant approximation from a linear time periodic model using a first order formulation. In this first order LTI formulation approach, there is no ambiguity in the treatment of LTP velocity states. Also, higher harmonic dynamics associated with degrees of freedom that are not explicitly expressed in second order form can be well captured . The authors also developed methodologies for assessing the fidelity of LTI approximations of LTP systems[13]. More recently, studies[23, 24, 63] at Penn State have used the LTI models of coupled body/rotor/inflow dynamics of Refs [13] and [62] for the development of life extending control schemes in the form of load alleviation control (LAC) strategies.

This thesis aims to extend the use of the LTI model of helicopter coupled body/rotor/inflow dynamics in two ways. First, the LTI model is used to synthesize a physics-based model for online estimation of rotating frame loads that are not easily amenable for measurement. Second, the LTI model is used in the development of novel life-extending control schemes for critical components in the rotating frame. More specifically, two life- extending control schemes are proposed: a load limiting control scheme and a load alleviation control scheme based on active rotor control.

1.2.5 Singular Perturbation Method for Model Order Reduction

High-fidelity models representative of real-life processes are usually complex, have multiple time scales (i.e., fast and slow modes), and are high-dimensional. In many cases, when using such high-fidelity models in numerical simulations, real-time performance is usually not possible.

Reduced order modeling is a technique that aims to reduce the complexity and dimension of high-fidelity mathematical models without too much loss of fidelity. In a sense, reduced order modeling alleviates the computational burden that comes with the use of high-fidelity models by generating a much simpler model which is generally referred to as a reduced order model. Therefore, such a reduced order model is more suitable for real-

time implementation[64]. The field of reduced order modeling is very mature for linear systems but not for nonlinear systems. For linear systems, various reduced order modeling techniques have been proposed in the literature. Among them are the balanced truncation and singular perturbation methods.

Model reduction via balanced truncation[65, 66] was proposed by Moore in 1981. This technique is based on principal component analysis where a coordinate transformation is applied to the state vector of the linear system, which renders the controllability and observability grammians balanced (i.e., the grammians are equal and diagonal). The main drawback of this method is that the obtained reduced order model does not have physical states but rather energy states.

Singular perturbation is another method used for the model order reduction of linear systems. This method is based on timescale separation where the system dynamics is decomposed into fast and slow modes[67, 68]. Model order reduction via singular perturbation can be best illustrated with the following example.
Consider the following set of differential equations

$$\dot{x} = f(x, z, u, \mu, t) \tag{1.1}$$

$$\mu\dot{z} = g(x, z, u, \mu, t) \tag{1.2}$$

Many physical phenomena can be modeled using Eqs. (1.1) and (1.2) where μ (≥ 0) is a small constant value which represents all the small parameters to be neglected[65, 66]. Typically, in a generic system, it is not clear apriori what dynamic modes one needs to capture in the reduced order model to obtain a model with a higher level of accuracy. In the singular perturbation technique, the μ parameter is introduced to decouple the original system into fast and slow modes, which facilitates the selection of the dynamic modes to retain in the reduced order model. As μ is small, the dynamics of Eq. (1.2) can be much

faster than that of Eq. (1.1) (i.e., when μ is small, $\dot{z} = \frac{g}{\mu}$ can be very large and furthermore $\frac{\dot{z}}{\dot{x}}$ can be of order $\frac{1}{\mu}$). The dynamical model represented by Eqs. (1.1) and (1.2) is more commonly known in the literature as a singularly perturbed system.

For the special case where f and g are linear and do not depend on μ the following equations are obtained

$$\dot{x} = A_{11}x + A_{12}z + B_1u \tag{1.3}$$

$$\mu\dot{z} = A_{21}x + A_{22}z + B_2u \tag{1.4}$$

Given that the dynamics of Eq. (1.4) is much faster than that of Eq. (1.3) a unique reduced order model (i.e., a quasi steady-state model) can be obtained by setting $\dot{z}$ to zero and using the obtained algebraic equation to generate a relationship between z, x, and u. The resultant reduced order model can be written as follows

$$\dot{x} = (A_{11} - A_{12}A_{22}^{-1}A_{21})x + (B_1 - A_{12}A_{22}^{-1}B_2)u \tag{1.5}$$

The reduced order model obtained through singular perturbation captures the low frequency and steady state of the original model accurately but the high frequency dynamics are neglected. Another very important fact here is that the state vector of the obtained reduced order model has physical significance. This is not the case when using other model reduction methods such as balanced realization. One drawback of the singular perturbation method is that converting any dynamical system to a singularly perturbed system is not easy. It is usually unclear how one should pick the parameter μ. More details about this method, including the mathematical properties the functions f and g need to satisfy, can be found in Refs.[65, 66].

The LTI model of helicopter coupled body/rotor/inflow dynamics extracted for the development of rotor system load monitoring and life extending control schemes can be very

large depending on the number of harmonic states retained. In this thesis, the singular perturbation method is used to derive a reduced order LTI model suitable for real-time implementation.

1.2.6 Individual Blade Control

Helicopter vibration and noise are usually induced by the rotor system. Vibration and noise are big concerns as they are the main cause of general public and passenger discomfort, flight safety issues, and deterioration of fatigue lives of structural components. Through various research efforts, active rotor control has been identified as a viable technique to arrive at vibration and noise reduction. Active rotor control aims at reducing vibration and noise at the source (i.e., at the rotor level).

Individual Blade Control (IBC) is a form of active rotor control where each blade is actuated independently [69]. In the literature, IBC has been mainly used for vibration and noise control. For instance, in Ref. [13], application of closed loop IBC in vibration control has been shown to be very effective at reducing vibration while having very little impact on handling qualities. Various other theoretical and experimental investigations [70–75] have shown the benefits of closed and open loop IBC on vibration and noise reduction.

This thesis aims to develop a novel load-alleviation control scheme using individual blade control. More specifically, this thesis seeks to understand if IBC could be used as a life extending control scheme rather than a vibration and noise reduction scheme.

1.3 Contributions of this Research

The contributions of this research are summarized as follows:

- In the literature, all the methods for real-time rotor component load and fatigue life estimation are based on models that are constructed using either neural networks or some form of statistical-based method and that make use of fixed system measurements (i.e., either load and flight parameter measurements). These methods are

data-driven (i.e, require expansive data) and aircraft specific. To overcome these issues, this dissertation provides a novel approach, namely a purely physics-based approach. In fact, this is the first investigation that proposes a purely physics-based approach to real-time estimation of rotating frame loads that are not easily amenable for measurement using fixed system measurements.

- Concepts from carefree maneuvering and model predictive control theory are used in the synthesis of a novel component life extension control strategy entitled LLC. The scheme is less conservative and more efficient than current life extending control schemes available in the literature. This is because the proposed scheme is not only able to discern between aggressive and non-aggressive maneuvers, but also takes into account the effect of harmonic loads on localized damage.

- The integration of the LLC scheme within an automatic flight control system for the development of an integrated flight and component load-limiting controller is studied. Such a controller is essential in understanding the trade-off between maneuver performance and component load limiting during maneuvering flight. Two integration methods are identified. For each integration technique a detailed analysis of the pros and cons is provided. This analysis helps to identify the integration method that is best suited for a particular application and minimizes maneuver performance degradation while performing load limiting.

- Traditionally, Individual Blade Control has been used for vibration and noise control. In this work, a novel Load Alleviation Control scheme (i.e., LAC via IBC) for critical helicopter component life extension is proposed. The scheme is innovative as it demonstrates how Individual Blade Control (IBC) and model prediction can be combined using higher-order Linear Time Invariant (LTI) models to develop a life-extending control scheme. The proposed LAC via IBC scheme is less conservative than the traditional LAC scheme, and no trade-off is involved between vehicle ma-

neuver performance and the impact of ensuing maneuver on a component life usage.

1.4 Objective

The objective of this work is to develop real-time algorithms for estimation of component-level dynamic loads as well as novel control schemes for critical component life extension with little impact on vehicle handling qualities. The developed algorithms and control designs were implemented in the Georgia Tech Re-configurable Rotorcraft Flight Simulator to carry out piloted simulation evaluations. Specifically, the following objectives are studied:

1. Extract LTI model from a high-fidelity nonlinear model using the harmonic decomposition methodology.

2. Validate the nonlinear and extracted LTI models using flight test-data (i.e., validate body/rotor dynamics and rotating frame loads prediction).

3. Use the extracted LTI model for the development of schemes for online estimation of rotating frame loads.

4. Use the extracted LTI model to develop novel control strategies for component life extension (i.e., Load Limiting Control and Load Alleviation Control via IBC schemes).

5. Assess the performance of the developed control schemes using nonlinear model simulations. Perform a handling qualities analysis for each control scheme to understand how the schemes impact the handling qualities performance of the helicopter.

6. Integrate the load-limiting control scheme with a visual cueing system. Use the resulting architecture to perform piloted simulation in

the Georgia Tech Re-configurable Rotorcraft Flight Simulator.

CHAPTER 2

LTI, LTI/LQE: PHYSICS-BASED MODELS FOR ONLINE ESTIMATION OF DYNAMIC LOADS IN THE ROTATING FRAME

The purpose of this chapter is to introduce a purely physics-based approach to online estimation of rotor system loads. The harmonic decomposition method and Linear Quadratic Estimator (LQE) are tools used in this investigation. Using the harmonic decomposition method, a higher order LTI model is derived. The extracted higher order LTI model provides real-time estimates of the effect of control inputs on component level dynamic loads and hence provides real-time load monitoring capability. The focus of this chapter is a mathematical formulation of the higher order LTI model along with required prior steps necessary to obtain such a model. These steps begin with the modeling of a high fidelity nonlinear FLIGHTLAB® model from which is extracted a Linear Time Periodic (LTP) model. First, the modeling details used to develop the nonlinear helicopter model in FLIGHTLAB® are described. Next, two formulations are presented: the formulation of an LTP model from a nonlinear helicopter simulation model, and the formulation of the higher order LTI model in terms of harmonic coefficient of the LTP model. Finally, the extracted higher order LTI system is evaluated in simulation using the developed high fidelity FLIGHTLAB® simulation model for on-line prediction of rotor blade pitch link loads arising from vehicle maneuvers.

The research in this chapter results in a new LTI/LQE model which is formulated by combining the LTI model with a Linear Quadratic Estimator(LQE) to understand the benefits of using fixed system load measurements to improve the load estimates from the LTI model alone. A time domain metric, namely the Theil Inequality Coefficients (TIC) is introduced to quantify the accuracy of the load predictions from the LTI/LQE and LTI models.

2.1 Nonlinear Model

This research makes use of FLIGHTLAB®[76] to develop a bare-airframe high fidelity nonlinear model. FLIGHTLAB® is a widely used flight software for rotorcraft dynamics modeling and simulation. The dynamics of very complex flying vehicles can be modeled in FLIGHTLAB®. Once a model is developed, various analyses can be undertaken such as aeroelastic stability, stability and control, aerodynamic and structural loads, etc.

The nonlinear model considered in this study is based on Ref. [77]. The high-fidelity nonlinear model is a generic single main rotor helicopter, similar in size and weight to the UH-60 developed in FLIGHTLAB®. The nonlinear helicopter model weighs approximately 17,000 lbs. and has an articulated rotor system with elastic blades. To accurately capture the rotor loads, the nonlinear model includes flexible blades with representative in-plane/out-of-plane and torsional-bending modes. Furthermore, the model uses a 33 state Peters-He dynamic inflow model, complete nonlinear aerodynamic look-up tables for airframe and rotor blade aerodynamic coefficients, swashplate and tail rotor actuator models, and the Bailey tail rotor model.

2.2 Linear Time Periodic Model

This section describes the extraction of a linear time period (LTP) model from a NL helicopter model using a first order formulation. The following nonlinear system of equations are representative of the dynamics of the nonlinear helicopter model:

$$0 = f(\dot{x}, x, u) \tag{2.1}$$

$$y = g(\dot{x}, x, u) \tag{2.2}$$

where x, y, and u are the state, control, and output vectors, respectively. Let $\tilde{x}(\psi)$ and $\tilde{u}(\psi)$

represent a periodic equilibrium solution of Eq. (2.1) such that

$$\tilde{x}(\psi + 2\pi) = \tilde{x}(\psi) \tag{2.3}$$

$$\tilde{u}(\psi + 2\pi) = \tilde{u}(\psi) \tag{2.4}$$

$$\psi = \Omega t \tag{2.5}$$

Hence, the equilibrium solution is periodic with a period of 2π. Here, ψ and Ω are parameters known as the azimuth angle and rotor angular velocity, respectively. A linearization of Eq. (2.1) can be obtained by first considering changes from equilibrium as given in Eqs. (2.6) and (2.7) and doing a Taylor- series expansion of Eq. (2.1) about the periodic equilibrium solution up to the first order (i.e.,Eq. (2.8))

$$\Delta x(\psi) = x(\psi) - \tilde{x}(\psi) \tag{2.6}$$

$$\Delta u(\psi) = u(\psi) - \tilde{u}(\psi) \tag{2.7}$$

$$f(\dot{\tilde{x}}, \tilde{x}, \tilde{u}) + [\frac{\partial f}{\partial \dot{x}}\bigg|_{x=\tilde{x}(\psi),u=\tilde{u}(\psi)}]\Delta\dot{x} + [\frac{\partial f}{\partial x}\bigg|_{x=\tilde{x}(\psi),u=\tilde{u}(\psi)}]\Delta x + [\frac{\partial f}{\partial u}\bigg|_{x=\tilde{x}(\psi),u=\tilde{u}(\psi)}]\Delta u = 0 \tag{2.8}$$

Given that the periodic equilibrium solution must satisfy Eq. (2.1), the above equation can be simplified as follows:

$$[\frac{\partial f}{\partial \dot{x}}\bigg|_{x=\tilde{x}(\psi),u=\tilde{u}(\psi)}]\Delta\dot{x} + [\frac{\partial f}{\partial x}\bigg|_{x=\tilde{x}(\psi),u=\tilde{u}(\psi)}]\Delta x + [\frac{\partial f}{\partial u}\bigg|_{x=\tilde{x}(\psi),u=\tilde{u}(\psi)}]\Delta u = 0 \tag{2.9}$$

Eq. (2.9) is arranged into the following form

$$M(\psi)\Delta\dot{x} = F(\psi)\Delta x + G(\psi)\Delta u \tag{2.10}$$

where

$$M(\psi) = \left.\frac{\partial f}{\partial \dot{x}}\right|_{x=\tilde{x}(\psi),u=\tilde{u}(\psi)} \tag{2.11}$$

$$F(\psi) = -\left.\frac{\partial f}{\partial x}\right|_{x=\tilde{x}(\psi),u=\tilde{u}(\psi)} \tag{2.12}$$

$$G(\psi) = -\left.\frac{\partial f}{\partial u}\right|_{x=\tilde{x}(\psi),u=\tilde{u}(\psi)} \tag{2.13}$$

In Eq. (2.10), M is known as the mass matrix. If this mass matrix is nonsingular, then Eq. (2.9) can be rewritten as follows:

$$\Delta\dot{x} = F(\psi)\Delta x + G(\psi)\Delta u \tag{2.14}$$

where

$$F(\psi) = -[\left.\frac{\partial f}{\partial \dot{x}}\right|_{x=\tilde{x}(\psi),u=\tilde{u}(\psi)}]^{-1}[\left.\frac{\partial f}{\partial x}\right|_{x=\tilde{x}(\psi),u=\tilde{u}(\psi)}] \tag{2.15}$$

$$G(\psi) = -[\left.\frac{\partial f}{\partial \dot{x}}\right|_{x=\tilde{x}(\psi),u=\tilde{u}(\psi)}]^{-1}[\left.\frac{\partial f}{\partial u}\right|_{x=\tilde{x}(\psi),u=\tilde{u}(\psi)}] \tag{2.16}$$

At the periodic equilibrium solution, the output equation is given by

$$\tilde{y} = g(\dot{\tilde{x}}, \tilde{x}, \tilde{u}) \tag{2.17}$$

A Taylor- series expansion of the output equation, Eq. (2.2), up to the first order, results in a linearized form

$$y = g(\dot{\tilde{x}}, \tilde{x}, \tilde{u}) + [\frac{\partial g}{\partial \dot{x}}\Big|_{x=\tilde{x}(\psi),u=\tilde{u}(\psi)}]\Delta\dot{x} + [\frac{\partial g}{\partial x}\Big|_{x=\tilde{x}(\psi),u=\tilde{u}(\psi)}]\Delta x + [\frac{\partial g}{\partial u}\Big|_{x=\tilde{x}(\psi),u=\tilde{u}(\psi)}]\Delta u \tag{2.18}$$

Substituting Eqs. (2.14) and (2.17) into Eq. (2.18) results in

$$\Delta y = P(\psi)\Delta x + R(\psi)\Delta u \tag{2.19}$$

where

$$\Delta y(\psi) = y(\psi) - \tilde{y}(\psi) \tag{2.20}$$

$$P(\psi) = [\frac{\partial g}{\partial \dot{x}}\Big|_{x=\tilde{x}(\psi),u=\tilde{u}(\psi)}]F(\psi) + [\frac{\partial g}{\partial x}\Big|_{x=\tilde{x}(\psi),u=\tilde{u}(\psi)}] \tag{2.21}$$

$$R(\psi) = [\frac{\partial g}{\partial \dot{x}}\Big|_{x=\tilde{x}(\psi),u=\tilde{u}(\psi)}]G(\psi) + [\frac{\partial g}{\partial u}\Big|_{x=\tilde{x}(\psi),u=\tilde{u}(\psi)}] \tag{2.22}$$

In this research, a numerical scheme is used to obtain a first order LTP representation of the nonlinear model. The numerical scheme can be summarized with the following two steps. First, the nonlinear FLIGHTLAB® model is trimmed to reach a periodic equilibrium solution. After the periodic equilibrium solution has been found, the nonlinear model is linearized to obtain an LTP model with first-order representation. The linearization is done by performing numerical perturbations over one rotor revolution (i.e., from $\psi = 0^\circ$ to $\psi = 360^\circ$, with an increment of $\Delta\psi = 1^\circ$) .

2.3 Linear Time Invariant Model

The extraction of a higher order LTI model from a Linear Time Periodic model (LTP) is described in this section. To develop this LTI model, the method described in Ref. [13]

is applied using harmonic decomposition of LTP states, with a first order representation (i.e., separate displacement and velocity states) from a full vehicle nonlinear (NL) FLIGHTLAB® model.

The following equations represent an LTP model of the form given by Eqs. (2.23) and (2.24)

$$\dot{x} = F(\psi)x + G(\psi)u \tag{2.23}$$

$$y = P(\psi)x + R(\psi)u \tag{2.24}$$

where F, G, P and R are periodic matrices and satisfy the following equations:

$$F(\psi + 2\pi) = F(\psi) \tag{2.25}$$

$$G(\psi + 2\pi) = G(\psi) \tag{2.26}$$

$$P(\psi + 2\pi) = P(\psi) \tag{2.27}$$

$$R(\psi + 2\pi) = R(\psi) \tag{2.28}$$

Such an LTP model with a first order representation can be obtained from a full vehicle nonlinear (NL) FLIGHTLAB® model by performing linearization about a periodic equilibrium at every azimuthal position, as described in the previous section.

Harmonic decomposition for the extraction of an LTI model assumes the approximation for the state vector, x , in Eq. (2.29)

$$x = x_0 + \sum_{n=1}^{N} [x_{nc} cos(n\psi) + x_{ns} sin(n\psi)] \tag{2.29}$$

where x_0 is the average component and x_{nc} and x_{ns} are, respectively, the n/rev cosine and sine harmonic components of x. Likewise, the control u is expanded in terms of harmonic components as

$$u = u_0 + \sum_{m=1}^{M} [u_{mc} cos(m\psi) + u_{ms} sin(m\psi)] \tag{2.30}$$

u_0 is the average component and u_{mc} and u_{ms} are, respectively, the m/rev cosine and sine harmonic components of u.

The output y is expanded in a similar fashion

$$y = y_0 + \sum_{l=1}^{L} [y_{lc} cos(l\psi) + y_{ls} sin(l\psi)] \tag{2.31}$$

where y_0 is the average component and y_{lc} and y_{ls} are, respectively, l/rev cosine and since harmonic components of y.

An LTI approximation of the LTP model given by Eqs. (2.23) and (2.24) can be obtained by substituting for harmonic expansions[13, 62] of x, u, and y, i.e., Eqs. (2.29), (2.30) and (2.31) into Eqs. (2.23) and (2.24). The resulting equations can be represented in state-space matrix form by defining an augmented state vector as:

$$X = [x_0^T .. x_{ic}^T \;\; x_{is}^T .. x_{jc}^T \;\; x_{js}^T ..]^T \tag{2.32}$$

and an augmented control vector as

$$U = [u_0^T .. u_{mc}^T \;\; u_{ms}^T ..]^T \tag{2.33}$$

Likewise, an augmented output vector as

$$Y = [y_0^T..y_{lc}^T \;\; y_{ls}^T..]^T \tag{2.34}$$

where x_0 is the average component, x_{ic} and x_{is} are, respectively, the i^{th} cosine and sine harmonic components of x. Similarly, u_0 is the average component and u_{mc} and u_{ms} are, respectively, the m^{th} cosine and sine harmonic components of u. The state-space representation of the resulting LTI model is

$$\dot{X} = [A]X + [B]U \tag{2.35}$$

$$Y = [C]X + [D]U \tag{2.36}$$

A detailed derivation of the LTI model can be found in the appendix section. The LTP model extracted through linearization from the NL model includes 8 body states, 33 inflow states (Peters-He Finite state inflow with 4 harmonics and a maximum radial variation power of 8), and 48 multi-blade coordinate (MBC) rotor states that include rigid flap, rigid lead-lag, and coupled elastic modes. Thus, the total number of LTP states is 89. Each of these LTP states is then decomposed into 0-8/rev harmonic components, resulting in 1513 total LTI model states. It should be noted that all 0-8 harmonics may not be required to achieve acceptable fidelity in the LTI model[13, 62]. The nonlinear model is trimmed at 120 knots.

2.4 Model Validation

2.4.1 Frequency Domain

This section evaluates the fidelity of the extracted higher order LTI model in the frequency domain. More specifically, the LTI model is validated using frequency domain flight data of a UH-60 aircraft at 80 knots provided by the U.S. Army Aviation Development Directorate

(ADD). The validation is performed at 80 knots since it is the only flight condition where flight data in the frequency domain is available. This flight data was gathered for the Army/NASA Rotorcraft Aircrew Systems Concepts Airborne Laboratory (i.e., RASCAL) program. This step compares the on-axis, open-loop, frequency response for the body angular velocities (P, Q, R), coning angle (β_0), longitudinal flapping (β_{1c}), and lateral flapping (β_{1s}) . Figures 2.1 and 2.2 suggest that there is very good match between the higher order LTI model frequency response and the flight data for high coherence values (i.e., $coherence > 0.6$).

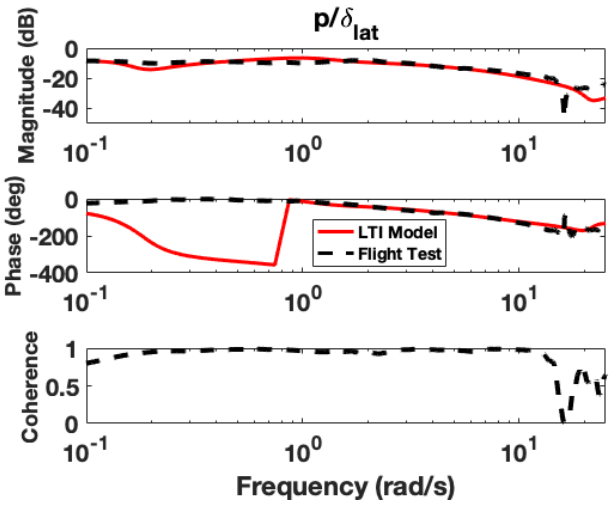

(a)

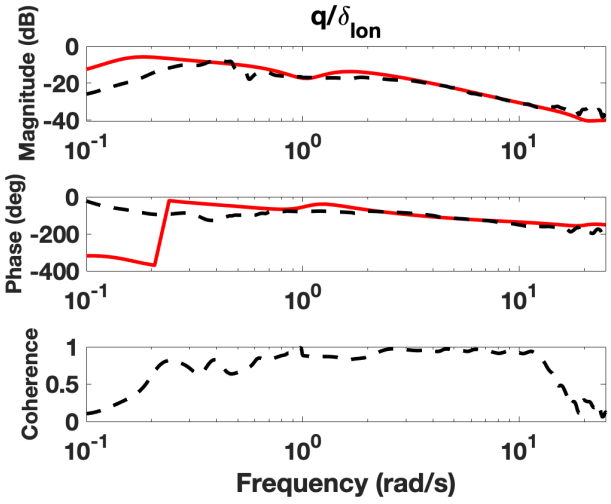

(b)

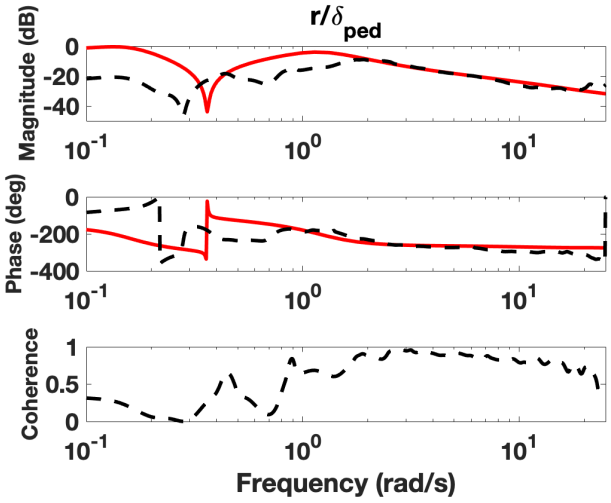

(c)

Figure 2.1: On-axis frequency domain response comparison.

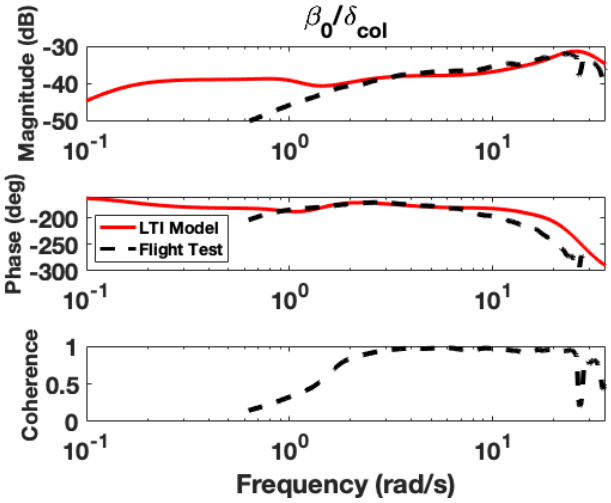

(a)

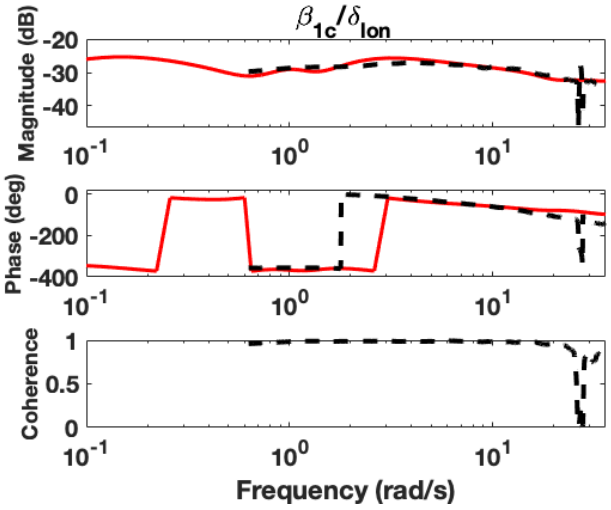

(b)

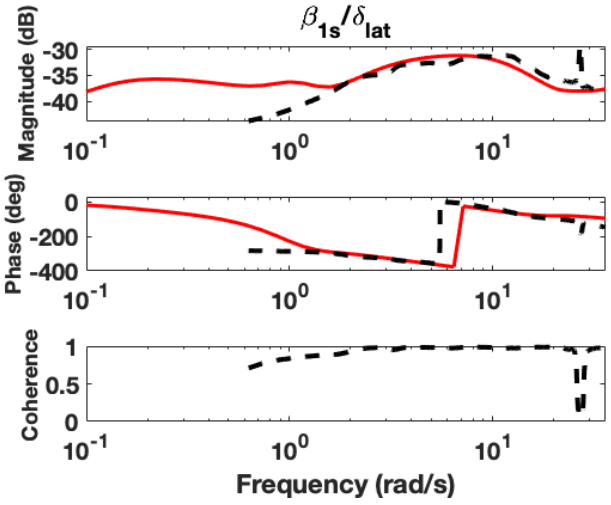

(c)

Figure 2.2: On-axis frequency domain response comparison.

A metric based on weighted sum of magnitude and phase squared errors can be used to quantify the fidelity of a simulation model frequency response. This metric was first introduced by Hogkinson and later improved by Tischler[78]. The mathematical expression of the metric is given as follows

$$J = \frac{20}{n_\omega} \sum_{\omega 1}^{\omega_{n_\omega}} W_\gamma [W_g (|\hat{T}_c| - |\hat{T}|)^2 + W_p (\angle \hat{T}_c - \angle \hat{T})^2] \tag{2.37}$$

where:

- $|.|$ is the magnitude in decibels at each frequency ω.
- $\angle$ is the phase in degrees at each frequency ω.
- n_ω is the number of frequency points.
- ω_1 and ω_{n_ω} are the starting and ending frequencies of fidelity assessment.

In Eq. (2.37), W_g and W_p are relative weighting coefficients for the magnitude and phase squared errors, respectively. A standard practice is to select $W_g = 1.0$ and $W_p = 0.01745$ [78]. Such a selection of the weighting coefficients yields 1 dB of magnitude error to be equivalent to $7.57\ ^\circ$ of phase error. W_γ is a weighting coefficient that is biased towards data with high coherence values. This is done to give a high-priority to reliable flight test data and neglect unreliable data. The level of reliability of the flight test data at each frequency, ω, can be determined using the coherence function i.e., γ^2_{xy}.

$$W_\gamma(\omega) = [1.58(1 - e^{-\gamma^2_{xy}})]^2 \tag{2.38}$$

The metric (J) is used to quantify the fidelity of the higher order LTI model through comparison with the flight test data in the frequency domain (see Figs. 2.1 and 2.2).

Table 2.1: Quantification of error response between higher order LTI and flight data using frequency domain metric

Frequency Response	Frequency Range (rad/s)	Value of Cost function (J)
p/δ_{lat}	0.6-20	66.5
q/δ_{on}	0.6-20	32.3
r/δ_{ped}	0.6-20	247.5
β_0/δ_{col}	0.62-20	45.6
β_{1c}/δ_{lon}	0.62-20	39.4
β_{1s}/δ_{lat}	0.62-20	119.4

From Table 2.1, it may be observed that across all frequency responses an average cost function value of 91.8 ($J = 91.8$) is obtained. The guideline provided by Ref. [78] suggests that a cost function value less than 100 ($J < 100$) represents an acceptable level of accuracy for flight dynamics modelling. Hence, this finding suggests that the extracted higher order LTI model provides an accurate modeling of the flight dynamics of a UH-60 aircraft. The finding also suggests that the developed nonlinear model is representative of a UH-60 aircraft in terms of the body, coning, longitudinal, and lateral flapping responses.

2.4.2 Time Domain

Given that the rotating pitch link is the component of interest in the rotating system, it is essential for the developed nonlinear model to give pitch link load variation that is close to what a UH-60 aircraft would experience. As such, the reference blade pitch-link load variation in steady-state at 120 knots flight condition from the nonlinear model is compared with flight data of a UH-60 aircraft at the same airspeed (i.e., 120 knots) provided by the U.S. Army. Figure 2.3 is a plot of the reference blade pitch link load variation with time at equilibrium from the nonlinear model and flight-test data. These are axial loads where a positive and negative load value represent, respectively, a tensile and compressive load. Figure 2.3 shows that the nonlinear model captures well the peak-to-peak value of the pitch link load. Furthermore, the nonlinear model predicts a peak-to-peak value of 1000 lb. whereas the flight data gives a peak-to-peak value of 957 lb. This yields a peak-to-

peak pitch link load prediction error of roughly 4.5%. Therefore, it may be concluded that the nonlinear model, at steady-state, gives reasonable pitch-link load prediction in forward flight.

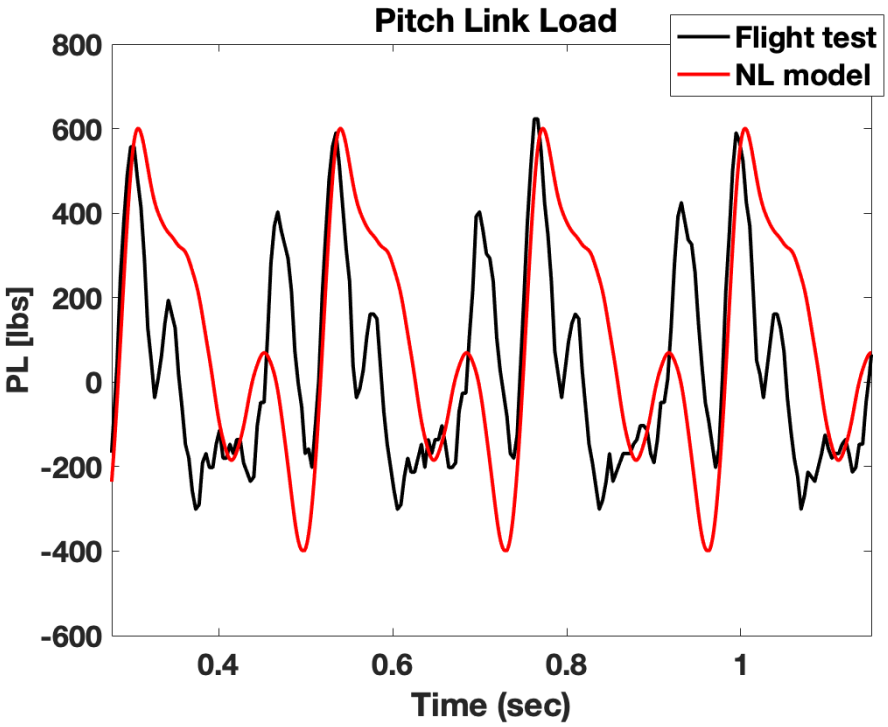

Figure 2.3: Reference blade pitch link load in steady state at 120 knots.

2.5 LTI System for Real-Time Rotor Component Load Estimation

The extracted LTI model is evaluated in simulation for the case of on-line estimation of blade pitch-link loads arising from vehicle maneuvers. Predictions of the reference blade pitch-link load from the LTI model are compared with the LTP and nonlinear model predictions in order to quantify the model mismatch between the models. This comparison also can validate the effectiveness of the harmonic decomposition methodology used for the extraction of an LTI model from an LTP model.

Figure 2.4 is a plot of the percentage change in longitudinal cyclic control variation used in this study. The input profiles shown in Fig. 2.4 are obtained by passing ramp doublets of 0.1 s raise time through an actuator model with a time constant of 0.1s. All other controls

are held fixed at their trim values.

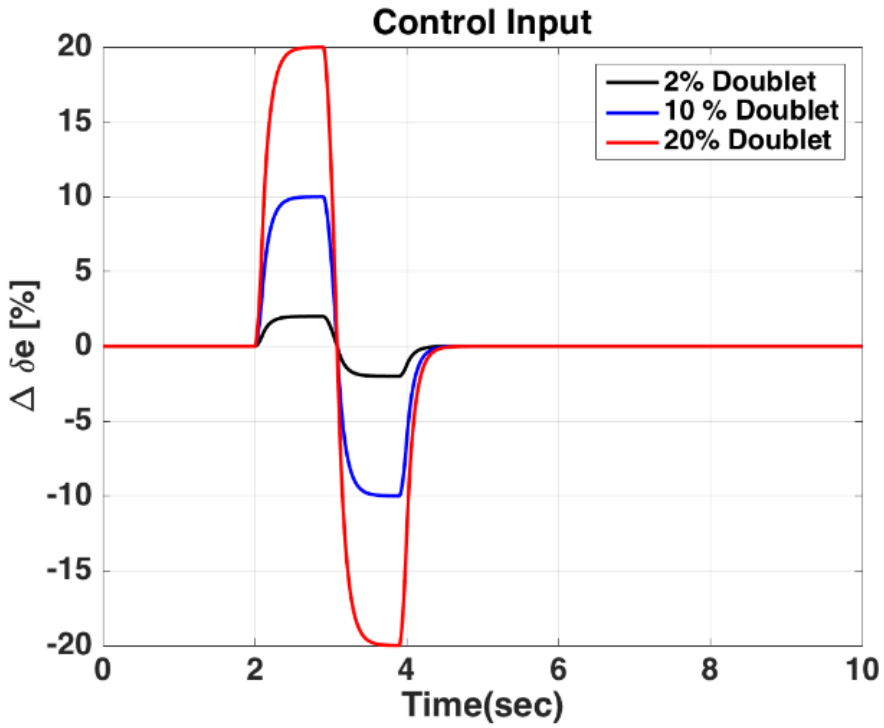

Figure 2.4: Percentage change from trim of longitudinal cyclic control input.

The 20% longitudinal doublet input is applied to both the LTI and LTP models. The resulting vehicle angular rate responses from trim (ΔP, ΔQ, ΔR) and body velocity component responses from trim (ΔU, ΔV, ΔW) from the LTP and LTI models are shown in Figs. 2.5 and 2.6. It is seen from Figs. 2.5 and 2.6 that the LTI model predictions of body velocity and angular rate responses are indistinguishable from the LTP model responses.

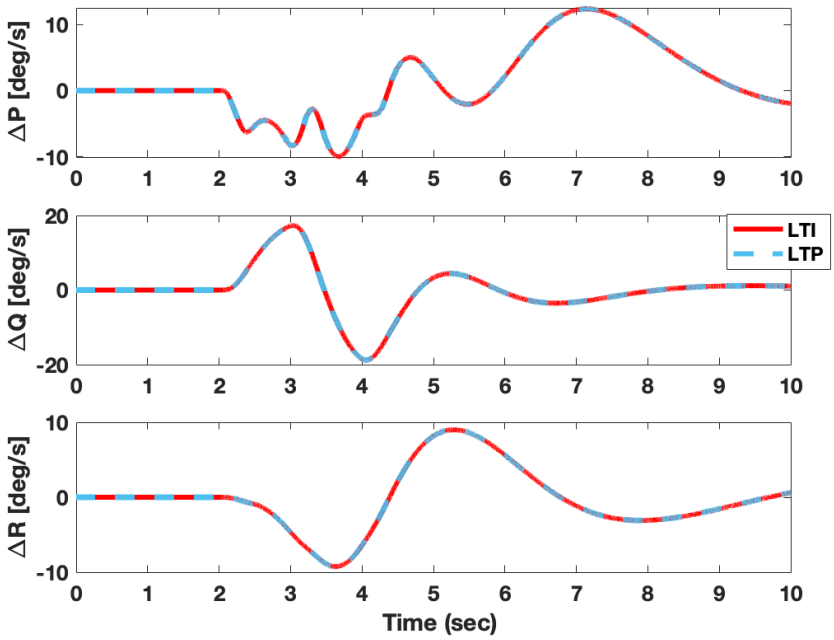

Figure 2.5: Body angular rate response from the LTP and LTI models for the 20% longitudinal control input (see Fig. 2.4).

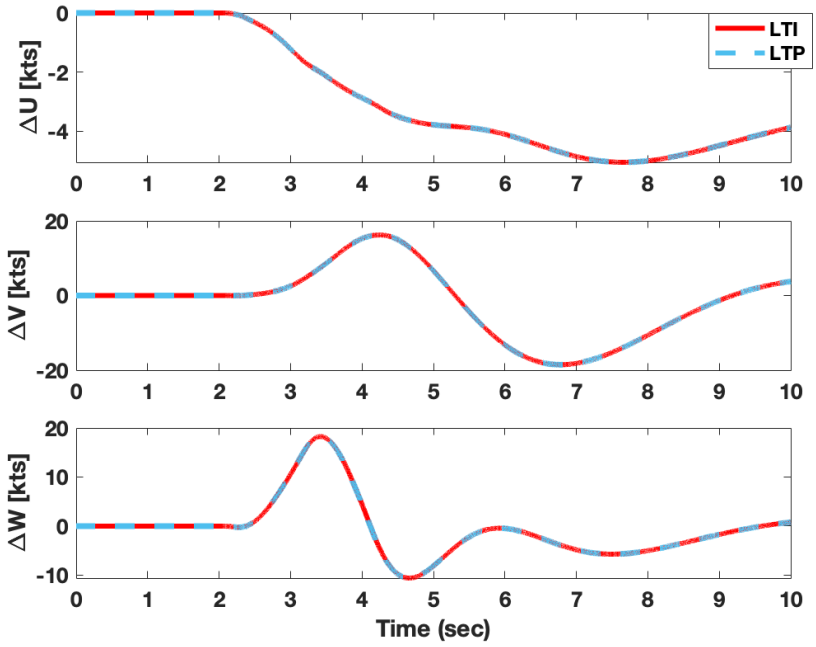

Figure 2.6: Body velocity response from the LTP and LTI models for the 20% longitudinal control input (see Fig. 2.4).

The reference blade pitch-link load variation from trim as predicted by the LTI model is compared with that from the LTP model in Fig. 2.7 for 20% longitudinal doublet input of Fig. 2.4.

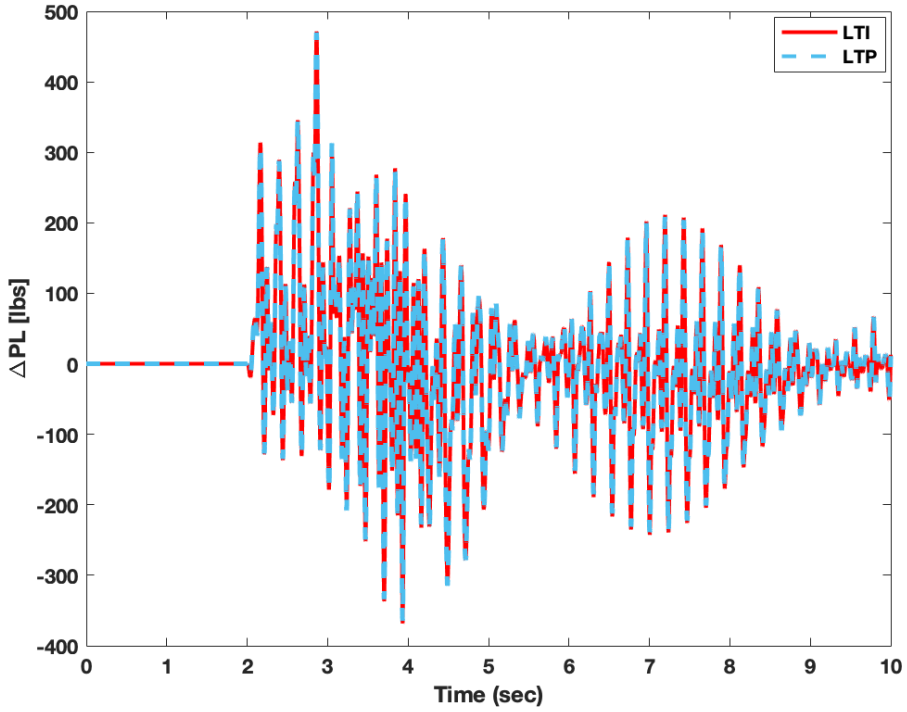

Figure 2.7: Pitch link load comparison between LTI and LTP models for the 20% longitudinal control input (see Fig. 2.4).

As the results in Fig. 2.7 show, the LTI model predictions of pitch-link load variation arising from the 20% longitudinal doublet input considered in this study are nearly same as that from the LTP model. No difference between the two models can be seen.

To quantify the accuracy of the pitch link load variation predicted by the LTI model when compared to the LTP model, a time domain fidelity metric similar to the frequency domain metric is necessary, as introduced in section 2.4 of this thesis.

The Theil Inequality Coefficient (TIC) defined in Eq. (2.39) provides a measure of the accuracy of a set of predictions generated from a selected model[79]. The TIC can only take values between 0 and 1. A value of 0 indicates that the model has perfect predictive

capability, whereas as value of 1 corresponds to a model that has no predictive capability. Table 2.2 taken from Ref. [79] gives a guideline for the interpretation of model fidelity using the TIC metric.

$$TIC = \frac{\sqrt{\frac{1}{n_t}\sum_{i=1}^{n_t}[(PL_{data}(i) - PL_{model}(i))^2]}}{\sqrt{\frac{1}{n_t}\sum_{i=1}^{n_t}[(PL_{data}(i))^2]} + \sqrt{\frac{1}{n_t}\sum_{i=1}^{n_t}[(PL_{model}(i))^2]}} \tag{2.39}$$

Table 2.2: Thiel Inequality Coefficient (TIC) criteria for model fidelity evaluation[23]

Thiel Inequality Coefficient	Accuracy of model
= 0	Model with perfect predictive capability
$\leq$ 0.25 *to* 0.30	Model with good predictive capability
= 1	Model with no predictive capability

The LTI model fidelity with respect to the LTP model using the TIC metric for 20% pitch maneuver case of Fig. 2.4 is computed using Eq. (2.39). A TIC value of 0.0190 is obtained.

Given the low TIC value obtained, it can concluded that the LTI model is a model with almost perfect predictive capability when compare to the LTP model. This suggests that the LTI model is nearly indistinguishable from the LTP model.

Next the LTI and nonlinear models predictions are compared. The longitudinal cyclic control variation shown in Fig 2.4 is applied to both the LTI and nonlinear models. Applying inputs of different magnitude is sought in order to analyze the effect of an increase in maneuver aggressiveness on the prediction capability of the LTI model when compared to the NL model. The resulting vehicle angular rate responses (P, Q,R) and body velocity component responses (U, V,W) from the nonlinear and LTI models are shown in Figs. 2.8 and 2.9. It may be noted from Figs. 2.8 and 2.9 that the LTI model predictions of body velocity and angular rate responses are close to the nonlinear model response predictions.

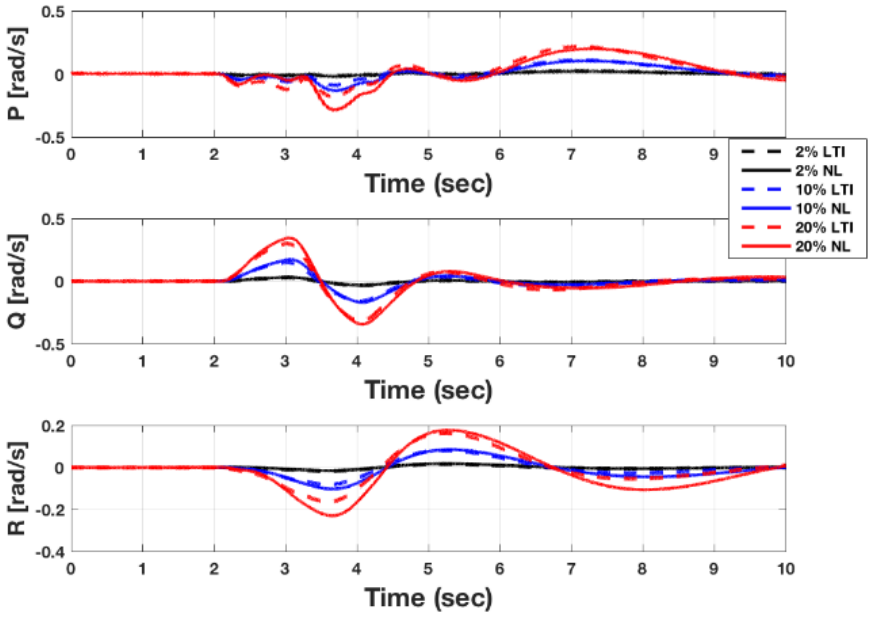

Figure 2.8: Body angular rate response from the nonlinear and LTI models for the selected longitudinal control inputs (see Fig. 2.4).

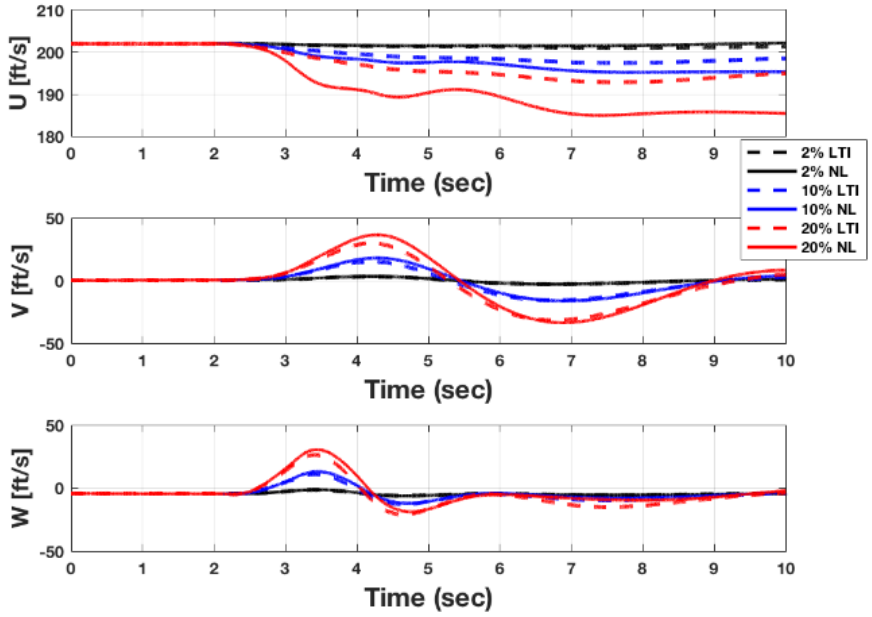

Figure 2.9: Body velocity response from the nonlinear and LTI models for the selected longitudinal control inputs (see Fig. 2.4).

The reference blade pitch link load variations from trim predicted by the LTI model are compared with the nonlinear model predictions in Fig. 2.10 for the three input cases of Fig. 2.4.

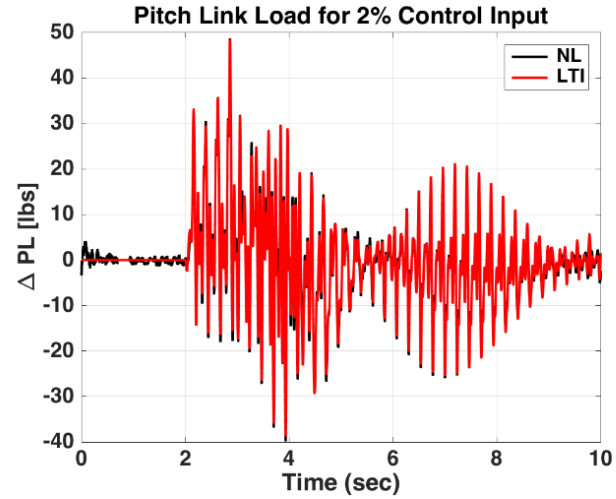

(a)

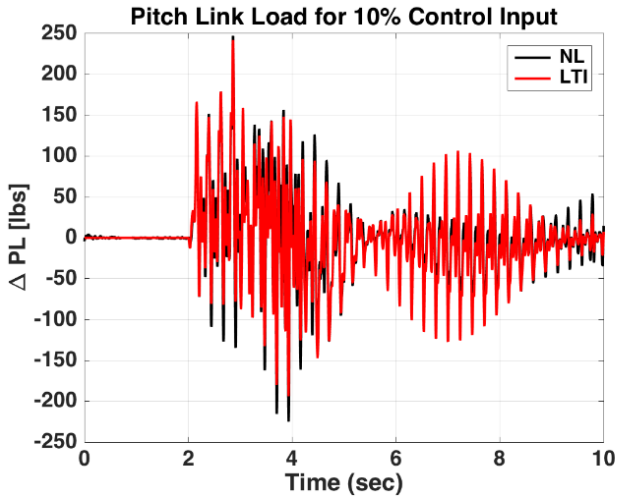

(b)

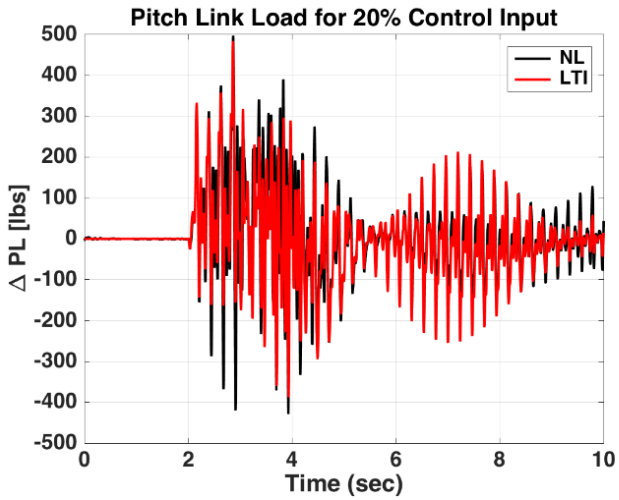

(c)

Figure 2.10: Pitch link load comparison between LTI and Nonlinear models.

At first glance, it appears from the results in Fig. 2.10 that the LTI model predictions of the blade pitch-link load variations from trim for the three maneuvers considered are within the same range as the nonlinear model predictions. However, some differences can be seen between the LTI and nonlinear models predictions. Such differences can be quantified via the use of the TIC metric. The LTI model fidelity with respect to the nonlinear model using the TIC metric for the three pitch maneuver cases of Fig. 2.10 are computed using Eq. (2.39) and are included in Table 2.3.

Table 2.3: LTI model fidelity using TIC for three different pitch maneuver

	2% Input Case	10% Input Case	20% Input Case
TIC	0.0710	0.1505	0.2813

From the results shown in Table 2.3, it is notable that as the magnitude of the input is increased, the TIC value increases, indicating that the predictions from the LTI model lose accuracy as the maneuver aggressiveness is increased. This loss of accuracy is expected for two reasons: nonlinear effects, and the significant change in vehicle response from the trim condition about which the LTI model is extracted. In light of these results, the following section proposes a novel approach to improve the LTI model predictions of pitch link load.

2.6 LTI/LQE Scheme

The previous section demonstrated that the extracted LTI model can be used for real-time rotor component load estimation. However, the estimated loads may have to be corrected for errors due to LTI model approximations for large deviations from trim, nonlinearities, etc. To address this problem, this research next focuses on the development of a novel model entitled LTI/LQE model for online estimation of rotor component loads. The LTI/LQE model is synthesized using the higher order linear time invariant model of helicopter coupled body-rotor-inflow dynamics and a linear quadratic estimator that corrects LTI model state response using available fixed system measurements during flight.

A scheme for combining LTI models with a Linear Quadratic Estimator (Kalman Filter) was developed in Ref. [16]. However, the focus of the study of Ref. [16] was to use the developed method as a harmonic analyser in which individual harmonic components of hub loads could be extracted from total hub load measurements in real time. The use of the developed method as a harmonic analyser was successfully demonstrated for real-time decomposition of total hub load data into individual harmonics using simulated data from a comprehensive nonlinear model of the UH-60 Black Hawk helicopter in FLIGHTLAB. While providing reasonably accurate estimates of harmonic loads, the developed method has been shown to be impervious to filter time delays typically present when one uses standard FFT techniques for real-time harmonic analysis.

For the construction of an LTI/LQE model, the LTI model of Eqs. (2.35) and (2.36) are represented in discrete form including process and measurement noise terms as Eqs. (2.40) and (2.41)

$$X_k = [L]X_{k-1} + [N]U_{k-1} + w_{k-1} \tag{2.40}$$

$$Y_k = [C]X_k + [D]U_k + v_{k-1} \tag{2.41}$$

where the random variables, w and v, represent the process and measurement noise, respectively. They are assumed to be independent, zero-mean white and with normal probability distributions given by Eqs. (2.42) and (2.43)

$$p(w) \sim N(0, Q_0) \tag{2.42}$$

$$p(v) \sim N(0, R_0) \tag{2.43}$$

where Q_0 and R_0 are the process noise covariance and measurement noise covariance ma-

trices, respectively. Large control input will likely cause the nonlinear model to drift away from the periodic equilibrium condition about which the LTI model was extracted. As noted in earlier sections, this will cause the load predictions from the LTI model to be different from the nonlinear model at the new flight condition the nonlinear model drifted to. Furthermore, when extracting the LTI model from the LTP model, a finite (0-8/rev) rather than an infinite expansion of the LTP states and outputs was performed. This will likely introduce modeling errors due to the finite truncation considered. Finally, the LTI model will likely not be able to capture highly nonlinear effects that are inherent in the nonlinear model. In the design of the LTI/LQE scheme, all the previously listed effects (i.e., drift away from periodic equilibrium condition, unmodeled dynamics, and nonlinearities) are well accounted for in the form of process or measurement noise.

The goal of the LQE (Kalman filter) is to compute a posteriori state estimate, $\hat{X}_k$, as a linear combination of an a priori estimate, $\hat{X}^-$, and the weighted difference between an actual measurement, z_k, and a measurement prediction, s_k , as shown in Eq. (2.44).

$$\hat{X}_k = \hat{X}^- + K_k(z_k - s_k) \tag{2.44}$$

The difference (z_k-s_k) is called the measurement innovation, or the residual, and K is referred to as the Kalman gain matrix, which minimizes the a posteriori error covariance. The Kalman filter algorithm estimates a process by predicting future response using the previous state estimate, current control input, and the system model, then corrects that prediction using current measurement data. As such, the equations for the Kalman filter fall into two groups: time update equations and measurement update equations. The time update equations first project (forward in time) the system state and error covariance estimates using the current control vector to predict the future states and error covariance, given the estimate from the previous time step and the system model. These equations are presented as Eqs. (2.45) and (2.46) [80].

$$\hat{X}^{-} = [L]\hat{X}_{k-1} + [N]U_{k-1} \tag{2.45}$$

$$P_k{}^{-} = FP_{k-1}F^T + Q_0 \tag{2.46}$$

The measurement update equations (i.e., Eqs. (2.47), (2.48) and (2.49)) generate an improved a posteriori estimate by correcting the a priori estimate with current measurement data weighted against the a priori estimate using the estimated error covariance.

$$K_k = \hat{P}_k{}^{-}C^T(CP_k{}^{-}C^T + R_0)^{-1} \tag{2.47}$$

$$\hat{X}_k = \hat{X}^{-} + K_k(z_k - s_k) \tag{2.48}$$

$$P_k = (I - K_kC)P_k{}^{-} \tag{2.49}$$

Since the objective of the proposed LTI/LQE scheme is to correct the LTI model state response using fixed system measurements, and, in turn, use the corrected LTI state response for the estimation of rotating system component loads, this study considers the total hub loads as the measurement, z. Since the total hub loads can be obtained as a linear combination of the LTI outputs, the measurement equation used to determine s is defined as follows:

$$s_k = E(\psi)\hat{Y}_k^{-} = E(\psi)C\hat{X}_k^{-} + E(\psi)DU_{k-1} \tag{2.50}$$

$$\begin{aligned} E(\psi) = [I \quad ...Icos(i\Omega t) \quad Isin(i\Omega t)... \\ Icos(j\Omega t) \quad Isin(j\Omega t)...] \end{aligned} \tag{2.51}$$

where E is the time-periodic linear combination of LTI system outputs which comprises the total hub loads in the fixed frame. The measurement update equations are thus updated to reflect this augmented output as follows.

$$K_k = \hat{P}_k^{\,-} C^T E(\psi)^T (E(\psi) C P_k^{\,-} C^T E(\psi)^T + R_0)^{-1} \tag{2.52}$$

$$P_k = (I - K_k E(\psi) C) P_k^{\,-} \tag{2.53}$$

With all system matrices and noise covariance matrices being constant or time periodic, the steady state solution to the Kalman gain matrix, K of Eq. (2.52), is periodic. Since calculation of the periodic steady state Kalman gain matrix does not depend on system state or time, it may be pre-computed offline for a given set of output and noise covariance matrices to improve the computation time associated with application of the LTI/LQE scheme. Thus, Eqs. (2.46), (2.52) and (2.53), can be iteratively solved a priori for selected values of the process noise covariance (Q_0) and the measurement noise covariance (R_0) in Eqs. (2.42) and (2.43). A block diagram representation of the LTI/LQE scheme for rotor component load estimation using fixed-system measurements is illustrated in Fig. 2.11.

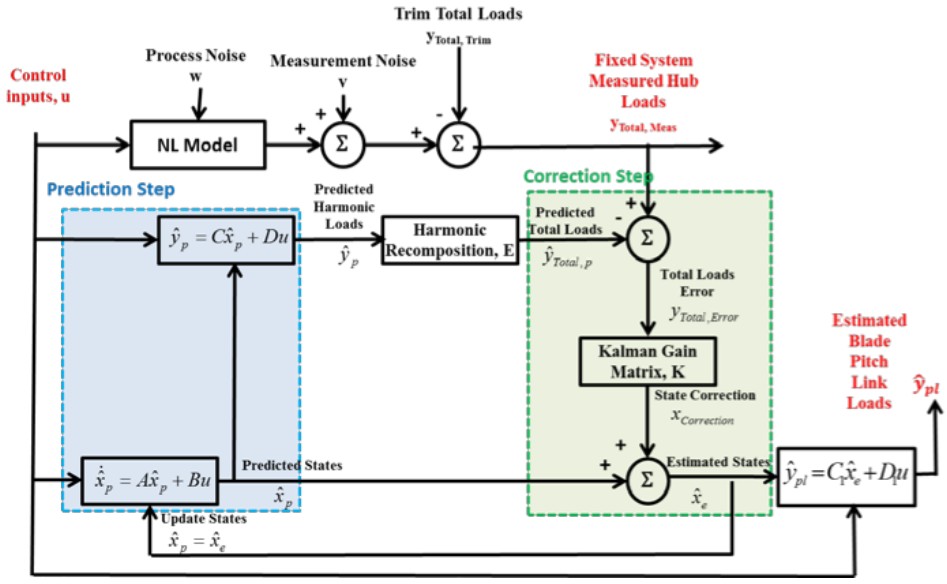

Figure 2.11: Block diagram of the LTI/LQE scheme for rotor component load estimation.

2.6.1 LTI/LQE Fidelity Evaluation

The LTI/LQE scheme is evaluated in simulation for the case of estimation of blade pitch-link loads arising from vehicle maneuvers using the nonlinear FLIGHTLAB® model developed in section 2.1 of this chapter. The LTI and LTI/LQE predictions of pitch link loads are compared to highlight the impact of the addition to the LTI model of a linear quadratic estimator that uses fixed system measurements. The form of the noise covariance matrices Q_0 and R_0 of Eqs. (2.42) and (2.43) for the Kalman filter design are selected to be diagonal as given in Eq. (2.54)

$$Q_0 = q_0 * I \quad R_0 = r_0 * I \tag{2.54}$$

where I is the identity matrix, Q_0 is a diagonal square matrix with size equal to the total number of states, and R_0 is a diagonal square matrix with size equal to the total number of measurements. For this study, the values of q_0 and r_0 in Eq. (2.54) are set to 10 and $10e^{-8}$, respectively. Since no explicit noise is added to the fixed system hub load response data, it is expected that the selected values of q_0 and r_0 would allow the estimator to trust the nonlinear hub load response much more than that of the LTI model response, and hence correct the LTI model response in order to make the LTI model predictions of the fixed system hub loads match those of the nonlinear model. This aspect is verified by comparing the hub load predictions from the LTI and LTI/LQE with that of the nonlinear predictions for the 10% input case of Fig. 2.4.

Figure 2.12 compares the fixed system hub loads (forces F_x, F_y and F_z and moments M_x, M_y and M_z) variations from trim as predicted by the LTI model with those of the nonlinear model for the 10% control input case. With the nonlinear model predictions representing the truth data, errors in LTI model predictions of hub loads can be seen in Fig. 2.12. The observed errors in LTI model predictions of hub loads are corrected by the LTI/LQE scheme as seen in the results presented in Fig. 2.13, where estimates of hub load variations from trim from the LTI/LQE are compared with those from the nonlinear model. These

observations are better illustrated in Fig. 2.14 where two sets are compared: the errors between the LTI and the nonlinear model, as well as the errors between the LTI/LQE and the nonlinear model of the hub loads predictions. While the errors in LTI/LQE predictions stay near zero, significant errors in LTI predictions are seen in Fig. 2.14.

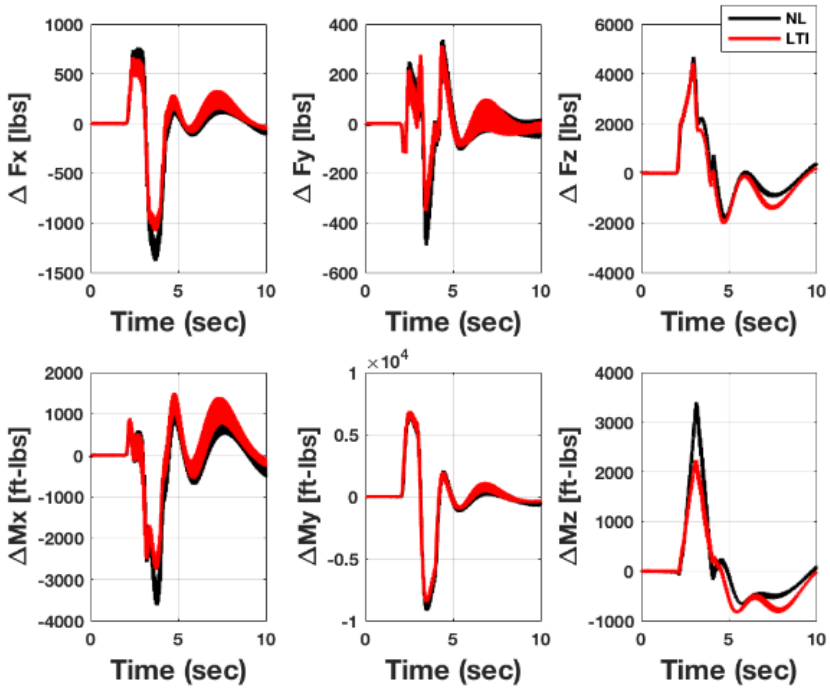

Figure 2.12: Comparison of fixed system hub loads variations from trim between nonlinear (NL) model and LTI.

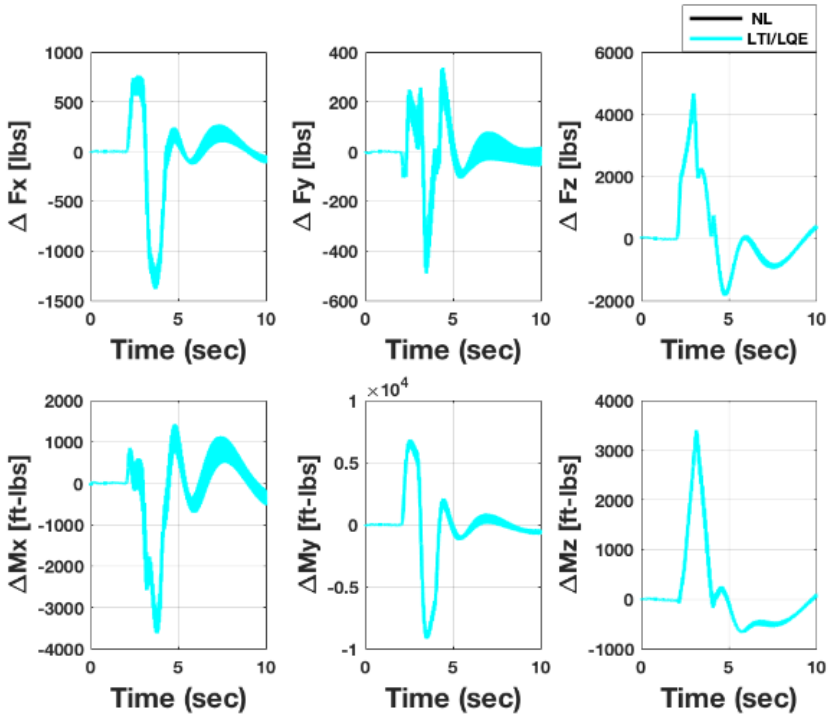

Figure 2.13: Comparison of fixed system hub load variations from trim between nonlinear model(NL) and LTI/LQE.

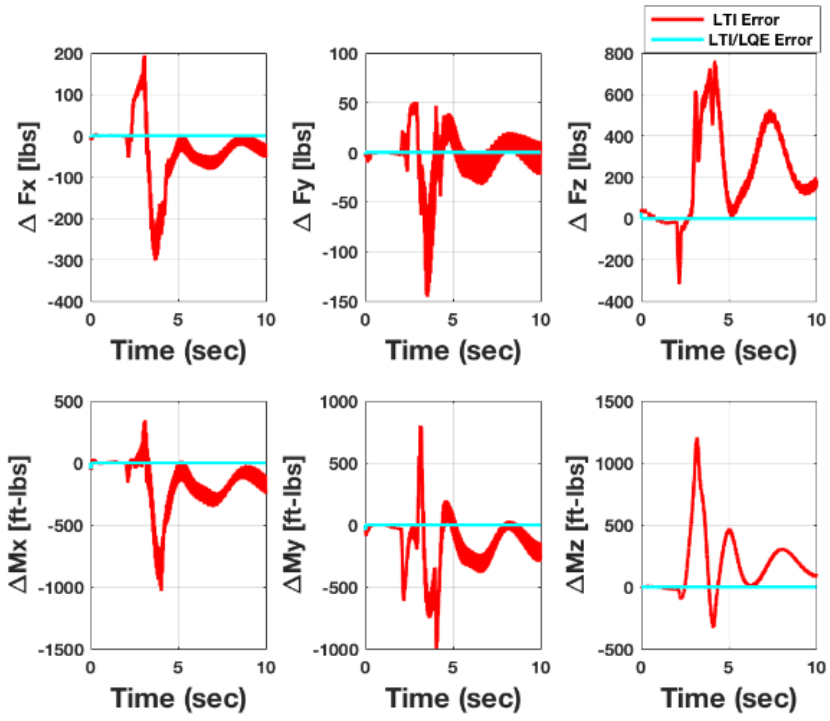

Figure 2.14: Comparison of error in fixed system hub loads between LTI and LTI/LQE.

From the results presented in Figs. 2.12, 2.13 and 2.14, it is seen that the LTI/LQE model adjusts the LTI state responses in order to make its hub load predictions match those of the nonlinear model. Hence, correction to the LTI model prediction of blade pitch-link loads can be expected, provided all or at least the important harmonic states of the LTI model are observable in the selected fixed system measurements.

Figure 2.15 compares prediction of blade pitch-link load variations from trim between LTI, LTI/LQE and NL models, while Fig. 2.16 compares errors (compared to the NL model) in the blade pitch-link load predictions between LTI and LTI/LQE. As expected, the LTI/LQE pitch-link load predictions have less error when compared to that of the LTI model. While the LTI model predictions are improved by the LTI/LQE scheme, significant errors are still seen. This is believed to be due to the non-observability of certain harmonic components of the LTI model states in the fixed-system hub load responses. Though not shown, similar trends have been observed for the 20% input case as well.

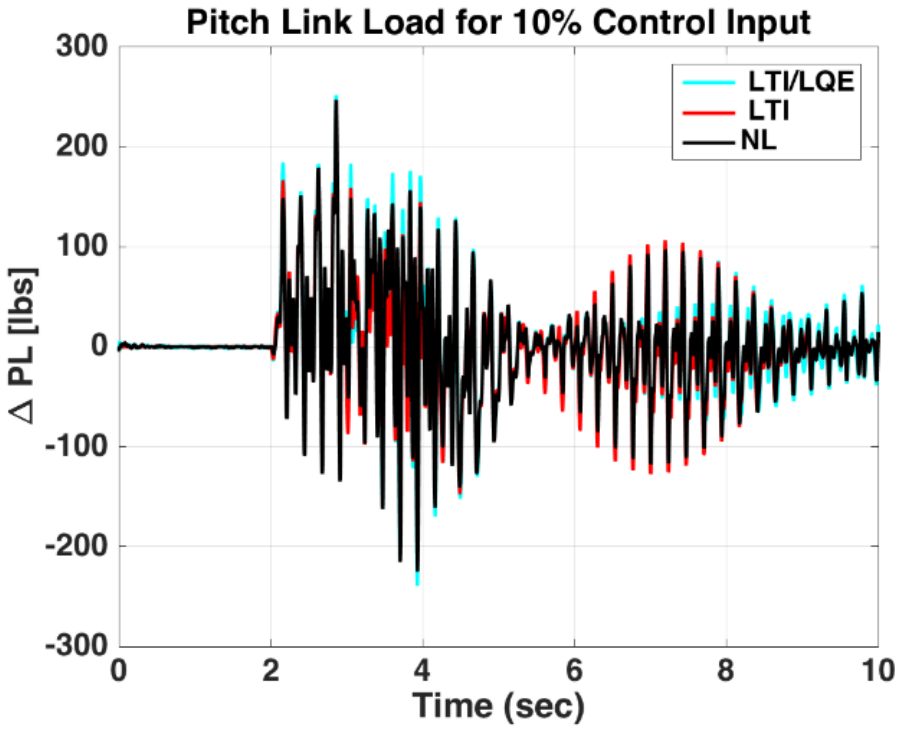

Figure 2.15: Comparison of blade pitch link load predictions between LTI, NL and LTI/LQE.

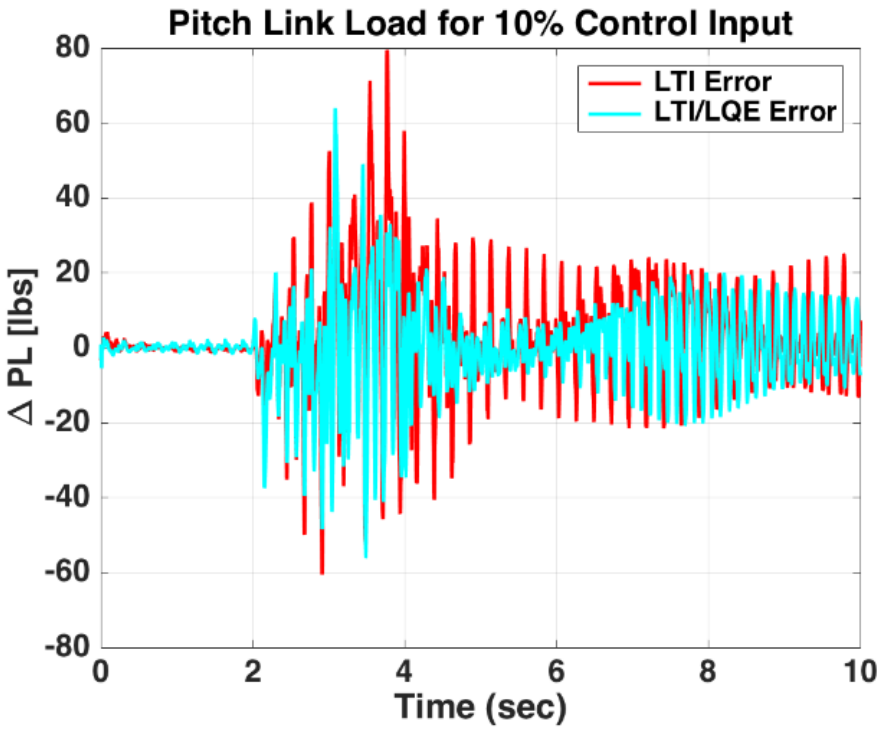

Figure 2.16: Comparison of error in reference blade pitch link load predictions between LTI and LTI/LQE.

The LTI/LQE model fidelity for pitch-link load predictions in terms of TIC (computed using Eq. (2.39) for the 10% and 20% input cases) are computed and included in Table 2.4. From a comparison of TIC results from Tables 2.3 and 2.4, it is seen that LTI model fidelity is improved with the addition of LQE for both the 10% and 20% input cases considered. With the LTI/LQE scheme, online prediction of pitch link loads is improved by 21.7% and 12.8% for the 10% and 20% input cases, respectively.

Table 2.4: LTI/LQE model fidelity using TIC metric for two different pitch maneuvers

	10% Input Case	20% Input Case
TIC	0.1178	0.2453

2.6.2 Redesign of LTI/LQE using Fixed-System Harmonic Load Measurements

In order to improve the estimation fidelity of the LTI/LQE scheme, it is important to consider the observability of the LTI model states in a selected set of fixed system measure-

ments, and in turn, improvements to individual harmonic components of a rotating system component loads using the LTI/LQE scheme.

As a first step, harmonic components of hub loads in place of total hub loads are used as measurements in the LTI/LQE scheme, as illustrated by the block diagram shown in Fig. 2.17. Individual harmonic components of hub loads are obtained by passing total loads from the nonlinear simulation through a double-sided Fast Fourier Transform (FFT) in order to capture both magnitude and phase.

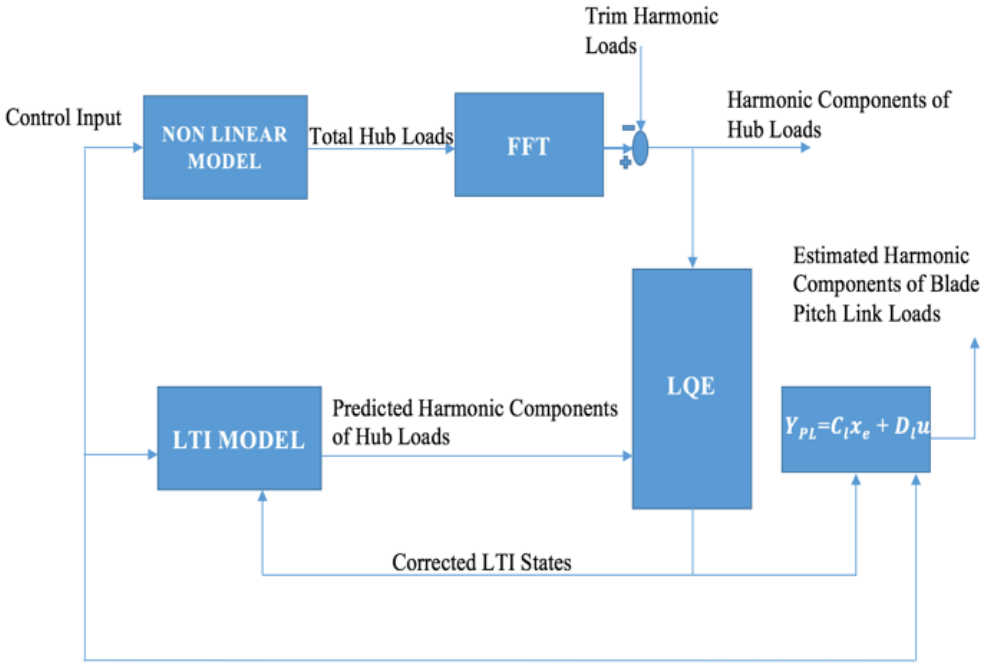

Figure 2.17: Block diagram of the LTI/LQE scheme with harmonic component of hub load measurements.

The performance of the LTI/LQE scheme is re-evaluated with this change using the 10% and 20% input profiles of Fig. 2.4. The variation of 1/rev and 4/rev harmonic component magnitudes of blade pitch-link loads as predicted by the Noninear (NL), LTI, and LTI/LQE models are shown in Fig. 2.18 for the 10% input case and Fig. 2.19 for the 20% input case. For the four-bladed rotor example considered in this study, the vibratory fixed system hub loads are mostly dominated by 4/rev. It is therefore expected that the relevant LTI states contributing significantly to 4/rev hub loads would be corrected by the LTI/LQE,

leading in turn to the corrections of 4/rev pitch link loads. This indeed is the case from the results of 4/rev pitch link load predictions shown in Fig. 2.18 (10% control input case) and Fig. 2.19 (20% control input case). Furthermore, it is notable that the LTI/LQE model fidelity in the prediction of 4/rev harmonic component of pitch link load is very good, even for the more aggressive 20% control input. While the 4/rev harmonic component magnitude of pitch link load prediction from LTI/LQE matches with that of the nonlinear model, the same is not the case with the 1/rev component as shown in Fig. 2.18 for the 10% input case and Fig. 2.19 for the 20% input case. These findings are not surprising, as they are a consequence of weak observability of 1/rev rotor states in fixed system hub load measurements of a four-bladed rotor. For a helicopter with 4 blades, the rotor acts as a filter since the forces and moments from all 4 blades cancel each other, except for the N/rev and (N $\pm$ 1)/rev forces and moments, when they get transferred from the rotating frame to the fixed frame through the rotor hub. This in turn gives rise to only N/rev (N=4, 8, etc.) hub forces and moments in the fixed-frame. This explains the weak observability of 1/rev rotor states in the fixed system hub load measurement of a four-bladed rotor; and also explains the strong observability of 4/rev rotor states in the fixed system hub load measurement of a four-bladed rotor.

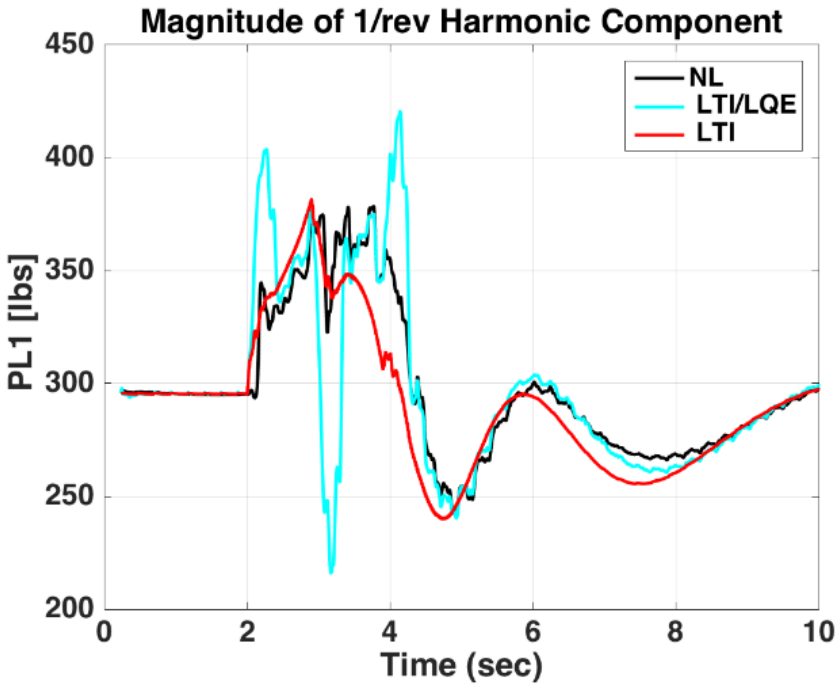

(a)

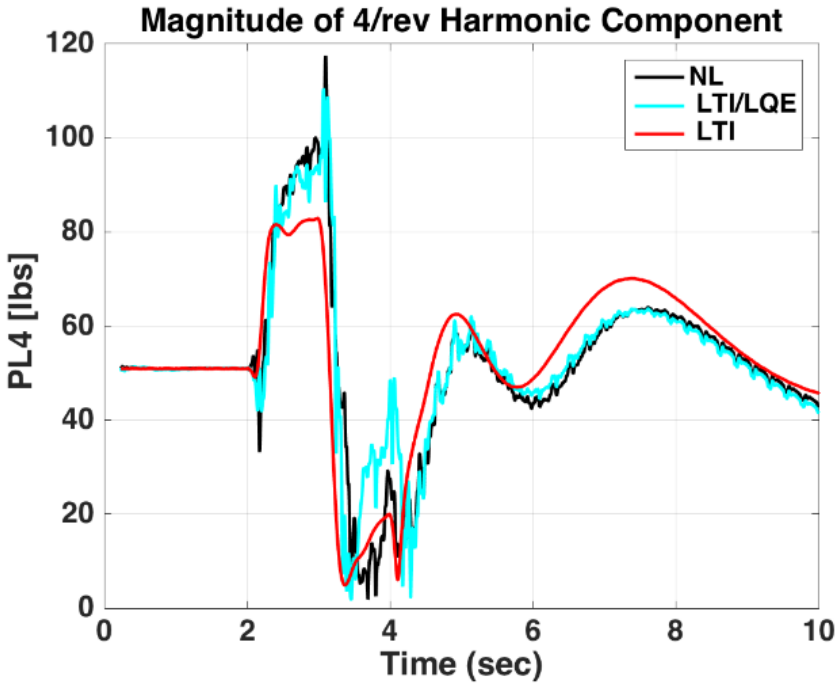

(b)

Figure 2.18: Variation of harmonic component of blade pitch link loads for the 10% control input case.

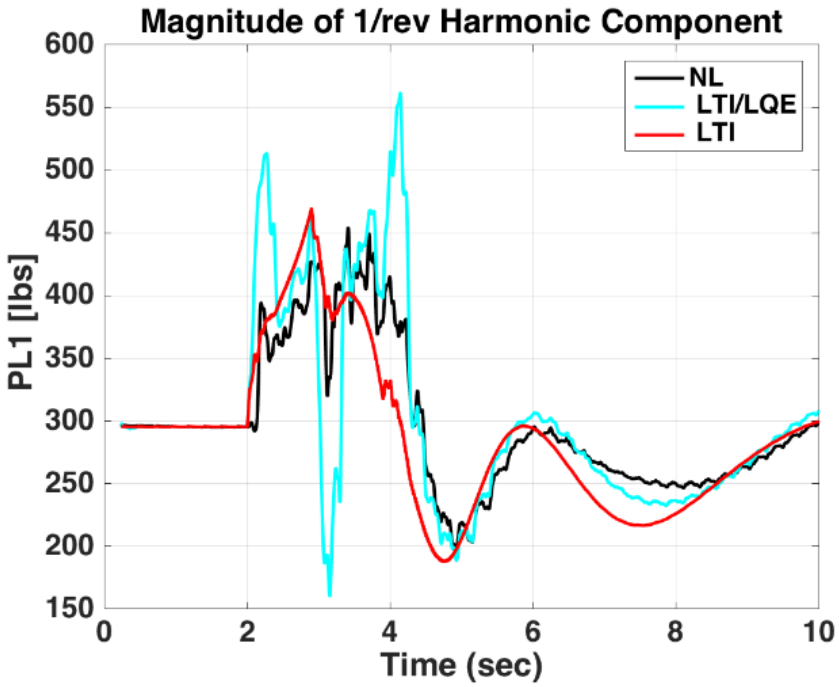

(a)

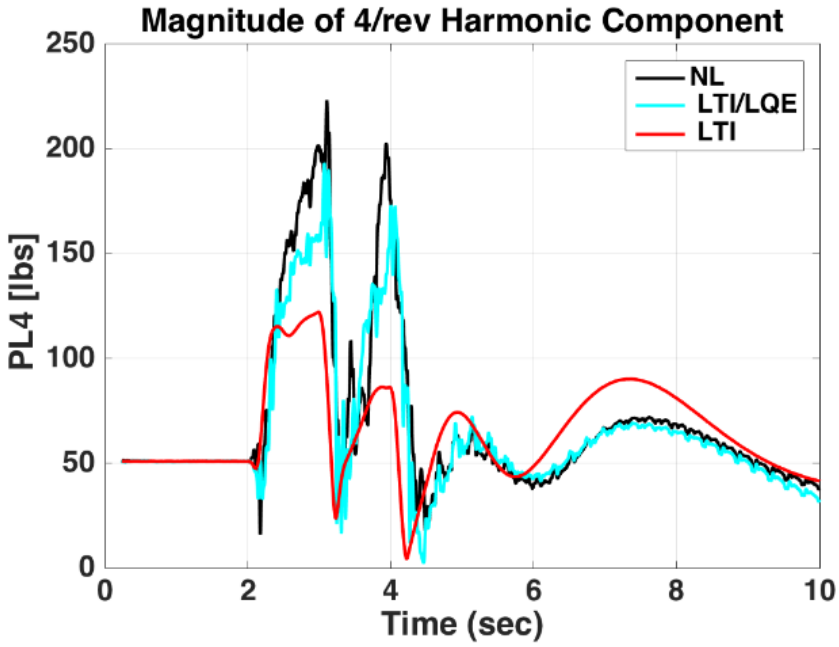

(b)

Figure 2.19: Variation of harmonic component of blade pitch link loads for the 20% control input case.

Another observation that can be made from the results shown in Figs. 2.18 and 2.19 is that the error in the prediction of 1/rev harmonic component of pitch link load appears to be prominent when the harmonic load reaches its peak magnitude. This observation suggests an alternate way of quantifying model fidelity, in addition to TIC factor, especially in studies involving harmonic component load predictions. Accordingly, the errors in the prediction of peak magnitudes of 1/rev and 4/rev harmonic pitch link load variation in Figs. 2.18 and 2.19 are shown as bar charts in Figs. 2.20 and 2.21, for the cases of 10% and 20% control inputs, respectively.

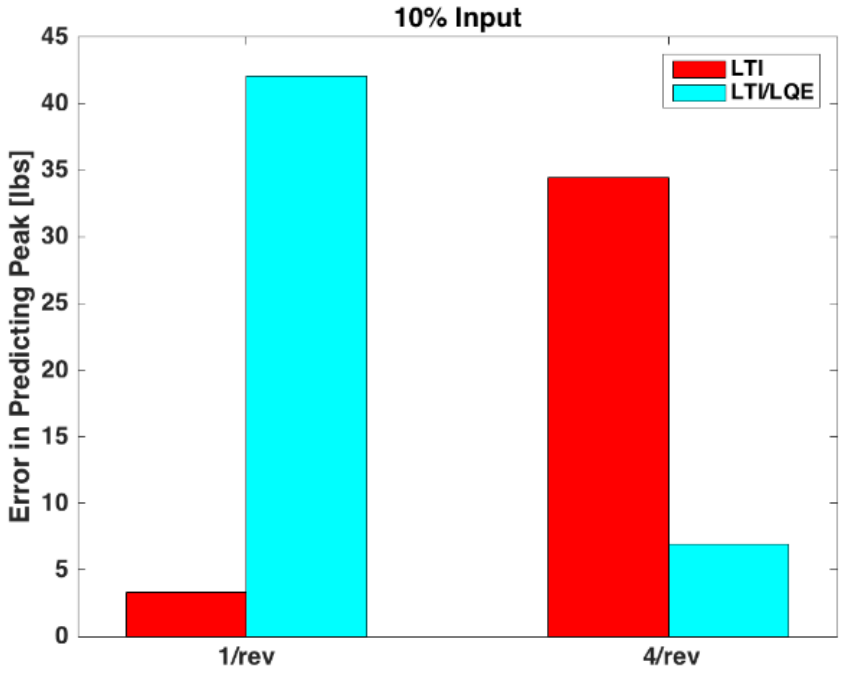

Figure 2.20: Comparison of error in peak magnitude prediction of harmonic loads between LTI and LTI/LQE.

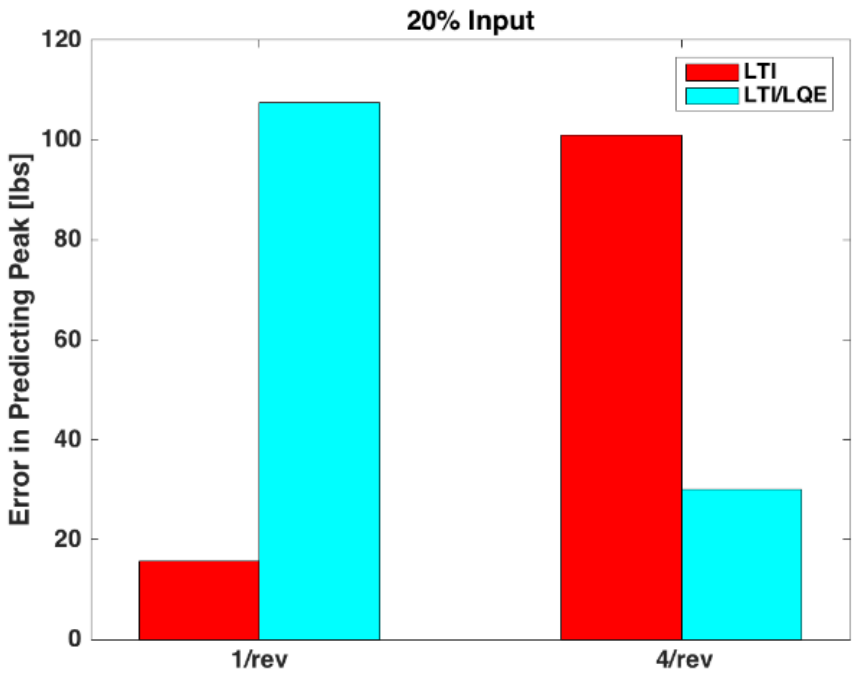

Figure 2.21: Comparison of error in peak magnitude prediction of harmonic loads between LTI and LTI/LQE.

A comparison of harmonic component peak magnitude predictions between LTI and LTI/LQE in Figs. 2.20 and 2.21 shows that while LTI/LQE significantly reduces the error in the prediction of the 4/rev peak magnitude, its prediction of the 1/rev peak magnitude becomes worse for both input cases. This finding is in line with the previous assertion of weak observability of 1/rev rotor states in fixed system hub load measurements of a four-bladed rotor.

2.6.3 Number of Sensors for LTI/LQE

An important consideration in the development of real-time algorithms for estimation of rotor component dynamic loads using the LTI/LQE scheme is the choice of number of sensors and their locations for the fixed system measurements. As blade pitch-link loads arise from blade root feathering moment variations, which in turn contribute to the fixed system hub pitching moment (M_y) and rolling moment (M_X), the performance of the LTI/LQE

is reevaluated using only harmonic components of hub moments M_X and M_y as measurements. The 1/rev and 4/rev harmonic component responses are presented for the 10% control input profile (see Fig. 2.4) in Fig. 2.22 and for the 20% control input profile (see Fig. 2.4) in Fig. 2.23. The resulting errors in harmonic peak magnitude predictions are shown as bar charts for the 10% control input profile in Fig. 2.24 and for the 20% control input profile in Fig. 2.25.

A comparison of the results obtained with all six components of hub loads as measurements (Figs. 2.18, 2.19, 2.20 and 2.21) and the results obtained with only hub moments (M_x and M_y) as measurements (Figs. 2.22, 2.23, 2.24 and 2.25) reveals that the LTI/LQE performance is very similar between the two sets of results, suggesting that the LTI model corrections by the LTI/LQE come mostly from the hub moment measurements.

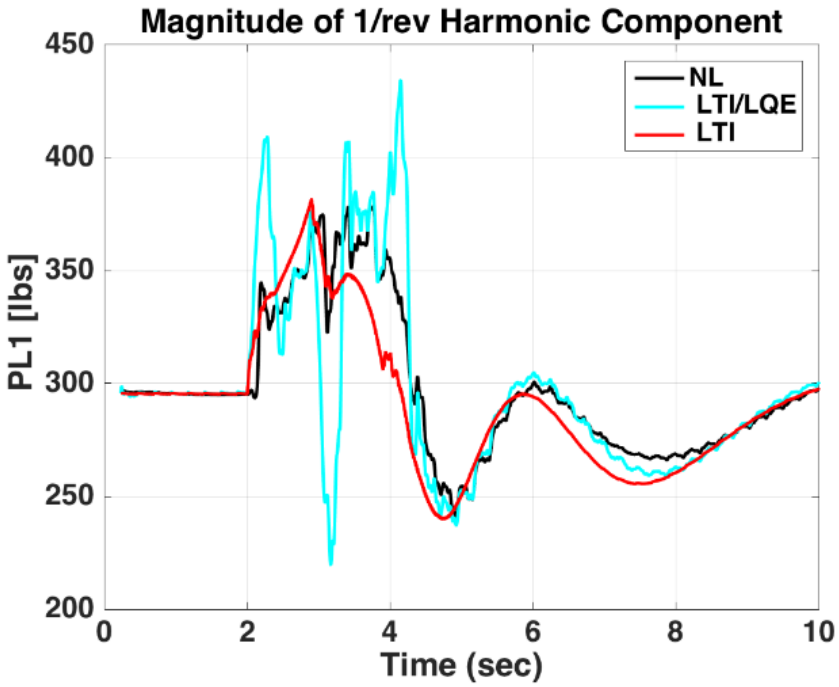

(a)

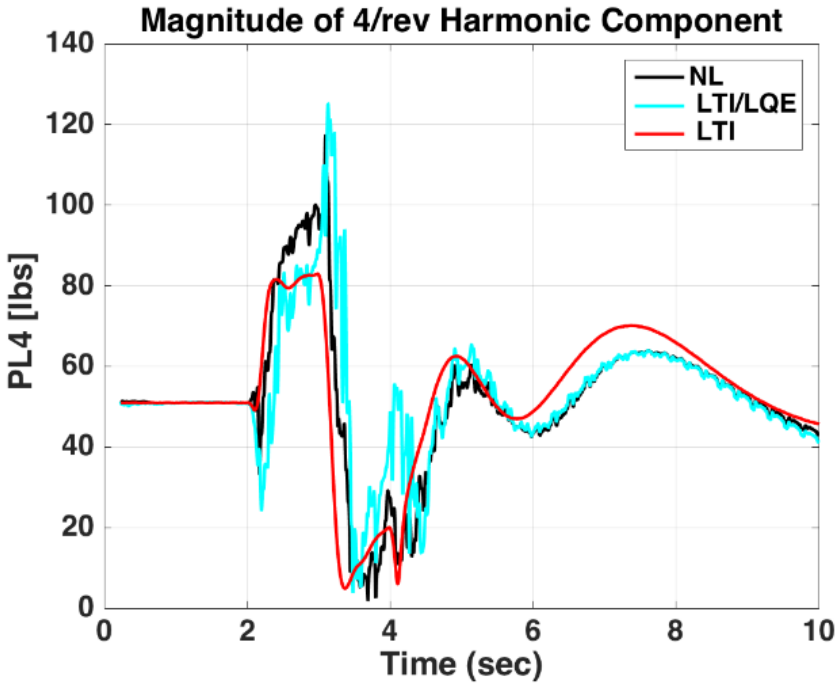

(b)

Figure 2.22: Variation of harmonic component of blade pitch link loads for the 10% control input case.

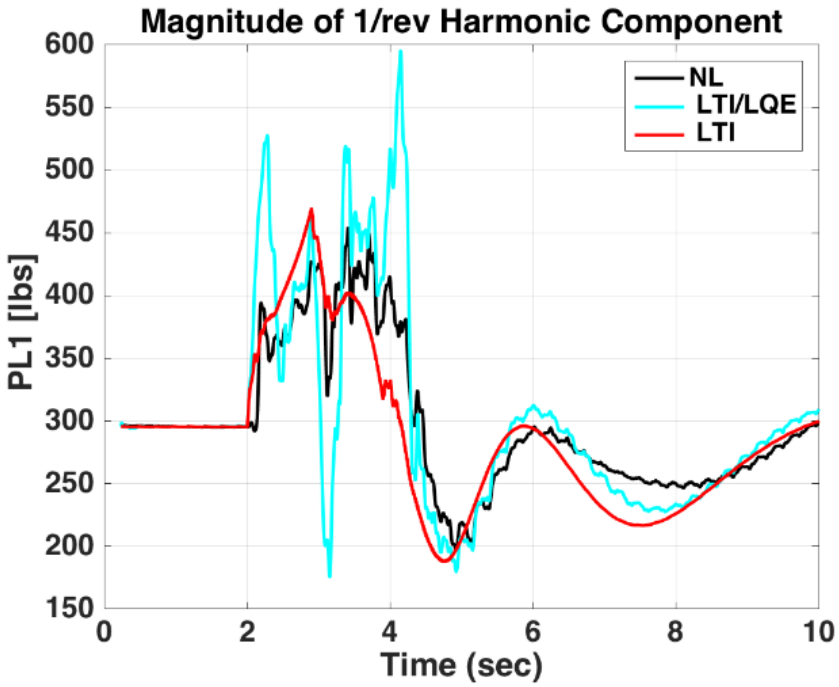

(a)

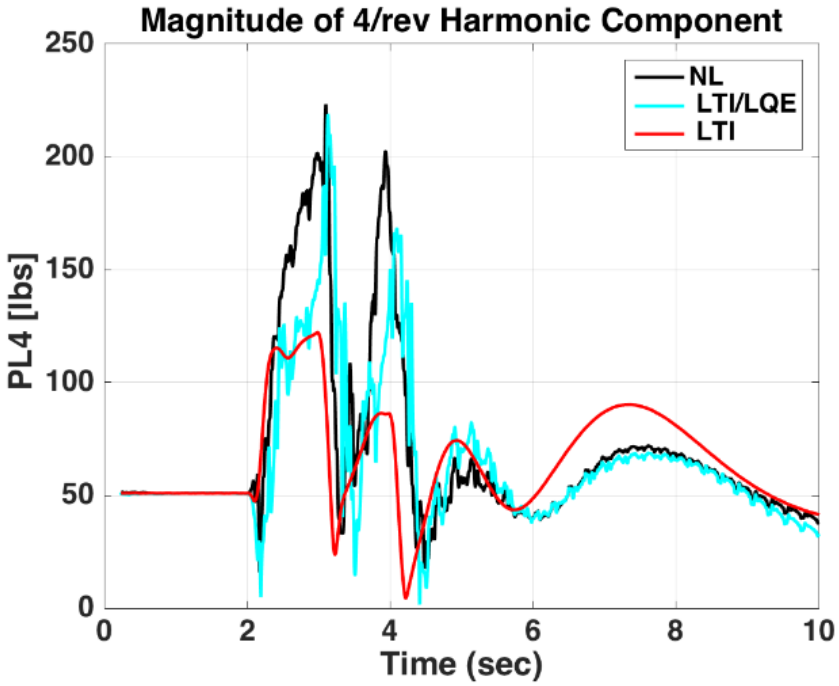

(b)

Figure 2.23: Variation of harmonic component of blade pitch link loads for the 20% control input case.

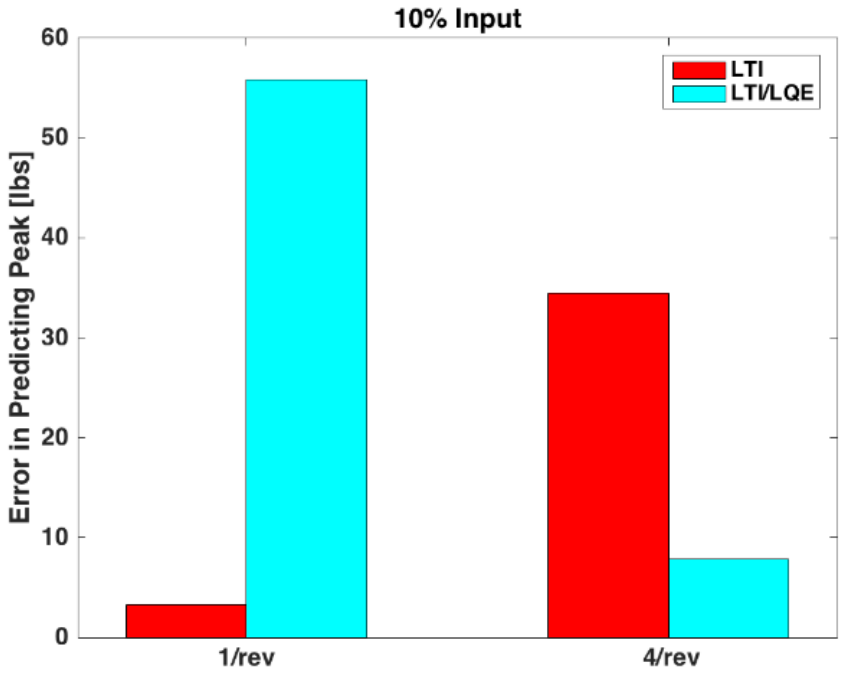

Figure 2.24: Comparison of error in peak magnitude prediction of harmonic loads between LTI and LTI/LQE.

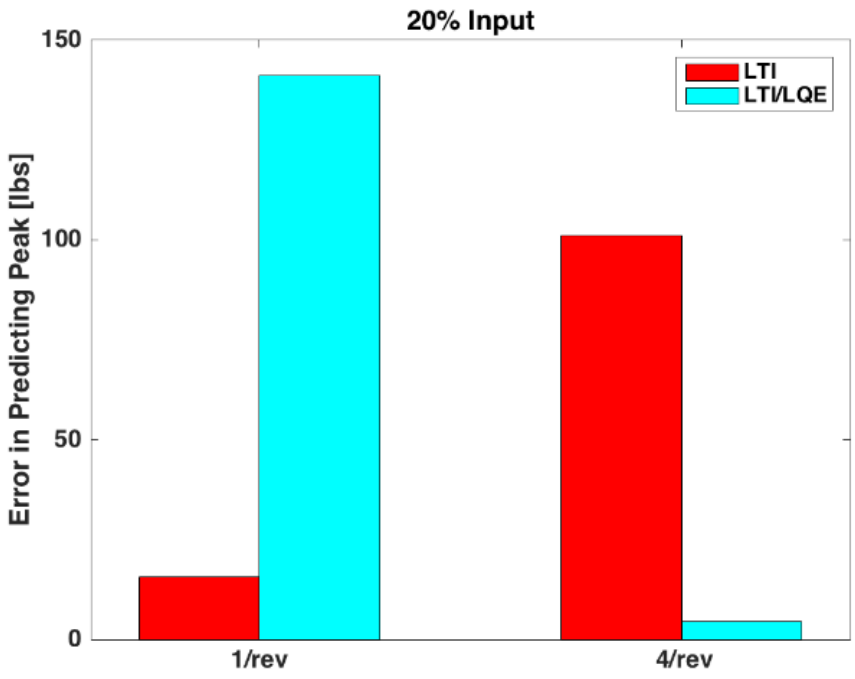

Figure 2.25: Comparison of error in peak magnitude prediction of harmonic loads between LTI and LTI/LQE.

2.7 Summary and Technical Findings

In this chapter, a purely physics-based approach to rotor load estimation has been proposed. In the literature various models were developed for estimation of rotating frame loads using fixed frame measurements. These models were developed using neural networks, a statistical-based approach, or a combination of both. The main drawbacks of these models are that they require a lot of data as they are data-driven, and they are aircraft specific. A physics-based approach would allow remediating these issues.

A higher order LTI model of coupled rotor/body/inflow dynamics and a Linear Quadratic Estimator (LQE) were used in this investigation. First, the LTI model load prediction capability was evaluated in simulation using a high fidelity nonlinear model of a generic UH-60 helicopter for on-line prediction of rotor blade pitch-link loads arising from vehicle maneuvers. The load predictions from the LTI model were compared to the nonlin-

ear model using a time-domain metric. It was observed that as the maneuver aggressiveness increased, the load predictions from the LTI model lost accuracy. An LTI/LQE model was formulated by combining the LTI model with a Linear Quadratic Estimator(LQE) to understand the benefits of using fixed system load measurements to improve the load estimates from the LTI model alone. The LTI/LQE scheme revealed an interesting finding. It was found that the N/rev (where N is the number of blades) fixed system load measurements have information that can be leveraged to make an inference about the N/rev dynamical loads in the rotating system. More specifically, it was found that fixed system hub forces and moments can be used to obtain accurate real-time estimates of the magnitude of 4/rev rotating blade pitch-link load. Overall, this chapter proves that coupling physics-based models with fixed system load measurements can be a viable method to obtain real-time estimates of dynamical loads in the rotating system.

CHAPTER 3

LOAD LIMITING CONTROL FOR COMPONENT LIFE EXTENSION

This chapter focuses on the development of a novel life extending control scheme for critical helicopter components. In particular, the synthesis of a more efficient and less conservative life extending control scheme compared to what is available in the literature is the primary objective of this chapter. A Load Limiting Control (LLC) scheme is proposed as a viable method that could solve many issues current life extending control schemes suffer from. An example of such issues is the total negligence of fatigue damage induced by harmonic component of loads. The proposed LLC scheme borrows concepts from carefree maneuvering. More specifically, the scheme treats desired harmonic load limits as limit boundaries and using a limit detection and avoidance module recasts the problem of load limiting as a vehicle limit through the computation of the available Control Margin (CM). The computed CM is used as a cue to the pilot. The limit detection and avoidance module comprises of an optimization algorithm, a model predictive controller, and a computationally simple on-board dynamical model.

In the previous chapter, a higher order LTI model was developed. The developed LTI model has 1513 states and can be used for real-time estimation of rotor component harmonic loads. The question of interest in this chapter is the following. Would it be possible to leverage the load prediction capability of the LTI model in the synthesis of a novel life extending control scheme ? In the literature, it is fairly common practice to take a Load Alleviation Control (LAC) approach to component life extension. An LAC is an inefficient and conservative design due to two reasons. First, it is incapable to discern aggressive from non-aggressive maneuvers. Second, it totally neglects the effect of harmonic loads on localized damage (i.e., no distinction is made between different harmonic load effects on accumulated component fatigue). In fact, a recent study showed that different harmonic loads have different effects on fatigue damage[81]. Therefore, during flight, it makes sense to track and limit the most damage threatening harmonic loads.

In this chapter, an LLC scheme for component life extension is proposed. The LLC scheme is a more efficient and less conservative scheme than the traditional LAC scheme since it is not only able to discern between aggressive and non-aggressive maneuvers but also takes into account the effect of harmonic loads on localized damage.

The development of an LLC scheme comes with many challenges which are addressed in this chapter. The first challenge is the need of a computationally simple on-board dynamical model to achieve real-time performance. The second challenge resides in the formulation of the scheme. In other words, using the on-board model, how can one recast the problem of harmonic load limiting as a vehicle limit in maneuvering flight. Once the problem is well posed and a suitable on-board dynamical model has been identified, the third challenge is the need of an optimization tool that can be used to solve in real-time the posed problem.

The LTI model developed in the previous chapter is indeed a great candidate for the on-board model. However, its very large size which is directly related to the number of harmonic states, inputs, and outputs retained can pose problem for real-time implementa-

tion. This might be the case in applications where very large number of harmonic states, inputs, and outputs might be required to capture accurately the relevant harmonic loads acting on a specific component. As such, the reduction of the full-order LTI model to a reduced order model using a two-time scale method is described next.

3.1 Model Order Reduction using Singular Perturbation Method

In this section, using the singular perturbation method, a reduced order LTI model is obtained. The higher order LTI model contains dynamics with different time scales. More specifically, the rotor and inflow dynamics happen at a must faster time scale than the body dynamics. This interaction between fast and slow dynamics in the higher order LTI model can cause problem associated with stiffness. Furthermore, the LLC scheme requires estimates of the initial values of the state vector of the on-board model for online estimation of harmonic loads. States associated with vehicle speed, body rates and attitudes can be measured while such is not the case for higher-order rotor and inflows states. As such, it is convenient to reduce the state-space dimension of the higher order LTI model.

The singular perturbation method for model order reduction can be summarized in two steps[82]. First, the system under consideration needs to be transformed into a singularly perturbed system with the introduction of the μ parameter (see Chapter 1, section 1.2.5). This step allows to obtain a two-time scale representations of the original system (i.e, decompose original system into fast and slow modes). Then, a reduced order model of the original system is obtained by performing a quasi-steady representation of the fast dynamics of the singularly perturbed system. In this step, it is assumed that the fast states reach their equilibrium instantaneously with respect to the slow states (i.e., the dynamics of the fast states are much faster than that of the slow states)

A two time-scale representation of the higher order LTI model can be obtained by using the fact that the rotor and inflow dynamics happen at a must faster time scale than the body dynamics. Therefore, for this particular case, since the fast and slow modes of the system

are known apriori the introduction of the μ parameter is not needed to decompose the system. The state vector of the higher-order LTI model is divided into slow and fast states as shown below

$$X = \begin{bmatrix} X_s \\ X_f \end{bmatrix} \tag{3.1}$$

where X_s=slow states and X_f=fast states

Such a decomposition of the state vector guarantees that $\frac{\dot{X}_f}{\dot{X}_s}$ is very large. In order words, $\frac{\dot{X}_f}{\dot{X}_s}$ is of order $\frac{1}{\mu}$ where μ is a very small real number. Using Eq. (3.1), the following dynamical system is obtained.

$$\begin{bmatrix} \dot{X}_s \\ \dot{X}_f \end{bmatrix} = \begin{bmatrix} A_s & A_{sf} \\ A_{fs} & A_f \end{bmatrix} \begin{bmatrix} X_s \\ X_f \end{bmatrix} + \begin{bmatrix} B_s \\ B_f \end{bmatrix} U \tag{3.2}$$

With the higher-order LTI model decomposed into fast and slow modes, a reduced order model is obtained by assuming that the fast states reach their equilibrium instantaneously with respect to the slow states (i.e., quasi-steady approximation of the fast dynamics). What follows is a derivation of the new reduced order dynamical system and functional relationship that maps the controls and slow states to the limit parameters. In this thesis, the rotating pitch link is selected as the component in the rotating frame of interest. Hence, for this study, specific harmonic components of pitch link loads are selected as limit parameters.

As per the assumption that the fast states reach steady state very quickly, $\dot{X}_f$ can be set to zero and an expression for X_f can be obtained.

$$A_{fs}X_s + A_fX_f + B_fU = 0 \tag{3.3}$$

$$X_f = A_f^{-1}[-A_{fs}X_s - B_fU] \tag{3.4}$$

By substituting for X_f from Eq. (3.4) into Eq. (3.2) the dynamic equation for the reduced system becomes

$$\dot{X}_s = [\hat{A}]X_s + [\hat{B}]U \tag{3.5}$$

where

$$\hat{A} = A_s - A_{sf}A_f^{-1}A_{fs} \tag{3.6}$$

$$\hat{B} = B_s - A_{sf}A_f^{-1}B_f \tag{3.7}$$

The output equation is also rewritten in terms of the slow states and control as

$$Y = \begin{bmatrix} C_s & C_f \end{bmatrix} \begin{bmatrix} X_s \\ X_f \end{bmatrix} + \begin{bmatrix} D \end{bmatrix} U \tag{3.8}$$

$$Y = [\hat{C}]X_s + [\hat{D}]U \tag{3.9}$$

where

$$\hat{C} = C_s - C_f A_f^{-1} A_{fs} \tag{3.10}$$

$$\hat{D} = D - C_f A_f^{-1} B_f \tag{3.11}$$

Using the model order reduction procedure described above, a 10^{th} order reduced order LTI model is considered. The reduced order model is derived with slow states consisting of 0^{th} harmonic components of body velocities (U, V, W), body angular velocities (P, Q, R), body pitch and roll attitudes, (θ,ϕ), and the 0^{th} harmonics of the longitudinal (β_{1c_0}) and lateral flapping (β_{1s_0}). The resultant slow state vector is defined as

$$X_s = [x_{B_o}^T \ \beta_{1c_0} \ \beta_{1s_0}]^T \tag{3.12}$$

The obtained 10^{th} order model allows for capturing the low-frequency cyclic flap mode in addition to the body modes as part of the slow dynamics

A study conducted in Ref. [83] assessed the fidelity of different reduced order LTI models for prediction of blade root pitch-link loads, vehicle angular rate and body velocity component responses. The study concluded that the reduced 10^{th} order LTI model provided a relatively good representation of the higher order LTI model in the prediction of harmonic of pitch link loads. Hence, a 10^{th} order LTI model is used in this research for the synthesis of the load limiting controller.

3.2 Load Limiting Control Scheme

This section describes the proposed LLC scheme in detail, highlighting the major features that make this scheme innovative. The use of Model Predictive Control (MPC) for the estimation of control margins associated with vehicle performance limit boundaries was developed in Ref. [42]. This control margin estimation via MPC is adopted here to develop a load-limiting control scheme by making use of a model predictive receding-horizon control formulation.

Given a load limit (y_{max}) that is not to be exceeded, the LLC scheme uses an on-board dynamical model representative of the true vehicle dynamics, a cost function defined over a finite time horizon of T_p, and an optimizer to compute, at each instant in time, future extremal control input (u_{ext}) that would lead the component harmonic load (y_p) to reach its limit without exceeding it. This process is illustrated in Fig. 3.1. Thus, the LLC scheme treats the load limit (y_{max}) as a limit boundary and uses Model Predictive Control (MPC) to arrive at an optimal control profile that would give rise to a harmonic load response reaching the limit boundary within a time horizon of T_p. The shaded area in Fig. 3.1b gives

a graphical representation of the cost function used by the LLC scheme. The calculated extremal control profile is used to form the quantity known as Control Margin (CM). The control margin is given by the following equation

$$CM(t) = u_{ext}(t_0 + \Delta t) - u_{pilot}(t) \tag{3.13}$$

The control margin is an important quantity that can be provided to the pilot in the form of a cue. This would allow informing the pilot, at each instant in time, how much control deflection is permitted before the harmonic load exceeds the maximum limit. The LLC scheme can also be used as an automatic load limiting system. In this case, the extremal control input estimates (i.e., allowable control travel estimates) are directly used to automatically constrain the pilot control inputs to keep the selected harmonic load within the desired maximum value. If integrated with a cueing system, the LLC scheme provides the benefit of allowing for a pilot's decision to prioritize between load limiting and maneuver aggressiveness. Therefore, the pilot has the choice to follow the cues to avoid load limit exceedance or disregard them in order to prioritize maneuver performance at the expense of component load limit violations.

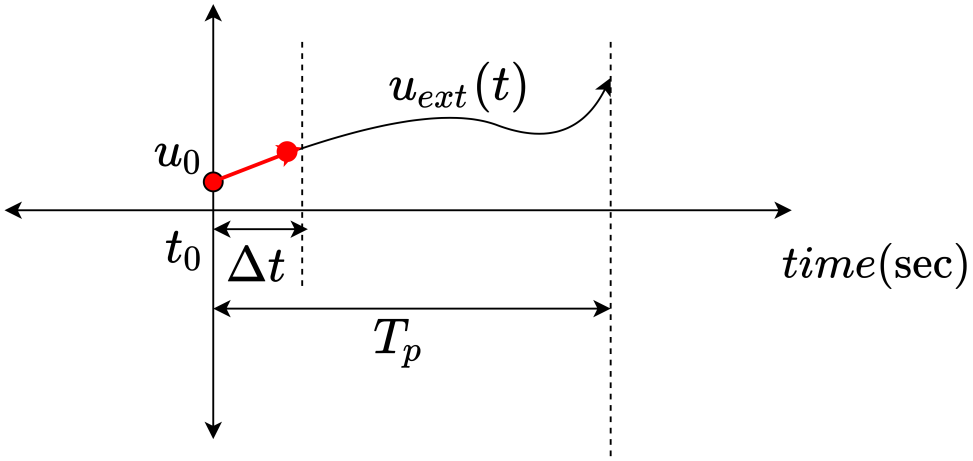

(a) Extremal control profile

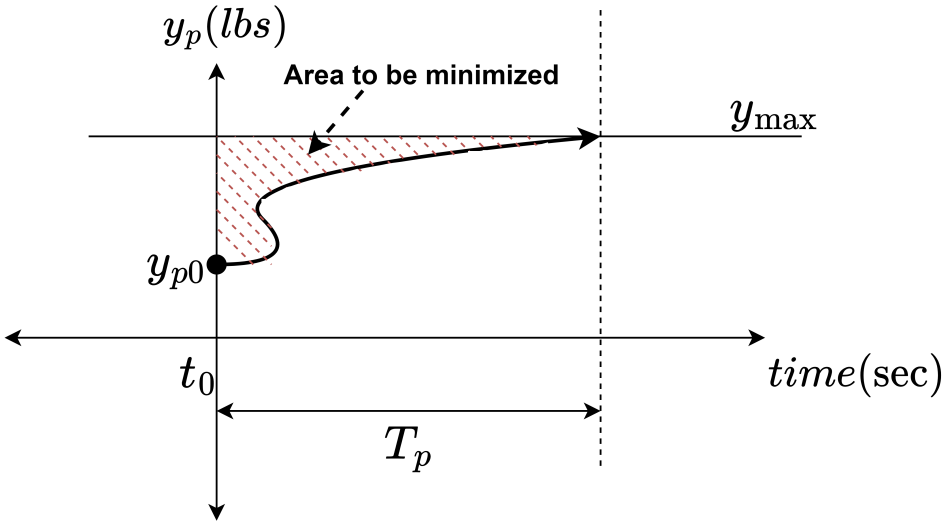

(b) Load profile

Figure 3.1: LLC scheme.

The LLC scheme trades between maneuver performance for harmonic load limiting and maneuver performance only when load exceedance occurs. Therefore, for non-aggressive maneuvers that do not cause load exceedance, no trade-off is required. Unlike the LAC scheme, the LLC scheme allows for limiting component dynamic loads within a prescribed maximum value. This prescribed maximum value can be wisely selected to reflect a threshold after which significant fatigue damage on the component is very likely to occur. Another important property of the proposed LLC schemes is its ability to estimate future

values of the limit parameter. This is essential in the early detection of limit violation, which allows the pilot to have enough time to take preventive actions. A block diagram representation of the LLC scheme is presented in Fig. 3.2.

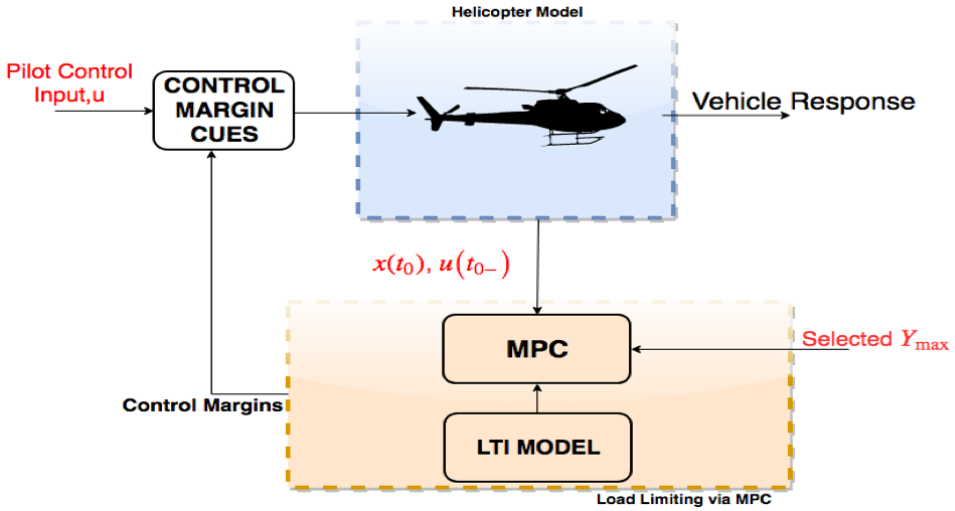

Figure 3.2: Load limiting algorithm via cueing.

In Fig. 3.2, $x(t_0)$ represents the current value of the on-board LTI model state vector and $u(t_{0-})$ represents control vector prior to pilot input at t_0. The LLC scheme assumes that the LTI model states are available from on-board measurements and stored values of component harmonic loads at trim. Two facts are important to note here. First, the on-board LTI model uses these measurements in order to estimate the component harmonic loads at t_0. Second, when the LTI model states are not available from on-board measurements, one can obtain an estimate of the component harmonic loads at t_0 directly using the LTI model or even the LTI/LQE model. The LLC scheme calculates the extremal control input by solving, at each time instant, a constrained optimization problem of a quadratic cost function using a 10^{th} order LTI model. The determination of extremal control boundary associated with component load limit is posed as a receding horizon model-predictive algorithm and is formulated in terms of the following optimal control problem:

$$min_U[J], J = \int_{t_0}^{t_o+T_p} L(\|Y_{harm}\|_2, U)dt \tag{3.14}$$

subj:

$$\dot{X}_s = [\hat{A}]X_s + [\hat{B}]U \tag{3.15}$$

$$\|Y_{harm}\|_2 \leq y_{max} \tag{3.16}$$

$$U_{min} \leq u(t_{0-}) + U \leq U_{max} \tag{3.17}$$

where $\|Y_{harm}\|_2$ is the two norm or magnitude of the specific pitch link harmonic load and y_{max} is a selected value of its limit.

The cost function integrand is defined as follows:

$$\begin{aligned} L(\|Y_{harm}\|_2, U) = \ & (\|Y_{harm}\|_2 - y_{max})^T Q(\|Y_{harm}\|_2 - y_{max}) + \\ & (U - u(t_{0-}))^T R(U - u(t_{0-})) \end{aligned} \tag{3.18}$$

where Q and R are symmetric positive definite matrices of design coefficients that penalize the limit parameter tracking error in reaching its boundary in the selected time horizon, T_p, and control activity, respectively. y_{max} is a user selected value of pitch link harmonic load limit. A and B are the 10^{th} order LTI state and input matrices, respectively.

A challenge that comes with the LLC scheme is its computational complexity. Solving the optimization problem posed in Eqs. (3.14), (3.15), (3.16) and (3.17) for the determination of extremal control input or equivalently, control margin estimates can be a challenge. This is due to the dynamics of the selected harmonic load (Y_{harm}) that is being limited. The harmonic load can have a mathematical expression that is highly nonlinear. Due to the computational benefit that comes with solving a convex optimization problem, one viable method to solve the posed optimization problem in real time is to first convexify the problem and subsequently use an ad-hoc solver (i.e, CVXGEN solver) [11, 12]. However, it is important to note that the ability to convexify the problem solely depends on the ability to

obtain a linear mathematical expression that accurately approximates the dynamics of the harmonic load. This might not always be feasible.

As a proof-of-concept, the 1/rev pitch link harmonic load is selected as the harmonic load of interest. The expression for the two norm of the 1/rev pitch link harmonic load is given by:

$$\|Y_{harm}\|_2 = \sqrt{(y_{1c_{(trim)}} + y_{1c})^2 + (y_{1s_{(trim)}} + y_{1s})^2} \tag{3.19}$$

The limit parameter, $\|Y_{harm}\|_2$, is the total 1/rev harmonic load (i.e., trim + change from trim).

The posed optimization problem can be convexified by performing a linear approximation of Eq. (3.19) as

$$\|Y_{harm}\|_2 \overset{\text{approx}}{\approx} a + by_{1c} + cy_{1s} \tag{3.20}$$

where a, b and c $\in \mathbb{R}$ and are given by

$$a = \sqrt{(y_{1c_{(trim)}})^2 + (y_{1s_{(trim)}})^2} \tag{3.21}$$

$$b = \frac{y_{1c_{(trim)}}}{\sqrt{(y_{1c_{(trim)}})^2 + (y_{1s_{(trim)}})^2}} \tag{3.22}$$

$$c = \frac{y_{1s_{(trim)}}}{\sqrt{(y_{1c_{(trim)}})^2 + (y_{1s_{(trim)}})^2}} \tag{3.23}$$

The MPC formulation expressed by Eqs. (3.14), (3.15), (3.16), (3.17) and (3.18) makes use of Eq. (3.20) as a representation of the magnitude of the 1/rev harmonic pitch link load.

The solution to the optimal control problem provides estimates of the control margin boundaries associated with 1/rev pitch link load limit and are given as cues to the pilot.

3.3 Batch Simulation Results

In this section, an investigation of the performance of the proposed load limiting controller at 120 knots forward flight is presented. Specifically, limiting of the magnitude of the 1/rev pitch link load is considered. For the proof-of-concept study considered here, the prediction horizon T_p is set at 0.0065 seconds. Two different models are considered as representation of the truth model (aircraft model). For each of the truth models considered, the pilot's control input is taken to be the longitudinal cyclic doublet input from trim as shown in Fig. 3.3.

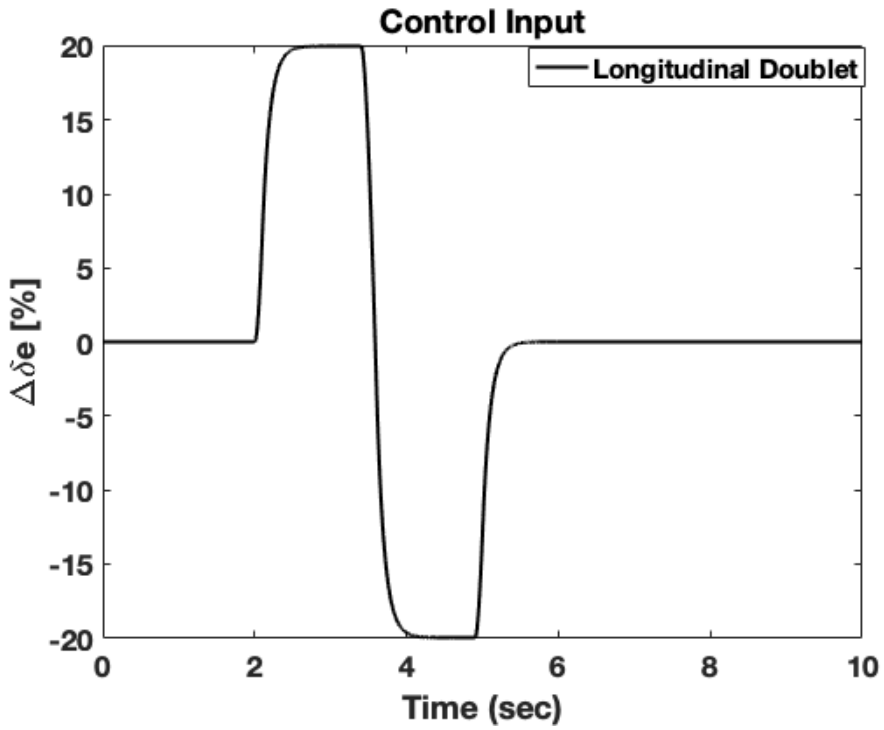

Figure 3.3: Percentage change from trim of longitudinal cyclic control input.

The proposed LLC scheme applies limits to the pilot's control input based on the MPC solution of the control limits that correspond to the user selected harmonic load limit.

3.3.1 Study with a Higher Order LTI Model as the Aircraft Model

In this section, the full-order LTI model extracted from the nonlinear model (NL) of the generic helicopter in FLIGHTLAB® is used as the truth model. The reason for using the higher order LTI model as the vehicle truth model is to assess the performance of the LLC scheme without the effect of nonlinearities and significant model mismatch between the on-board and vehicle truth models. Furthermore, having no significant model mismatch is ideal in selecting the design parameters for the load limiting controller (Q and R matrices). The upper limit for the pitch link 1/rev load magnitude is arbitrarily set at 350 lbs. Simulation results of the reference blade root pitch-link 1/rev load magnitude without (labeled 'No LLC') and with the proposed load limiting scheme (labeled 'LLC with...') are shown in Fig. 3.4 for the case of the longitudinal cyclic doublet input of Fig. 3.3. It can be observed from Fig. 3.4 that with LLC, the 1/rev magnitude of the pitch link load stays within the selected limit.

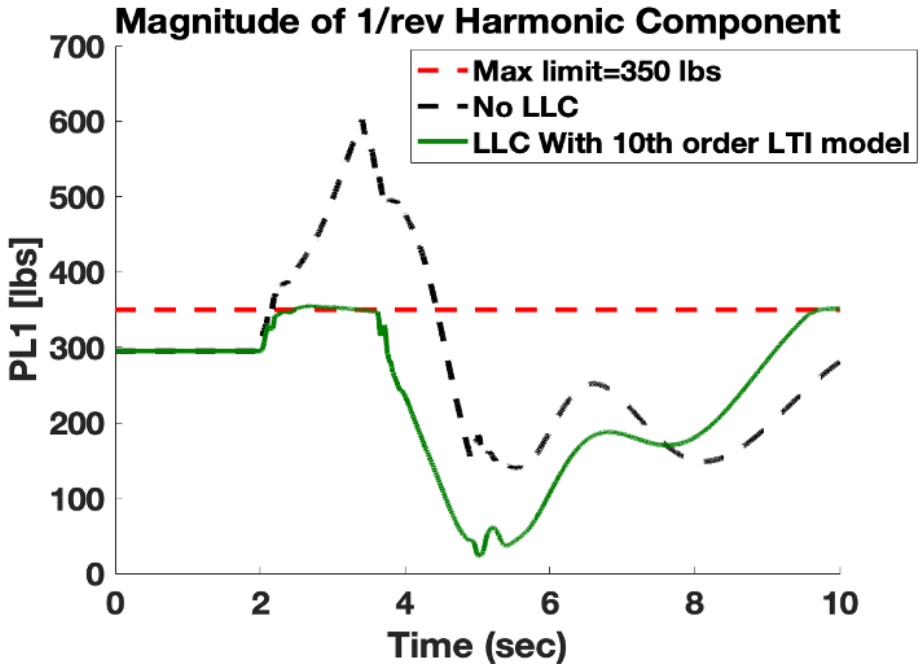

Figure 3.4: Variation of 1/rev harmonic component of reference blade pitch link loads with and without LLC.

The LLC, in this case, does result in the limit parameter to perfectly ride the limit boundary whenever limit exceedence occurs. This is due to the fact that the on-board 10^{th} order LTI model is a good representation of the aircraft model and as such estimation of the limit parameter using the on-board LTI model is accurate. The load limiting controller (LLC) is seen to be very effective.

The root mean square errors for limit exceedance for the case with no LLC and LLC with 10^{th} order LTI model are evaluated to be respectively, 138 lbs and 2.8 lbs (98% reduction), which indicates that the 10^{th} order LTI model leads to good load-limiting performance.

Furthermore, Fig. 3.5, wherein the longitudinal cyclic control input with and without LLC are compared, the pilot control input is modified whenever the 1/rev load exceeds the selected limit (i.e., the proposed LLC scheme takes corrective action in altering the pilot control input only when necessary). Load limiting comes with a reduction in the maneuver aggressiveness as seen from Fig. 3.6. The maximum pitch rate that can be achieved without LLC for the selected control input is not reached for the case with LLC. Moreover, it is noted that when the selected limit is not exceeded, the pitch rate response for the case with LLC is somewhat similar to the case without LLC.

The angular rates (yaw and roll rates), attitudes (roll and pitch attitudes), and velocities (i.e., x,y,z-axis body velocities) responses from trim for the cases with and without LLC are shown in Figs. 3.7, 3.8 and 3.9, respectively.

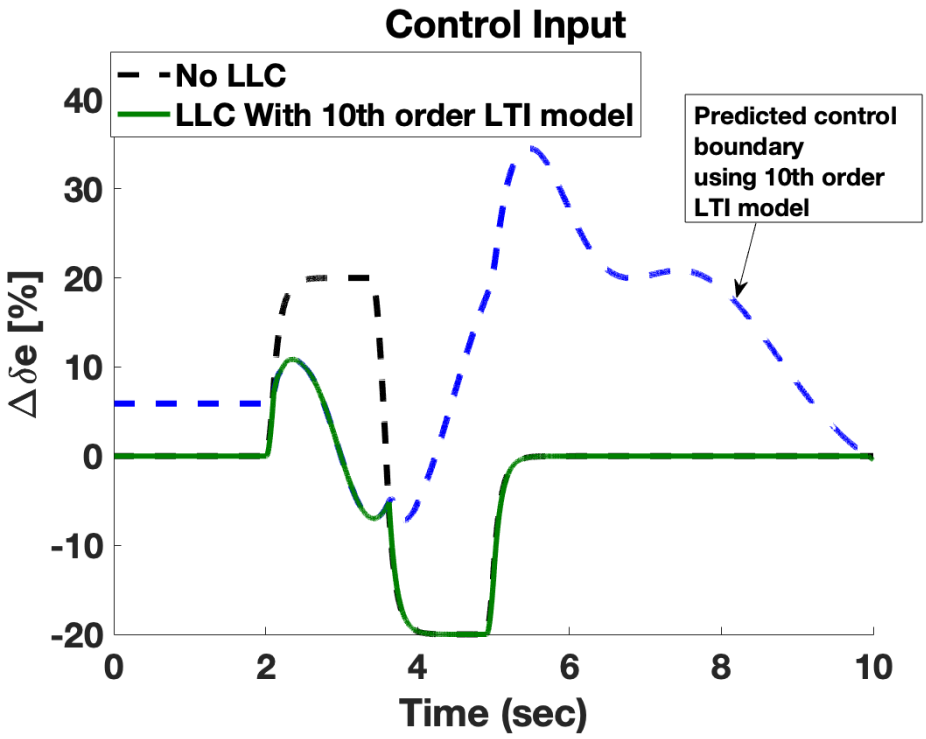

Figure 3.5: Percentage change from trim of longitudinal cyclic control input with and without LLC.

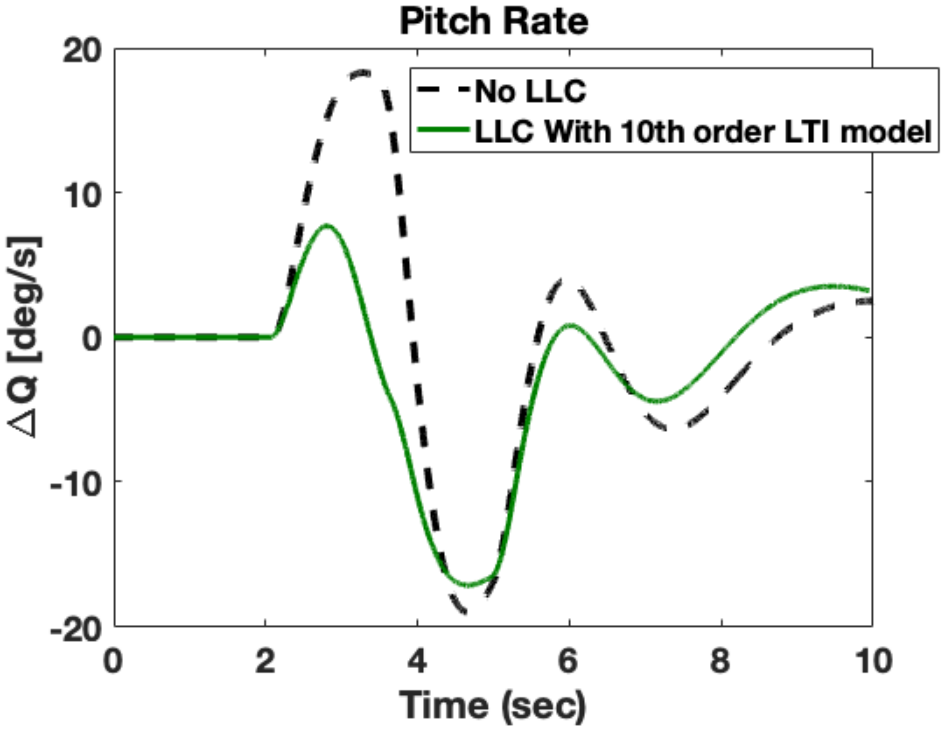

Figure 3.6: Body pitch rate response with and without LLC.

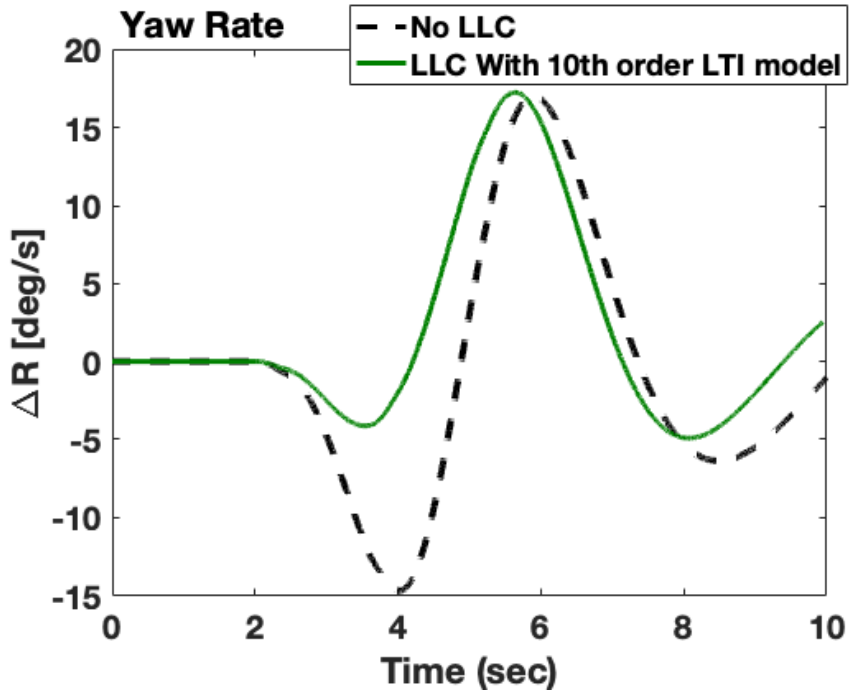

(a)

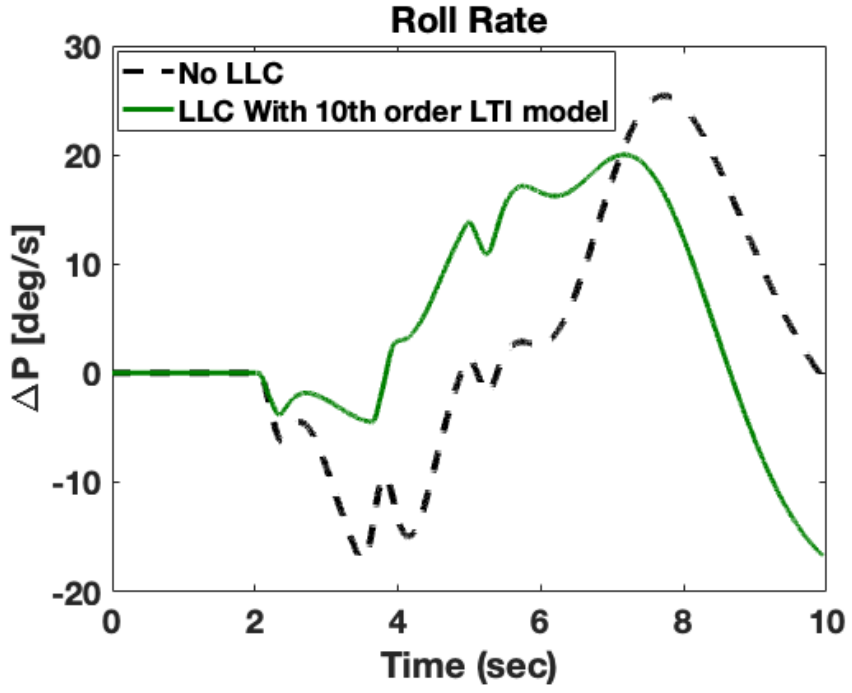

(b)

Figure 3.7: Body rate response with and without LLC.

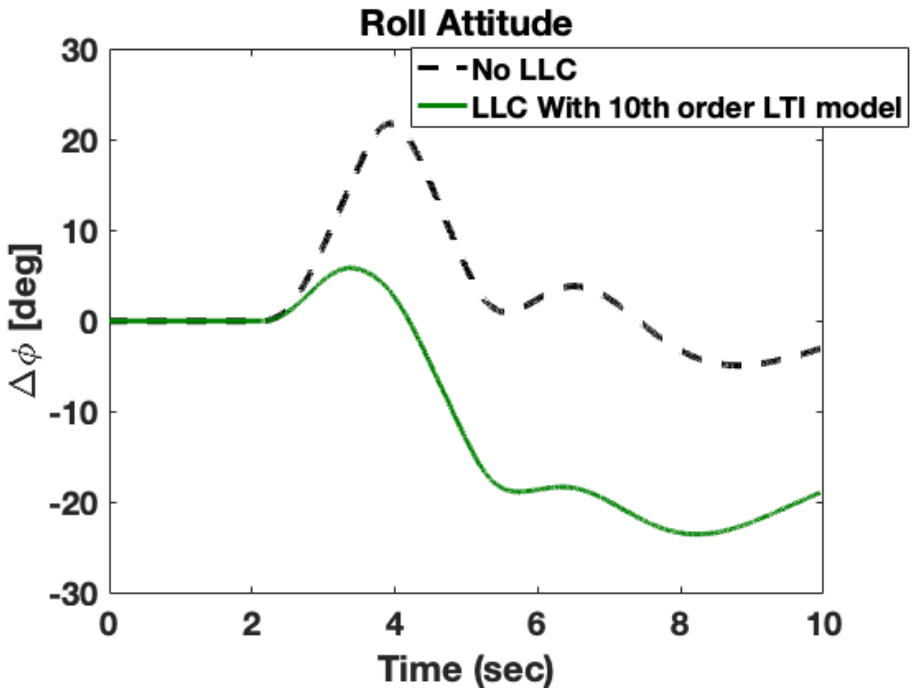

(a)

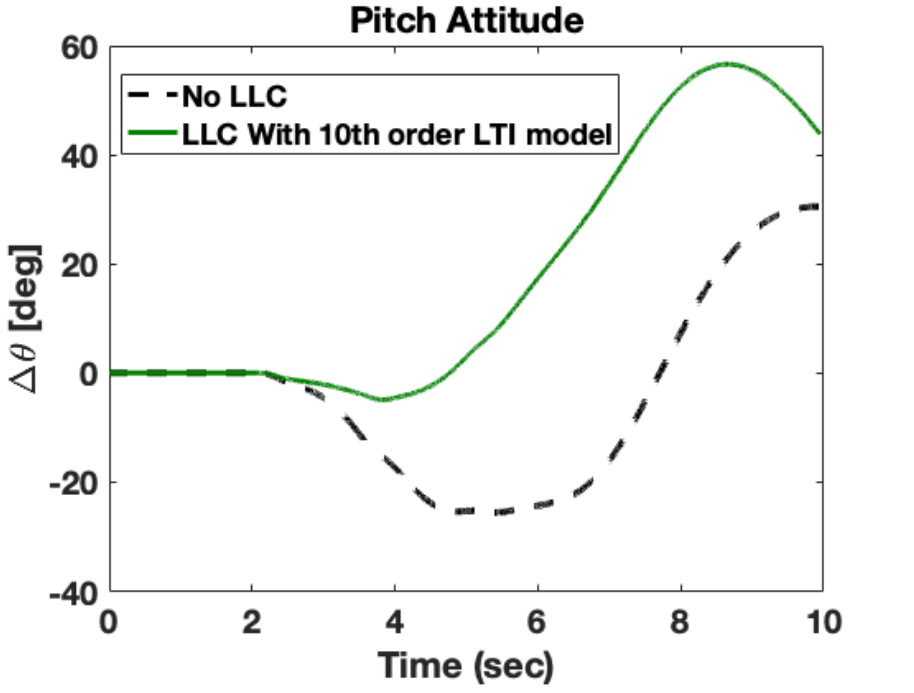

(b)

Figure 3.8: Body attitude response with and without LLC.

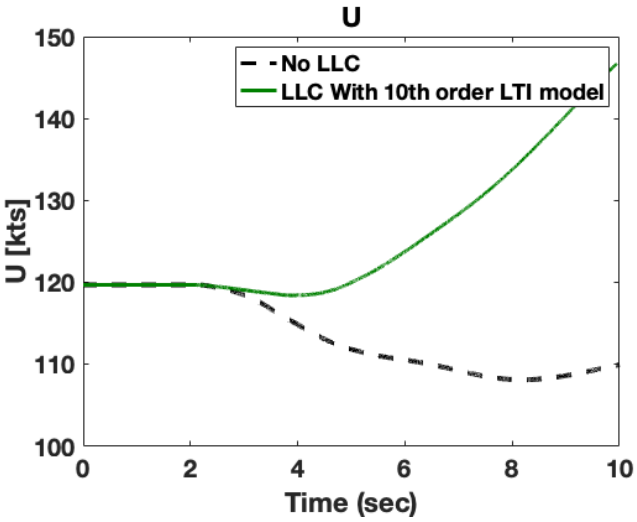

(a)

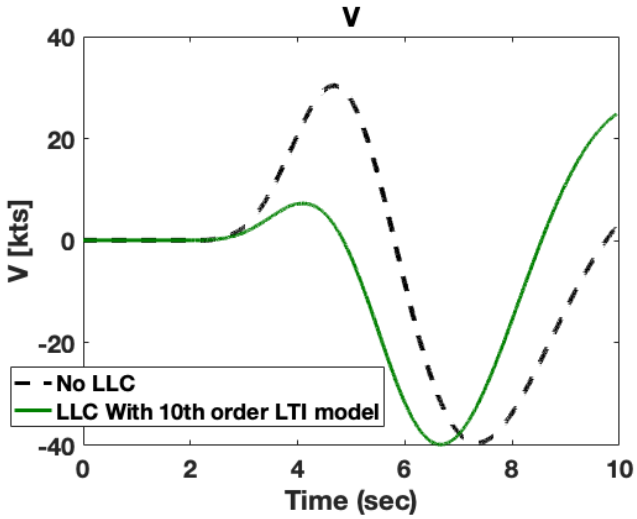

(b)

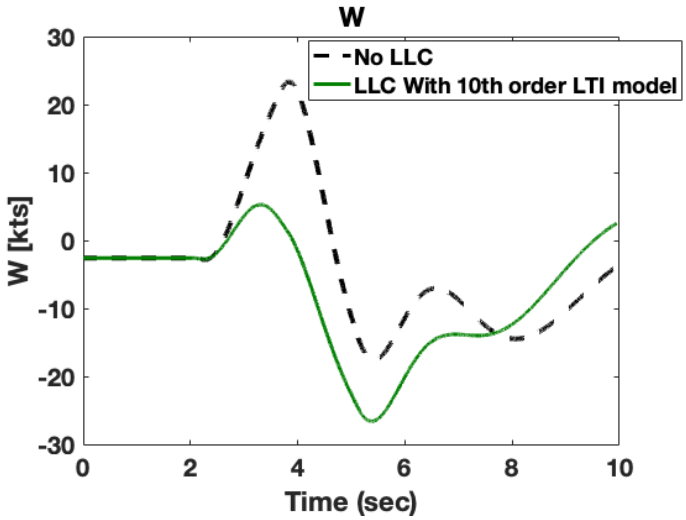

(c)

Figure 3.9: Body velocity response with and without LLC.

3.3.2 Study with a High Fidelity Nonlinear Model as the Aircraft Model

A more realistic application of the proposed load limiting control scheme presented in this thesis would be to use a high fidelity nonlinear model as the truth model. This would allow investigating the performance of the proposed LLC in the presence of nonlinearities and model mismatch between the on-board and vehicle truth models. Therefore, the high fidelity full vehicle nonlinear model (NL) in FLIGHTLAB®, from which the higher-order LTI model is generated, is used as the aircraft model in this section. For consistency and ease of performance comparison with previous results, the upper limit for the pitch link 1/rev load magnitude is kept at 350 lbs. Figures 3.10, 3.11 and 3.12 show example results using the proposed LLC scheme, demonstrating the plots of longitudinal control input and the resulting magnitude of 1/rev component of pitch link load and body pitch rate variation with and without LLC. These results demonstrate once again the effectiveness of the proposed LLC scheme.

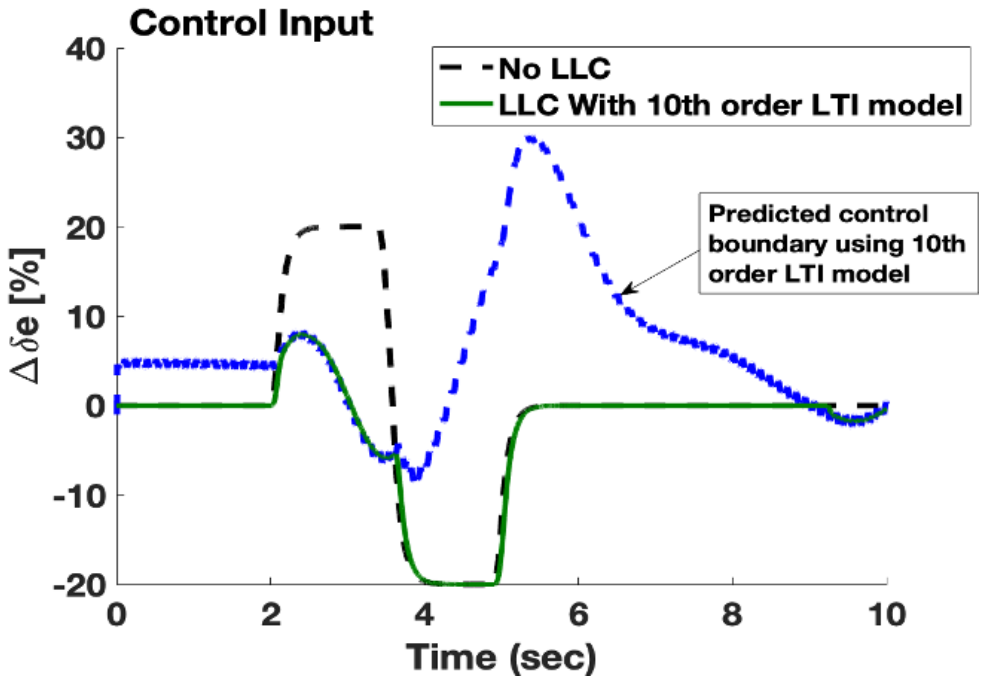

Figure 3.10: Percentage change from trim of longitudinal cyclic control input with and without LLC.

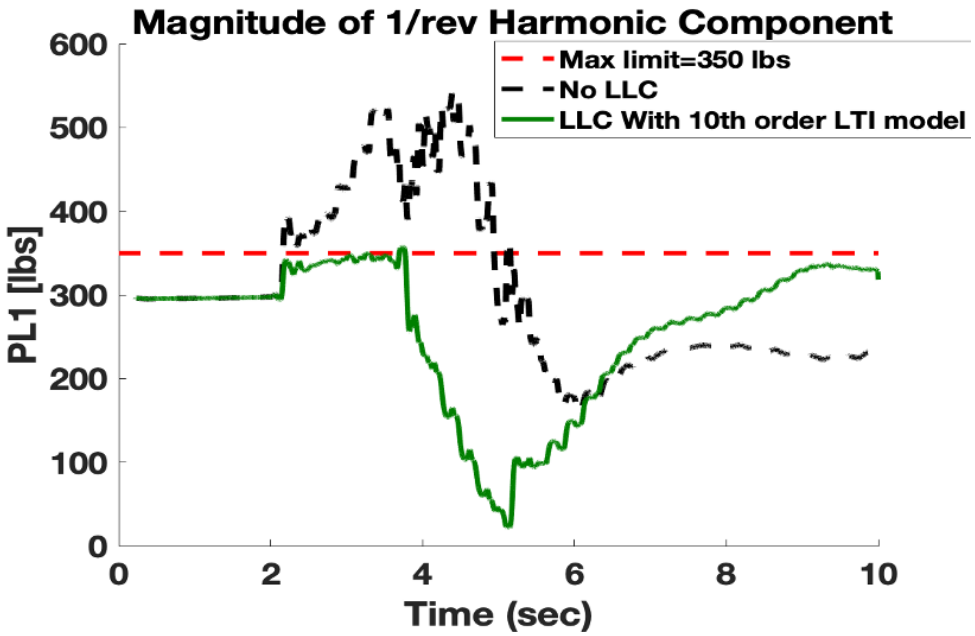

Figure 3.11: Variation of 1/rev harmonic component of reference blade pitch link loads with and without LLC.

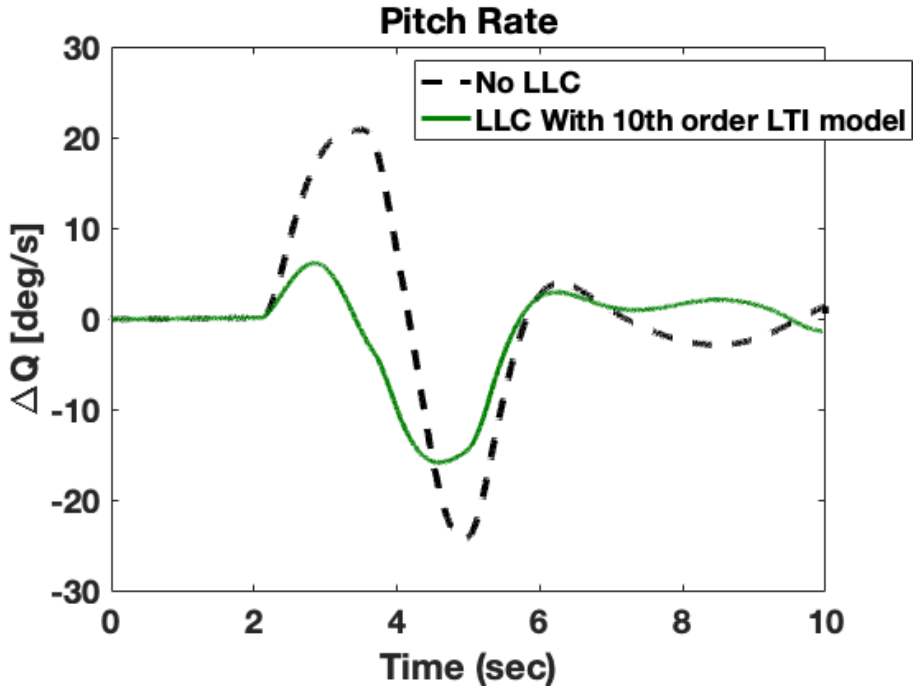

Figure 3.12: Body pitch rate response with and without LLC.

It is important to note that even though the on-board reduced order LTI model is a simple lower order model, the real-time component load estimates it generates are relatively accurate as can be seen in Fig. 3.11 where no limit exceedance is observed. This suggests that the singular perturbation algorithm for system order reduction is a viable technique to reduce the state-space dimension of physics-based models that are used for the development of life extending control schemes. The root mean square values of limit exceedance for the case without and with LLC are evaluated to be, respectively, 108 lbs and 5.9 lbs (95% reduction).

For this simulation, the angular rates (yaw and roll rates), attitudes (roll and pitch attitudes), and velocities (i.e., x,y,z-axis body velocities) responses for the cases with and without LLC are shown in Figs. 3.13, 3.14 and 3.15, respectively.

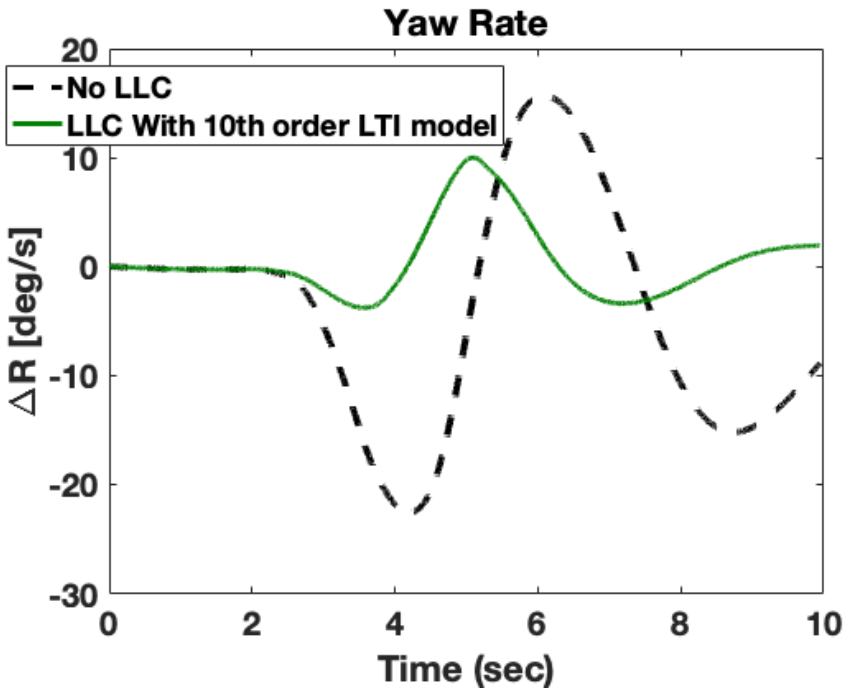

(a)

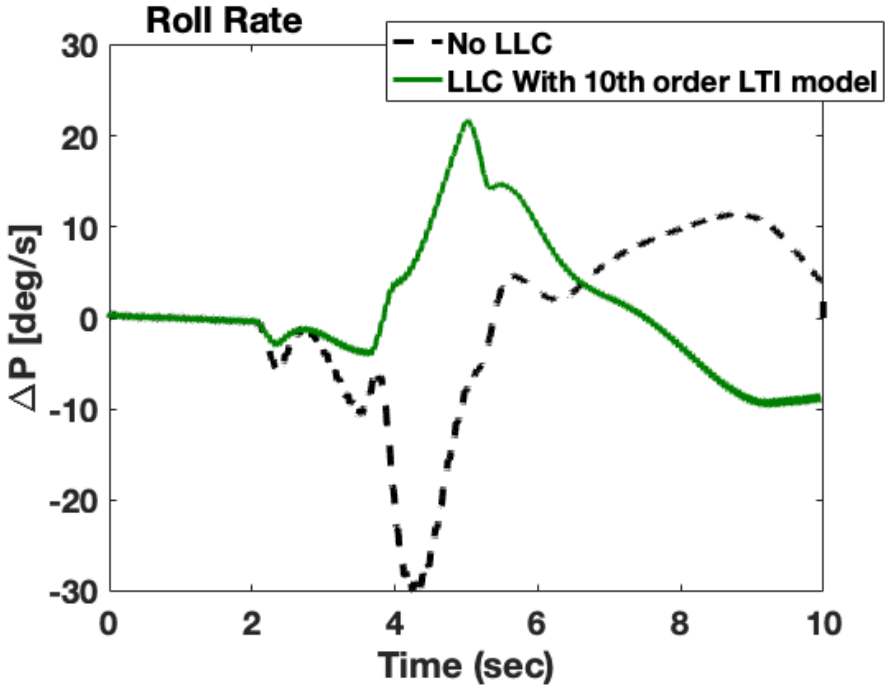

(b)

Figure 3.13: Body angular rate response with and without LLC.

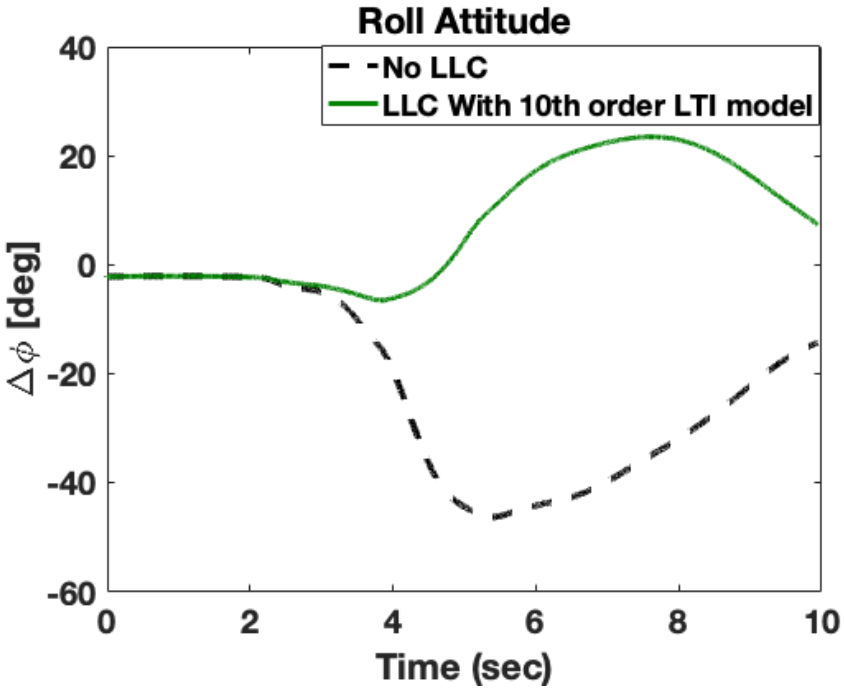

(a)

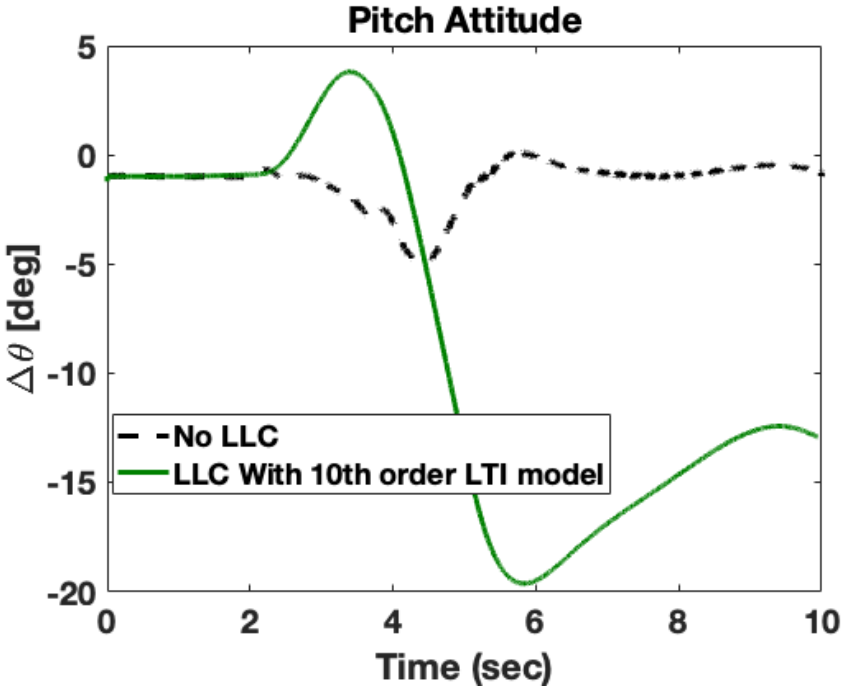

(b)

Figure 3.14: Body attitude response with and without LLC.

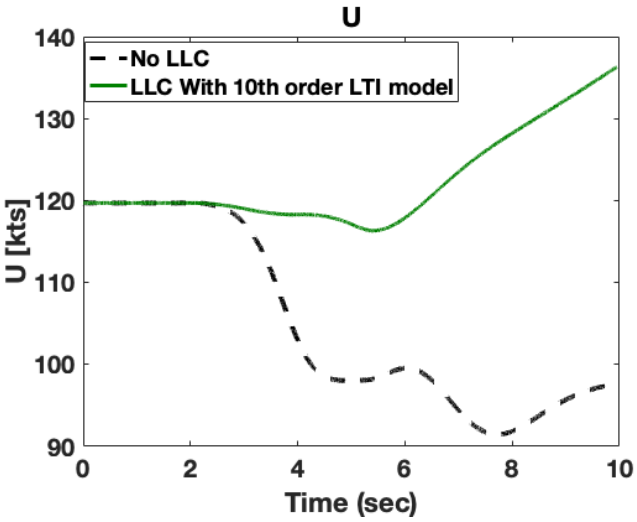

(a)

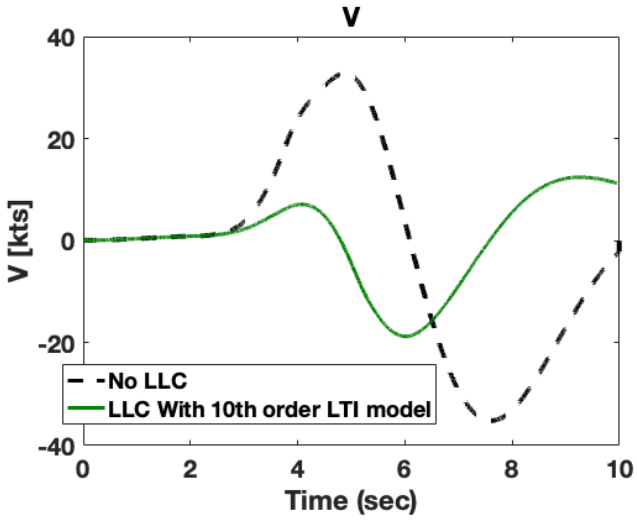

(b)

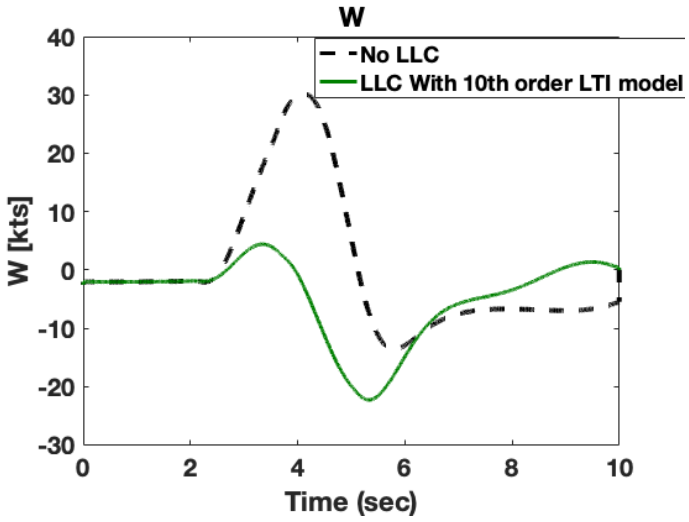

(c)

Figure 3.15: Body velocity response with and without LLC.

3.4 Piloted Simulation Results

This section considers an integration of the LLC scheme with a visual cueing system and piloted simulation evaluations of the resulting architecture. More specifically, the LLC scheme is implemented within the Georgia Tech Re-configurable Rotorcraft Flight Simulator and piloted simulation evaluations are carried out. The real time control margin estimates are provided as visual cues to the pilot for their use in limiting the aggressiveness of the maneuver for a selected value of the rotating pitch link 1/rev harmonic load limit (i.e., 350 lbs).

The Georgia Tech Re-configurable Rotorcraft Flight Simulator is a fixed-base simulator utilizing the cockpit of a OH-58D helicopter. The simulator imagery is generated using the UNIGENE image generation software and displayed onto a 16 feet diameter and 270° screen. The flight dynamics is generated using FLIGHTLAB®. Furthermore, the simulator is equipped with a mechanically linked control system with no advanced features (i.e, no ACAH/RCAH modes). A picture of the simulator is shown in Fig. 3.16.

A former US. Army Black Hawk pilot conducted the piloted study and helped in deciding a visual cue strategy that would lead to minimal effects on the pilot attention and no increase in pilot workload. Based on his comments, the 2D visual cue shown in Fig. 3.17 was implemented.

Figure 3.16: The Georgia Tech Re-configurable Rotorcraft Flight Simulator.

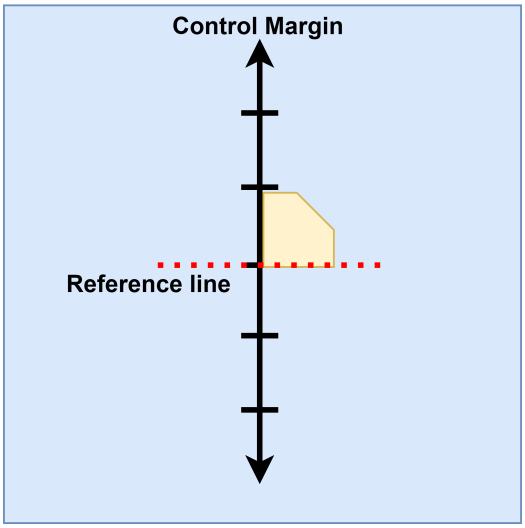

(a) Nominal case with control margin

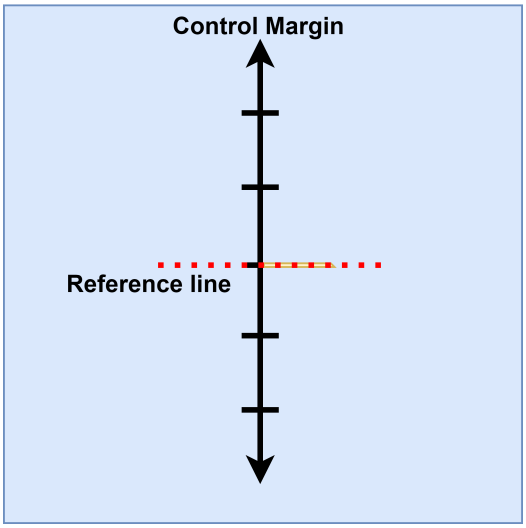

(b) Case with zero control margin

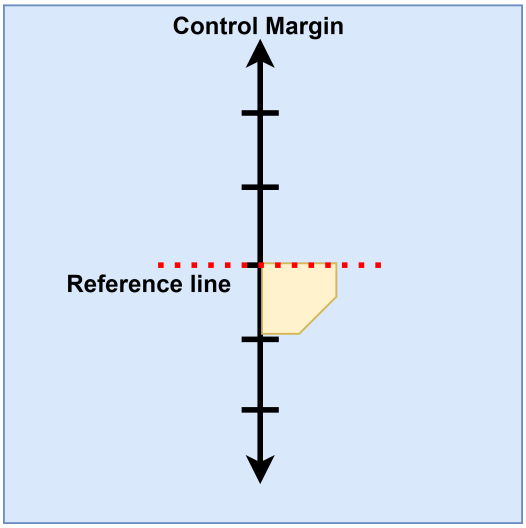

(c) Case with negative control margin

Figure 3.17: 2D visual cue.

The 2D-cue shown in Fig. 3.17 is a vertical bar. One side of the vertical bar is aligned with a fixed reference line, whereas the other side is free to move vertically. Hence, the height of the vertical bar changes with time. The width of the vertical bar is fixed and selected by the pilot to enhance the effectiveness of the visual cue. At each instant in time, the vertical bar enables the pilot to gauge the amount of control deflection required to take the harmonic load of interest from its current value to its limit. When the vertical bar has a height equal to zero (i.e., Fig. 3.17b: both sides of the vertical bar are at the reference

line), the control margin is zero. A zero control margin value implies that the harmonic load (i.e., 1/rev load) is at the load limit. When the vertical bar is below the reference line (i.e., Fig. 3.17c), this implies a negative control margin which represents load exceedance (i.e., the harmonic load exceeded the maximum load value). On the other hand, a positive control margin illustrated by the vertical bar being above the reference line (i.e., Fig. 3.17a) implies that the load limit is not exceeded.

Piloted simulation evaluations were carried out by considering two maneuvers at a forward flight speed of 120 knots in order to assess the effectiveness of the visual cue in limiting maneuver aggressiveness for component load limiting. The first maneuver is a pitch doublet maneuver similar to Fig. 3.5. During this maneuver, the pilot is asked to keep both the collective stick and pedal at their trim value and avoid lateral motion. This is done because the LLC scheme is currently only tuned to act on the longitudinal cyclic channel. Figure 3.18 shows an overlay of the actual longitudinal control input from the pilot and estimated control limit (corresponding to component load limit) as a visual cue to the pilot. The other pilot control inputs are shown in Fig. 3.19. The resulting pitch rate response is shown in Fig. 3.20. In this case, the pilot is asked to ignore the visual cue for load limiting provided to him (i.e., cue-off case), resulting in the rotating pitch link 1/rev load to exceed the selected limit of 350 lbs (shown in Fig. 3.24). In Fig. 3.21, the simulation is repeated, except in this case, the pilot is asked to limit the control input to the estimated control limit provided to him in the form of a visual cue (i.e., cue-on case), resulting in the 1/rev load to be roughly limited to the selected maximum value (shown in Fig. 3.24). The lateral, collective and pedal control inputs from the pilot for the cue-on case are shown Fig. 3.22. The pitch rate response for the case with cue-on is shown in Fig. 3.23. As expected, the vehicle response with cue-on shown in Fig. 3.23 becomes restricted compared to that for the cue-off shown in Fig. 3.20, thus trading vehicle maneuver performance with component load limiting.

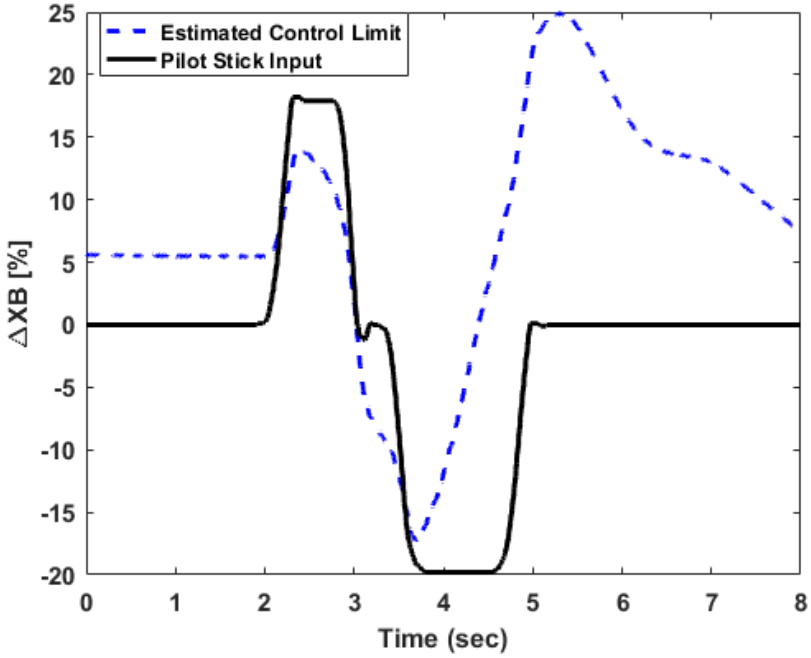

Figure 3.18: Pilot longitudinal stick input with cue-off.

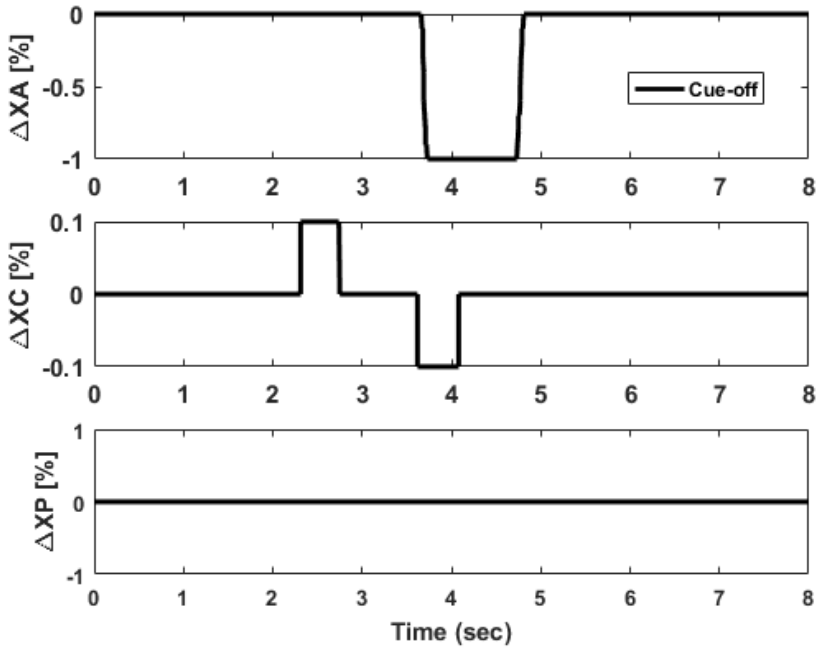

Figure 3.19: Pilot stick input with cue-off.

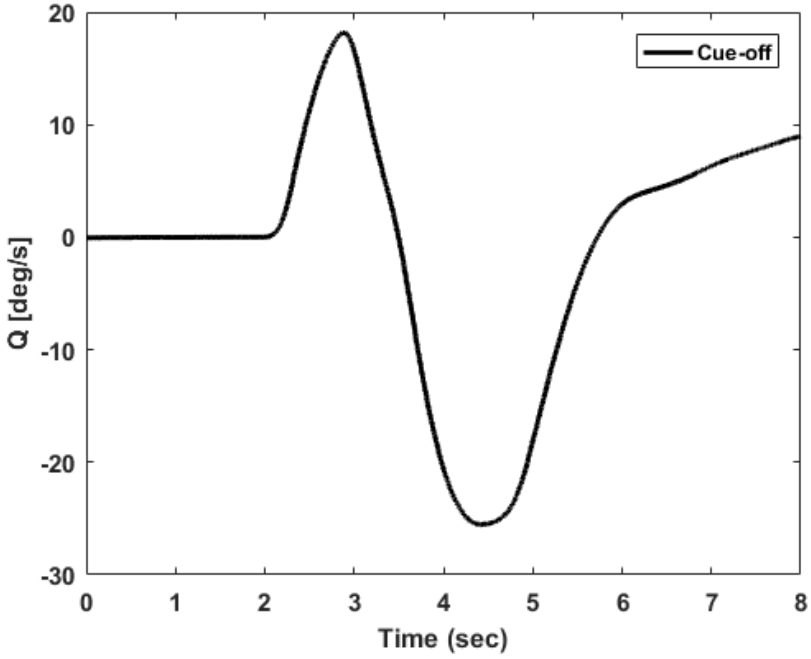

Figure 3.20: Pitch rate response with cue-off

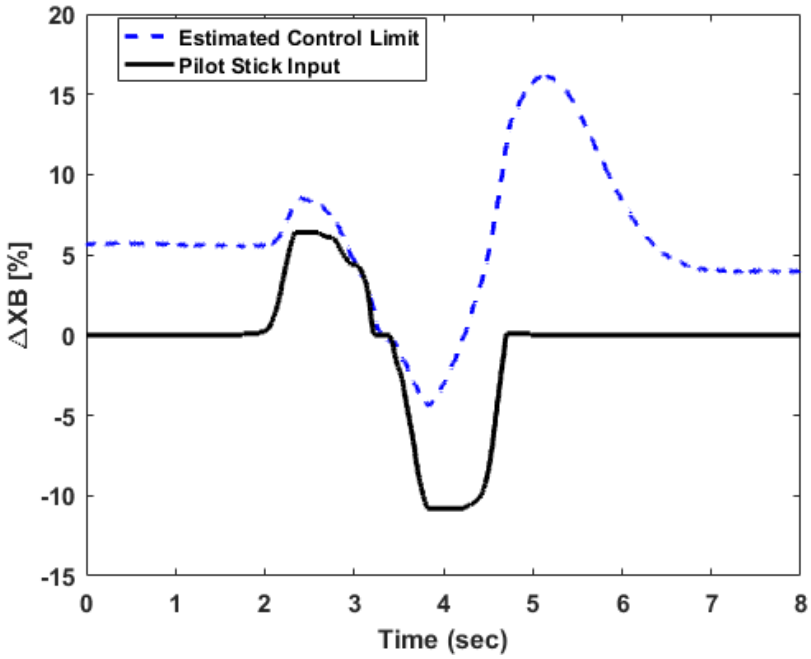

Figure 3.21: Pilot longitudinal stick input with cue-on.

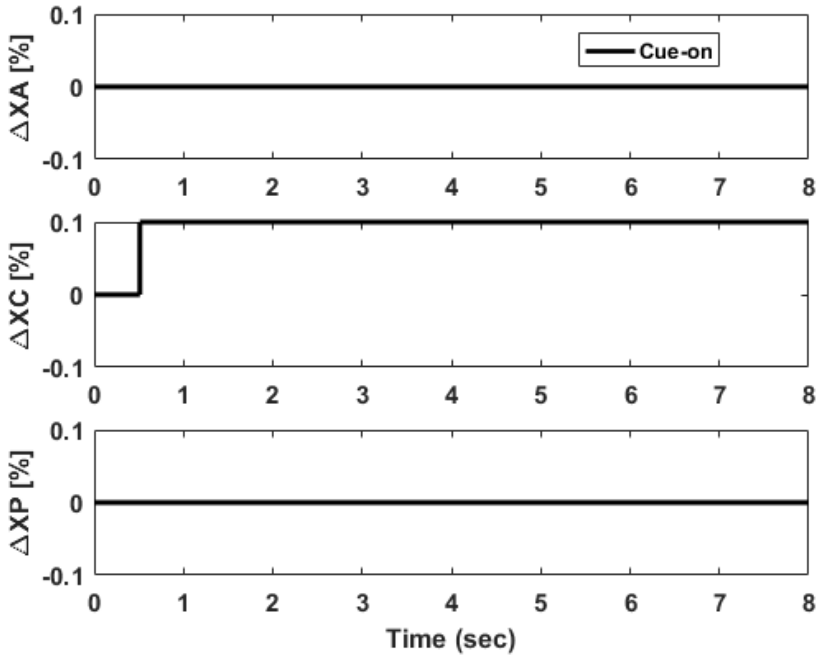

Figure 3.22: Pilot stick input with cue-on.

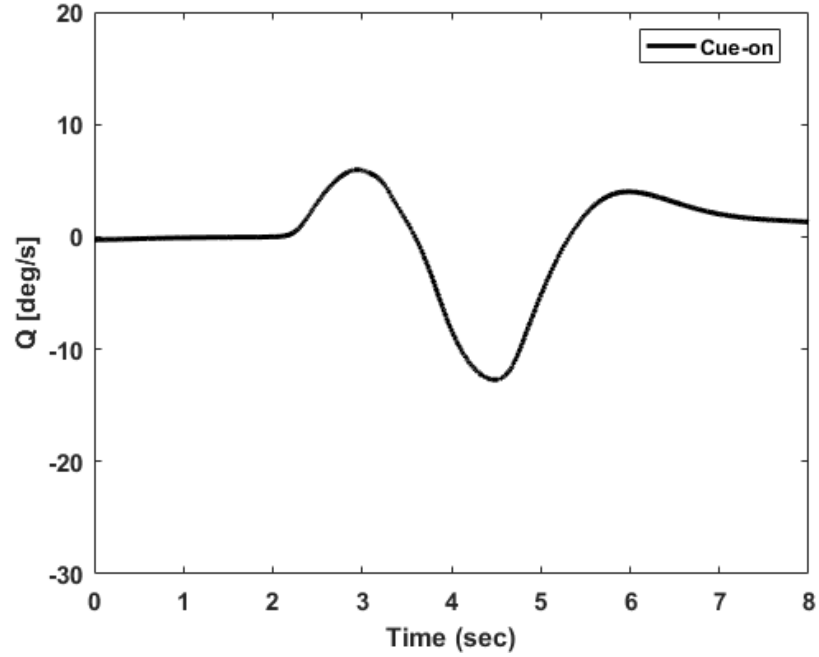

Figure 3.23: Pitch rate response with cue-on

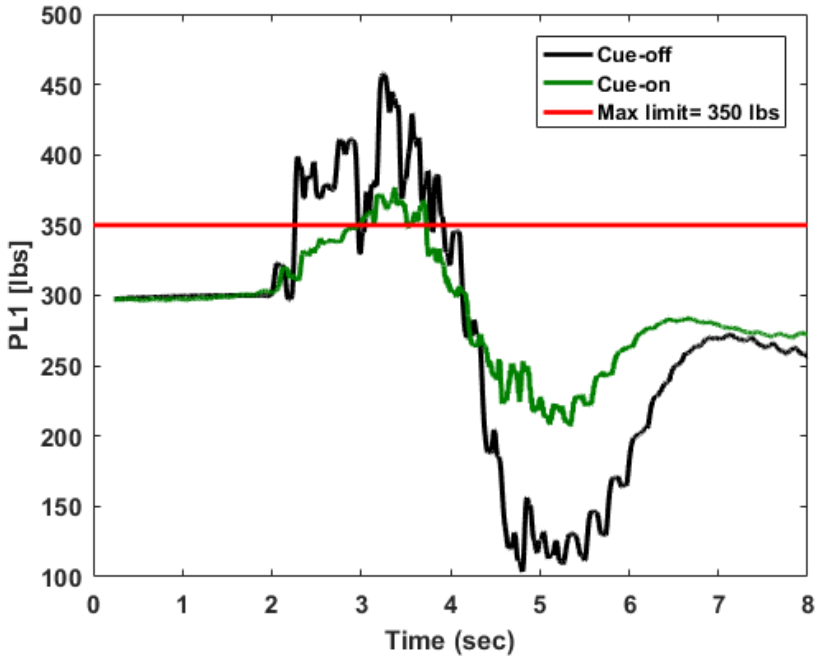

Figure 3.24: Magnitude of 1/rev harmonic pitch link load

The second maneuver is a pull-up maneuver. This maneuver has a duration of 9 seconds and is performed to test the ability of the pilot to track the visual cue. Initially, the pilot is asked to ignore the visual cue (i.e., cue-off case). The pilot is then asked to repeat the same maneuver but this time to pay attention and track the visual cue to the best of his ability (i.e., cue-on case). In Figs. 3.25 and 3.26, an overlay of the actual longitudinal control input from the pilot and estimated control limit as a visual cue to the pilot are shown for the cue-off and cue-on cases, respectively. For the cue-on case, it can be observed that the pilot tracks the visual cues fairly well. One important observation is that when the cue changes rapidly due to vehicle speed changes, the pilot's ability to track the cue slightly degrades. This can be attributed to the time delay inherent in a visual cueing system. For the cue-off case, the pilot control input exceeds the estimated control limit. Figure 3.27 shows the rotating pitch link 1/rev load resulting from both runs. It is notable that when the pilot uses the visual cue, the 1/rev load stays near the load limit. Due to the significant speed

change introduced by the maneuver under consideration, the prediction from the on-board LTI model deteriorates. This explains the noticeable load exceedance for the cue-on case. The LLC scheme developed in this thesis is a fixed-point controller extracted at a true air speed of 120 knots. Therefore, the LLC scheme might not perform well when the aircraft's speed deviates far from 120 knots. Adopting a control scheduling methodology would take into account the variation in operating point, and hence, improve the performance of the LLC scheme.

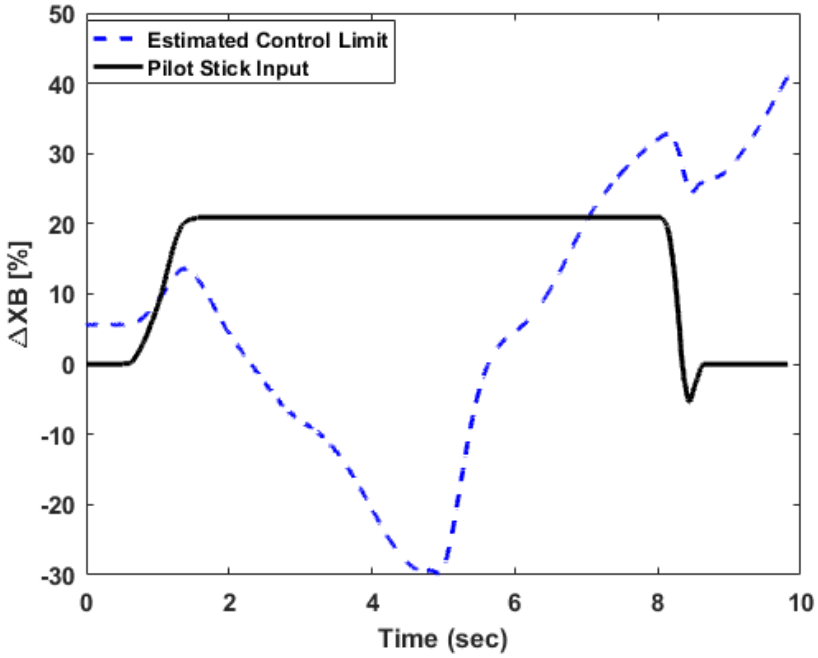

Figure 3.25: Pilot longitudinal stick input with cue-off.

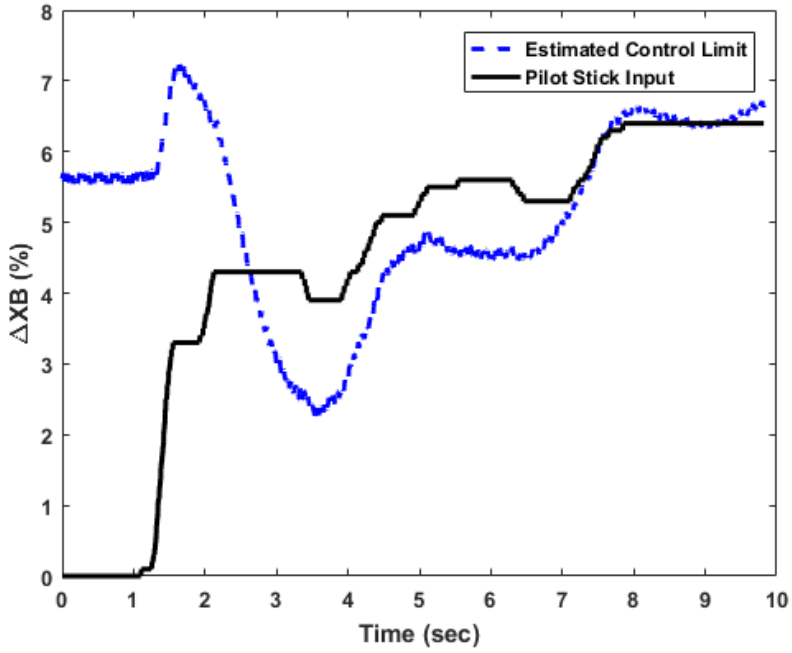

Figure 3.26: Pilot longitudinal stick input with cue-on.

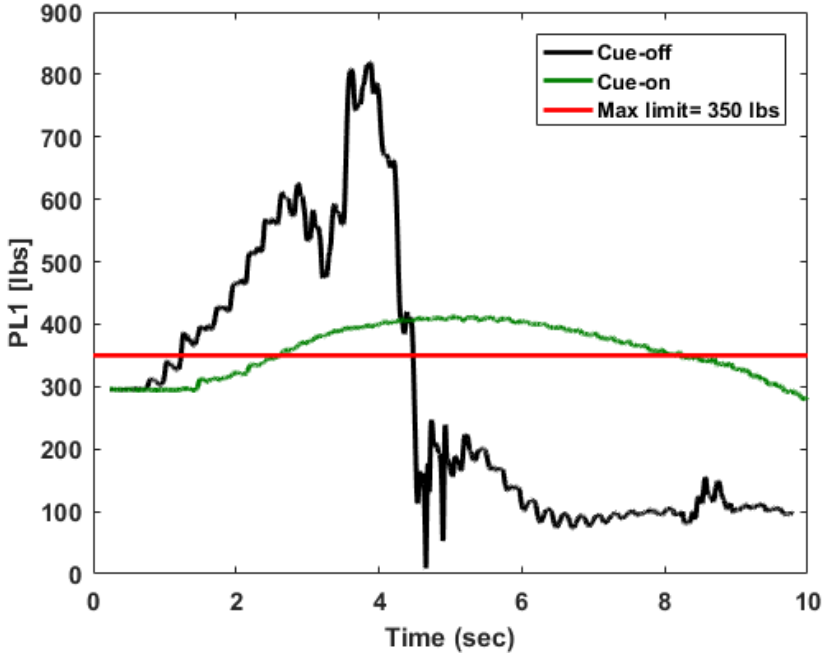

Figure 3.27: Magnitude of 1/rev harmonic pitch link load.

3.5 Summary and Technical Findings

In this Chapter, a novel life-extending control scheme for critical helicopter components is proposed. The scheme is innovative mainly for three reasons. First, it combines concepts from carefree maneuvering and model predictive control theory in the synthesis of a component life-extension control strategy. Second, in light of a new study[81] that shows that different harmonic loads have different impacts on fatigue damage, it is important to determine, in real-time, which harmonic load has the most impact on the fatigue life usage of the component, and then limit such harmonic load during flight. The proposed scheme takes into account the impact of harmonic load on fatigue damage by limiting the most damage-threatening harmonic load to a user selected value. This is the second reason why this scheme is innovative. It is important to note that even though this thesis is not focused on the determination in real-time of the most damage-threatening harmonic load, such a task can be achieved by using a decision-making tool in the form of a damage mitigation control metric [81]. The LLC scheme coupled with this damage mitigation control metric would allow to track and limit in real-time the most damage-threatening harmonic load. Lastly, the proposed scheme is innovative because it trades maneuver performance for component load limiting only during aggressive maneuvers that cause significant fatigue damage and at the pilot's request. This contrasts with current life extending control schemes, such as the load alleviation control scheme, where the trade-off between maneuver performance and load alleviation is always present, irrespective of maneuver aggressiveness.

The proposed scheme was implemented in a high fidelity nonlinear simulation model (i.e., FLIGHTLAB) and evaluated in its ability to limit the magnitude of 1/rev pitch link load during pitch maneuvers in the forward flight regime. The scheme was seen to work well in limiting the magnitude of 1/rev pitch link load to a user prescribed value. One finding was that, using the singular perturbation technique for system order reduction, a computationally simple on-board model can be obtained for online prediction of harmonic

pitch loads. The LLC scheme was integrated with a visual cueing system and the resulting architecture was implemented within the Georgia Tech Re-configurable Rotorcraft Flight Simulator. From the piloted study performed, it was found that the time delay inherent in a visual cueing system can impede the overall performance of an LLC system.

CHAPTER 4

INTEGRATED FLIGHT AND LOAD LIMITING CONTROLLER

This chapter provides an in-depth study of the trade-off between maneuver performance and component load limiting. The interaction between a nonlinear flight controller and the developed real-time component load limiting scheme is explored. The synthesis of an integrated flight and component load limiting controller is achieved via both a command limiting and a control limiting architectures. The resultant flight controllers obtained from this synthesis are used to understand the trade-off between maneuver performance and component load limiting through extensive nonlinear model simulations.

A challenge that comes with the LLC scheme is its integration within an Automatic Flight Control System (AFCS). Such an integration should be done in a way to minimize maneuver performance degradation while performing load limiting.

Rotorcraft are known to exhibit unstable bare-airframe flight dynamics and high inter-axis coupling. The pilot is, therefore, forced to manually suppress the inter-axis coupling and stabilize the aircraft through the use of the 4 primary controls (collective, lateral and longitudinal cyclic, and pedal). The use of an AFCS helps in circumventing these issues. An AFCS is able to eliminate the inter-axis coupling and provide a stable dynamic response. This greatly reduces the pilot workload, hence improving the handling qualities of the vehicle. Given that most helicopters use an AFCS, the integration of the LLC scheme within an AFCS would be of interest. The interaction between the automatic flight control system and LLC scheme is essential in understanding the trade-off between maneuver performance and component load limiting during maneuvering flight. The LLC scheme can be integrated within an AFCS in two ways. One way is through a control limiting architecture ("control limiting LLC") where an estimate of the allowable control travel for each control channel is calculated and used to avoid load exceedance via a constraint imposed on the AFCS output (u) as can be seen in Fig. 4.1. The modeling required to obtain a mapping from the AFCS output (u) to the limit parameter (y_p) is shown in Fig. 4.2. Hence, as can be seen in Figs. 4.1 and 4.2, to generate the allowable control travel estimates, the on-board dynamical model used in the LLC scheme should provide a mapping from the AFCS output (u) to the limit parameter (y_p). An alternative to the control limiting architecture is the command limiting architecture ("command limiting LLC"). In a command limiting architecture, the input to the AFCS is constrained based on allowable command travel estimates computed by the LLC scheme as can be seen in Fig. 4.3. To generate the allowable command travel estimates, the on-board dynamical model used in the LLC scheme should provide a mapping from the controller's input (δ_{cmd}) to the limit parameter (y_p) as shown in Fig. 4.4. It may be noted that, for the LLC via command limiting, the complexity of the on-

board dynamical model is increased with the inclusion of the AFCS. This can drastically increase the computational complexity of the proposed LLC scheme.

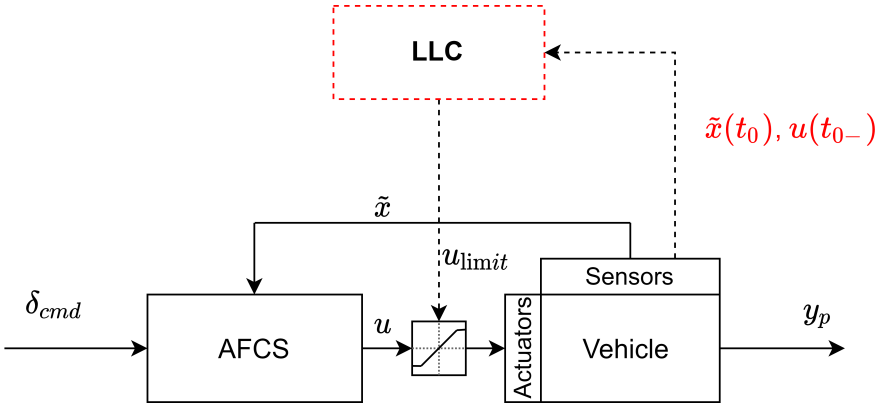

Figure 4.1: Load Limiting via control limiting.

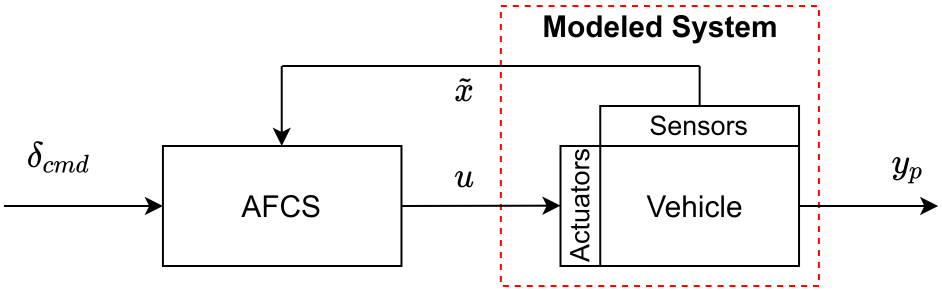

Figure 4.2: On-board model needed for LLC via control limiting.

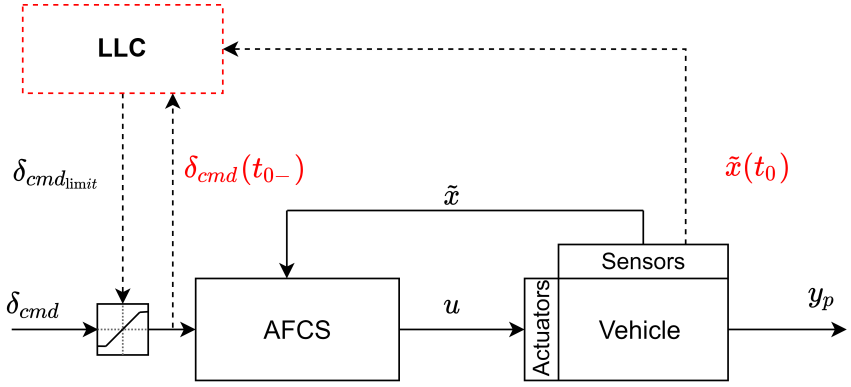

Figure 4.3: Load Limiting via command limiting.

As in the previous chapter, the limit parameter is chosen to be the magnitude of 1/rev harmonic component of the rotating pitch link load. Furthermore, a dynamic inversion controller[77] is used as the flight controller. The dynamics inversion controller of Ref. [77]

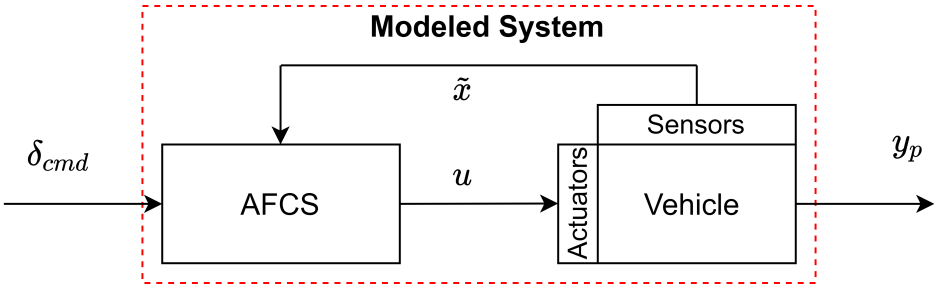

Figure 4.4: On-board model needed for LLC via command limiting.

is augmented with a Damage Mitigation Control (DMC) scheme that limits selected aircraft states such as the pitch rate to indirectly reduce the fatigue damage caused to critical hub components. The dynamic inversion controller considered in this study does not include the DMC scheme.

It is important to note that the proposed load limiting scheme is not limited to this specific choice of limit parameter and flight controller, and a more complicated flight controller as well as a different limit parameter could be used without difficulty. Following is a description of the flight controller used in this study and a detailed development of the component load limiting scheme using control and command limiting architectures.

4.1 Flight Controller

In this section, a description of the flight controller used in this study is presented.

4.1.1 Dynamic Inversion Controller

Rotorcraft flight control design is a very challenging task, mainly because of the strong cross-coupling effects. Dynamic inversion control law provides a suitable solution as it allows for the decoupling of the plant dynamics. Furthermore, dynamic inversion is very attractive as it eliminates the need to gain schedule controllers in order to cover the entire flight envelope[77]. Thus, a dynamic inversion controller is used as the flight controller.

The dynamic inversion controller considered in this study[77] makes use of linearized aircraft dynamics in an inner feedback loop to invert the plant model using feedback lin-

earization. The linear models are generated about different airspeeds ranging from 0 to 160 knots with an increment of 20 knots. A block diagram representation of the controller is shown in Fig. 4.5

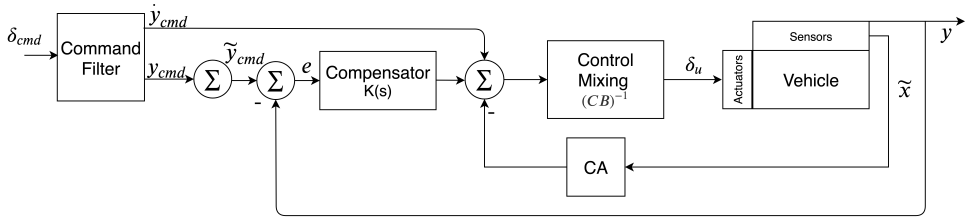

Figure 4.5: Dynamic inversion control law.

In this control architecture, the signal y is forced to follow the reference signal y_{cmd}. A PID controller is used for feedback compensation. The matrices A, B, and C are functions of airspeed, as stated earlier. The transfer function in the command filter dictates the desired dynamics of the closed-loop or the nature of the desired response type. One instance of response type is Attitude Command/Attitude Hold (ACAH). ACAH response relates a pilot stick displacement to a vehicle attitude. Another response type is Rate Command/Attitude Hold (RCAH). RCAH response relates a pilot stick displacement to a vehicle angular rate. The selection of the response type heavily depends on the usable cue environment[84] (UCE).

It is important to note that the command model has design parameters that are tuned manually to meet desired aircraft response to piloted inputs as characterized by ADS-33 requirements[84].

4.1.2 Integral Anti-Windup Scheme

As stated before, the integration of the LLC scheme within an AFCS should be done in a way to minimize maneuver performance degradation while performing load limiting. A drawback of using a control limiting LLC is that due to the contradictory nature of the constraints placed on the flight and the load limiting controllers, the maneuver performance can be severely affected[85]. For the control limiting LLC case, the battle between the

flight and the load limiting controllers can cause the well-known phenomenon of integral windup, also known as integrator windup[40, 86–88]. The integral windup effect is a non-linear phenomenon that is common to controllers with PID feedback compensation. It is attributed to a saturation at the actuator level. Due to the saturation, the nominal input commanded by the PID controller cannot be achieved; therefore, the feedback path is broken, which essentially leaves the controller to operate in open-loop. Applied to the context of the control limiting LLC, as the load limiting controller changes the aircraft's response to keep the load within the selected maximum value by limiting the control effector commands, the flight controller tries to force the response to follow the reference trajectory; this could essentially cause input saturation (i.e., the output of the flight controller and the input to the vehicle are inconsistent), which forces the flight controller to operate in open-loop. During input saturation, the error (e) accumulates, which in turn leads to a large increase of the integral of the error (i.e., the integral term becomes very large). As a consequence of such a phenomenon, the system experiences large overshoot and poor transient response.

An anti-windup scheme is a system that is added to the original flight controller in order to prevent the integral windup phenomenon; the scheme functions by preventing the integral term of the error from building up excessively. Various anti-windup schemes have been proposed in the literature[31–34]. These schemes can be categorized into two groups, namely, conditional integration and back-calculation. Conditional integration-based anti-windup schemes freeze the integral compensation when a certain set of conditions are met (i.e., set of conditions that predict the onset of input saturation). On the other hand, back calculation-based anti-windup schemes make use of the difference between the desired and the actual control input as a feedback signal to the integral term.

Among anti-windup schemes, one based on conditional integration has been found to work best[88]. Such an anti-windup scheme is depicted in Fig. 4.6. As can be seen in Fig. 4.6, the integral compensation is stopped when two conditions are met simultaneously:

1. The controller saturates.

2. The system error and the uncontrolled input have the same sign.

i.e., if $u(t) \neq u_s(t)$ & $e(t).u(t) > 0 => K_I = 0$

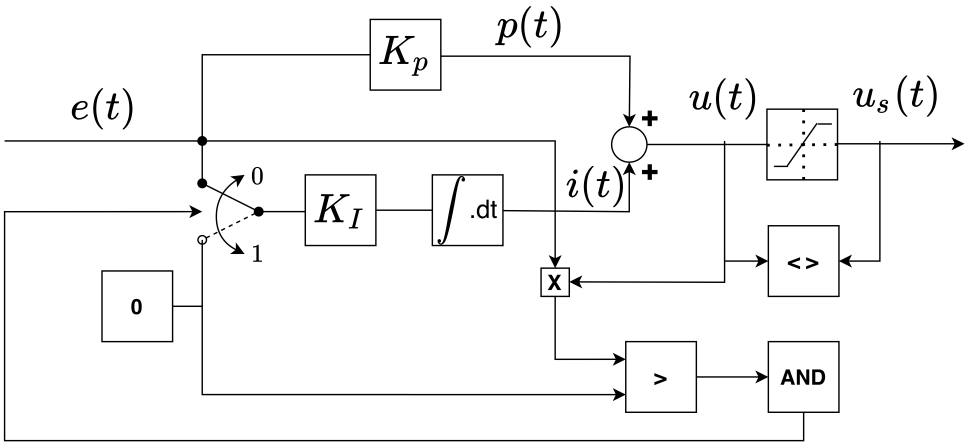

Figure 4.6: Integral Anti-Windup Scheme.

The anti windup scheme presented in Fig. 4.6 is implemented in the dynamic inversion controller to avoid feedback integrator windup that would be caused as a result of the interaction between the flight controller and the LLC scheme.

4.2 Control Limiting LLC

The control limiting LLC makes use of the on-board 10^{th} order LTI model to compute, at each instant in time, future extremal control input that would result in the component load reaching its limit boundary without exceeding it. The 10^{th} order LTI model provides a means of obtaining a mapping from u to y_p (see Fig. 4.2). The calculated extremal control inputs are then used as bounds on the control effector commands. A block diagram representation of the LLC scheme integrated within the dynamic inversion controller via a control limiting architecture is shown in Fig. 4.7.

In Fig. 4.7, $x(t_0)$ represents the current values of the reduced order LTI model state vector and $\delta\tilde{u}(t_{0-})$ represents control vector prior to input at t_0. The control limiting LLC

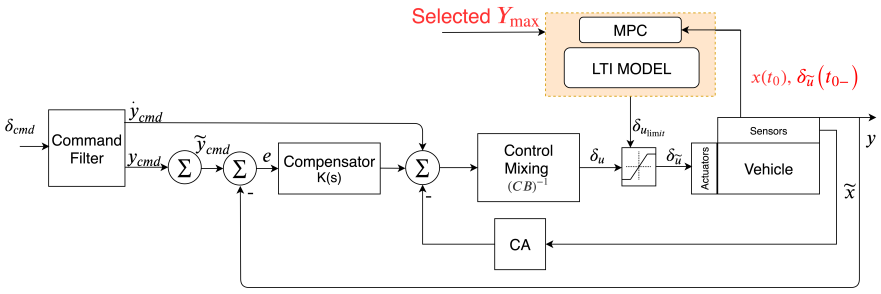

Figure 4.7: Dynamic Inversion control law with control limiting LLC.

scheme calculates the extremal control input by solving, on-line, at each instant in time a constrained optimization problem of a quadratic cost function using the reduced order LTI model. Such a constrained optimization problem is posed in Eqs. (3.14), (3.15), (3.16) and (3.17)

The solution to this problem provides estimates of the control margin boundaries (i.e., extremal control input estimates) associated with pitch link load limits.

4.3 Command Limiting LLC

For the command limiting architecture, the on-board dynamical model needs to provide a mapping between δ_{cmd} and y_p (see Fig. 4.4). The following provides a formulation of the on-board dynamical model for the command limiting LLC. Then the derived on-board model is used to give a mathematical formulation of the command limiting LLC. The on-board dynamical model uses the 10^{th} order LTI model as a representation of the truth bare-airframe vehicle dynamics (see Eqs. (3.5) and (3.9)).

Let the flight controller dynamics be represented in the following form:

$$\dot{x}_c = f(x_c, x_s, \delta cmd) \tag{4.1}$$

$$\delta u = g(x_c, x_s, \delta cmd) \tag{4.2}$$

where x_c is the flight controller's state vector, δu and δ_{cmd} are chosen to be the controller's output and input, respectively (see Fig. 4.5). Equations (4.1) and (4.2) can be combined with the 10^{th} order LTI model for the determination of command margin as follows:

$$\|Y_{harm}\|_2 = \sqrt{(y_{1c_{(trim)}} + \Delta y_{1c})^2 + (y_{1s_{(trim)}} + \Delta y_{1s})^2} \tag{4.3}$$

where

$$\Delta y_{1c} = [\hat{C}_{1c}]X_s + [\hat{D}_{1c}]g(x_c, x_s, \delta cmd) \tag{4.4}$$

$$\Delta y_{1s} = [\hat{C}_{1s}]X_s + [\hat{D}_{1s}]g(x_c, x_s, \delta cmd) \tag{4.5}$$

$$\dot{X}_s = [\hat{A}]X_s + [\hat{B}]g(x_c, x_s, \delta cmd) \tag{4.6}$$

The model predictive control formulation can be expressed as follows:

$$min_{\delta cmd}[J], J = \int_{t_0}^{t_o+T_p} L_{cmd}(\|Y_{harm}\|_2, \delta cmd)dt \tag{4.7}$$

subj:

$$\dot{X}_s = [\hat{A}]X_s + [\hat{B}]g(x_c, x_s, \delta cmd) \tag{4.8}$$

$$\dot{x}_c = f(x_c, x_s, \delta cmd) \tag{4.9}$$

$$\|Y_{harm}\|_2 \leq y_{max} \tag{4.10}$$

$$\delta cmd_{min} \leq \delta cmd(t_{0-}) + \delta cmd \leq \delta cmd_{max} \tag{4.11}$$

The cost function integrand is defined as follows:

$$L_{cmd}(\|Y_{harm}\|_2, \delta cmd) = (\|Y_{harm}\|_2 - y_{max})^T Q(\|Y_{harm}\|_2 - y_{max}) + (\delta cmd - \delta cmd(t_{0-}))^T R(\delta cmd - \delta cmd(t_{0-})) \tag{4.12}$$

where Q and R are symmetric positive definite matrices of design coefficients that penalize the limit parameter tracking error in reaching its limit boundary in the selected time horizon, T_p, and command activity, respectively. As defined before, y_{max} is a user selected value of pitch link harmonic load limit. A block diagram representation of the LLC scheme integrated within the dynamic inversion controller using a command limiting architecture is shown in Fig. 4.8.

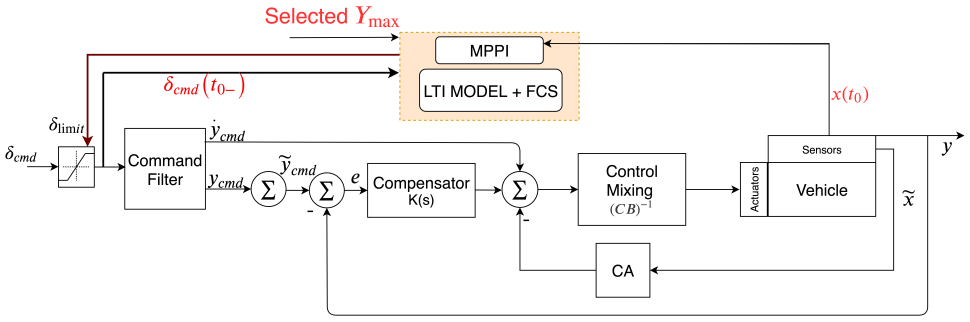

Figure 4.8: Dynamic inversion control law with command limiting LLC.

Solving in real-time the optimization problem posed in the control limiting LLC for the determination of allowable control travel estimates could be done using the convex scheme described in the previous chapter of this thesis. However, it is important to note that the convexification of the problem relies heavily on the ability to obtain an accurate linearized expression for the selected limit parameter,$\|Y_{harm}\|_2$. For low frequency loads such as the 1/rev pitch load, such a linear approximation can be obtained. For higher-harmonic loads (i.e., N/rev Pitch Link load; N=2,3,4, etc.) an accurate linearized expression might not be obtainable. This is due to the fact that the dynamics of such higher-harmonic loads are more driven by secondary effects. As for the command limiting LLC, solving the optimization

problem posed for the determination of allowable command travel estimates is difficult and cannot be done using the convex scheme. This is attributed to the fact that the on-board dynamical model (flight controller + bare-airframe model) is nonlinear and its complexity highly depends on the complexity of the vehicle as well as of the flight controller models. An attempt to use a linearization method to remove the nonlinearity might be a solution for some special cases where the flight controller is simple. However, if the flight controller is very complicated and highly nonlinear, such a method might not work. In order to circumvent these obstacles, it is important to have an optimizer that can be used to solve such optimization problems (i.e., for the command and control limiting LLC) no matter the complexity of the flight controller, vehicle dynamics, and parametric expression of the selected harmonic load. An implicit optimization technique from the literature[89–91] called the Model Predictive Path Integral (MPPI) method is a potential candidate.

4.4 MPPI Approach for Optimization

Model predictive control scheme heavily depends on explicit optimization. However, that dependence on explicit optimization is the source of major drawbacks. One significant challenge with explicit optimization is its inability to handle complex system models without a significant sacrifice in solution fidelity [89]. In order to overcome the challenges that come with explicit optimization, indirect methods such as Model Predictive Path Integral (MPPI) approach [90] have been used. MPPI approach is based on implicit optimization where the solution to the optimization problem is obtained via an averaging of multiple (of the order of 1000) stochastic sample of trajectories. The parallel computing capability of such a technique is a huge benefit for real-time implementation.

The MPPI methodology has been successfully proven to work in shipboard landing problems [89, 91] where the goal was to use an implicit optimization technique for trajectory guidance. The current study adapts the MPPI approach towards the development of a control and command limiting LLC scheme. More specifically, the MPPI implicit opti-

mization is used to solve the optimization problems posed in Eq. (3.14) through Eq. (3.18) and Eq. (4.7) through Eq. (4.12).

The following section reformulates the optimization problems to a form that is suitable for the implicit optimization algorithm. Since implicit optimization techniques cannnot handle equality and inequality constraints, this formulation drops the inequality and equality constraints given in Eq. (3.15) through Eq. (3.17) and Eq. (4.8) through Eq. (4.11). Dropping the equality constraints (i.e., Eqs. (3.15), (4.8) and (4.9)) does not affect the posed optimization problems, as those equations are associated with the dynamics of the on-board model and therefore are part of the structure imposed on the problems already. Furthermore, this formulation can easily drop the inequality constraint associated with the control and command input bounds (i.e., Eqs. (3.17) and (4.11)) since direct access to them is possible when using an implicit optimization method. The inequality constraints on the limit parameter (i.e., Eqs. (3.16) and (4.10)) are treated as soft limits by the quadratic cost terms in Eqs. (3.18) and (4.12). Hence, when those inequality constraints are not considered, solutions with slight load limit violations can be obtained. In this study, slight load exceedance is acceptable since the user defined maximum limit is a soft limit rather than a hard limit. The resultant optimization problems for the command and control limiting LLC are posed as follows, respectively:

$$min_{\delta cmd}[J], J = \int_{t_0}^{t_o+T_p} L_{cmd}(\|Y_{harm}\|_2, \delta cmd)dt \tag{4.13}$$

$$min_{\delta u}[J], J = \int_{t_0}^{t_o+T_p} L_{ctrl}(\|Y_{harm}\|_2, \delta u)dt \tag{4.14}$$

With both optimization problems reformulated in a form that is suitable for the MPPI algorithm, attention is turned to how the MPPI algorithm is used to arrive at a solution to the optimization problems posed in Eqs. (4.13) and (4.14). The following describes the MPPI approach with a special focus on the command limiting LLC. The exact same procedure is

valid for the control limiting LLC. The MPPI approach determines an optimal command based on the evaluation of a well-defined performance measure using an on-board model. Using an initial estimate δcmd for the command vector over t_0 to t_0+T_p, several sample command vectors (δcmd_i) are constructed as random perturbations ($d\delta cmd$) from the initial command vector.

$$\delta cmd_i = \delta cmd + d\delta cmd_i \tag{4.15}$$

i=1 to M

In the equation above, M is the total number of sample command vectors. For each δcmd_i, the corresponding sample limit parameter is obtained using the on-board model, and simultaneously, the chosen performance index (J_i) for the sample limit parameter is evaluated. Following that, the updated command vector δcmd_p is obtained using the weighted averaging of the random perturbations ($d\delta cmd_i$)

$$\delta cmd_p = \delta cmd + \frac{1}{M}\sum_{i=1}^{M}[(d\delta cmd_i)e^{-J_i}] \tag{4.16}$$

It is important to note that the inclusion of the exponential weighting leads to a command update δcmd_p which is heavily biased towards command vectors with lower cost values J_i, and hence, implicitly forcing δcmd_p towards the optimal solution. The procedure described above is repeated by replacing δcmd in Eq. (4.15) with the command update from Eq. (4.16) . At each instant, the procedure used by the MPPI algorithm in order to calculate an estimate of the command limit can be summarized as:

1) Generation of random command vectors and the corresponding limit parameter vectors

2) Evaluation of the performance measure (J_i) for each command vector

3) Stochastic averaging to obtain updated command

Commands which yield very large cost function value are rejected for solution conver-

gence. Hence, it can be easily seen that the exponential averaging performed in Eq. (4.16) enhances the rate of convergence of the algorithm. Typically, the optimal command can be reached within two or three iterations [89]. As stated earlier, the exact same procedure is valid for the control limiting LLC.

The MPPI algorithm for command margin estimation described above is presented in Algorithm 1.

Algorithm 1: MPPI for Component Load Limiting

Result: Command Margin

Number of sample command vectors: M;

Define max limit: y_{max};

Define epsilon: ϵ;

Assume initial solution: δ_{cmd};

while $|\ y_p\text{-}y_{max}| > \epsilon$ **do**

1- Apply random perturbations: $\delta_{cmd_i} = \delta_{cmd} + d\delta_{cmd_i}$*;*

2- Use on-board model to evaluate performance index: J_i*;*

3- Perform exponential weighting: $\delta cmd_p = \delta cmd + \frac{1}{M}\sum_{i=1}^{M}[(d\delta cmd_i)e^{-J_i}]$*;*

if $\#$ *of rejected commands* $> 90\%$ **then**

4- Increase perturbation magnitude;

5- Go to Step 1;

end

5- Use on-board model to compute limit parameter: y_p*;*

6- $\delta_{cmd} \leftarrow \delta cmd_p$

end

4.5 Performance Evaluation of Integrated Flight and Load Limiting Controller

This section presents an investigation of the performance of the dynamic inversion controller with control and command limiting LLC . Specifically, limiting of the 1/rev pitch link load is considered. Moreover, the impact of such load limiting on the maneuver performance for both command and control limiting architectures is also investigated. For this study, the prediction horizon (T_p) is arbitrarily set to 0.0065 seconds. Likewise, the number of command vectors (M) and perturbations ($d\delta cmd_i$) are set to 1500 and 10%, respectively. For both command and control limiting architectures, the on-board model uses the 10^{th} order LTI model. For simulation evaluation purposes, the high fidelity full vehicle nonlinear model (NL) in FLIGHTLAB®, from which the higher order LTI model is generated, is used as the vehicle truth model. Two maneuvers were conducted. The first maneuver is an attitude command maneuver where the flight controller is set to give an Attitude Command/Attitude Hold (ACAH) response in the pitch axis. The second maneuver is a rate command maneuver where the flight controller is set to give a Rate Command/Attitude Hold (RCAH) response in the pitch axis. The LLC scheme applies bounds, based on the MPPI solution, to the input coming out of the flight controller for the case where a control limiting architecture ("control limiting LLC") is used while the bounds are applied to the command input going into the flight controller for the case where a command limiting architecture ("command limiting LLC") is selected. To avoid confusion, the load limiting controller via control limiting is denoted as "control limiting LLC" and the load limiting controller via command limiting is denoted as "command limiting LLC". Furthermore, when no command limiting nor control limiting is used, this case is denoted as "No LLC".

4.5.1 Performance of the Flight Controller

In order to test the attitude command/attitude hold and rate command/attitude hold capabilities of the dynamic inversion controller, simulation with LLC turned off ("No LLC")

is first considered. For the attitude and rate command maneuvers, the transfer function in the command model is appropriately selected to give an attitude command/attitude hold or a rate command/attitude hold response type. For the attitude command maneuver, the longitudinal cyclic stick input from the pilot is taken to be desired pitch attitude command input. The attitude command is tested first. Figure 4.9 shows the pilot stick command, the commanded attitude and the resulting vehicle (NL-model) attitude. As a result of the step input command from the pilot, the vehicle is commanded to reach a specified attitude and hold it approximately constant until removal of the step input. This is indeed the case as the vehicle pitch attitude is seen to converge to the desired attitude. Figure 4.9 also shows the pitch attitude response prediction from the on-board 10^{th} order model. It is also important to note that subsequent to the start of the pilot stick command, the vehicle attitude is approximately constant (about 20 deg) between 6 and 12 seconds following the step input. Therefore, it may be concluded that the dynamic inversion controller provides a response that can be characterized as an attitude command/attitude hold response-type in the pitch axis[92]. Figure 4.10 shows the reference blade root pitch link 1/rev load magnitude resulting from the pitch attitude command of Fig. 4.9.

For the rate command maneuver, the pilot control input is taken to be pitch rate command as shown in Fig. 4.11. The doublet input has a duration of 2 seconds. Similar to the previous maneuver case, the rate command/attitude hold capability of the dynamic inversion controller is tested first by turning off the LLC ("No LLC"). As a result of the rate command doublet, the vehicle is commanded to reach a specified pitch rate as can be seen in Fig. 4.11. Figure 4.11 also shows the pitch rate response prediction from the on-board 10^{th} order model. Figure 4.12 shows the reference blade root pitch link 1/rev load magnitude resulting from the command doublet input of Fig. 4.11. The pilot commands a pitch rate doublet of $\pm$ 28 deg/s while the vehicle reaches a maximum pitch rate of 26 deg/s and -28 deg/s approximately for both vehicle models. From this analysis, it can be concluded that the dynamic inversion controller performs reasonably well and that the on-board 10^{th}

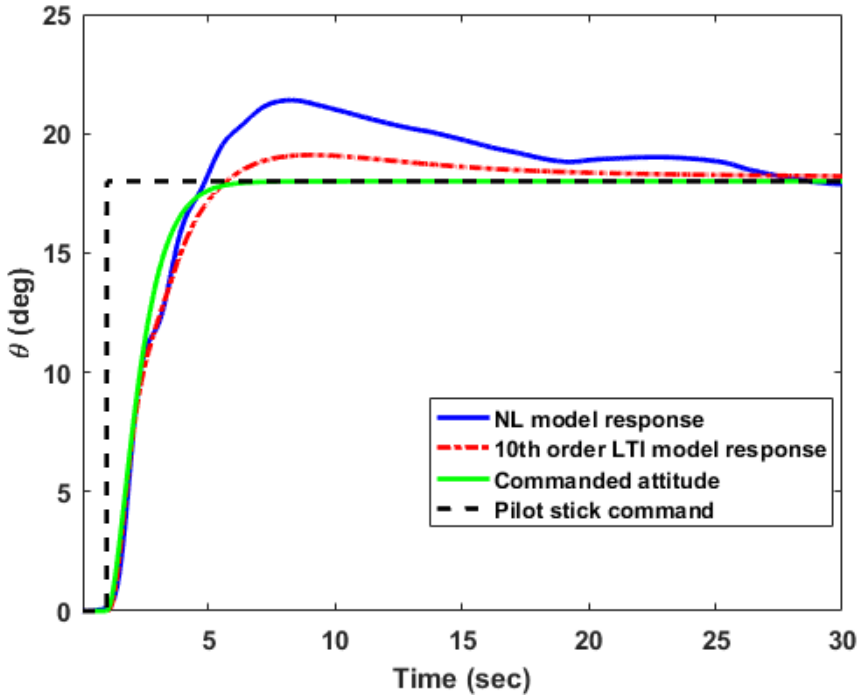

Figure 4.9: Body pitch attitude response comparison between pilot stick command and vehicle response.

order model captures the 1/rev pitch link load reasonably well.

The following section investigates the performance of the control and command limiting LLC for both the rate command/attitude hold and attitude command/attitude hold maneuvers. The limit for the pitch link 1/rev load magnitude is arbitrarily set to 350 lb.

4.5.2 Results

As mentioned in earlier sections, two maneuvers are considered:

1. Attitude command.

2. Rate command.

The control and command limiting LLC schemes are achieved by using the controllers in Figs. 4.7 and 4.8, respectively.

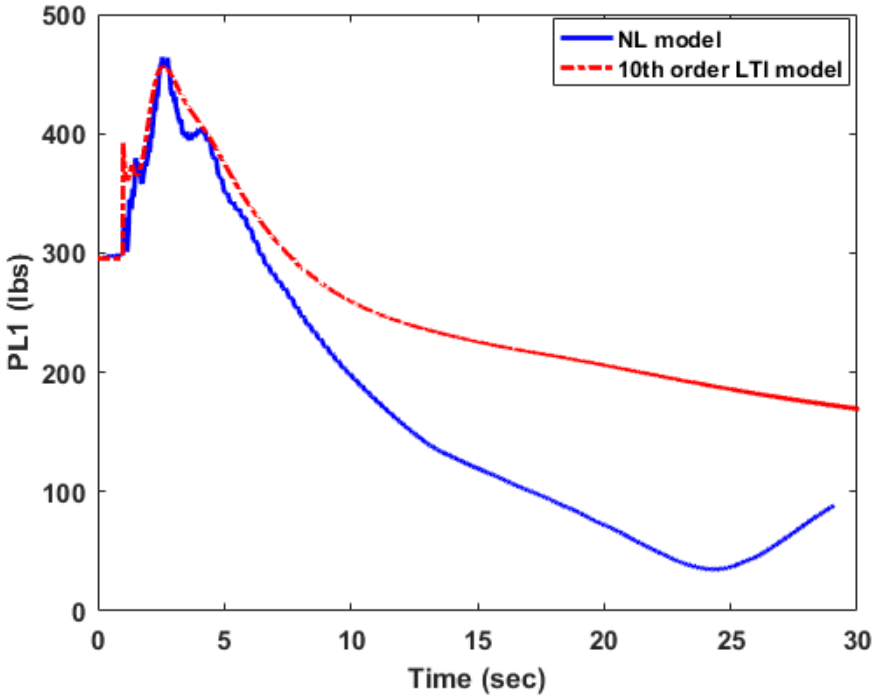

Figure 4.10: Variation of 1/rev harmonic component of reference blade pitch link load without LLC.

Attitude Command Maneuver:

Simulation results of the reference blade root pitch link 1/rev load magnitude without LLC (labeled 'No LLC'), with control limiting LLC, and with command limiting LLC are shown in Fig. 4.13. It can be observed from Fig. 4.13 that the 1/rev magnitude of the pitch link load stays within the selected 350 lb for both command and control limiting LLC. However, slight load exceedance is noticeable. This can be attributed to two factors. Firstly, even though the reduced order LTI model used in the formulation of the proposed LLC scheme can be used for real-time component load estimation, the estimated loads may have to be corrected for error due to LTI model approximation and nonlinearities[40–42]. As such, to a large input, the on-board linear model may lose fidelity. Secondly, the MPPI algorithm treats the limit parameter as a soft limit rather than a hard one. It is therefore normal to expect some limit exceedance. Nevertheless, the command and control limiting LLC are seen to perform well at limiting the magnitude of 1/rev pitch link load as very negligible

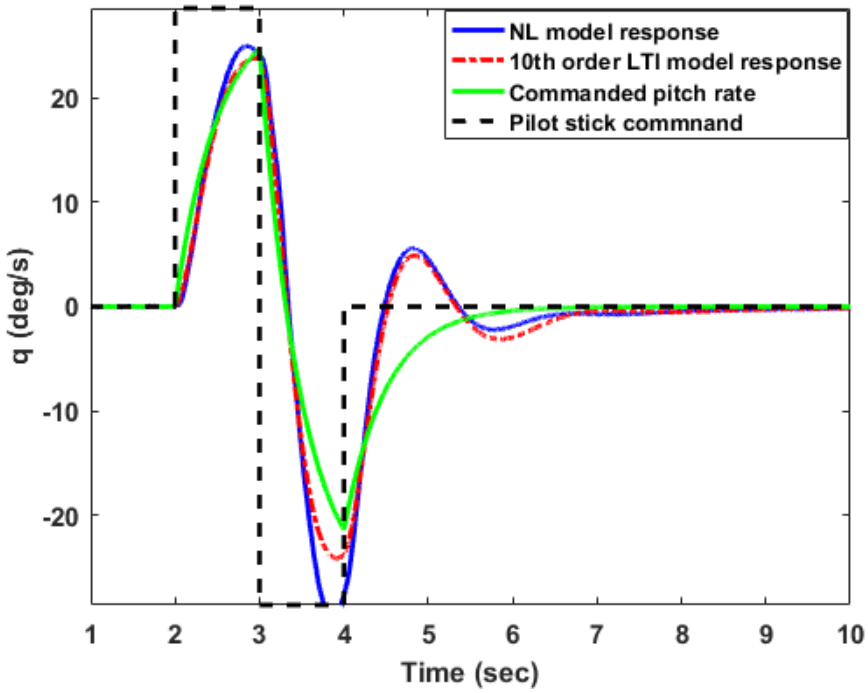

Figure 4.11: Body pitch rate response comparison between pilot stick command and vehicle response.

limit exceedance is observed.

The effect of the load limiting control strategy via command and control limiting on the helicopter maneuver performance can be illustrated by comparing the achieved pitch attitude for the cases with command limiting LLC, with control limiting LLC and without LLC.

Figure 4.14, where the pitch attitude variation with command limiting LLC, with control limiting LLC and without LLC are compared, shows that with both command and control limiting LLC, the desired pitch attitude is achieved. The trade-off between load limiting and maneuver performance resides in the time needed to reach the desired attitude. For both command and control limiting LLC, the maneuver aggressiveness is limited in order to limit the resulting 1/rev magnitude of pitch link load, which, in turn, causes the desired pitch attitude to be reached with some delay.

It is important to note that with the addition of the integrator anti-windup scheme in the

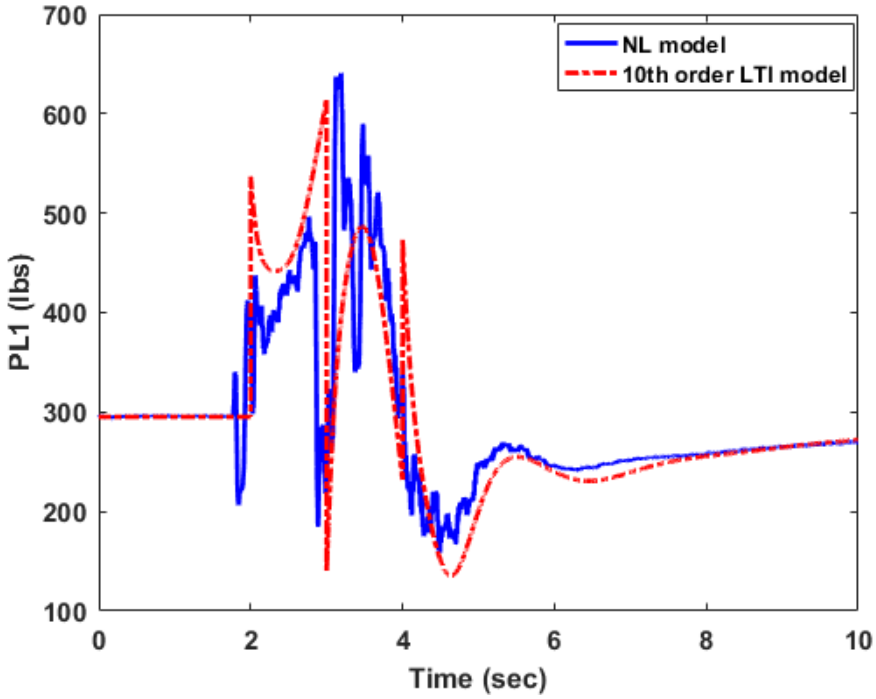

Figure 4.12: Variation of 1/rev harmonic component of reference blade pitch link load without LLC.

flight controller, the control limiting LLC does not lead to large attitude overshoot. The anti-windup scheme resolves the integrator windup issue highlighted in Ref. [85], where large attitude overshoot was observed as a result of the conflict between the flight and load limiting controllers for the control limiting LLC architecture. Therefore, it is crucial to embed an anti-windup scheme within the flight controller when using a control limiting architecture. Figure 4.15 (where the longitudinal cyclic control input variation with command limiting LLC, with control limiting LLC, and without LLC are compared) shows that, for both control and command limiting LLC schemes, the longitudinal cyclic control input is modified to allow the pitch link load to remain within the selected limit of 350 lb.

Another important observation is that the command and control limiting LLC schemes introduce some oscillations (i.e., chattering) near the limit boundary (see Fig. 4.13) which in turn affect the vehicle pitch attitude response (see Fig. 4.14). This phenomenon is more apparent for the command limiting LLC. This chattering phenomenon is a known issue in

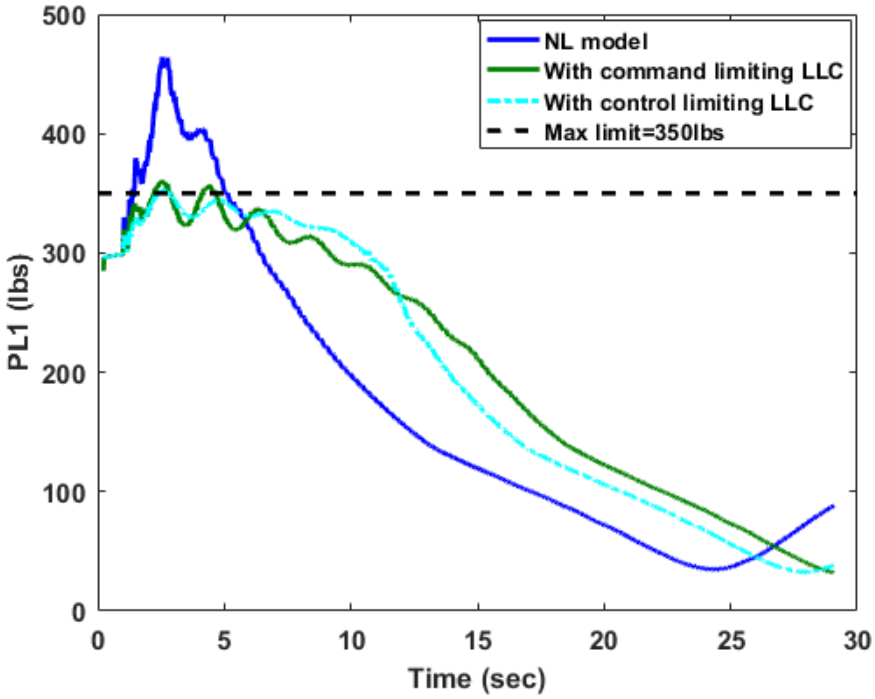

Figure 4.13: Variation of 1/rev harmonic component of reference blade pitch link load with and without LLC.

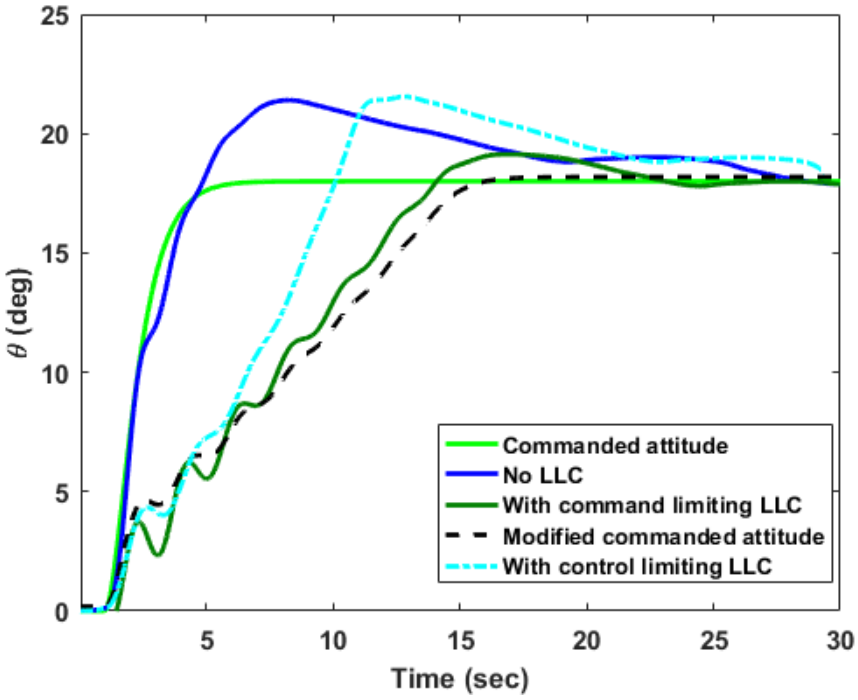

Figure 4.14: Body pitch attitude response with and without LLC

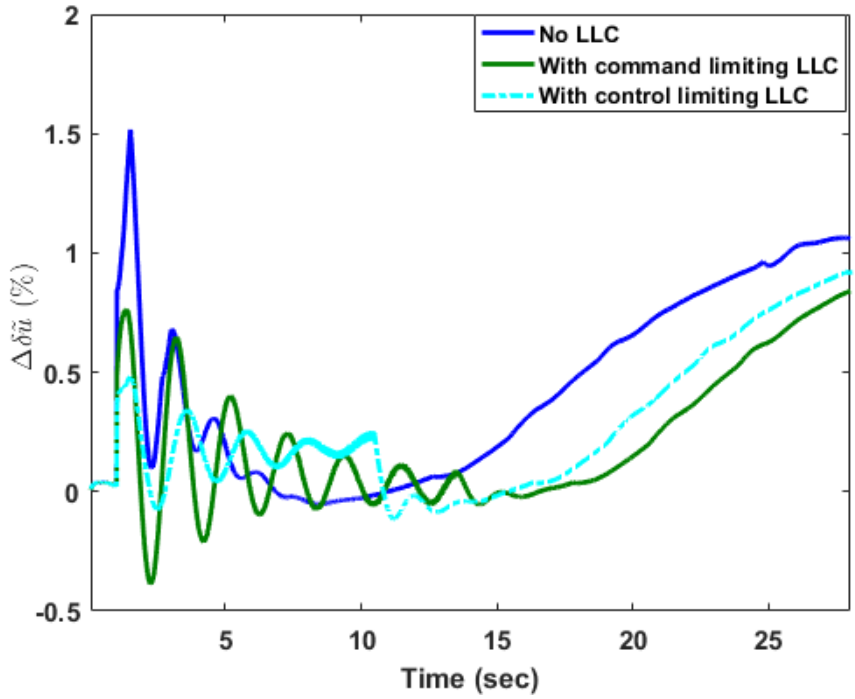

Figure 4.15: Change in control with and without LLC.

the literature that comes with limiting of control/command inputs near the limit boundary (i.e., this has been noticed for envelope protection systems)[31, 41]. Near the limit boundary, control/command limiting algorithms can behave like a nonlinear feedback controller with high gain which may cause the observed oscillations. As a remedy to this problem, Ref. [41, 93] suggest the use of smoothing algorithms or logics at the limit boundary.

Rate Command Maneuver:

Simulation results of the reference blade root pitch link 1/rev load magnitude without LLC (labeled 'No LLC'), with control limiting LLC and with command limiting LLC are shown in Fig. 4.16 for the case of the pitch rate command doublet of Fig. 4.11.

It can be observed from Fig. 4.16 that the 1/rev magnitude of the pitch link load stays within the selected limit value of 350 lb for both command and control limiting LLC. In fact, both control and command limiting LLC are seen to perform very well at limiting the magnitude of 1/rev pitch link load.

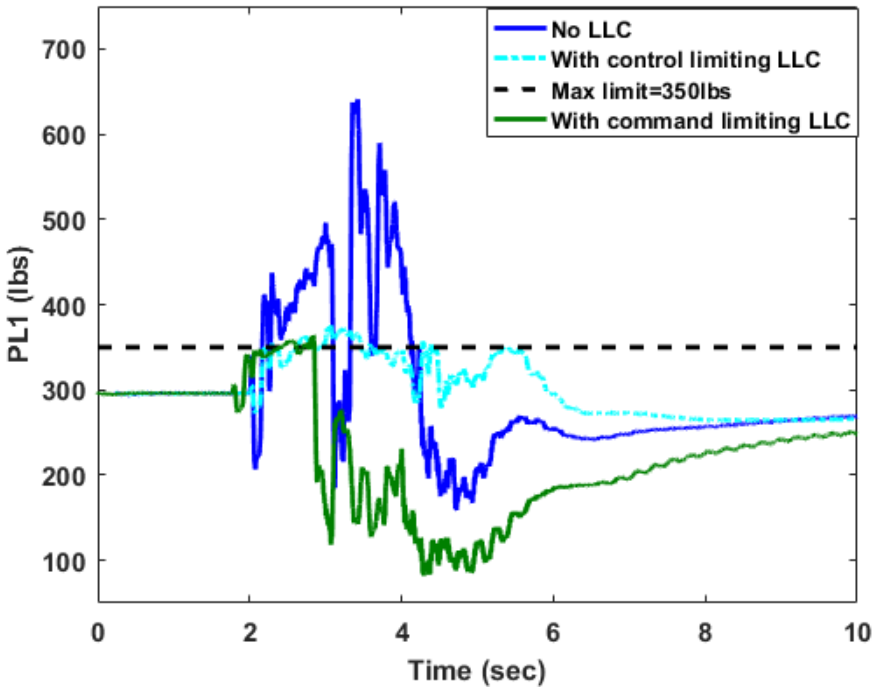

Figure 4.16: Variation of 1/rev harmonic component of reference blade pitch link load with and without LLC.

Load limiting comes at the expense of reduced pitch rate maneuver performance. This can be observed in Fig. 4.17, where the variation of body pitch rate response with command limiting LLC, with control limiting LLC and without LLC are compared. It is notable that with control limiting LLC, the resulting pitch rate is reduced, whenever necessary, in order to arrive at load limiting. However, this leads to a severe degradation of the maneuver as can be seen in the pitch rate profile for the control limiting LLC case in Fig. 4.17. As for the command limiting LLC, the pitch rate response does not reach its desired value in the pitch up part of the maneuver; however, in the pitch down part of the maneuver the pitch rate response is not greatly affected. This is not the case for the control limiting LLC where the pitch up and down part of the maneuver are severely affected. These results suggest that the pitch rate maneuver is less compromised at the expense of load limiting when the command limiting architecture is used instead of the control limiting architecture. With these results, it becomes apparent that care must be taken when integrating an LLC scheme

within an AFCS. Such an integration needs to be done in a seamless way to minimize maneuver performance degradation while performing load limiting.

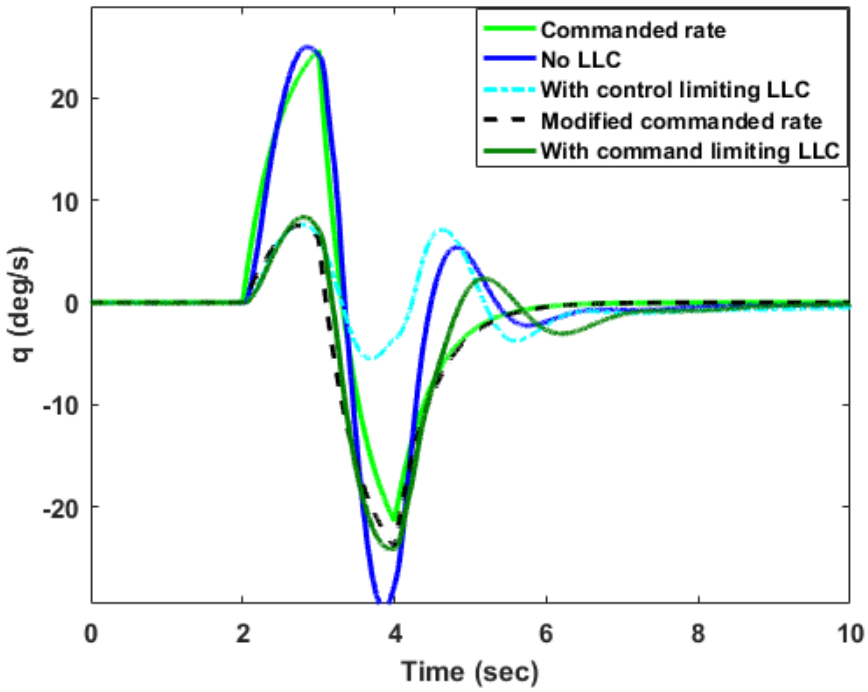

Figure 4.17: Body pitch rate response with and without LLC.

Figure 4.18, where the control input variation with command limiting LLC, with control limiting LLC and without LLC are compared, shows that for both control and command limiting LLC schemes, the control input is modified to allow the pitch link load to remain within the selected limit of 350 lb.

4.6 Handling Qualities Analysis

This section analyzes the impact of the command limiting LLC and control limiting LLC on the quantitative handling qualities specifications during pitch maneuvers in the forward flight regime. Specifically, the maximum achievable load factor, the pitch attitude quickness, the agility quickness, and the load quickness parameters are used as metrics to quantify the impact of both LLC architectures on the handling qualities performance of the helicopter.

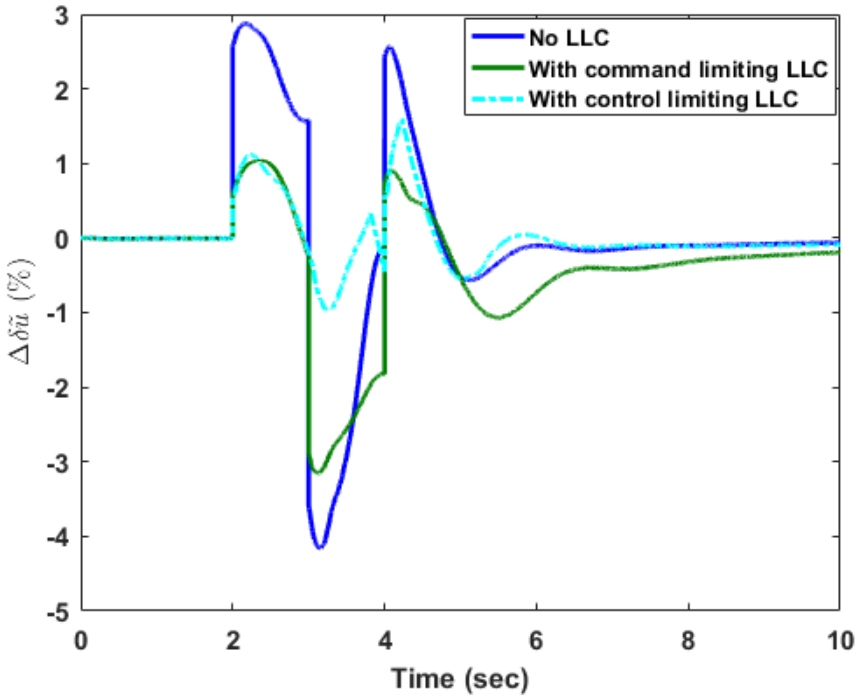

Figure 4.18: Change in control with and without LLC.

4.6.1 Maximum Achievable Load Factor

The maximum achievable load factor ($n_{z_{max}}$) can be used as a metric to quantify the impact of the LLC schemes on the handling qualities during pitch maneuvers in forward flight (Ref. [94]). To quantify the impact of the LLC schemes on the handling qualities using the maximum achievable load factor metric, a step pitch rate command input of magnitude 34.4 deg/s is considered. The maximum achievable load factor for the cases with control limiting LLC, with command limiting LLC, and without LLC ("No LLC") resulting from this step command input are recorded and compared. Figures 4.19 and 4.20 show the load factor and magnitude of 1/rev component of pitch link load resulting from the step pitch rate command input. The maximum achievable load factor for the cases with control limiting LLC, with command limiting LLC and without LLC ("No LLC") is determined (Table 4.1). With the baseline controller ("No LLC") a maximum load factor of 2.45g is achieved whereas for the cases with control and command limiting LLC the maximum achievable load factor

Table 4.1: Maximum achieved load factor

Cases	$n_{z,max}(g)$
No LLC	2.45
With control limiting LLC	1.24 (-49.4%)
With command limiting LLC	1.27 (-48.2%)

drops to $1.24g$ (49.4% reduction) and $1.27g$ (48.2% reduction) respectively. These results are not surprising as the load factor is probably the biggest correlated parameter to pitch link load (i.e., higher thrust necessarily implies higher pitch link load). The chosen limit of 350 lb is very low which explains such drastic decrease in load factor for both the control and command limiting LLC.

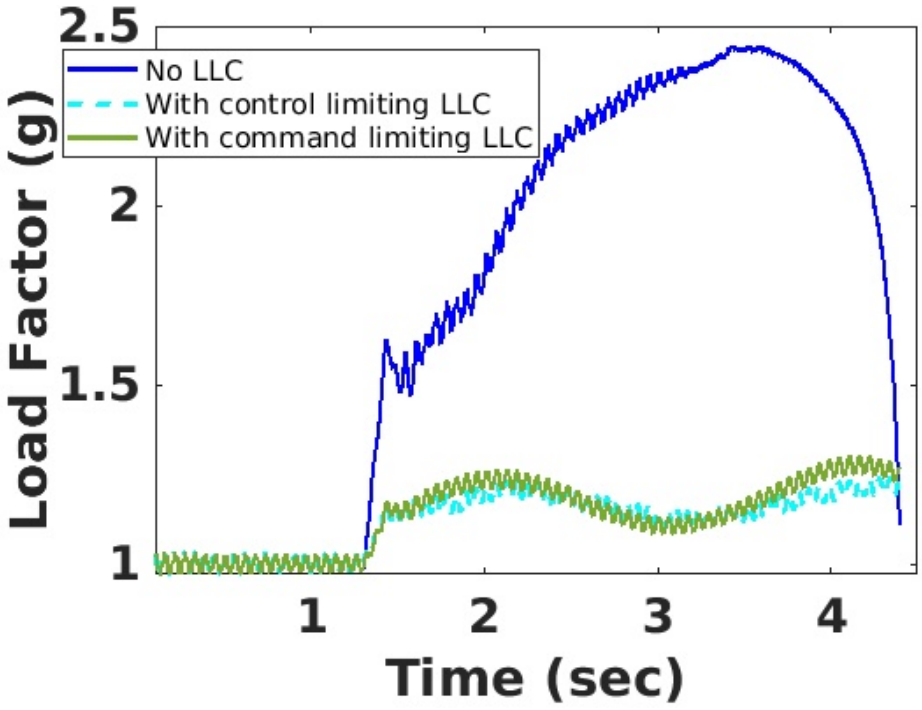

Figure 4.19: Load factor with and without LLC.

It can be concluded that for a load limit of 350 lb. the control and command limiting LLC have similar impacts on the maximum achievable load factor.

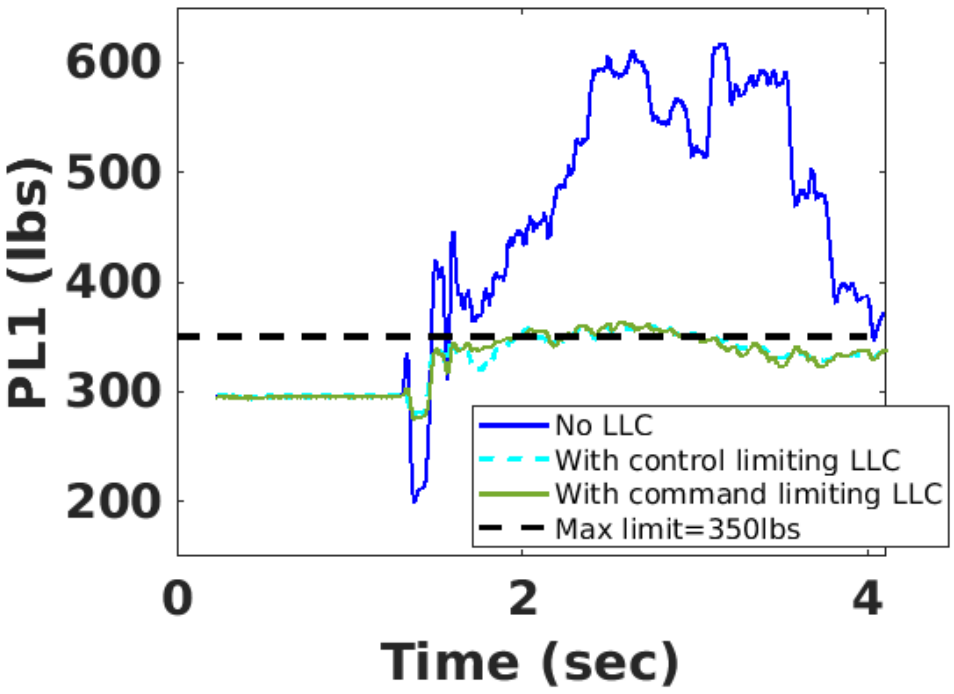

Figure 4.20: Magnitude of 1/rev pitch link load with and without LLC.

4.6.2 Pitch Attitude Quickness

In the pitch axis, an important flying qualities criterion is the pitch attitude quickness. The pitch attitude quickness parameter gives a measure of the agility of the helicopter during vertical maneuvers. It does so by measuring the ability of the helicopter to perform rapid and precise moderate-amplitude pitch attitude changes (i.e., $5^o < \theta < 30^o$) during pitch maneuvers (Ref.[92]). The pitch attitude quickness parameter (Q_θ) is defined as the ratio of the peak pitch rate (q_{pk}) to the peak attitude angle change ($\Delta\theta_{pk}$)

$$Q_\theta = \frac{q_{pk}}{\Delta\theta_{pk}} \tag{4.17}$$

The ADS-33 handling qualities boundary associated with the pitch attitude quickness is defined as a function of the minimum attitude change ($\Delta\theta_{min}$). Figure 4.21 shows the handling qualities boundary for the pitch attitude quickness for a general MTE at hover and low speed (Ref. [92]).

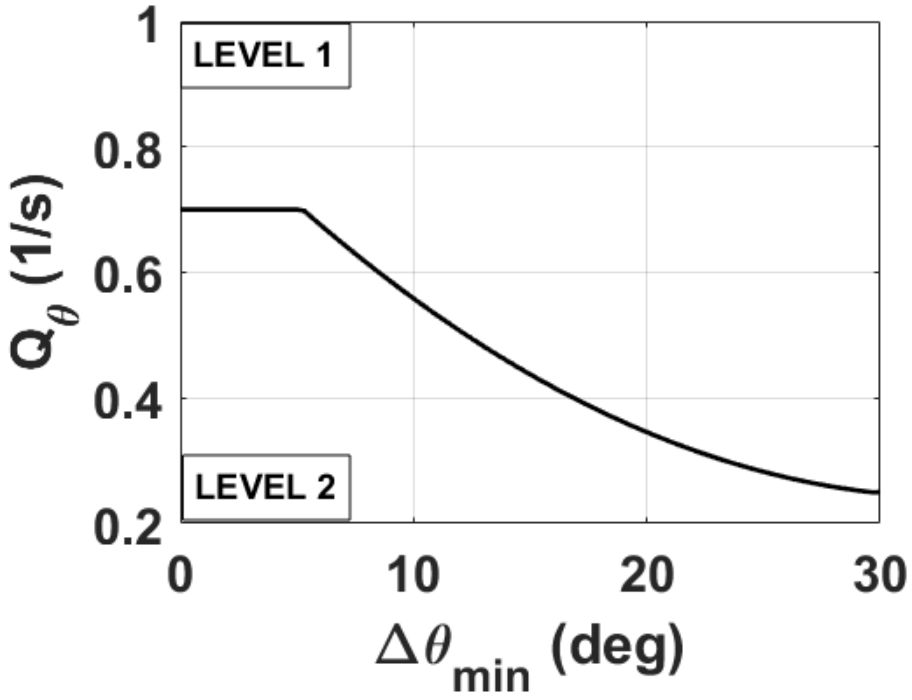

Figure 4.21: ADS-33 level 1-2 pitch attitude quickness boundary for a general MTE.

For a helicopter with a flight controller that provides a rate command response type in the pitch axis, the pitch attitude quickness parameter can be computed from the response of a pulse command input (Ref. [95]). Figure 4.22 shows a typical ADS-33E-PRF pulse command input.

Figures 4.23 and 4.24 show the pitch rate and attitude responses resulting from the pulse command input of Fig. 4.22. From Figs. 4.23 and 4.24, the values of peak pitch rate (q_{pk}), peak attitude angle change ($\Delta\theta_{pk}$), and minimum attitude change ($\Delta\theta_{min}$) can be extracted.

The pitch attitude quickness as a function of the minimum attitude change can then be obtained from pulse command input responses of different durations. The impact of both the command and control limiting LLC on the agility of the helicopter can be assessed by comparing the pitch attitude quickness with and without LLC. Figure 4.25 shows the pitch attitude quickness for the cases with control limiting LLC, with command limiting LLC and without LLC ("No LLC"). Looking at Fig. 4.25, one main conclusion can be drawn. The control and command limiting LLC result in identical loss in agility. In addition, for

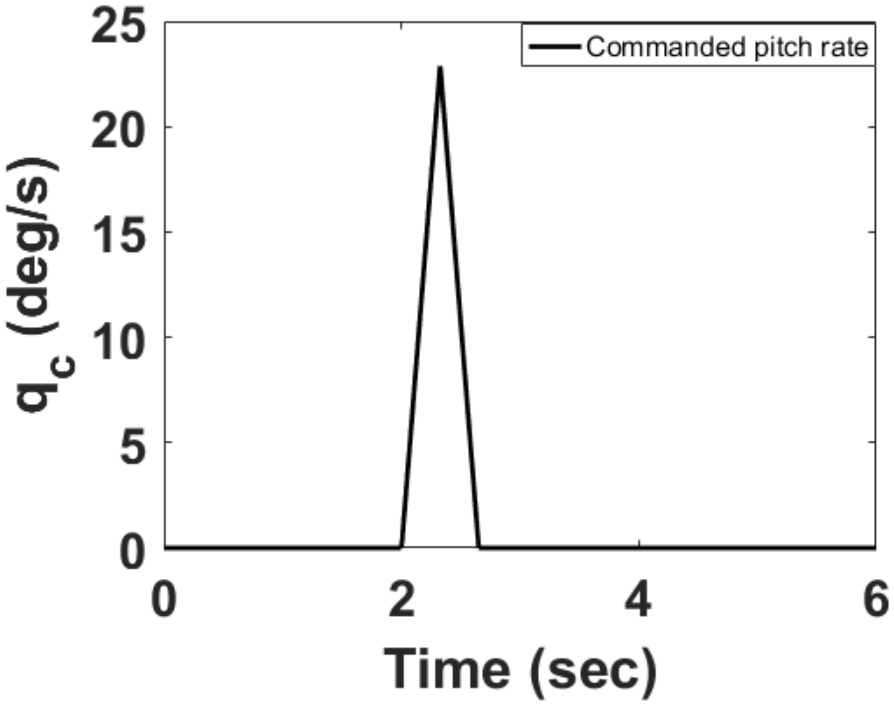

Figure 4.22: Pulse command input of 0.65 sec.

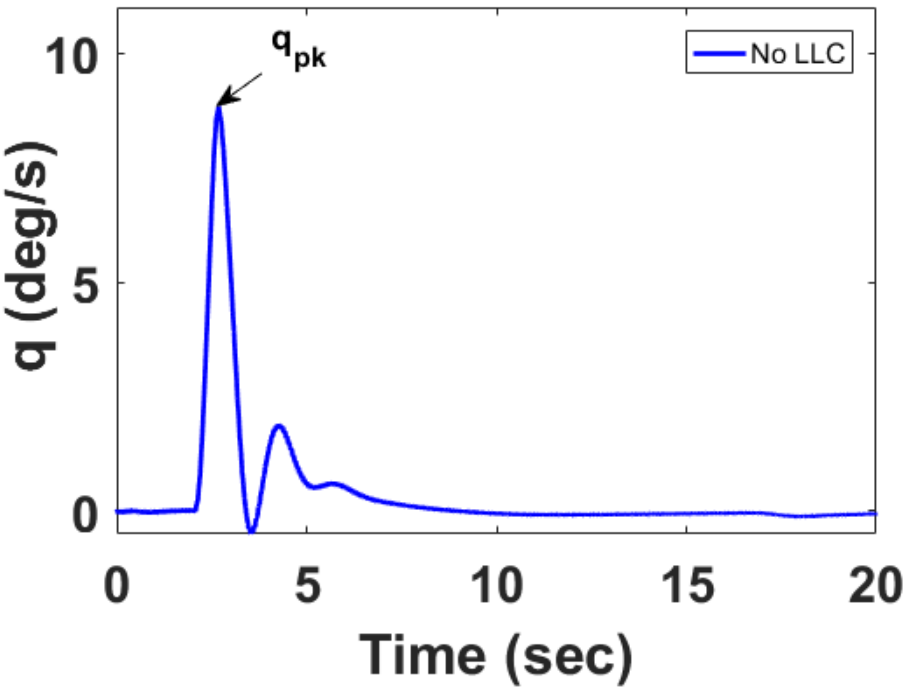

Figure 4.23: Body pitch rate response.

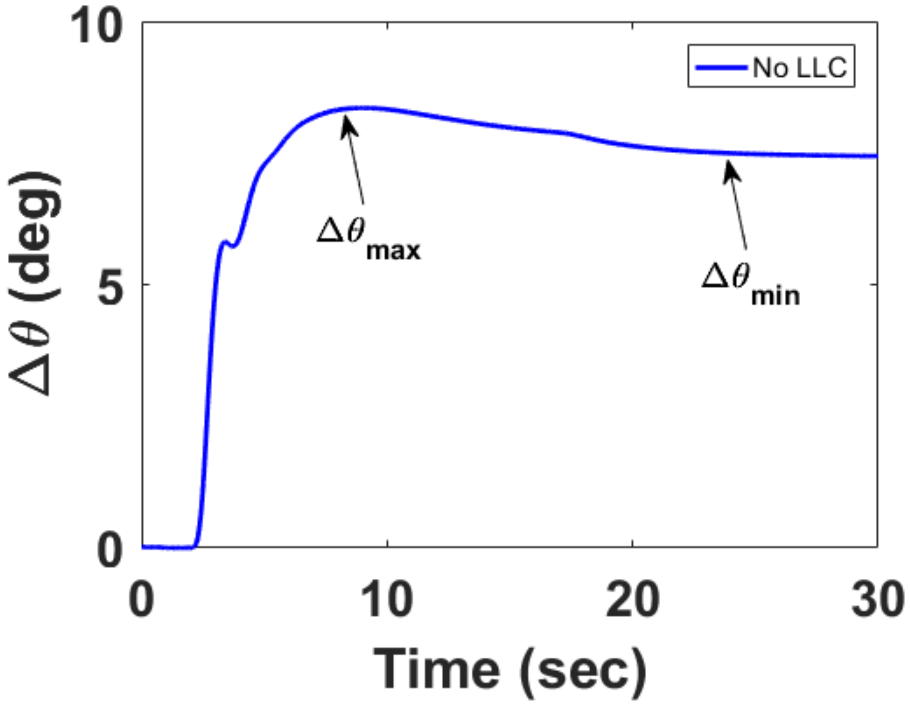

Figure 4.24: Body pitch attitude response.

both control and command limiting LLC the pitch attitude quickness remains within level 1. It is important to note that although the pitch attitude quickness parameter is only defined at hover and low speed, it still remains a good metric to quantify the change in handling qualities introduced by the command and control limiting LLC (Ref. [94]) .

4.6.3 Agility Quickness

An alternative parameter that can be used to quantify the agility of a helicopter in forward flight is the agility quickness parameter. The agility quickness parameter is a metric introduced in Ref. [96] as a replacement for the conventional ADS-33 pitch attitude quickness parameter. In forward flight, during maneuvers in the vertical axes, the pilot is far more interested in the flight path angle change than in the pitch attitude change (Refs. [96], [97]). Hence, in forward flight, the agility of a helicopter in the pitch axes should be related to the flight path angle instead of the pitch attitude angle. The agility quickness parameter, Q_γ, is defined as follows

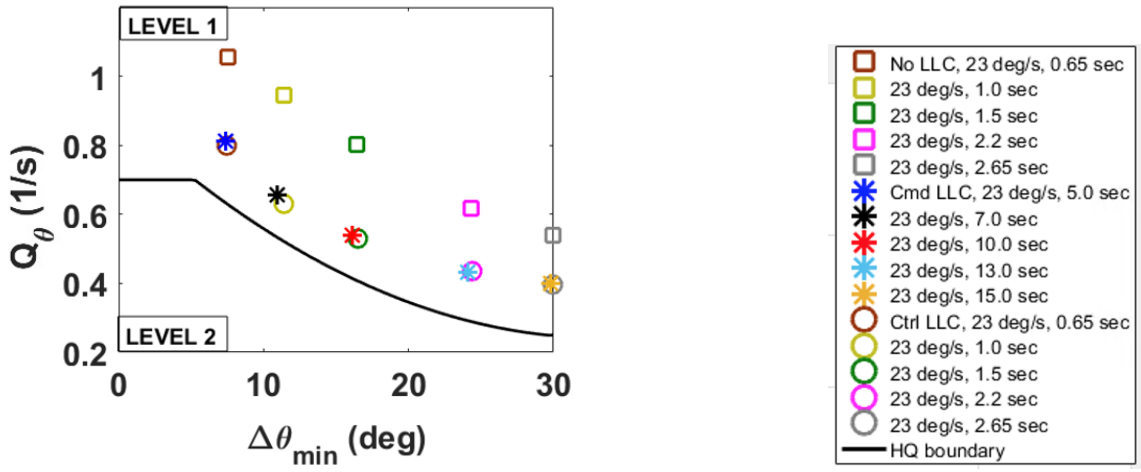

(a) Pitch attitude quickness with and without LLC (b) Legend

Figure 4.25: Impact of control and command limiting LLC on the pitch attitude quickness

$$Q_\gamma = \frac{\dot{\gamma}_{pk}}{\Delta\gamma} \tag{4.18}$$

where $\dot{\gamma}_{pk}$ is the peak values of the rate of change of the flight path angle during a specific maneuver and $\Delta\gamma$ is the change in flight path angle. It can be readily seen that the agility quickness parameter has the same units as the pitch attitude quickness parameter, which facilitates their comparison. For a helicopter with a flight controller that provides a rate command response type in the pitch axis, the agility quickness parameter can be computed from the response of a pulse command input in the pitch axes.

Similar to the pitch attitude quickness, the agility quickness can be obtained from pulse command input responses of different durations. The impact of both the command and control limiting LLC on the agility of the helicopter can be assessed by comparing the agility quickness with and without LLC. Figure 4.26 shows the agility quickness for the cases with control limiting LLC , with command limiting LLC and without LLC ("No LLC"). It can be observed from Fig. 4.26 that the command limiting LLC performs better than the control limiting LLC. At low to medium flight path angle changes, the agility of the helicopter is less compromised with the command limiting LLC when compared to the control

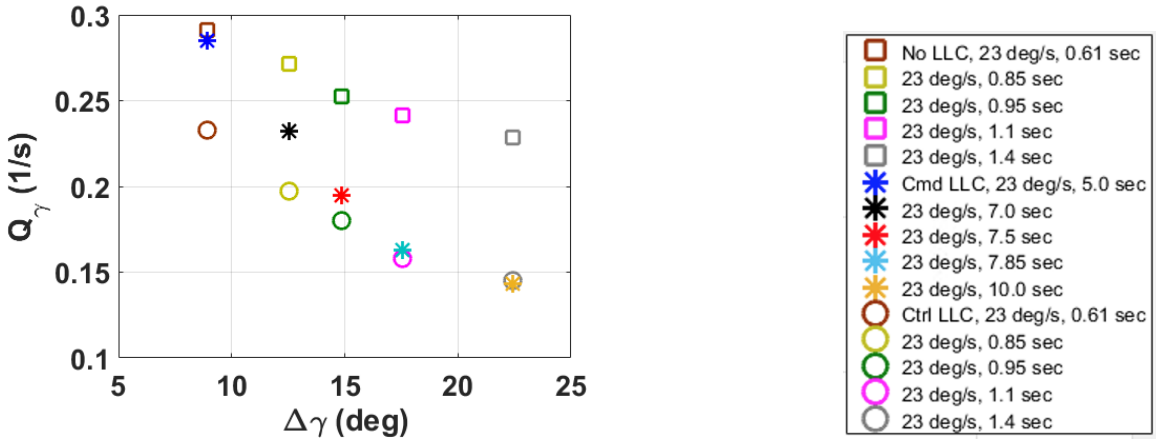

(a) Agility quickness with and without LLC

(b) Legend

Figure 4.26: Impact of control and command limiting LLC on the agility quickness.

limiting LLC. At large flight path angle changes, the agility is near-identical. Hence, using the agility quickness parameter, it can be concluded that the command limiting LLC has less detrimental effect than the control limiting LLC on the agility of the helicopter.

4.6.4 Load Quickness

The load quickness parameter is a handling qualities metric for structural loading during maneuvering flight (Refs. [94], [96], [97]). It was introduced to quantify the buildup of loads in the rotor during maneuvering flight (Refs. [96, 97]). Therefore, this metric can be used to quantify the effectiveness of the control and command limiting LLC. The load quickness parameter is given as follows:

$$Q_l = \frac{|F|_{max}}{W\Delta\gamma} \tag{4.19}$$

where F is the maximum absolute value of the load during a specific maneuver, W is the weight of the helicopter, and $\Delta\gamma$ is the flight path angle change. Similar to the pitch attitude quickness, the load quickness can be obtained from pulse command input responses of different durations. Figure 4.27 shows the load quickness for the cases with control limiting LLC, with command limiting LLC, and without LLC ("No LLC"). It can observed that the

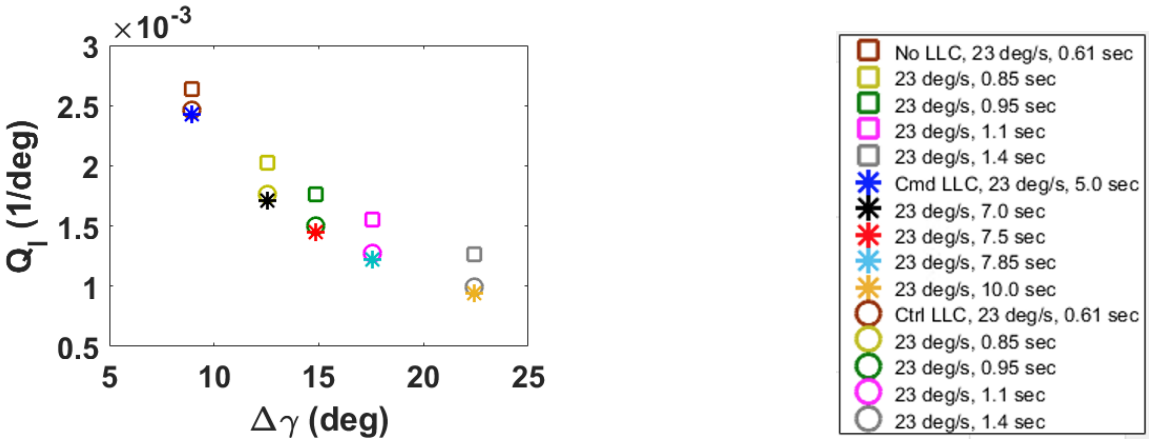

(a) Load quickness with and without LLC

(b) Legend

Figure 4.27: Impact of control and command limiting LLC on the load quickness.

1/rev load build-up on the pitch link for the control and command limiting LLC is near-identical.

4.7 Discussion

The command limiting LLC can be implemented with a soft-stop that would allow the pilot to override it for safety reasons. In addition, since it is not in the loop, it does not affect the overall stability of the system. Hence, for the command limiting LLC, stability will not be sacrificed to avoid the excessive build-up of load on the component during maneuvering flight. On the other hand, while the control limiting LLC can affect the overall stability of the system, it allows for setting an absolute load limit and not exceeding it, no matter what the control system or pilot commands.

In light of the results obtained in this research, it is evident that the command limiting LLC and control limiting LLC have similar performance in component load limiting. In addition, the command limiting LLC allows for more rapid changes in the flight path angle when compared to the control limiting LLC. Hence, the command limiting LLC allows for a more agile aircraft when compared with the control limiting LLC. It is important to note that when designing either a command limiting LLC or control limiting LLC scheme for

component load limiting, the agility quickness and load quickness parameters can be used to optimize between component load limiting and helicopter maneuverability.

4.8 Summary and Technical Findings

In this chapter, the investigation of trade-off between maneuver performance and component load limiting was presented. This was done via the development of an integrated flight and load limiting controller where the LLC scheme is seamlessly merged within an AFCS. Two design methodologies for the development of such a controller have been identified: command and control limiting architectures.

In the control limiting architecture, the LLC scheme limits the control effector commands to achieve load limiting while in the command limiting architecture the LLC scheme limits directly the pilot's command to achieve load limiting. From the time domain simulation and handling qualities results, it was found that choosing one architecture over the other for a particular application can lead to non-negligible repercussions on the maneuver performance. Therefore, care must be taken when integrating an LLC scheme within an AFCS. Such an integration needs to be done in a way to minimize maneuver performance degradation while performing load limiting.

CHAPTER 5

LOAD ALLEVIATION VIA INDIVIDUAL BLADE CONTROL

This chapter presents the synthesis of a novel load alleviation scheme based on active rotor control for critical helicopter component life extension. The proposed load alleviation scheme is innovative as it demonstrates how Individual Blade Control (IBC) and model prediction can be combined using higher-order Linear Time Invariant (LTI) models to develop a life extending control scheme. Using a 10^{th} order LTI model on-board the vehicle and a cost function, cost-minimizing higher harmonic individual blade control (IBC) inputs are computed over a selected time horizon and used to reduce selected harmonics of component loads during maneuvering flight. The component load alleviation using IBC scheme is implemented in a comprehensive nonlinear model of a generic helicopter to evaluate the performance of the scheme.

The 10^{th} order LTI model used in the development of the LAC via IBC scheme is constructed from an LTP model similar to the one developed in chapter 2. The only difference between the two LTP models resides in the control vector. For the current study, the input vector of the LTP model is composed of the main rotor lateral, collective and longitudinal swashplate inputs (θ_{1C}, θ_0, θ_{1S}), the tail rotor collective swashplate input (θ_{TR0}), and 2/rev cosine and sine individual blade pitch inputs (θ_{2C}, θ_{2S}).

The proposed component load alleviation scheme presented in this chapter is based on active rotor control. More specifically, it is an on-board system that uses model prediction to reduce selected harmonic(s) of pitch link loads. The component load alleviation scheme has two main components. The first component is an on-board dynamical model that provides real-time estimates of the effect of pilot command and higher harmonic individual blade pitch inputs on pitch link harmonic loads. The second component is a IBC controller that uses the harmonic pitch link load estimates from the first component (i.e., on-board dynamical model) to provide optimally calculated higher harmonic individual blade pitch inputs to reduce the selected harmonic loads. Hence, both the modeling of the on-board dynamical model that can provide such load estimates and the IBC controller are crucial for the successful implementation of the proposed scheme.

5.1 On-Board Dynamical Model

In this section, to illustrate the effectiveness of the proposed scheme, the 2/rev pitch link load is selected as the harmonic load of interest. The on-board dynamical model is used to provide real-time estimates of pitch link harmonic loads resulting from the pilot control and higher harmonic individual blade pitch inputs. Given that the higher order LTI model contains the swashplate inputs and 2/rev cosine and sine individual blade pitch inputs, the 10^{th} order LTI model readily provides a mapping from the 2/rev individual blade pitch inputs to the harmonic pitch link loads. One way to enable the on-board dynamical model to provide real-time estimation of the effect of pilot command inputs on harmonic loads is to

feed the swashplate inputs generated by the flight controller as input to the 10^{th} order LTI model. Equations (5.1) and (5.2) represent the mathematical model of the on-board dynamical model. The control vector is partitioned into two parts as can be seen in Eqs. (5.3) and (5.4). Using this model, one can obtain real-time estimates of the effect of flight control (referred to as δ_{FC} in the sequel) and higher harmonic individual blade pitch inputs (referred to as δ_{IBC} in the sequel) on the 2/rev cosine and sine harmonic pitch link loads.

$$\dot{X}_s = [\hat{A}]X_s + [\hat{B}_{FC}]\delta_{FC} + [\hat{B}_{IBC}]\delta_{IBC} \tag{5.1}$$

$$\begin{bmatrix} y_{2c} \\ y_{2s} \end{bmatrix} = [\hat{C}]X_s + [\hat{D}_{FC}]\delta_{FC} + [\hat{D}_{IBC}]\delta_{IBC} \tag{5.2}$$

where

$$\delta_{FC} = \begin{bmatrix} \theta_0 \\ \theta_{1C} \\ \theta_{1S} \\ \theta_{TR0} \end{bmatrix} \tag{5.3}$$

$$\delta_{IBC} = \begin{bmatrix} \theta_{2C} \\ \theta_{2S} \end{bmatrix} \tag{5.4}$$

5.2 Harmonic Individual Blade Controller

This section presents a derivation of the IBC controller, using model prediction. The IBC controller is developed based on a T-matrix approach [11]. In this approach, the T-matrix of component load sensitivity to selected harmonic components of Individual Blade Control (IBC) inputs is extracted using the 10^{th} order LTI model as follows. The transfer function from 2/rev IBC inputs to 2/rev cosine and sine pitch link loads obtained using Eqs. (5.1)

and (5.2) is given by

$$G(s) = [\hat{C}(sI - \hat{A})^{-1}\hat{B}_{IBC} + \hat{D}_{IBC}] \tag{5.5}$$

Hence, one can obtain the continuous time DC gain matrix of the transfer function as follows

$$DC\ gain\ matrix = -\hat{C}(\hat{A})^{-1}\hat{B}_{IBC} + \hat{D}_{IBC} \tag{5.6}$$

The T-matrix of 2/rev load sensitivity to 2/rev individual blade control inputs is the DC gain matrix (as shown in Eq. (5.6)).

Hence, the T-matrix is a simple gain matrix that provides, at steady state, a static mapping between the 2/rev pitch link loads (sine and cosine components) and 2/rev IBC inputs as can be seen in Eq. (5.7)

$$Y_{IBC} = T\ \delta_{IBC} \tag{5.7}$$

Equation (5.7) represents the continuous time representation of the T-matrix operator. Y_{IBC} is the vector composed of 2/rev cosine and sine components of the pitch link load due to IBC inputs alone.

At any given instant in time, the proposed load alleviation scheme uses the on-board dynamical model and the T-matrix to compute the needed current IBC control action to reduce harmonic loads. Let Y_{FC} represent the 2/rev harmonic load changes arising from the flight control inputs over a duration of one time step. Y_{FC} is obtained by integrating Eqs. (5.1) and (5.2) over one time step and adding the trim loads. As defined in Eq. (5.7), Y_{IBC} is the 2/rev harmonic load changes due to application of IBC inputs alone. The aim is to reduce the effect of the flight control inputs on the 2/rev pitch link load using IBC inputs. Therefore, the following cost function is defined as

$$J = (Y_{IBC} + Y_{FC})^T Q\ (Y_{IBC} + Y_{FC}) + \delta_{IBC}^T\ R\ \delta_{IBC} \tag{5.8}$$

The optimization problem is defined as follows

$$\min_{\delta_{IBC}} [J] \tag{5.9}$$

As the optimization problem suggests, the goal is to find the optimal IBC input that allows minimizing the effect of the flight controller on the 2/rev pitch link load.

The working of the proposed scheme is as follows. Using the current pilot control inputs and the previous time step IBC control inputs, the on-board dynamical model provides change in harmonic components of loads at the next time step. This quantity added to the 2/rev trim loads (i.e., 2/rev cosine and sine trim loads) represents the value of Y_{FC} which is an estimate of the effect of the flight control inputs on the 2/rev pitch link load. From the static optimization problem, an optimal control action in terms of individual blade pitch inputs necessary to reduce this anticipated increase in load is obtained. More specifically, the gain of the harmonic individual blade controller is extracted from this optimization problem. The solution of the optimization problem posed in Eq. (5.9) can be obtained by applying the first order necessary condition of optimally. The resultant harmonic individual blade controller is given by Eq. (5.10):

$$U_{IBC\,opt} = \hat{T} Y_{FC} \tag{5.10}$$

where

$$\hat{T} = -(T^T Q T + R)^{-1} T^T Q \tag{5.11}$$

The weighting matrices Q and R are selected as follows:

$$R = r_{\text{IBC}} \begin{bmatrix} 1 & 0 \\ 0 & 1 \end{bmatrix} \tag{5.12}$$

$$Q = q_{\text{IBC}} \begin{bmatrix} 1 & 0 \\ 0 & 1 \end{bmatrix} \tag{5.13}$$

where

$$q_{\text{IBC}}, r_{\text{IBC}} \in \mathbb{R}_{+} \tag{5.14}$$

A block diagram representation of the proposed load alleviation control scheme for component life extension is shown in Fig. 5.1. The estimated trim values of the limit parameter (i.e., 2/rev cosine and sine components of pitch link load) are assumed to be known.

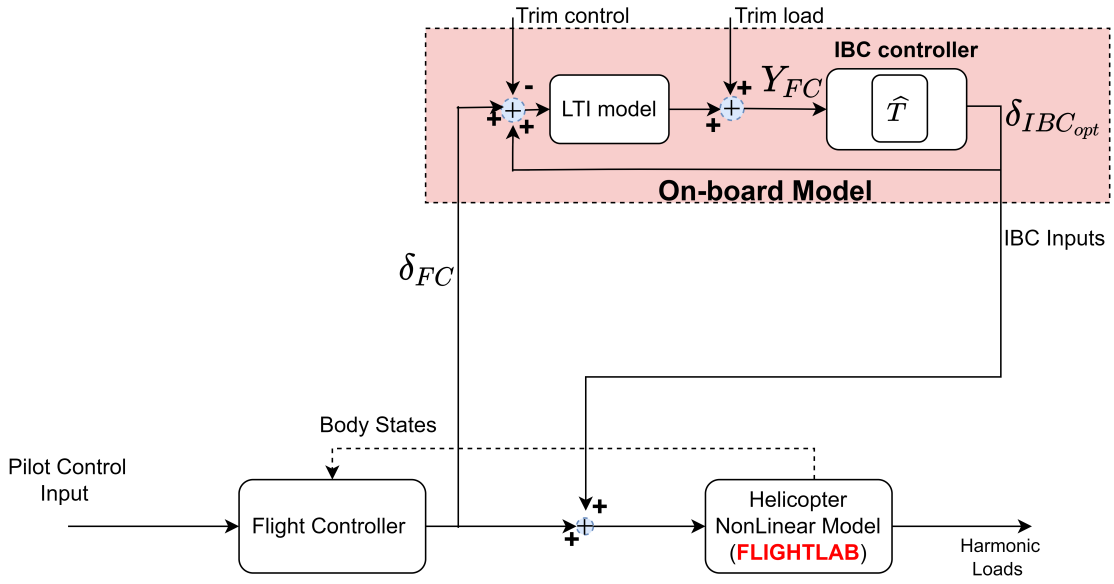

Figure 5.1: Individual Blade Control (IBC) for component load alleviation.

5.3 Results

This section presents an investigation of the performance of the load alleviation scheme for component life extension. Specifically, reduction of the 2/rev pitch link load using 2/rev cosine and sine individual blade pitch inputs is considered. Moreover, the following is also investigated: the impact of such load reduction on the maneuver performance, other harmonic pitch link loads, peak-to-peak total pitch link load, and vibratory hub loads (i.e., 4/rev hub loads). For simulation evaluation purposes, the high fidelity full vehicle nonlinear model in FLIGHTLAB®, from which the higher order LTI model is generated, is used as the vehicle truth model. To avoid confusion, cases where the load alleviation scheme is used are denoted as "With IBC" and cases where the load alleviation scheme is not used are denoted as "No IBC".

The maneuver considered in this study is a rate command maneuver where the flight controller is set to give a Rate Command/Attitude Hold (RCAH) response in the pitch axis. More specifically, a pitch rate doublet of magnitude 20 deg/s is considered. The flight controller used is a dynamic inversion controller as described in the previous chapter.

Figure 5.2 shows the commanded pitch rate and the resulting vehicle pitch rate. The magnitude of 2/rev pitch link load arising from this rate command maneuver as predicted by the nonlinear and the on-board LTI models is presented in Fig. 5.3. For this simulation result, where the IBC controller is turned off, the interest is to compare the 2/rev harmonic component magnitude of pitch link load prediction from the on-board LTI and the nonlinear models. The magnitude of 2/rev pitch link load prediction from the on-board LTI model is computed by using the trim loads as follows

$$PL2 = \sqrt{[y_{2c} + (y_{2c})_{trim}]^2 + [y_{2s} + (y_{2s})_{trim}]^2} \tag{5.15}$$

It can observed from Fig. 5.3 that the predictions from the on-board LTI and the nonlinear models are close. This result suggests that the on-board LTI model can be used for

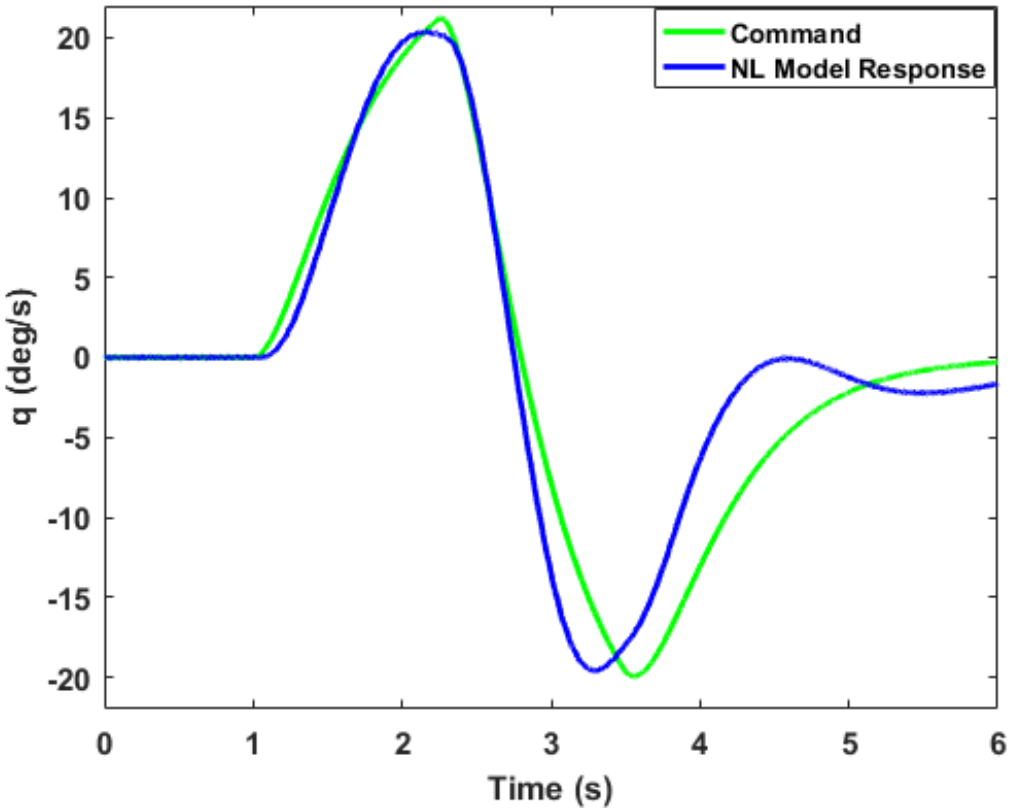

Figure 5.2: Body pitch rate response comparison between commanded and vehicle response.

on-line estimation of 2/rev harmonic component magnitude of pitch link load.

To select the design parameters (Q and R matrices), the ratio $\frac{q_{\text{IBC}}}{r_{\text{IBC}}}$ is varied and the percent improvement in 2/rev RMS and peak magnitude of the "With IBC" case over the "No IBC" case are recorded and compared. The RMS and peak magnitude for the 2/rev pitch link load are computed as follows:

$$RMS = \sqrt{\frac{1}{N}\sum_{n=1}^{N}[PL2(n)]^2} \tag{5.16}$$

$$Peak \;\; Magnitude = \max_{n}[PL2(n)] \tag{5.17}$$

where PL2 $\in \mathbb{R}^N$

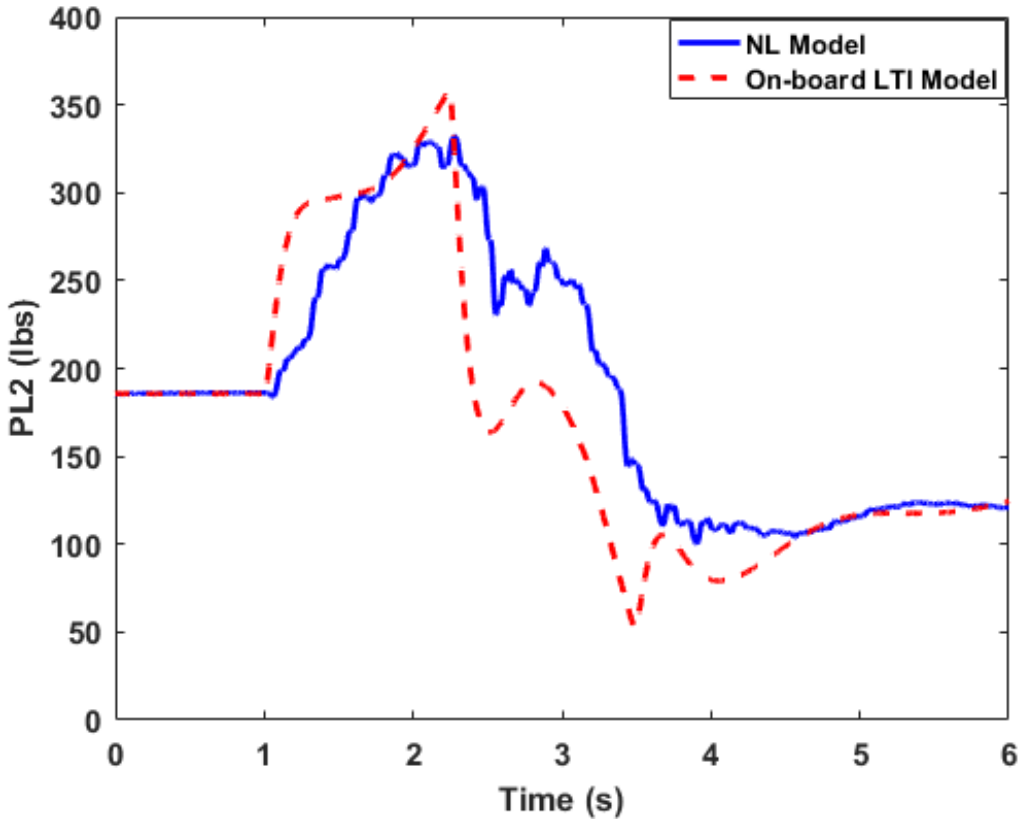

Figure 5.3: Variation of 2/rev harmonic component of reference blade pitch link load without IBC.

The root mean square (i.e., Eq. (5.16)) gives a measure of the size or magnitude of the total response, whereas the peak metric (i.e., Eq. (5.17)), as the name suggests, quantifies the peak value of the total response. The use of the peak metric is justified by the fact that an increase in peak load can potentially lead to a significant increase in fatigue damage. It is therefore ideal for the load alleviation scheme to decrease the RMS and peak values of the magnitude of 2/rev pitch link load.

Figure 5.4 shows the RMS and peak magnitude percent improvement for the magnitude of 2/rev pitch link load as the ratio $\frac{q_{\text{IBC}}}{r_{\text{IBC}}}$ is varied. As expected, as $\frac{q_{\text{IBC}}}{r_{\text{IBC}}}$ is increased the RMS and peak values for the 2/rev pitch link load decrease. The load alleviation scheme is seen to be very effective, since an RMS percent improvement of 65% is achieved for the 2/rev load. It may be observed that 0.1 is the minimum value of the q_{IBC} to r_{IBC} ratio that gives the

maximum RMS and peak magnitude percent improvements for the 2/rev pitch link load. Therefore, for the reminder of this chapter, the performance of the proposed load alleviation scheme is assessed with q_{IBC} and r_{IBC} selected to be 0.1 and 1, respectively. This ratio value allows using the minimum higher harmonic individual blade pitch input needed for best performance of the load alleviation scheme.

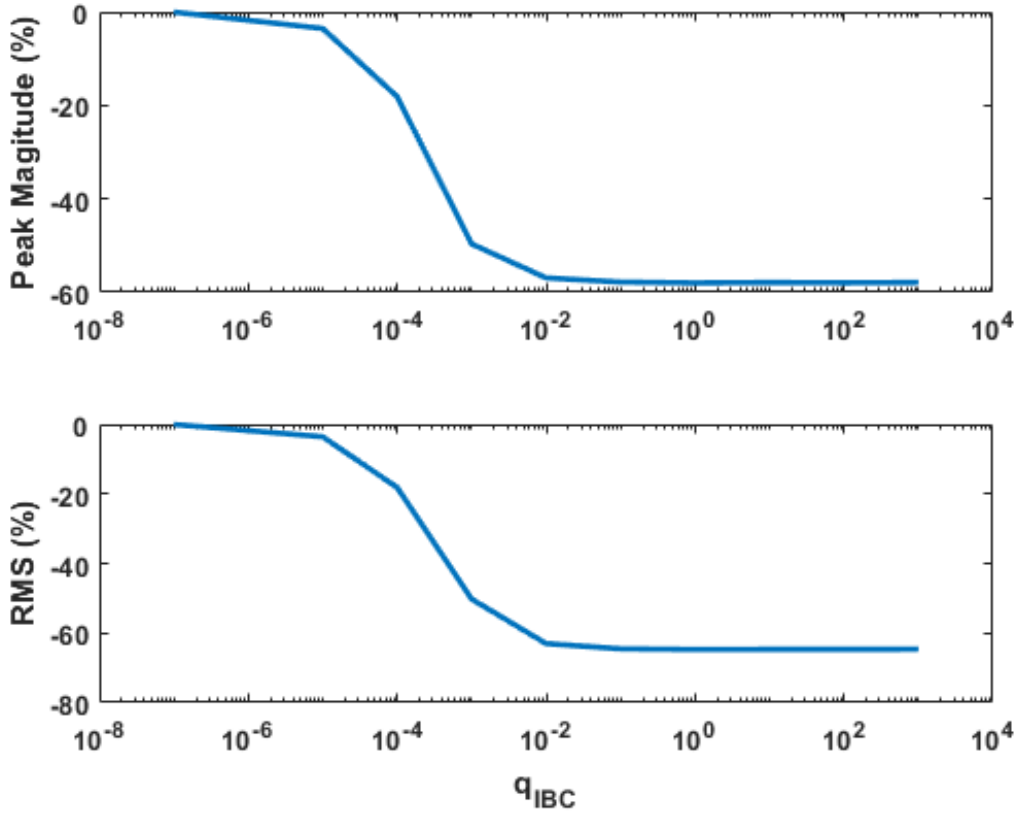

Figure 5.4: Percent improvement for 2/rev pitch link load.

Simulation results of the pitch link 2/rev load magnitude with the load alleviation scheme (labeled "With IBC") and without the load alleviation scheme (labeled "No IBC") are shown in Fig. 5.5 for the case of the pitch rate doublet input of Fig. 5.2. It can be observed that the proposed load alleviation scheme significantly reduces the magnitude of the 2/rev pitch link load of the nonlinear model.

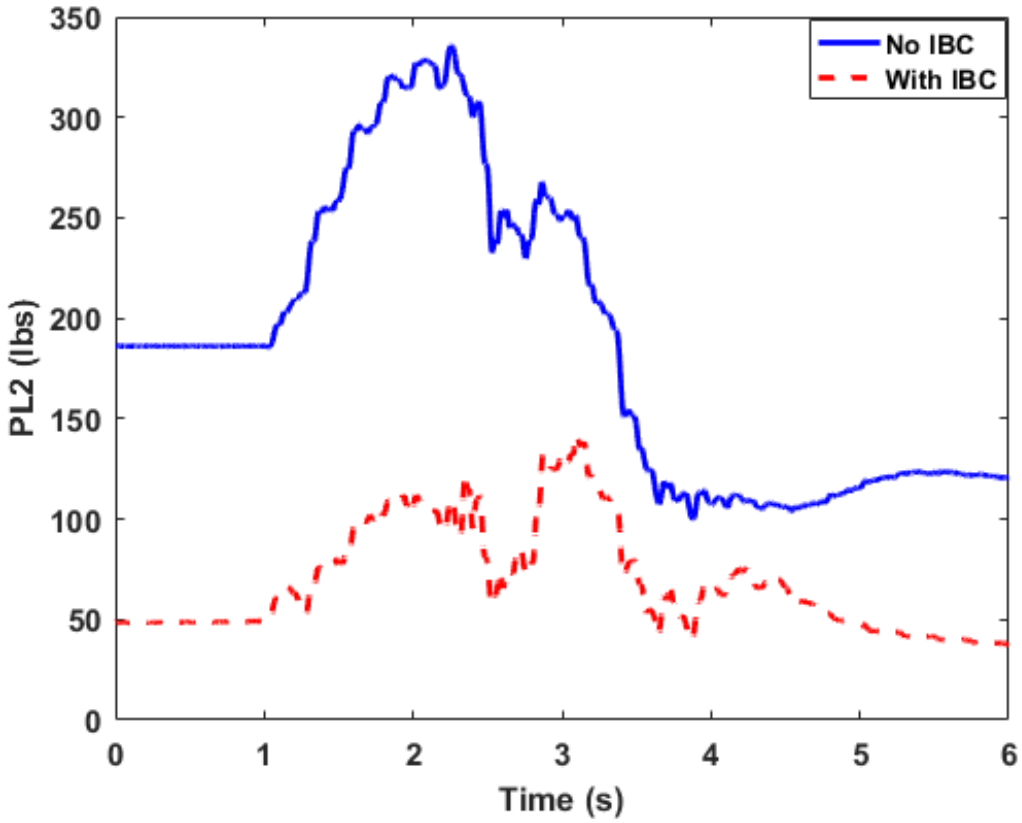

Figure 5.5: Variation of 2/rev harmonic component of reference blade pitch link load with and without IBC.

The effect of the load alleviation scheme on uncontrolled harmonic loads (i.e., 1/rev, 3/rev and 4/rev pitch link loads) is shown in Fig. 5.6. It can be noticed that the load alleviation scheme does not seem to have significant detrimental effects on uncontrolled harmonic pitch link loads.

To characterize the load alleviation performance, each harmonic component magnitude of pitch link load is examined in terms of RMS and peak values. For each magnitude of pitch link harmonic load, the RMS and peak values for the case with IBC are computed and included in Table 5.1. Furthermore, the percent improvement of the "With IBC" case over the "No IBC" case is also provided in Table 5.1 (shown in parenthesis). A negative percentage represents a decrease whereas a positive percentage is an increase.

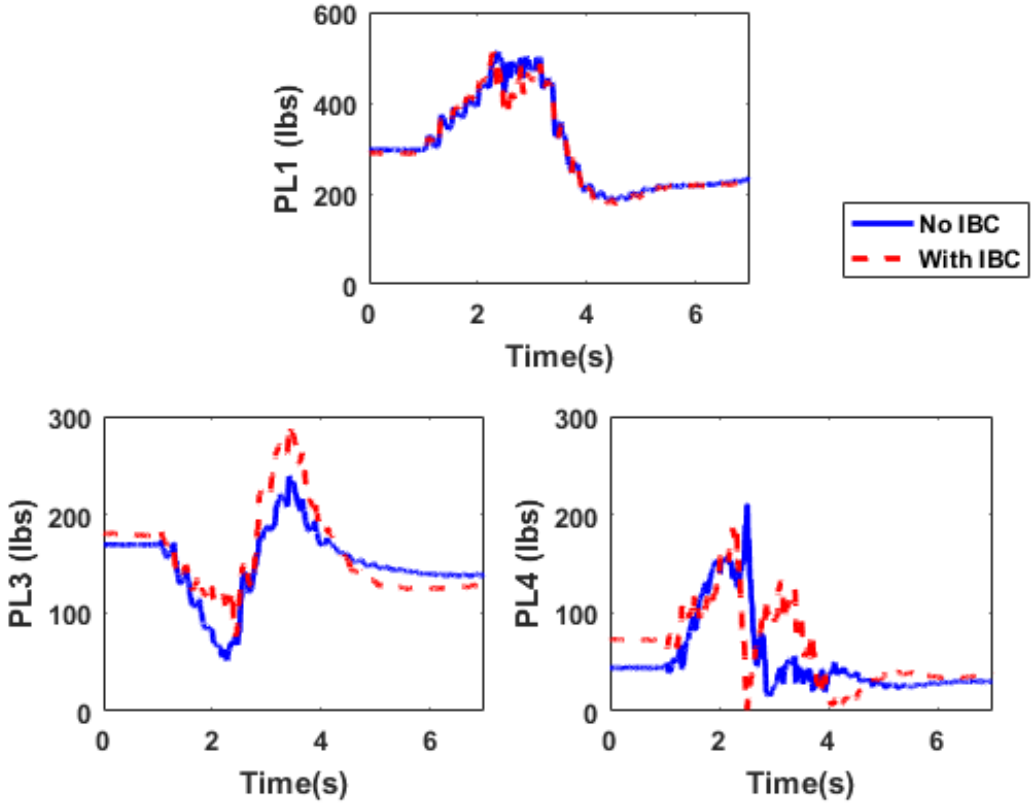

Figure 5.6: Variation of harmonic component of reference blade pitch link load with and without IBC.

Table 5.1: RMS and Peak metrics for load alleviation performance quantification

PL Load	RMS (lb)	Peak Magnitude (lb)
1/rev	308(-2%)	511 (-1%)
2/rev	68 (-65%)	142 (-58%)
3/rev	168 (7%)	292 (22%)
4/rev	74 (16%)	186 (-12%)
Average	155 (-11%)	262 (-12%)

From Table 5.1, it is clear that the load alleviation scheme leads to significant decreases in RMS and peak values for the magnitude of 2/rev pitch link load. More specifically, a decrease of 65% and 58% for the RMS and peak values, respectively, is notable. The average percent improvement in RMS and peak values of the "With IBC" case over the "No IBC" case across all harmonic loads is shown in the last row of Table 5.1. It can

also be observed that in terms of average RMS and peak values, the "With IBC" case is improved over the "No IBC" case. This suggests that the load alleviation scheme has overall beneficial effects on all harmonic components of pitch link load. Therefore, it can be concluded that the proposed load alleviation scheme performs well.

From the harmonic loads, the total pitch link load can be reconstructed. Reduction in peak-to-peak total pitch link load can result in substantial reduction in low-cycle fatigue life usage. Therefore, it would be ideal for the load alleviation scheme to reduce the peak-to-peak total pitch link load as a direct result of individual harmonic component load reduction. Figure 5.7 shows the time history of the peak-to-peak total pitch link load for the cases "With IBC" and "No IBC" based on rotor revolution. Figure 5.7 is obtained by extracting, for each rotor revolution, the pair of maximum and minimum peak total pitch link load values. It may be observed that the peak-to-peak total pitch link load is reduced for the case "With IBC" when compared to the "No IBC" case. The maximum peak-to-peak total pitch link load for the cases "With IBC" and "No IBC" are recorded to be 1201 lb. (occurring at the 10^{th} revolution) and 1341 lb. (occurring at the 11^{th} revolution), respectively. This represents a reduction of 10.4%.

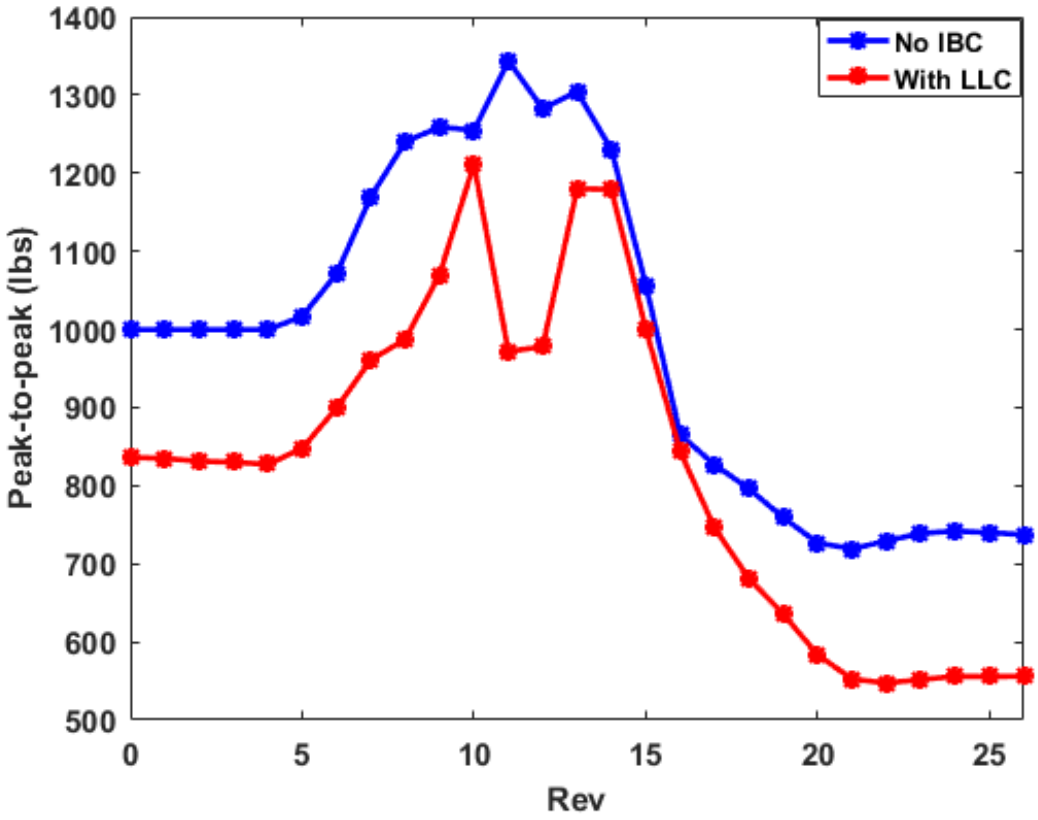

Figure 5.7: Peak-to-peak pitch link load.

The impact of the load alleviation scheme on the maneuver performance can be illustrated by comparing the vehicle pitch rate and airspeed profiles for the cases "With IBC" and "No IBC" (see Fig. 5.8). It may be noted that the body responses are not significantly changed. Hence, it can be concluded that the load alleviation scheme does not have a negative effect on the maneuver performance.

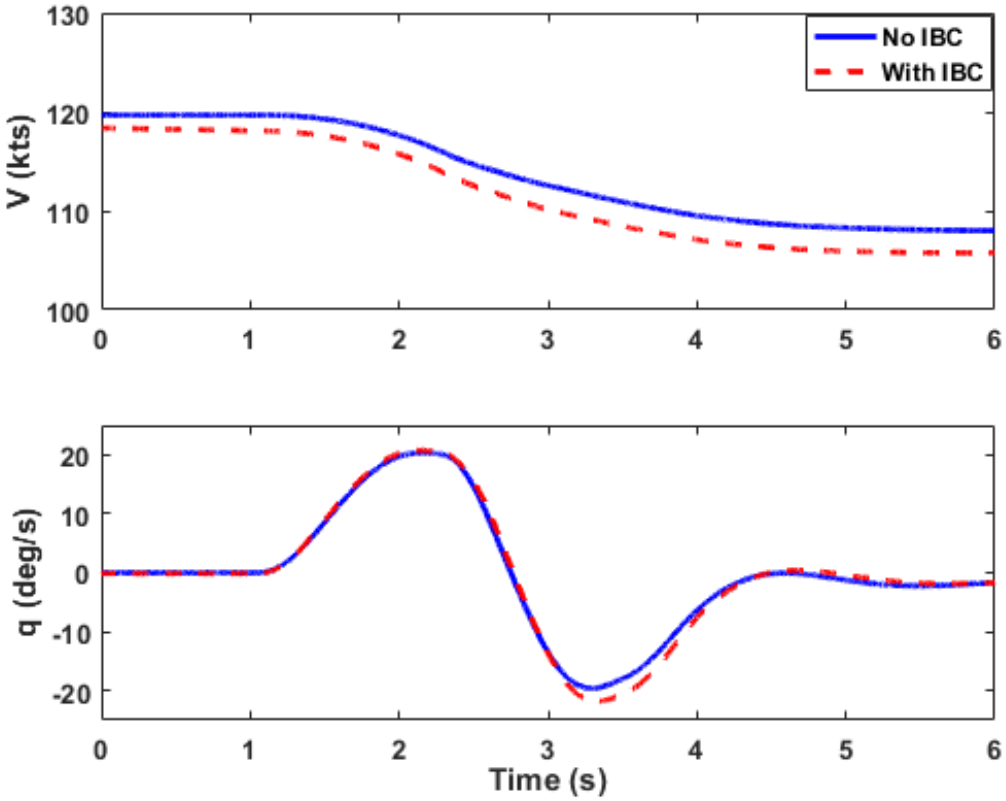

Figure 5.8: Body response with and without IBC.

Figures 5.9 and 5.10 show the flight controller and higher harmonic individual blade pitch inputs, respectively. From Fig. 5.9, it may be observed that the flight controller inputs remain unchanged. The dynamic inversion controller considered in this study is designed to leave the collective stick open-loop. Therefore, for a pitch rate maneuver, the main rotor swashplate collective pitch input is kept at its trim value for the duration of the maneuver as can be observed in Fig. 5.9. It is seen from Fig. 5.10 that for the selected set of weighting matrices Q and R (i.e., q_{IBC} =0.1 and r_{IBC}=1) the 2/rev blade pitch variations stay roughly within 2 degrees of magnitude, while achieving substantial reduction in 2/rev pitch link load (see Fig. 5.5).

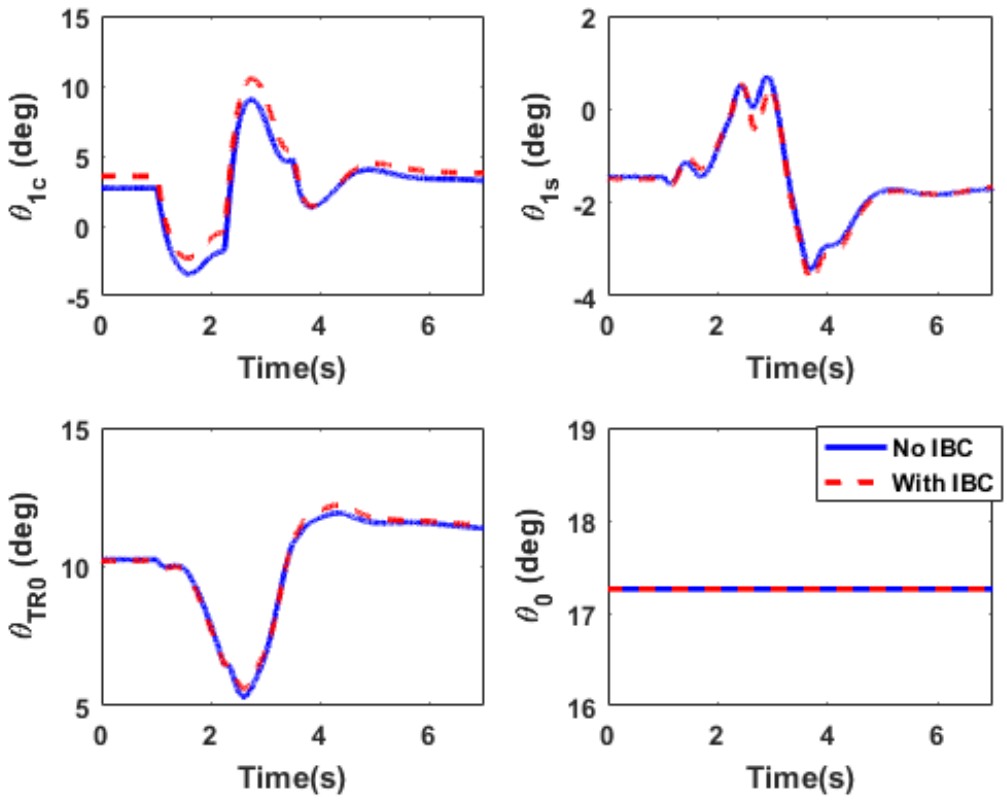

Figure 5.9: Swashplate inputs variations with and without IBC.

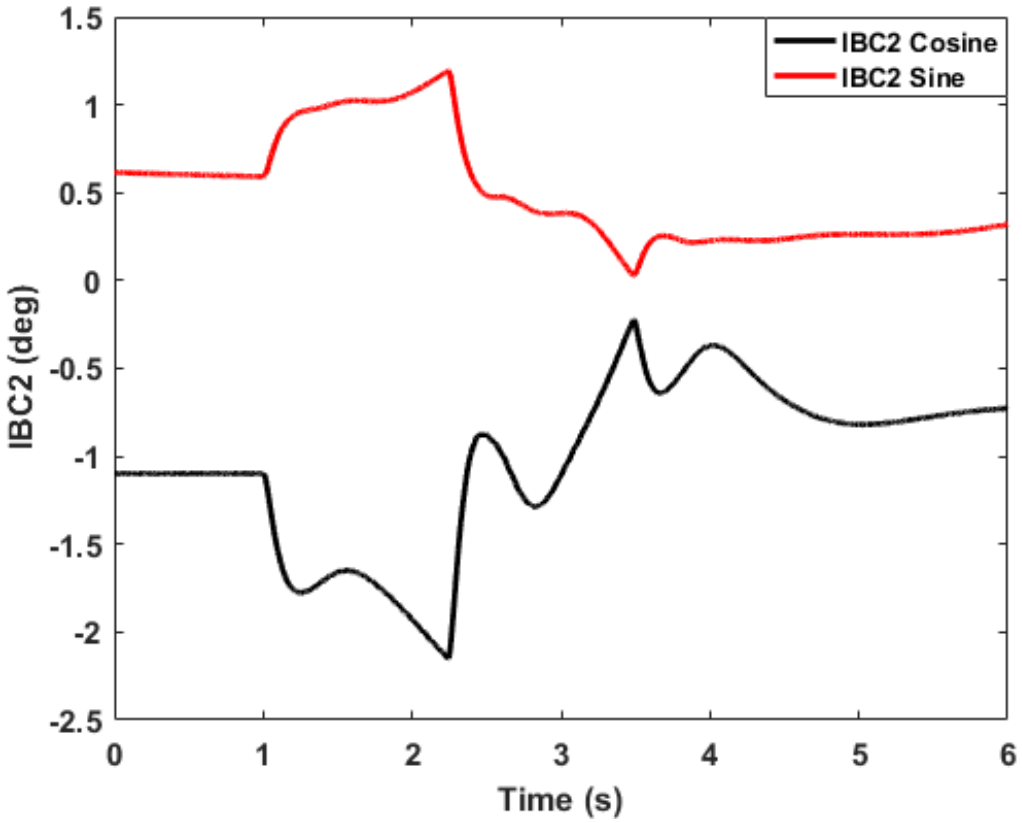

Figure 5.10: Individual blade control inputs variations.

In the literature, various control strategies using individual blade control have been proposed for vibration control. Ref. [98] and Ref. [99] are examples of such research, which demonstrates that individual blade pitch inputs of magnitude 2° or less can have significant effects on vibration (i.e., IBC has the potential to either significantly increase or decrease vibration). Therefore, it is important to assess the impact of the proposed load alleviation scheme on the vibratory hub loads. Simulation results of the magnitude of 4/rev vibratory hub loads (forces: Fx4, Fy4, and Fz4 and moments: Mx4, My4, and Mz4) variations without (labeled "No IBC") and with the proposed load alleviation scheme (labeled "With IBC") are shown in Fig. 5.11 for the case of the pitch rate doublet input of Fig. 5.2. Note that the reduction in 4/rev hub load responses prior to the maneuver is a consequence of the presence of 2/rev IBC inputs throughout the simulation, as shown in Fig. 5.10. To quantify the changes in 4/rev vibratory hub loads introduced by the load

alleviation scheme, the RMS and Peak metrics of Eqs. (5.16) and (5.17) are used. The average RMS and peak percent improvements of the "With IBC" case over the "No IBC" case for the 4/rev vibratory hub loads are -10% and 1%, respectively. As with the harmonic pitch link loads, a negative percentage represents a decrease whereas a positive percentage is an increase. In the computation of the average percent improvement, the 4/rev moments are weighted by $\frac{1}{\Delta Z}$ to put them into comparable units as the 4/rev forces. Here, ΔZ is the vertical displacement of the rotor hub from the vehicle center of gravity. From the average RMS and peak percent improvement values for the 4/rev hub loads, it may be noticed that the load alleviation scheme does not increase the magnitude of 4/rev vibratory hub loads.

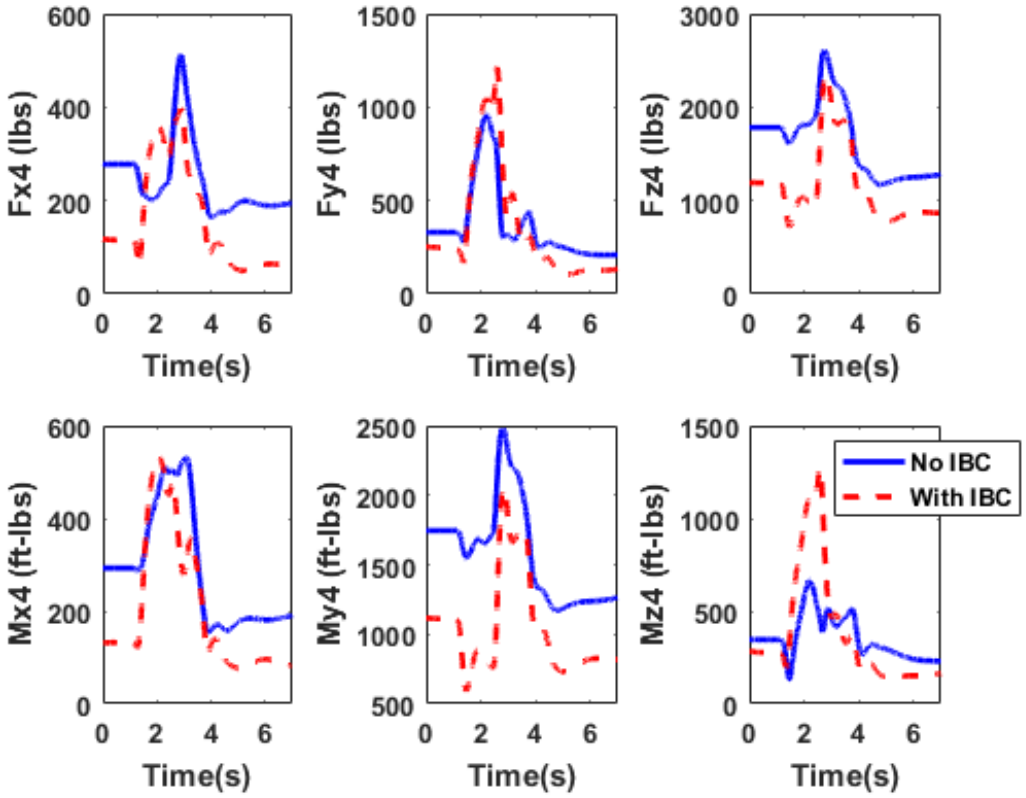

Figure 5.11: Vibratory hub loads variations with and without IBC.

Handling Quality Analysis

A handling quality analysis is needed to understand the impact of the load alleviation scheme on the handling qualities performance of the helicopter. The Handling quality analysis is done using the ADS-33E requirement for small amplitude pitch attitude changes in forward flight. To obtain the requirement for small amplitude pitch attitude changes, it is necessary to extract the bandwidth ($\omega_{BW\theta}$) and phase delay ($\tau_{p\theta}$) parameters. This is done by performing a frequency sweep. First, a frequency sweep is injected into the nonlinear helicopter model. Following that, aircraft responses such as vehicle angular rate responses resulting from this sweep are collected and converted to frequency domain plots. Finally, from the frequency domain plots, the bandwidth and phase delay parameters can be extracted. In this study, the frequency sweep is carefully selected to meet the criteria of the ADS-33E test guide [18]. According to the ADS-33E test guide, the frequency sweep input should be selected such that the aircraft's attitudes are within $\pm$ 10°, angular rates are within $\pm$ 10 deg/s, and the airspeed shall remain within $\pm$ 10 knots of trim.

A sample frequency response plot resulting from a frequency sweep input applied to the nonlinear model with IBC off and on is shown in Fig. 5.12. Figure 5.12 shows the closed-loop pitch attitude response to the commanded pitch rate in the frequency domain. The software CIFER® (Comprehensive Identification from Frequency Responses)[19] is used to convert the time domain data collected from the frequency sweep to the frequency-response plot shown in Fig. 5.12.

From such a frequency sweep, the closed-loop frequency response of the magnitude of 2/rev pitch link load to the commanded angular pitch rate can be computed. Such a plot is shown in Fig. 5.13. From Fig. 5.13, it can be seen that the load alleviation scheme is effective at frequencies ranging from 0.3 rad/s to 15 rad/s.

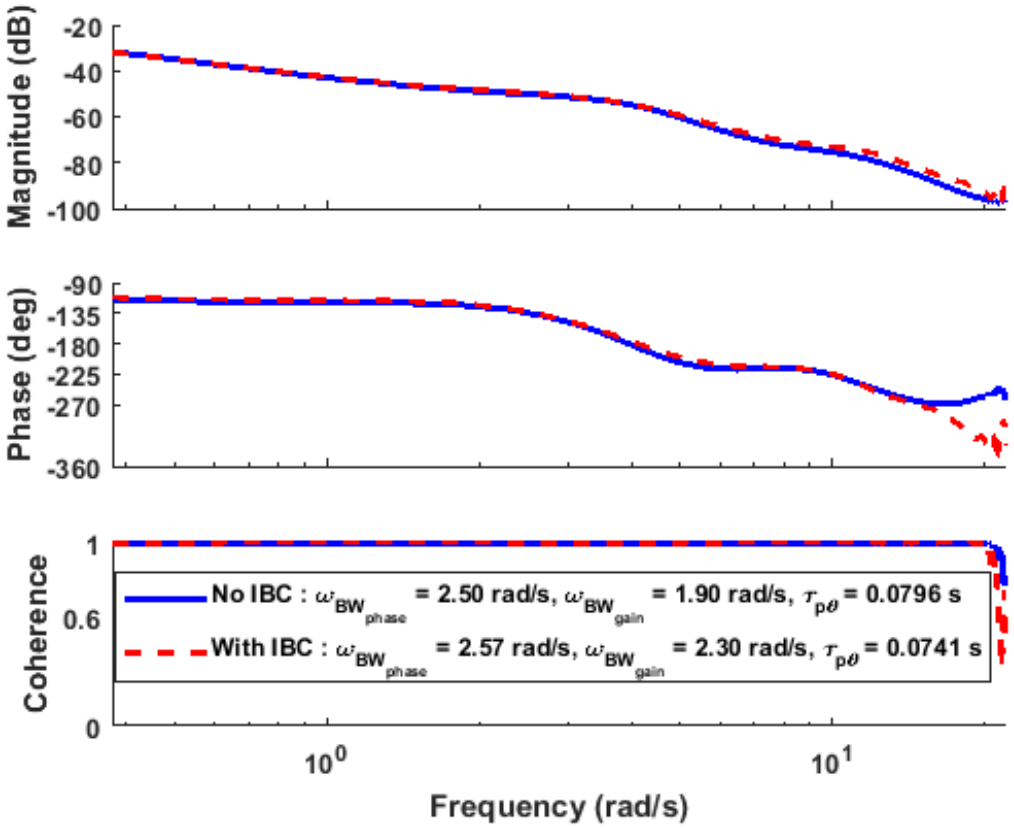

Figure 5.12: Frequency response of the pitch attitude due to pitch rate command with and without IBC.

For an aircraft with a rate command response type, ADS-33E defines the bandwidth and phase delay parameter as follows:

$$\tau_{p\theta} = -\frac{\phi_{2\omega_{180}} + 180^\circ}{57.3(2\omega_{180})} \tag{5.18}$$

$$\omega_{BW_\theta} = min\{\omega_{BW_{gain}}, \omega_{BW_{phase}}\} \tag{5.19}$$

where $\omega_{BW_{gain}}$ and $\omega_{BW_{phase}}$ are the frequency for 6 dB gain and 45° phase margins, respectively. Whereas ω_{180} and $\phi_{2\omega_{180}}$ are the neutral stability frequency and phase at twice the neutral stability frequency, respectively.

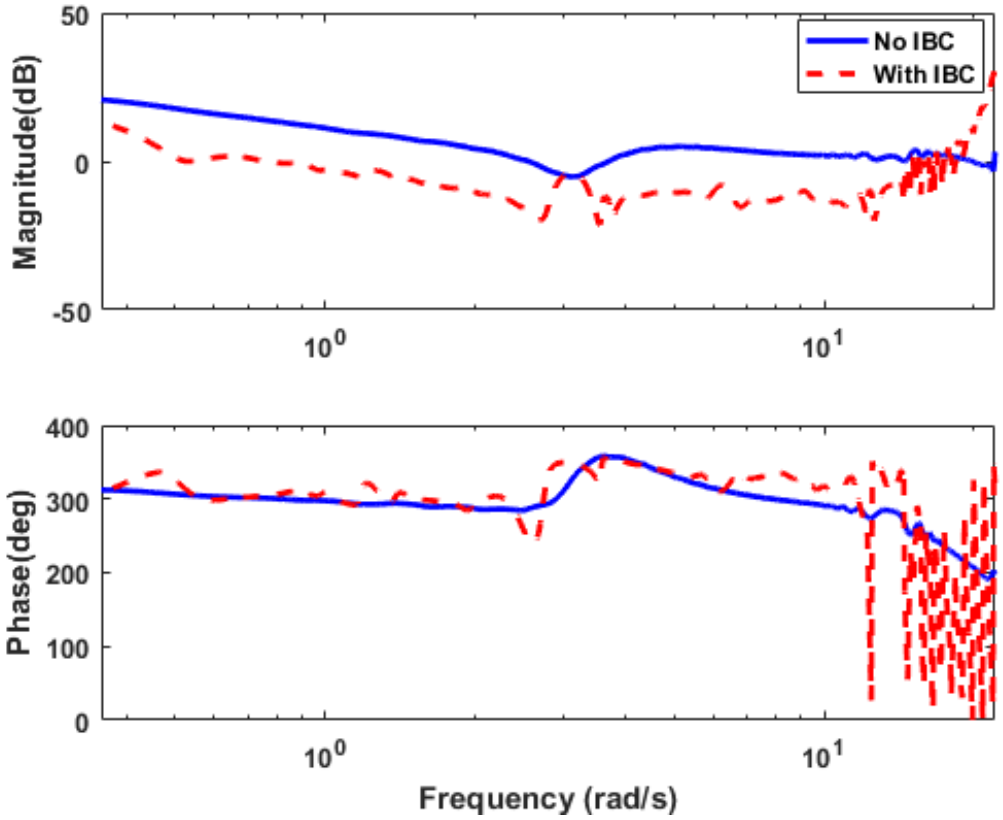

Figure 5.13: Frequency response of the magnitude of 2/rev pitch link load due to pitch rate command with and without IBC.

The bandwidth and phase delay specifications for pitch in the forward flight regime (i.e., 120 knots) are shown in Fig. 5.14. It is seen from Fig. 5.14 that the load alleviation scheme does not degrade the handling qualities for small amplitude pitch changes in forward flight.

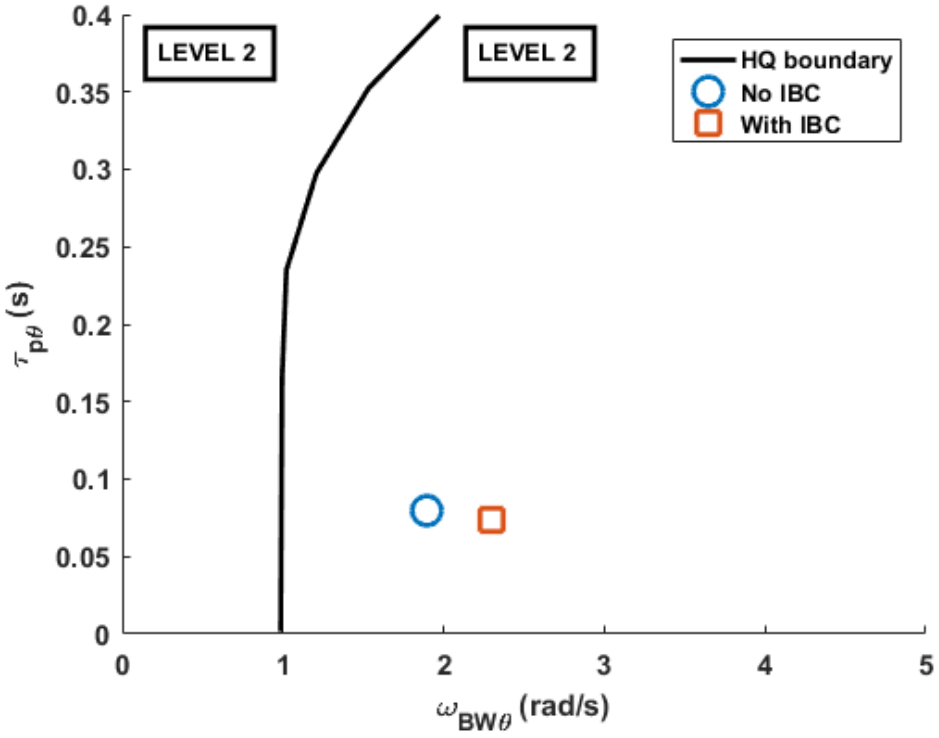

Figure 5.14: Bandwidth and phase delay with and without IBC evaluated against ADS-33E specifications for small-amplitude pitch attitude changes.

5.4 Summary and Technical Findings

In this chapter, a novel approach was presented for real-time load alleviation using active rotor control for reducing helicopter component dynamic loads during aggressive maneuvers. The proposed load alleviation scheme is an on-board system composed of two main components. The first component is a dynamical model that mimics the dynamics of the truth vehicle. This component provides real-time estimates of the effect of pilot control and higher harmonic individual blade pitch inputs on component dynamic loads. The second component is an IBC controller that uses the load estimates from the first component to calculate optimal higher harmonic individual blade pitch inputs to reduce the dynamic loads. Both of these components are developed using a higher-order Linear Time Invariant (LTI) model of helicopter coupled body/rotor/inflow dynamics. The proposed load alleviation scheme is formulated in a model predictive fashion where, using a selected prediction

time horizon, load estimates are generated and used to calculate optimal higher-harmonic individual blade-pitch inputs, which are then combined with the flight control blade pitch changes.

Nonlinear model simulation is performed using a full vehicle nonlinear FLIGHTLAB® model of a generic helicopter . The proposed load alleviation scheme is evaluated in vehicle nonlinear model simulations for its ability to reduce an individual harmonic component of pitch link loads (i.e., 2/rev pitch link load) arising from a rate command maneuver of magnitude 20 deg/s.

It is found that the load alleviation scheme is effective in reducing the 2/rev harmonic pitch link load at trim but also during maneuvering flight with no impact on the maneuver performance. Furthermore, it is revealed that 2/rev load reduction leads to no detrimental effects on uncontrolled harmonic pitch link loads and a reduction in the peak-to-peak total pitch link load. Another interesting finding is that the optimal higher harmonic individual blade pitch inputs generated by the load alleviation scheme have only a minor effect on vibratory hub loads. Furthermore, using the handling quality requirement for small amplitude pitch changes in forward flight, it is shown that the proposed scheme does not cause handling qualities degradation.

CHAPTER 6
CONCLUSIONS AND FUTURE WORK

6.1 Conclusions

In this thesis, research is presented that developed novel estimation methods for online estimation of rotor component loads and novel control methods for component life extension. More specifically, two models, namely LTI and LTI/LQE, were developed for real-time estimation of rotating frame loads that are not easily amenable for measurement; and two control schemes, namely LLC and LAC via IBC, were developed to limit fatigue life usage associated with harmonic loads for component life extension.

The LTI model was evaluated in simulation for estimation of rotor blade pitch link loads arising from vehicle maneuvers using a high-fidelity nonlinear model. While the LTI model can be used for real-time component load estimation, the estimated loads may have to be corrected for errors due to LTI model approximations for large deviations from trim, non-linearities, etc. To remediate this issue, the LTI/LQE model is proposed. The LTI/LQE model combines the LTI model with a Linear Quadratic Estimator (Kalman Filter), which is designed to correct LTI model state response using fixed system hub load measurements. The LTI/LQE was also evaluated in simulation for estimation of rotor blade pitch link loads arising from vehicle maneuvers using a high fidelity nonlinear model. It was shown that the LTI/LQE model gives more accurate load predictions than the LTI model alone. The LTI/LQE model evaluations revealed an interesting finding: the N/rev (where N is the number of blades) fixed system load measurements have information that can be leveraged to make an inference about the N/rev dynamical loads in the rotating system. More specifically, it was found that fixed system hub forces and moments can be used to obtain accurate real-time estimates of the magnitude of 4/rev rotating blade pitch link load. One issue that

arises with the LTI/LQE model is the non-observability of certain harmonic components of rotor states in fixed system measurements. Since the rotor acts as a filter of blade forces and moments, some harmonic states of the LTI model are unobservable in a selected set of fixed system measurements. One potential solution to this issue is the excitation of rotor response where individual blade responses over a rotor revolution is not repeated, which can give rise to vibration at not only N/rev but at all discrete frequencies.

The load limiting control (LLC) scheme is a novel life-extending control scheme that is proposed in this thesis as a potential substitute to the traditional Load Alleviation scheme via flight control modification (LAC via flight control modification). The proposed LLC scheme is an approach for real-time load limiting using Model Predictive Control (MPC) for limiting helicopter component loads during aggressive maneuver. For both the LLC and LAC via flight control modification schemes, a careful trade-off between vehicle maneuver performance and the impact of ensuing maneuver on a component life usage is involved. The LLC scheme was evaluated using nonlinear model simulations for its ability to limit an individual harmonic component of blade root pitch link loads arising from various maneuvers such as attitude and rate command maneuvers. It was observed that the proposed LLC scheme is effective in reducing specific harmonic components of rotor loads within a desired maximum value during aggressive maneuvers.

LAC via flight control modification is a conservative design for two reasons. First, it is incapable of discerning aggressive from non-aggressive maneuvers. Second, it totally neglects the effect of harmonic loads on localized damage. LLC is less conservative than LAC via flight control modification since it is not only able to discern between aggressive and non-aggressive maneuvers but also takes into account the effect of harmonic loads on localized damage. Furthermore, the proposed LLC scheme has the advantage of being integrable with a cueing system. Such cannot be achieved with LAC. Even though the proposed LLC scheme has significant benefits, implementation of this technology in a real system may face a few major roadblocks that should be highlighted. These roadblocks are

associated with the computational complexity of the LLC scheme and its integration within an automatic flight control system. An LAC design is computationally much simpler than the LLC scheme. This is because with the LLC scheme a dynamic optimization needs to be solved in real-time. For a particular application, it might be challenging to guarantee real-time performance of the LLC scheme. Even though the integration of the LLC scheme within an AFCS is merely a software implementation task, choosing the desired integration architecture for a particular application can be challenging. Care should be taken when choosing the integration architecture to minimize maneuver performance degradation while performing load limiting. Such an integration can be achieved in two ways. The first way is via a control limiting architecture ("Control limiting LLC") and the second way is via a command limiting architecture ("Command limiting LLC"). The control limiting LLC limits the control effector commands to achieve load limiting while the command limiting LLC directly limits the pilot's command to achieve load limiting. The command limiting can be implemented with a soft-stop or a visual cueing system that would allow the pilot to override it for safety reasons. On the other hand, implementing a cueing system with the control limiting LLC is not possible. To minimize maneuver performance degradation as a result of the integration of the LLC scheme within an AFCS, it is good practice to augment the AFCS with an anti-windup scheme. This is especially needed for the control limiting LLC since this integration architecture leads to a conflict between the AFCS and the LLC scheme.

The Load Alleviation via IBC (LAC via IBC) scheme is another novel life extending control scheme that is proposed in this thesis as a potential substitute to the traditional Load Alleviation scheme via flight control modification (LAC via flight control modification). LAC via IBC is an approach for real-time load alleviation using active rotor control for reducing helicopter component loads during flight. In this approach, as opposed to the LLC and LAC via flight control modification schemes, no trade-off between vehicle maneuver performance and the impact of ensuing maneuver on a component life usage is

involved. The LAC via IBC scheme is evaluated using nonlinear model simulations for its ability to reduce an individual harmonic component of blade root pitch link loads arising from a rate command maneuver in the forward flight regime. From the simulation results, it was observed that the LAC via IBC scheme is effective in reducing specific harmonic components of rotor loads during flight while not affecting the maneuver performance.

Like the LLC scheme, the LAC via IBC scheme is less conservative than the LAC via flight control modification scheme. This is the case since for this scheme, no trade-off between maneuver performance and load alleviation is present and the effect of harmonic loads on localized damage is taken into account. Another benefit of the LAC via IBC scheme is that it expands the control design space via the introduction of additional controls in the form of higher harmonic blade pitch inputs. One major roadblock for the implementation of this new technology in current and future aircrafts is the need to have actuators in the rotating frame.

It is important to note that in this thesis the robustness of the LLC and LAC via IBC schemes is not evaluated. The LLC and LAC via IBC schemes are fixed-point controllers. The nominal design conditions of both schemes are at a true air speed of 120 knots, steady level flight, an altitude of 1000 ft above sea level standard day and a gross weight of 17000 lbs. A robustness study similar to that of Ref [13] needs to be performed to understand how changes in flight conditions, gross weight, and CG location affect the performance of the fixed-point controllers (i.e., LLC and LAC via ICB schemes).

6.2 Future Work

The following work is recommended to future researchers:

1. Future research should explore ways to overcome the issue of non-observability of harmonic states other than N/rev to improve the proposed LTI/LQE model using fixed system hub load measurements.

2. Further understanding of the trade-off between maneuver performance and different harmonic component load limiting is needed.

3. Further work is needed to evaluate the robustness of the LLC and LAC via IBC schemes with respect to changes in flight condition, weight, and C.G. location. This would assist in determining if an appropriate control scheduling technique is needed to guarantee the effectiveness of the LLC and LAC via IBC schemes throughout the entire flight envelope.

4. In this work, the LTI model used by the LLC and LAC via IBC scheme is obtained by performing, offline, a two-step linearization procedure of a high-fidelity nonlinear model. Perhaps a better strategy would be to identify the LTI model in real-time using system identification methods.

5. Evaluation of the proposed LLC scheme through a visual cueing architecture was shown to be viable; however, for slow to moderate maneuvers, the pilot's ability to follow the visual cue was seen to be degraded for more aggressive maneuvers. Further work is needed to evaluate the effectiveness of LLC using more intuitive cues such as tactile cueing where it is expected that such a cueing system may perform better.

6. Further work is needed in the use of LAC via IBC for alleviation of different harmonic loads.

7. Further work is needed to understand how using the LTI/LQE model instead of the LTI model alone can improve the effectiveness of the LLC and LAC via IBC schemes.

8. Further work is needed in the integration of the proposed LLC scheme with real-time prediction of component fatigue damage models.

Appendices

APPENDIX A

DERIVATION OF HIGHER ORDER LINEAR TIME INVARIANT MODEL

Considering an LTP model of the form given by Eqs. (A.1) and (A.2)

$$\dot{x} = F(\psi)x + G(\psi)u \tag{A.1}$$

$$y = P(\psi)x + R(\psi)u \tag{A.2}$$

Where F, G, P and R are periodic matrices and satisfy the following equations:

$$F(\psi + 2\pi) = F(\psi) \tag{A.3}$$

$$G(\psi + 2\pi) = G(\psi) \tag{A.4}$$

$$P(\psi + 2\pi) = P(\psi) \tag{A.5}$$

$$R(\psi + 2\pi) = R(\psi) \tag{A.6}$$

Such an LTP model with a first order representation can be obtained from a full vehicle nonlinear (NL) FLIGHTLAB® model by performing a linearization about a periodic equilibrium at every azimuthal position as described in the chapter 2. Harmonic decomposition for the extraction of an LTI model assumes the approximation for the state vector, x, in Eq. (A.7).

$$x = x_0 + \sum_{n=1}^{N} [x_{nc} cos(n\psi) + x_{ns} sin(n\psi)] \tag{A.7}$$

where x_0 is the average component, x_{nc} and x_{ns} are, respectively, the n/rev cosine and sine harmonic components of x. Likewise, the control u is expanded in terms of harmonic components as

$$u = u_0 + \sum_{m=1}^{M} [u_{mc} cos(m\psi) + u_{ms} sin(m\psi)] \tag{A.8}$$

u_0 is the average component, u_{mc} and u_{ms} are, respectively, the m^{th} harmonic cosine and sine components of u.

The output y is expanded in a similar fashion

$$y = y_0 + \sum_{l=1}^{L} [y_{lc} cos(l\psi) + y_{ls} sin(l\psi)] \tag{A.9}$$

where y_0 is the average component, y_{lc} and y_{ls} are, respectively, the l^{th} harmonic cosine and sine components of y.

The time derivative of the state vector can be obtained by differentiating Eq. (A.7) with respect to time.

$$\dot{x} = \dot{x}_0 + \sum_{n=1}^{N} [\hat{x}_{nc} cos(n\psi) + \hat{x}_{ns} sin(n\psi)]; \tag{A.10}$$

where

$$\hat{x}_{nc} = \dot{x}_{nc} + n\Omega x_{ns} \qquad \forall n \in [1, 2, ..., \ N] \tag{A.11}$$

$$\hat{x}_{ns} = \dot{x}_{nc} - n\Omega x_{nc} \qquad \forall n \in [1, 2, ..., \ N] \tag{A.12}$$

We substitute Eqs. (A.7), (A.8) and (A.10) into Eq. (A.1).

$$\dot{x}_0 + \sum_{n=1}^{N}[\hat{x}_{nc}cos(n\psi) + \hat{x}_{ns}sin(n\psi)] =$$
$$[F(\psi)](x_0 + \sum_{n=1}^{N}[x_{nc}cos(n\psi) + x_{ns}sin(n\psi)]) + [G(\psi)](u_0 + \sum_{m=1}^{M}[u_{mc}cos(m\psi) + u_{ms}sin(m\psi)]) \tag{A.13}$$

Analogous to the method used in finding the coefficients of a fourrier series, we obtain $\dot{x}_0$ by normalizing Eq. (A.13) by the period (2π) and performing an integration over a full period.

$$\dot{x}_0 = \frac{1}{2\pi}\int_0^{2\pi}\Bigg\{[F(\psi)](x_0 + \sum_{n=1}^{N}[x_{nc}cos(n\psi) + x_{ns}sin(n\psi)]) + [G(\psi)](u_0 + \sum_{m=1}^{M} [u_{mc}cos(m\psi) + u_{ms}sin(m\psi)])\Bigg\}d\psi \tag{A.14}$$

For the cosine and sine components of the vector, $\dot{x}$, they are obtained by multiplying Eq. (A.13) by $\cos(i\psi)$ and $\sin(i\psi)$, respectively, normalizing the obtained expression by half a period (π), and performing an integration over a full period.

$$\dot{\hat{x}}_{ic} = \frac{1}{\pi}\int_0^{2\pi}\Bigg\{[F(\psi)](x_0 + \sum_{n=1}^{N}[x_{nc}cos(n\psi) + x_{ns}sin(n\psi)]) + [G(\psi)](u_0 + \sum_{m=1}^{M} [u_{mc}cos(m\psi) + u_{ms}sin(m\psi)])\Bigg\}cos(i\psi)d\psi$$
$$\forall i \in [1, 2, ..., N] \tag{A.15}$$

$$\dot{\hat{x}}_{is} = \frac{1}{\pi}\int_0^{2\pi}\Bigg\{[F(\psi)](x_0 + \sum_{n=1}^{N}[x_{nc}cos(n\psi) + x_{ns}sin(n\psi)]) + [G(\psi)](u_0 + \sum_{m=1}^{M} [u_{mc}cos(m\psi) + u_{ms}sin(n\psi)])\Bigg\}sin(i\psi)d\psi \quad \forall i \in [1, 2, ..., \ N] \tag{A.16}$$

To simplify Eqs. (A.14), (A.15) and (A.16), we introduce the following notation

$$F^{\text{nc}}(\psi) = F(\psi)cos(n\psi) \tag{A.17}$$

$$F^{\text{ns}}(\psi) = F(\psi)sin(n\psi) \tag{A.18}$$

$$G^{\text{nc}}(\psi) = G(\psi)cos(n\psi) \tag{A.19}$$

$$G^{\text{ns}}(\psi) = G(\psi)sin(n\psi) \tag{A.20}$$

Using the newly introducing notation, Eqs. (A.14), (A.15) and (A.16) can be simplified as follows

$$\dot{x}_0 = \frac{1}{2\pi}\int_0^{2\pi}\Bigg\{(F(\psi)x_0 + \sum_{n=1}^{N}[F^{\text{nc}}(\psi)x_{nc} + F^{\text{ns}}(\psi)x_{ns}]) + (G(\psi)u_0 + \sum_{m=1}^{M} [G^{\text{mc}}(\psi)u_{mc} + G^{\text{ms}}(\psi)u_{ms}])\Bigg\}d\psi \tag{A.21}$$

$$\dot{x}_{ic} = -i\Omega x_{is} + \frac{1}{\pi}\int_0^{2\pi}\Bigg\{(F(\psi)x_0 + \sum_{n=1}^{N}[F^{\text{nc}}(\psi)x_{nc} + F^{\text{ns}}(\psi)x_{ns}]) + (G(\psi)u_0 + \sum_{m=1}^{M} [G^{\text{mc}}(\psi)u_{mc} + G^{\text{ms}}(\psi)u_{ms}])\Bigg\}cos(i\psi)d\psi$$

$$\forall i \in [1, 2, ..., \ N] \tag{A.22}$$

$$\dot{x}_{is} = i\Omega x_{ic} + \frac{1}{\pi}\int_0^{2\pi}\Bigg\{(F(\psi)x_0 + \sum_{n=1}^{N}[F^{\text{nc}}(\psi)x_{nc} + F^{\text{ns}}(\psi)x_{ns}]) + (G(\psi)u_0 + \sum_{m=1}^{M} [G^{\text{mc}}(\psi)u_{mc} + G^{\text{ms}}(\psi)u_{ms}])\Bigg\}sin(i\psi)d\psi$$

$$\forall i \in [1, 2, ..., \ N] \tag{A.23}$$

We can further simplify Eqs. (A.21), (A.22) and (A.23) by introducing the following notation

$$H_{oM} = \frac{1}{2\pi}\int_0^{2\pi} M(\psi)d\psi \tag{A.24}$$

$$H_{icM} = \frac{1}{\pi}\int_0^{2\pi} M(\psi)cos(i\psi)d\psi \tag{A.25}$$

$$H_{isM} = \frac{1}{\pi}\int_0^{2\pi} M(\psi)sin(i\psi)d\psi \tag{A.26}$$

Substituting Eqs. (A.24), (A.25) and (A.26) into Eqs. (A.21), (A.22) and (A.23) we obtain the following simplified expressions

$$\dot{x}_0 = H_{oF}x_0 + \sum_{n=1}^{N}[H_{oF^{\mathrm{nc}}}x_{nc} + H_{oF^{\mathrm{ns}}}x_{ns}] + H_{oG}u_0 + \sum_{m=1}^{M}[H_{oG^{\mathrm{mc}}}u_{mc} + H_{oG^{\mathrm{ms}}}u_{ms}]$$

$$\forall i \in [1, 2, ..., \ N] \tag{A.27}$$

$$\dot{x}_{ic} = -i\Omega x_{is} + H_{icF}x_0 + \sum_{n=1}^{N}[H_{icF^{\mathrm{nc}}}x_{nc} + H_{icF^{\mathrm{ns}}}x_{ns}] + H_{icG}u_0 + \sum_{m=1}^{M}[H_{icG^{\mathrm{mc}}}u_{mc} + H_{icG^{\mathrm{ms}}}u_{ms}]$$

$$\forall i \in [1, 2, ..., \ N] \tag{A.28}$$

$$\dot{x}_{is} = i\Omega x_{ic} + H_{isF}x_0 + \sum_{n=1}^{N}[H_{isF^{\mathrm{nc}}}x_{nc} + H_{isF^{\mathrm{ns}}}x_{ns}] + H_{isG}u_0 + \sum_{m=1}^{M}[H_{isG^{\mathrm{mc}}}u_{mc} + H_{isG^{\mathrm{ms}}}u_{ms}]$$

$$\forall i \in [1, 2, ..., \ N] \tag{A.29}$$

Substituting Eqs. (A.7), (A.8) and (A.9) into Eq. (A.2) we obtain

$$y_0 + \sum_{l=1}^{L}[y_{lc}cos(l\psi) + y_{ls}sin(l\psi)] =$$
$$[P(\psi)](x_0 + \sum_{n=1}^{N}[x_{nc}cos(n\psi) + x_{ns}sin(n\psi)]) + [R(\psi)](u_0 + \sum_{m=1}^{M}[u_{mc}cos(m\psi) + u_{ms}sin(m\psi)]) \tag{A.30}$$

The coefficients y_0, y_{lc}, and y_{ls} are obtained in a similar fashion as for the coefficients $\dot{x}_0$, $\dot{x}_{ic}$, and $\dot{x}_{is}$ (see Eqs. (A.14), (A.15) and (A.16))

$$y_0 = \frac{1}{2\pi}\int_0^{2\pi}\Bigg\{[P(\psi)](x_0 + \sum_{n=1}^{N}[x_{nc}cos(n\psi) + x_{ns}sin(n\psi)]) + [R(\psi)](u_0 + \sum_{m=1}^{M} [u_{mc}cos(m\psi) + u_{ms}sin(m\psi)])\Bigg\}d\psi \tag{A.31}$$

$$y_{lc} = \frac{1}{\pi}\int_0^{2\pi}\Bigg\{[P(\psi)](x_0 + \sum_{n=1}^{N}[x_{nc}cos(n\psi) + x_{ns}sin(n\psi)]) + [R(\psi)](u_0 + \sum_{m=1}^{M} [u_{mc}cos(m\psi) + u_{ms}sin(m\psi)])\Bigg\}cos(l\psi)d\psi \quad \forall l \in [1, 2, ..., \ L] \tag{A.32}$$

$$y_{ls} = \frac{1}{\pi}\int_0^{2\pi}\Bigg\{[P(\psi)](x_0 + \sum_{n=1}^{N}[x_{nc}cos(n\psi) + x_{ns}sin(n\psi)]) + [R(\psi)](u_0 + \sum_{m=1}^{M} [u_{mc}cos(m\psi) + u_{ms}sin(m\psi)])\Bigg\}sin(l\psi)d\psi \quad \forall l \in [1, 2, ..., \ L] \tag{A.33}$$

To simplify Eqs. (A.31), (A.32) and (A.33), we introduce the following notation

$$P^{\text{nc}}(\psi) = P(\psi)cos(n\psi) \tag{A.34}$$

$$P^{\text{ns}}(\psi) = P(\psi)sin(n\psi) \tag{A.35}$$

$$R^{\text{nc}}(\psi) = R(\psi)cos(n\psi) \tag{A.36}$$

$$R^{\text{ns}}(\psi) = R(\psi)sin(n\psi) \tag{A.37}$$

Using the notation above, Eqs. (A.31), (A.32) and (A.33) become

$$y_0 = \frac{1}{2\pi}\int_0^{2\pi}\Bigg\{P(\psi)x_0 + \sum_{n=1}^{N}[P^{\text{nc}}(\psi)x_{nc} + P^{\text{ns}}(\psi)x_{ns}] + R(\psi)u_0 + \sum_{m=1}^{M} [R^{\text{mc}}(\psi)u_{mc} + R^{\text{ms}}(\psi)u_{ms}]\Bigg\}d\psi \tag{A.38}$$

$$y_{lc} = \frac{1}{\pi}\int_0^{2\pi}\Bigg\{P(\psi)x_0 + \sum_{n=1}^{N}[P^{\text{nc}}(\psi)x_{nc} + P^{\text{ns}}(\psi)x_{ns}] + R(\psi)u_0 + \sum_{m=1}^{M} [R^{\text{mc}}(\psi)u_{mc} + R^{\text{ms}}(\psi)u_{ms}]\Bigg\}cos(l\psi)d\psi \tag{A.39}$$

$$\forall l \in [1, 2, ..., \ L]$$

$$y_{ls} = \frac{1}{\pi}\int_0^{2\pi}\Bigg\{P(\psi)x_0 + \sum_{n=1}^{N}[P^{\text{nc}}(\psi)x_{nc} + P^{\text{ns}}(\psi)x_{ns}] + R(\psi)u_0 + \sum_{m=1}^{M} [R^{\text{mc}}(\psi)u_{mc} + R^{\text{ms}}(\psi)u_{ms}]\Bigg\}sin(l\psi)d\psi \tag{A.40}$$

$$\forall l \in [1, 2, ..., \ L]$$

Further simplification can be obtained by using the notation introduced in Eqs. (A.24), (A.25) and (A.26)

$$y_0 = H_{oP}x_0 + \sum_{n=1}^{N}[H_{oP^{\text{nc}}}x_{nc} + H_{oP^{\text{ns}}}x_{ns}] + H_{oR}u_0 + \sum_{m=1}^{M}[H_{oR^{\text{mc}}}u_{mc} + H_{oR^{\text{ms}}}u_{ms}] \tag{A.41}$$

$$y_{lc} = H_{lcP}x_0 + \sum_{n=1}^{N}[H_{lcP^{\text{nc}}}x_{nc} + H_{lcP^{\text{ns}}}x_{ns}] + H_{lcR}u_0 + \sum_{m=1}^{M}[H_{lcR^{\text{mc}}}u_{mc} + H_{lcR^{\text{ms}}}u_{ms}]$$

$$\forall l \in [1, 2, ..., \ L] \tag{A.42}$$

$$y_{ls} = H_{lsP}x_0 + \sum_{n=1}^{N}[H_{lsP^{\text{nc}}}x_{nc} + H_{lsP^{\text{ns}}}x_{ns}] + H_{lsR}u_0 + \sum_{m=1}^{M}[H_{lsR^{\text{mc}}}u_{mc} + H_{lsR^{\text{ms}}}u_{ms}]$$

$$\forall l \in [1, 2, ..., \ L] \tag{A.43}$$

In summary, we have the following sets of equations

$$\dot{x}_{harmonic} = \begin{cases} \dot{x}_0 = H_{oF}x_0 + \sum_{n=1}^{N}[H_{oF^{\text{nc}}}x_{nc} + H_{oF^{\text{ns}}}x_{ns}] + H_{oG}u_0 + \\ \qquad \sum_{m=1}^{M}[H_{oG^{\text{mc}}}u_{mc} + H_{oG^{\text{ms}}}u_{ms}] \\ \dot{x}_{ic} = -i\Omega x_{is} + H_{icF}x_0 + \sum_{n=1}^{N}[H_{icF^{\text{nc}}}x_{nc} + H_{icF^{\text{ns}}}x_{ns}] + H_{icG}u_0 + \\ \qquad \sum_{m=1}^{M}[H_{icG^{\text{mc}}}u_{mc} + H_{icG^{\text{ms}}}u_{ms}] \\ \dot{x}_{is} = i\Omega x_{ic} + H_{isF}x_0 + \sum_{n=1}^{N}[H_{isF^{\text{nc}}}x_{nc} + H_{isF^{\text{ns}}}x_{ns}] + H_{isG}u_0 + \\ \qquad \sum_{m=1}^{M}[H_{isG^{\text{mc}}}u_{mc} + H_{isG^{\text{ms}}}u_{ms}] \end{cases}$$

$$\forall i \in [1, 2, ..., \ N] \tag{A.44}$$

$$
y_{harmonic} = \begin{cases} y_0 = H_{oP}x_0 + \sum_{n=1}^{N}[H_{oP^{\text{nc}}}x_{nc} + H_{oP^{\text{ns}}}x_{ns}] + H_{oR}u_0 + \\ \qquad \sum_{m=1}^{M}[H_{oR^{\text{mc}}}u_{mc} + H_{oR^{\text{ms}}}u_{ms}] \\ \\ y_{lc} = H_{lcP}x_0 + \sum_{n=1}^{N}[H_{lcP^{\text{nc}}}x_{nc} + H_{lcP^{\text{ns}}}x_{ns}] + H_{lcR}u_0 + \\ \qquad \sum_{m=1}^{M}[H_{lcR^{\text{mc}}}u_{mc} + H_{lcR^{\text{ms}}}u_{ms}] \\ \\ y_{ls} = H_{lsP}x_0 + \sum_{n=1}^{N}[H_{lsP^{\text{nc}}}x_{nc} + H_{lsP^{\text{ns}}}x_{ns}] + H_{lsR}u_0 + \\ \qquad \sum_{m=1}^{M}[H_{lsR^{\text{mc}}}u_{mc} + H_{lsR^{\text{ms}}}u_{ms}] \\ \qquad\qquad\qquad\qquad \forall l \in [1, 2, ..., \ L] \end{cases} \tag{A.45}
$$

We can notice that Eqs. (A.44) and (A.45) represent systems of linear equations. Hence, Eqs. (A.44) and (A.45) can be represented in matrix form by defining the augmented state vector as

$$
X = [x_0^T..x_{ic}^T \ \ x_{is}^T..x_{jc}^T \ \ x_{js}^T..]^T \tag{A.46}
$$

and the augmented control vector as

$$
U = [u_0^T..u_{mc}^T \ \ u_{ms}^T..]^T \tag{A.47}
$$

Likewise, the augmented output vector as

$$
Y = [y_0^T..y_{lc}^T \ \ y_{ls}^T..]^T \tag{A.48}
$$

The state-space representation of the resulting LTI model is

$$
\dot{X} = [A]X + [B]U \tag{A.49}
$$

$$Y = [C]X + [D]U \tag{A.50}$$

The LTI model matrices of Eqs. (A.49) and (A.50) are obtained as

$$A = \begin{bmatrix}
H_{oF}\ldots & H_{oF^{ic}} & H_{oF^{is}} & \ldots & H_{oF^{jc}} & H_{oF^{js}} & \ldots \\
\vdots & & \vdots & \vdots & \vdots & \vdots & \ldots \\
H_{icF}\ldots & H_{icF^{ic}} & -i\Omega + H_{icF^{iS}} & \ldots & H_{icF^{jc}} & H_{icF^{js}} & \ldots \\
H_{isF}\ldots & i\Omega + H_{isF^{ic}} & H_{isF^{is}} & \ldots & H_{isF^{jc}} & H_{isF^{js}} & \ldots \\
\vdots & \vdots & \vdots & \vdots & \vdots & \vdots & \ldots \\
H_{jcF}\ldots & H_{jcF^{ic}} & H_{jcF^{is}} & \ldots & H_{jcF^{jc}} & -j\Omega + H_{jcF^{js}} & \ldots \\
H_{jsF}\ldots & H_{jsF^{ic}} & H_{jsF^{is}} & \ldots & j\Omega + H_{jsF^{jc}} & H_{jsF^{js}} & \ldots \\
\vdots & \vdots & \vdots & \vdots & \vdots & \vdots & \ldots
\end{bmatrix}$$

$$B = \begin{bmatrix}
H_{oG}\ldots & H_{oG^{ic}} & H_{oG^{is}} & \ldots & H_{oG^{jc}} & H_{oG^{js}} & \ldots \\
\vdots & \vdots & \vdots & \vdots & \vdots & & \\
H_{icG}\ldots & H_{icG^{ic}} & H_{icG^{is}} & \ldots & H_{icG^{jc}} & H_{icG^{js}} & \ldots \\
H_{isG}\ldots & H_{isG^{ic}} & H_{isG^{is}} & \ldots & H_{isG^{jc}} & H_{isG^{js}} & \ldots \\
\vdots & \vdots & \vdots & \vdots & \vdots & & \\
H_{jcG}\ldots & H_{jcG^{ic}} & H_{jcG^{is}} & \ldots & H_{jcG^{jc}} & H_{jcG^{js}} & \ldots \\
H_{jsG}\ldots & H_{jsG^{ic}} & H_{jsG^{is}} & \ldots & H_{jsG^{jc}} & H_{jsG^{js}} & \ldots \\
\vdots & \vdots & \vdots & \vdots & \vdots & &
\end{bmatrix}$$

$$C = \begin{bmatrix}
H_{oP}\ldots & H_{oP^{ic}} & H_{oP^{is}}\ldots & H_{oP^{jc}} & H_{oP^{js}} & \ldots \\
\vdots & \vdots & \vdots & \vdots & \vdots & \\
H_{lcP}\ldots & H_{lcP^{ic}} & H_{lcP^{is}}\ldots & H_{lcP^{jc}} & H_{lcP^{js}} & \ldots \\
H_{lsP}\ldots & H_{lsP^{ic}} & H_{lsP^{is}}\ldots & H_{lsP^{jc}} & H_{lsP^{js}} & \ldots \\
\vdots & \vdots & \vdots & \vdots & \vdots &
\end{bmatrix}$$

$$D = \begin{bmatrix} H_{oR} \dots & H_{oR^{ic}} & H_{oR^{is}} \dots & H_{oR^{jc}} & H_{oR^{js}} & \dots \\ \vdots & \vdots & \vdots & \vdots & \vdots & \\ H_{lcR} \dots & H_{lcR^{ic}} & H_{lcR^{is}} \dots & H_{lcR^{jc}} & H_{lcR^{js}} & \dots \\ H_{lsR} \dots & H_{lsR^{ic}} & H_{lsR^{is}} \dots & H_{lsR^{jc}} & H_{lsR^{js}} & \dots \\ \vdots & \vdots & \vdots & \vdots & \vdots & \end{bmatrix}$$

APPENDIX B

DERIVATION OF DYNAMIC INVERSION CONTROLLER

Consider the following dynamical system where the output y and δu have the same dimensions.

$$\dot{\tilde{x}} = [A]\tilde{x} + [B]\delta u \tag{B.1}$$

$$y = [C]\tilde{x} \tag{B.2}$$

The matrices A, B and C vary with flight condition and are scheduled with airspeed. The goal of a dynamic inversion controller is to control the output y so as to follow a reference signal. Hence, we differentiate the output equation until the control input appears.

$$\dot{y} = [C]\dot{\tilde{x}} = [C][A]\tilde{x} + [C][B]\delta u \tag{B.3}$$

In case $[C][B]$ is equal to zero y should be differentiate again to explicitly show the control input with a non-zero coefficient.

The reference signal to track is y_{cmd}. The tracking error can be formulated as follows

$$\vec{e} = y_{cmd} - y \tag{B.4}$$

The dynamics of the error is obtained as follows

$$\dot{\vec{e}} = \dot{y}_{cmd} - \dot{y} \tag{B.5}$$

Using Eqs. (B.3) and (B.5) we obtain

$$-\dot{\vec{e}} = [C][A]\tilde{x} + [C][B]\delta u - \dot{y}_{cmd} \tag{B.6}$$

In order to minimize the tracking error and stabilize the error growth, we add some compensation as follows

$$\mu = Ke = -\dot{\vec{e}} \tag{B.7}$$

We can solve for the control input, δu, (see Fig. 4.5) out of the control mixing by using Eqs. (B.6) and (B.7)

$$\vec{\delta u} = [CB]^{-1}(-CA\tilde{x} + Ke + \dot{y}_{cmd}) \tag{B.8}$$

We use the dynamic inversion controller in order to track command inputs. The higher order LTI model was reduced to a simple 3^{rd} order model of the angular rate dynamics with lateral, longitudinal and pedal inputs as control variables

$$\dot{\tilde{x}} = [A]\tilde{x} + [B]\delta u \tag{B.9}$$

$$y = [C]\tilde{x} \tag{B.10}$$

where

$$y = \tilde{x} = \begin{bmatrix} P \\ Q \\ R \end{bmatrix} \tag{B.11}$$

$$\delta u = \begin{bmatrix} \delta_{lat} \\ \delta_{lon} \\ \delta_{ped} \end{bmatrix} \tag{B.12}$$

REFERENCES

[1] G. D. Pathfield, *Helicopters Flight Dynamics*. WILEY, 2018.

[2] C. C. Crawford, "Rotorcraft analytical improvement needed to reduce developmental risk-the 1989 alexander a. nikolsky lecture," *JAHS*, vol. 35, pp. 3–22, 1 Jan. 1990.

[3] P. D. Schrage, "An overview of technical problems in helicopter rotor loads predictions methods," *AIAA Journal*, Sep. 1979.

[4] P. D. Schrage and A. J. O'Malley, "Performance and aeroelastic tradeoffs on recent rotor blade designs," *JAHS*, vol. 50, pp. 238–248, 3 Jul. 2005.

[5] M. L. Mil, *Helicopters: Calculation and Design vol.11,Vibrations and Dynamic Stability*. NASA TT F-519., 1968.

[6] D. P. Davies, S. L. Jenkins, and F. R. Belben, "Survey of fatigue failures in helicopter components and some lessons learnt," *Engineering Failure Analysis*, vol. 32, pp. 134–151, 9 2013.

[7] M. Kaye, "Dynamic Health and Usage Monitoring System - Program Update," Proceedings of the Fifteenth European Rotorcraft Forum., Amsterdam, Netherland, Sep. 1989.

[8] G. Jeram and J. V. R. Prasad, "Open architecture for helicopter tactile cueing systems," *JAHS*, vol. 50, pp. 238–248, 3 Jul. 2005.

[9] P. Pawar and R. Ganguli, "Helicopter rotor health monitoring – a review," *Journal of Aerospace Engineering*, vol. 211, pp. 631–647, 2007.

[10] D. J. Haas, J. Milano, and L. Flitter, "Prediction of helicopter component loads using neural networks," *Journal of the American Helicopter Society*, vol. 40, no. 1, pp. 72–82, 1995.

[11] D. J. Haas, L. Flitter, and J. Milano, "Helicopter flight data feature extraction for component load monitoring," *Journal of Aircraft*, vol. 33, no. 1, pp. 37–47, 1996.

[12] M. M. Kelley, L. Flitter, and D. J. Haas, "Development and flight test evaluation of a rotor system load monitoring technology," *Journal of the American Helicopter Society*, vol. 45, no. 1, pp. 19–27, 2000.

[13] M. J. S. Lopez, "Linear time invariant approximations of linear time periodic systems for integrated flight and vibration control," Ph.D. dissertation, Georgia Institute of Technology, 2016.

[14] F. E. Olcer, "Linear Time Invariant Models for Integrated Flight and Rotor Control," Ph.D. dissertation, Georgia Institute of Technology, 2011.

[15] J. V. R. Prasad, F. E. Olcer, L. N. Sankar, and C. He, "Linear Time Invariant Models for Integrated Flight and Rotor Control," Proceedings of the 35^{th} European Rotorcraft Forum., Hamburg, Germany, Sep. 2009.

[16] N. T. Morgan, C. S. Berrigan, M. J. S. Lopez, and J. V. R. Prasad, "Application of linear quadratic estimation to harmonic analysis of rotorcraft vibration," *Journal of Guidance, Control, and Dynamics*, vol. 40, no. 9, pp. 1–7, 2017.

[17] D. G. Miller, T. M. Black, and M. Joglekar, "Tiltrotor control law design for rotor loads alleviation using modern control techniques," in *1991 American Control Conference*, 1991, pp. 2488–2493.

[18] D. G. Miller, "Active Control of TiltRotor In-plane Loads duirng Maneuvers," M.S. thesis, Massachusetts Institute of Technology, 1988.

[19] D. Popelka and A. Agnihotri, "Prediction and Alleviation of V-22 Rotor Dynamic Loads," American Helicopter Society National Specialists' Meeting on Rotorcraft Dynamics., Arlington, Texas, Nov. 1989.

[20] D. W. King, R. L. Dabundo, and A. Agnihotri, "V-22 load limiting control law development," Proceedings of the 49^{th} Annual Forum of the American Helicopter Society., St Louis, MO, May 1993.

[21] M. Voskuijl, M. D. Pavel, and Vorst, "Active Control Technology for Tiltrotor Structural Load Alleviation," Proceedings of the 30^{th} European Rotorcraft Forum., Marseille, France, Sep. 2004.

[22] M. M. Colella, G. Bernardini, and M. Gennaretti, "Alleviation of Tiltrotor Wing-Root Vibratory Loads Through Cyclic Control Approach," Proceedings of the 35^{th} European Rotorcraft Forum., Hamburg, Germany, Sep. 2009.

[23] U. Saetti and J. Horn, "Load alleviation flight control design using high-order dynamic models.," *Journal of the American Helicopter Society*, vol. 65, no. 3, pp. 1–15, 2020.

[24] U. Saetti, J. F. Horn, T. Berger, and M. B. Tischler, "Handling-qualities perspective on rotorcraft load alleviation control.," *Journal of Guidance, Control, and Dynamics*, vol. 43, no. 10, pp. 1792–1804, 2020.

[25] M. Whalley and M. Achache, "Joint U.S/France investigation of helicopter flight envelope limit cueing," Proceedings of the 52^{nd} Annual Forum of the American Helicopter Society., Washington, D.C, Jun. 1996.

[26] J. R. Mayo and V. N. Iannacci, "Rah-66 comanche flight envelope cueing system," Proceedings of the 55^{th} Annual Forum of the American Helicopter Society., Montreal, Canada, May 1999.

[27] M. S. Whalley, "A piloted simulation investigation of helicopter limit cueing," USAATCOM Technical report 94-A-020, Aeroflightdynamics Directorate, U.S.Army Aviation and Troop Command, Ames Research Center., Moffet Field,California, Oct. 1994.

[28] M. S. Whalley, B. Hindson, and G. Thiers, "Comparison of Active Sidestick and Conventional Inceptors for Helicopter Flight Envelope Tactile Cueing," NASA Ames Research Center., Moffet Field,California, Jan. 2000.

[29] A. J. Bateman, D. G. Ward, R. L. Barron, and M. S. Whalley, "Piloted simulation evaluation of a neural network limit avoidance system for rotorcraft," Proceedings of AIAA Atmospheric Flight Mechanics Conference., Portland, OR, Aug. 1999.

[30] J. Horn, "Flight Envelope Limit Detection and Avoidance," Ph.D. dissertation, Georgia Institute of Technology, 1999.

[31] I. Yavrucuk, "Adaptive Limit Margin Detection and Limit Avoidance," Ph.D. dissertation, Georgia Institute of Technology, 2003.

[32] P. K. Menon, V. R. Iragavarapu, and M. S. Whalley, "Estimation of Rotorcraft Limit Envelopes Using Neural Networks," Proceedings of the 52^{nd} Annual Forum of the American Helicopter Society., Washington, DC, Jun. 1996.

[33] I. Yavrucuk, J. Prasad, and A. Calise, "Carefree maneuvering using adaptive neural networks," Proceedings of AIAA Atmospheric Flight Mechanics Conference., Monterey, California, Aug. 2002.

[34] I. Yavrucuk, J. Prasad, and A. Calise, "Adaptive limit detection and avoidance for carefree maneuvering," Proceedings of AIAA Atmospheric Flight Mechanics Conference., Montreal, Canada, Aug. 2001.

[35] I. Yavrucuk, J. V. R. Prasad, and A. Calise, "Adaptive limit and control margin prediction and limit avoidance," Proceedings of the 58^{th} Annual Forum of the American Helicopter Society., Montreal, Canada, Jun. 2002.

[36] I. Yavrucuk and J. V. R. Prasad, "Adaptive limit margin prediction and control cueing for carefree maneuvering of vtol aircraft," Proceedings of the AHS Flight Control and Crew Design Technical Specialists Meeting., Philadelphia, PA, Aug. 2001.

[37] S. Unnikrishnan, G. Jeram, and J. V. R. Prasad, "Tactile limit avoidance cueing using adaptive dynamic trim.," Proceedings of the 60^{th} Annual Forum of the American Helicopter Society., Baltimore, MD, Jun. 2004.

[38] J. V. R. Prasad, I. Yavrucuk, and S. Unnikrishnan, "Adaptive limit prediction and avoidance for rotorcraft," Proceedings of the 28^{th} European Rotorcraft Forum., Bristol, UK, Oct. 2002.

[39] I. Yavrucuk, S. Unnikrishnan, and J. V. R. Prasad, "Envelope protection in autonomous unmanned aerial vehicles.," Proceedings of the 60^{th} Annual Forum of the American Helicopter Society., Phoenix, AZ, May 2003.

[40] N. Sahani, "Envelope Protection Systems for Piloted and Unmanned Rotorcraft," Ph.D. dissertation, The Pennsylvania State University, 2005.

[41] S. Unnikrishnan, "Envelope Protection Systems for Piloted and Unmanned Rotorcraft," Ph.D. dissertation, Georgia Institute of Technology, 2006.

[42] C. L. Botasso and P. Montinari, "Rotorcraft flight envelope protection by model predictive control," *JAHS*, vol. 60, pp. 1–13, 2 Jan. 2017.

[43] F. G. Polanco, "Estimation of Structural Component Loads in Helicopters : A Review of Current Methodologies," *DSTO Aeronautical and Maritime Research Laboratory*, 1999.

[44] W. L. Gunsallus, W. L. Pellum, and W. Flannelly, "Holometrics: An Information Transformation Methodology," Proceedings of the 44^{th} Annual Forum of the American Helicopter Society., Washington, DC, Jun. 1988.

[45] W. L. Gunsallus, "Rotating System Load Monitoring Using Minimum Fixed System Instrumentation," American Helicopter Society National Specialist Meeting on Fatigue Methodology, Scottsdale, AZ, Oct. 1989.

[46] W. L. Gunsallus and E. Robeson, "AH-64A Rotating Load Usage Monitoring from Fixed System Information," American Helicopter Society Structures Specialist Meeting, Williamsburg, Virginia, Oct. 1991.

[47] S. S. Tang and L. J. O'Brien, "A Novel Method for Fatigue Life Monitoring of Non-Airframe Components," 32^{nd} Structures, Structural Dynamics, and Materials Conference, Baltimore, MD, Aug. 1991.

[48] G. L. Barndt and S. Moon, "Development of a Fatigue Tracking Program for Navy Rotary Wing Aircraft," Proceedings of the American Helicopter Society 50^{th} Annual Forum, Washington, DC, May 1997.

[49] D. J. Haas, "Determination of Helicopter Flight Loads from Fixed System Measurements," Proceedings of the AIAA/ASME/ASCE/AHS/ASC 32^{nd} Structures, Structural Dynamics, and Materials Conference, Baltimore, MD, 1991.

[50] D. J. Haas and R. Imber, "Identification of helicopter component loads using multiple regression," *Journal of Aircraft*, vol. 31, no. 4, 1994.

[51] S. S. Tang and J. Moffatt, "Flight Load Models for the On-Board Fatigue Usage Processing of Mechanical Components on Helicopters," AIAA Dynamics Specialists Conference, Apr. 1994.

[52] S. S. Tang and J. Moffatt, "Development of an on-board fatigue processor for helicopters," *International Journal of Fatigue*, vol. 18, no. 3, 1996.

[53] K. Funahashi, "On the approximate realization of continuous mappings by neural networks," *International Journal of Fatigue*, vol. 2, no. 3, pp. 183–192, 1989.

[54] A. B. Cook, C. R. Fuller, R. H. O'Brien, and R. H. Cabell, "Artificial neural networks for predicting nonlinear dynamic helicopter loads," *AIAA Journal*, vol. 32, no. 5, pp. 1072–1077, 1994.

[55] H. Azzam, "A Practical Approach for the Indirect Prediction of Structural Fatigue from Measured Flight Parameters," *Journal of Aerospace Engineering*, vol. 211, no. 5, pp. 29–38, 1997.

[56] M. E. Hoffman, "Improving Predictions for Helicopter Usage Monitoring," Proceedings of the USAF Structural Integrity Program Conference, San Antonio, TX, Dec. 1994.

[57] E. Matthieu, "Mémoire sur le mouvement vibratoire de une membrance de fore elliptique," *Journal Mathematique Pures at Appliquee*, 1868.

[58] G. W. Hill, "Mean Motion of the Lunar Perigee," *Acta Matematica*, vol. 8, Jan. 1886.

[59] D. J. Daniel, "Exact solutions of mathieu's equation," *Progress of Theoretical and Experimental Physics*, vol. 40, no. 1, pp. 1–14, 2020.

[60] F. E. Olcer, J. V. R. Prasad, L. N. Sankar, J. J. Bain, J. Zhao, and C. He, "Development and Evaluation of Reduced Order Models of On-Blade Control for Integrated Flight and Rotor Control," Annual Forum Proceedings - American Helicopter Society., Phoenix, Arizona, May 2010.

[61] M. J. S. Lopez, J. V. R. Prasad, M. B. Tischler, and M. D. Takahashi, "Simulating HHC/AFCS Interaction and Optimized Controllers using Piloted Maneuvers,"

Annual Forum Proceedings - American Helicopter Society., Phoenix, Arizona, May 2015.

[62] M. J. S. Lopez and J. V. R. Prasad, "Linear time invariant approximations of linear time periodic systems," *JAHS*, vol. 62, pp. 1–10, 1 Jan. 2017.

[63] M. Scaramal, J. F. Horn, and U. Saetti, "Load Alleviation Control using Dynamic Inversion with Direct Load Feedback," Proceedings of the 77^{th} Annual Forum of the American Helicopter Society., May 2020.

[64] K. Glover, "All optimal hankel-norm approximations of linear multivariable systems and their L^{∞} -error bounds," *International Journal of Control*, vol. 9, no. 5, pp. 1115–1193, 1984.

[65] B. Moore, "Principal component analysis in linear systems: Controllability, observability, and model reduction," *IEEE Transactions on Automatic Control*, vol. 26, no. 1, pp. 17–32, 1981.

[66] L. Silverman and L. Pernebo, "Model reduction via balanced state space representations," *IEEE Transactions on Automatic Control*, vol. 27, no. 2, pp. 382–387, 1982.

[67] P. V. Kokotovic, K. H. Khalil, and J. O'Reilly, "Time-scale modeling," in *Singular Perturbation Methods in Control: Analysis and Design*, ch. 1, pp. 1–46.

[68] P. V. Kokotovic, R. E. O'Malley, and P. Sannuti, "Singular perturbations and order reduction in control theory — an overview," *Automatica.*, vol. 12, pp. 123–132, 2 Mar. 1976.

[69] P. Friedmann and T. Millott, "Vibration reduction in rotorcraft using active control: A comparison of various approaches," *Journal of Guidance, Control, and Dynamics*, vol. 18, no. 4, 1995.

[70] C. Kessler, "Active rotor control for helicopters: Individual blade control and swashplateless rotor designs," *CEAS Aeronautical Journal*, vol. 1, no. 23, pp. 23–54, 2011.

[71] D. Patt, L. Liu, J. Chandrasekar, D. Bernstein, and P. Friedmann, "Higher-harmonic-control algorithm for helicopter vibration reduction revisited," *Journal of Guidance, Control, and Dynamics*, vol. 28, no. 5, 2005.

[72] D. Roth, "Advanced Vibration Reduction by IBC Technology," Delft, The Netherlands, Sep. 2004.

[73] T. R. Norman *et al.*, "Full-Scale Wind Tunnel Test of a UH-60 Individual Blade Control System for Performance Improvement and Vibration, Loads, and Noise Control," Grapevine, Texas, May 2009.

[74] U. T. P. Arnold and D. Furst, "Closed loop ibc results from ch-53g flight tests," *Aerospace Science and Technology*, vol. 9, no. 5, pp. 421–435, 2005.

[75] O. Dieterich, "Application of Modern Control Technology for Advanced IBC Systems," Marseilles, France, Sep. 1998.

[76] ART, Inc., "Flightlab® xanalysis user manual," Jul. 2013.

[77] D. B. Caudle, "Damage Mitigation for Rotorcraft through Load Alleviating Control," Master thesis, The Pennsylvania State University, 2014.

[78] M. B. Tischler and R. K. Remple, " Aircraft and Rotorcraft System Identification: Engineering Methods With Flight-test Examples," in AIAA, 2012.

[79] R. M. Leuthold, "One the use of theil's inequality coefficients.," *American Journal of Agricultural Economics*, vol. 57, 2 May 1975.

[80] G. Welch and G. Bishop, "An introduction to the kalman filter," *Department of Computer Science, University of North Carolina at Chapel Hill*, Jul. 2006.

[81] S. Shah, C. Mballo, J. V. R. Prasad, and J. J. Rimoli, "Effect of load limiting control on rotorcraft maneuver performance and component damage growth," Proceedings of the American Helicopter Society 77^{th} Annual Forum, Oct. 2021.

[82] S. Dobrila and R. K. Nada, "The system order reduction via balancing in view of the method of singular perturbation," *FME Transactions*, Oct. 2010.

[83] C. E. Mballo and J. V. R. Prasad, "Load Limiting Control Design for Rotating Blade Root Pitch Link Load Using Higher Order Harmonic LTI Models," Delft, The Netherlands, Sep. 2018.

[84] M. B. Tischler, T. Berger, C. M. Ivler, K. K. Mansur M. H.and Cheung, and J. Y. Soong, "Practical Methods for Aircraft and Rotorcraft Flight Control Design: An Optimization-Based Approach," in 2017.

[85] C. E. Mballo and J. V. R. Prasad, "Trade-off between maneuver performance and component load limiting," in *Proceedings of the* 76^{th} *Annual Forum of the American Helicopter Society*, Oct. 2020.

[86] M. T. Sergio Galeani Sophie Tarbouriech and L. Zaccarian, "A tutorial on modern anti-windup design," *European Journal of Control*, vol. 15, pp. 418–440, May 2009.

[87] L. R. da Silva, R. C. Flesch, and J. E. Normey-Rico, "Analysis of anti-windup techniques in pid control of processes with measurement noise.," *IFAC-PapersOnLine*, vol. 51, no. 4, pp. 948–953, 2018.

[88] A. Visioli, "Modified anti-windup scheme for pid controllers," *IEE proceedings. Control theory and applications*, vol. 150, no. 1, pp. 49–54, 2003.

[89] J. V. R. Prasad, V. Comandur, R. Walters, and D. Guerrero, "Model Predictive Path Integral Approach for Trajectory Guidance of Rotorcraft Shipboard Landing.," Proceedings of the 74^{th} Annual Forum of the American Helicopter Society.., Phoenix, AZ, May 2018.

[90] G. Williams, A. Aldrich, and E. A. Theodorou, "Model predictive path integral control: From theory to parallel computation," *JGCD*, vol. 40, pp. 344–357, 2 Feb. 2017.

[91] V. Comandur, J. V. R. Prasad, and R. Walters, "MPPI Parallel Trajectory Optimization for Guidance in Rotorcraft Shipboard Landing.," Proceedings of the 75^{th} Annual Forum of the American Helicopter Society., Philadelphia, PA, May 2019.

[92] "Handling Qualities Requirements for Military Rotorcraft," Aeronautical Design Standard, Performance Specification, ADS-33E-PRF. Redstone Arsenal, Alabama: United States Army Aviation and Missile Command, 2000.

[93] I. Yavrucuk, S. Unnikrishnan, and J. V. R. Prasad, "Envelope protection for autonomous unmanned aerial vehicles," *Journal of Guidance, Control, and Dynamics*, vol. 32, no. 1, pp. 248–261, 2009.

[94] M. Voskuijl and M. Verhagen, "Helicopter main rotor hub load alleviation using a variable incidence horizontal stabilizer," *American Helicopter Society. Journal*, vol. 63, 2017.

[95] C. Blanken, R. Hoh, D. Mitchell, and D. Key, "Test guide for ads-33e-prf," in *HAI Technical Report No. 1130-1*, 2008.

[96] M. Pavel and G. D. Padfield, "The extension of ADS-33 Metrics for agility Enhancement and structural Load Alleviation," *Journal of the American Helicopter Society*, vol. 51, pp. 319–330, 4 Oct. 2006.

[97] M. D. Pavel, "Rotorcraft design for maximized performance at minimized vibratory loads," in *Aeronautics and Astronautics*, M. Mulder, Ed., IntechOpen, 2011, ch. 8.

[98] M. J. S. Lopez, M. B. Tischler, M. D. Takahashi, K. K. Cheung, and J. V. R. Prasad, "Development and evaluation of a full flight envelope integrated flight and vibration controller," *Journal of the American Helicopter Society*, vol. 64, pp. 1–11, 1 Jan. 2019.

[99] D. Roth, "Advanced Vibration Reduction by IBC Technology," Proceedings of the 30^{th} European Rotorcraft Forum, Marseilles, France, Sep. 2004.

VITA

Chams Eddine Mballo was born in Dakar, Senegal. He received his bachelor's degree with a dual major in aerospace engineering and mechanical engineering in 2015 from the State University of New York (SUNY) at Buffalo. He joined the Georgia Institute of Technology in August 2016. He is the recipient of three master's degrees from the Georgia Institute of Technology: aerospace engineering (2019), electrical and computer engineering (2020), and mathematics (2021). While completing his PhD in Aerospace Engineering at Georgia Tech, he was a Marcus Dash Fellow, and an active participant in the Model-Based Life Extending Control for Rotorcraft project funded by the U.S. Army, U.S. Navy, and NASA under the Vertical Lift Research Center of Excellence at Georgia Tech. He is a previous member of the Georgia Tech Vertical Flight Society and a current member of the National Society of Black Engineers.